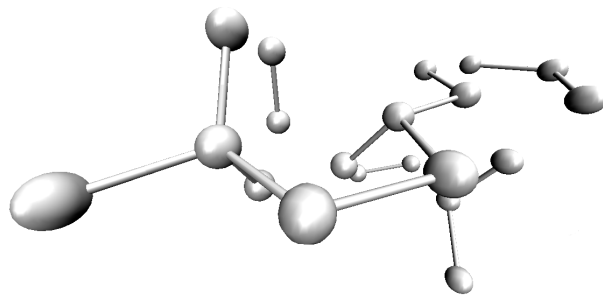*phd thesis*

Long-time simulations of viscous liquids
from strong correlations to crystallization

Ulf Rørbæk Pedersen

Supervisor: Thomas B. Schrøder

*Danish National Research Foundation Centre "Glass and Time",
IMFUFA, Department of Science, Systems and Models,
Roskilde University, Denmark*

January 30, 2009

Abstract

This philosophiæ doctor thesis has thirteen companion papers. The major part is a theoretical and simulation study of a class of liquids referred to as strongly correlating liquids. However, one chapter is dedicated to a study of thermodynamic fluctuations of simulated phospholipid membranes, and another to a simulation study of crystallization of a binary mixture. The thesis also includes a short introduction to supercooled viscous liquids and molecular dynamics simulations. The final chapter is an outlook. The conclusions are as follows:

A class of model liquids exhibit strong correlation in the thermal fluctuations of the virial and potential energy at constant volume. The origin of the correlation is explained for the Lennard-Jones liquid. The pair energy can to a good approximation be replaced by an inverse power-law plus a linear term. At constant volume only the inverse power-law gives a contribution to fluctuations, thereby explaining the correlation. Two quantities characterize a strongly correlating liquid: i) A correlation coefficient, R, that determine the degree of correlation and ii) a slope, γ, that determine the proportionality between virial and potential energy. If the correlation coefficient is close to unity the liquid is strongly correlating and 3γ equals the exponent of the inverse power-law.

For viscous liquids, the correlation coefficient equals the inverse square-root of a Prigogine-Defay ratio defined from three response functions. Also the slope can be determined from response functions. Literature values of the classical Prigogine-Defay suggests that van der Waals bonded liquids in general are strongly correlating.

Strongly correlating viscous liquids are more simple than viscous liquids in general: i) Slow dynamics are determined by a single relaxing parameter. Thus, time- and frequency-dependent response functions of a given ensemble are proportional. ii) Scale invariance is inherited from soft-sphere liquids though the effective inverse-power law. Thus, state points with the same value of ρ^{γ}/T have the same scaled structure and dynamics. These conclusions are verified in simulations.

Slow thermal fluctuations of volume and energy of simulated phospholipid membranes are strongly correlated. The origin of the strong correlation can be traced to the van der Waals bonded core of the membranes and, thus, have the same origin as simple strongly correlating liquids.

The last part of the thesis reports crystallization into the $MgZn_2$ Laves phase of the binary Lennard-Jones mixture suggested by Wahnström [1991]. The crystallization mechanism from the supercooled melt is investigated in detail.

Abstract in danish:

Denne philosophiæ doctor afhandling er ledsaget af tretten artikler. Hoveddelen er et teoretisk og simulerings studie af en klasse af væsker refereret til som stærkt korrelerede væsker. Dog er et kapitel dedikeret til et studie af termiske fluktuationer af simulerede phospholipidmembraner, og et kapitel til et simuleringstudie af krystallisering af en binær blanding. Afhandlingen inkluderer også en kort introduktion til underafkølede viskøse væsker samt molekyledynamik simuleringer. Det sidste kapitel omhandler fremtidige undersøgelser. Følgende er konkluderet:

En klasse af modelvæsker udviser ved konstant volumen en stærk korrelation i de termiske fluktuationer af virial og potentiel energi. Korrelationens ophav er forklaret for Lennard-Jones væsken. Parenergien kan med god tilnærmelse erstattes med en invers potensfunktion plus et lineært led. Ved konstant volumen er det kun den inverse potensfunktion som giver bidrag til fluktuationer, og derved forklarer korrelationen. To størrelser karakteriserer en stærkt korreleret væske: i) En korrelationskoefficient, R, som bestemmer graden af korrelation og ii) en hældning, γ, som bestemmer proportionaliteten mellem virial og potentiel energi. Hvis korrelationskoefficienten er tæt på én, er væsken stærkt korrelerende og 3γ er lig med eksponenten af den inverse potensfunktion.

For viskøse væsker er korrelationskoefficienten lig med den inverse kvadratrod af en Prigogine-Defay kvotient defineret ud fra tre responsfunktioner. Hældningen kan også bestemmes ud fra responsfunktioner. Værdier af den klassiske Prigogine-Defay kvotient fra litteraturen indikerer, at van der Waals væsker i almindelighed er stærkt korrelerede.

Stærkt korrelerede viskøse væsker er simplere end viskøse væsker i almindelighed: i) Langsom dynamik er styret af en enkelt relakserende parameter. Derved er de tids- og frekvensafhængige responsfunktioner for et givet ensemble proportionale. ii) Skaleringsinvarians af *soft sphere*-væsker nedarves gennem den inverse potensfunktion. Derfor har tilstande med samme værdi af ρ^γ/T den samme skallerede struktur og dynamik. Simuleringer bekræfter disse konklusioner.

Simulerede phospholipidmembraners langsomme termiske fluktuationer af volumen og energi er stærkt korrelerede. Forklaringen på den stærke korrelation skal findes i den indre van der Waalske del af membranen. Derved er oprindelsen den samme som for de stærkt korrelerede simple væsker.

Den sidste del af afhandlingen beretter om krystallisering ind i $MgZn_2$ Laves-fasen af den binære Lennard-Jones blanding foreslået af Wahnström [1991]. Mekanismen for krystallisering af den underafkølede smelte er undersøgt i detaljer.

iv

Preface

This is the philosophiæ doctor (Ph.D.) thesis of Ulf Rørbæk Pedersen. The Ph.D. was initiated February 1st 2006 and the thesis was submitted January 30th 2009, thus lasting the three years of the Danish Ph.D. program.

The thesis have thirteen companion papers (listed below). The purpose of the thesis is to guide the reader though these papers. The reader will, however, have to consult the papers to get the full story. Also, parts of the thesis goes beyond the papers.

Papers

Companion papers are listed below and reprinted in Appendix B.

Paper I: Niels L. Ellegaard, Tage Christensen, Peder Voetmann Christiansen, Niels Boye Olsen, Ulf R. Pedersen, Thomas B. Schrøder, Jeppe C. Dyre (2007) *Single-order-parameter description of glass-forming liquids: A one-frequency test.* J. Chem. Phys 126, 074502

Paper II: Ulf R. Pedersen, Nicholas P. Bailey, Jeppe C. Dyre, Thomas B. Schrøder (2007) *Crystallization of the Wahnström Binary Lennard-Jones Liquid.* arXiv:0706.0813

Paper III: Ulf R. Pedersen, Nicholas P. Bailey, Thomas B. Schrøder, Jeppe C. Dyre (2008) *Strong pressure-energy correlations in van der Waals liquids.* Phys. Rev. Lett. 100, 015701

Paper IV: Ulf R. Pedersen, Tage Christensen, Thomas B. Schrøder, Jeppe C. Dyre (2008) *Feasibility of a single-parameter description of equilibrium viscous liquid dynamics.* Phys. Rev. E 77, 011201

Paper V: Ulf R. Pedersen, Günther H. Peters, Thomas B. Schrøder, Jeppe C. Dyre (2008) *Volume-energy correlations in the slow degrees of freedom of computer-simulated phospholipid membranes.* AIP Conf. Proc. 982, 407-409

Paper VI: Nicholas P. Bailey, Tage Chistensen, Bo Jakobsen, Kristine Niss, Niels Boye Olsen, Ulf R. Pedersen, Thomas B. Schrøder, Jeppe C. Dyre (2008) *Glass-forming liquids: one or more 'order' parameters?* Journal of physics-condensed matter 20, 244113

Paper VII: Thomas B. Schrøder, Ulf R. Pedersen, Jeppe C. Dyre (2008) *Density scaling in a strongly correlating viscous liquid.* arXiv:0803.2199 [cond-mat.soft]

Paper VIII: Nicholas P. Bailey, Ulf R. Pedersen, Nicoletta Gnan, Thomas B. Schrøder, Jeppe C. Dyre (2008) *Pressure-energy correlations in liquids. I. Results from computer simulations.* J. Chem. Phys. 129, 184507

Paper IX: Nicholas P. Bailey, Ulf R. Pedersen, Nicoletta Gnan, Thomas B. Schrøder, Jeppe C. Dyre (2008) *Pressure-energy correlations in liquids. II. Analysis and consequences.* J. Chem. Phys. 129, 184508 (2008)

Paper X: Ulf R. Pedersen, Günther H. Peters, Thomas B. Schrøder, Jeppe C. Dyre (2008) *Computer simulations of phospholipid-membrane thermodynamic fluctuations.* arXiv:0811.3317 [physics.bio-ph]

Paper XI: Søren Toxvaerd, Ulf R. Pedersen, Thomas B. Schrøder, Jeppe C. Dyre (2008) *Stability of supercooled binary liquid mixtures.* arXiv:0811.1117v1 [cond-mat.soft]

Paper XII: Ulf R. Pedersen, Thomas B. Schrøder, Jeppe C. Dyre (2008) *Termiske fluktuationer — er der noget nyt under Solen?* (in danish) Kvant: Tidskrift for fysik og astronomi 16(4), 26-29. Dec 2008

Paper XIII: Thomas B. Schrøder, Ulf R. Pedersen, Nicholas Bailey, Søren Toxværd, Jeppe C. Dyre (2008) *Hidden scale invariance in molecular van der Waals liquids: A simulation study* arXiv:0812.4960v1 [cond-mat.soft]

Oral and poster presentations

Results of this thesis have also been presented at the following conferences and meetings.

Oral presentations:

Copenhagen 2008 *Long-lived structural fluctuations and crystallization of a binary Lennard-Jones mixture.* Presented at the international workshop Fragility of Viscous Liquids: Cause(s) and Consequences [Carlsberg Academy, Copenhagen, Denmark, October 8-10, 2008].

Nyborg Strand 2008 *Volume-energy correlations in the slow degrees of freedom of phospholipid membranes.* Presented at the Danish Physical Society Annual Meeting [Nyborg Strand Hotel, Denmark, June 17-18, 2008].

Søminestationen 2007 *Crystallization of the Wahnström binary Lennard-Jones liquid.* Presented at Viscous Liquids and the Glass Transition VI [Søminestationen, Holbæk, Denmark, June 29 - July 1, 2007].

Søminestationen 2006 *A tumbling model of toluene.* Presented at Viscous Liquids and the Glass Transition V [Søminestationen, Holbæk, Denmark, May 26-28, 2006].

Poster presentations:

Kyoto 2008 *Density scaling as a property of strongly correlating viscous liquids* and *Long-lived structural fluctuations and crystallization of a binary mixture.* Two posters presented at Unifying Concepts in Glass Physics IV (UCGP2008) [Kyoto, Japan, November 25-28 2008].

Sitges 2008 *Equilibrium fluctuations of volume and energy of simulated phospholipid membranes.* Presentedat the XXI Sitges Conference on Statistical mechanics: Statistical Mechanics of Molecular Biophysics [Sitges, Barcelona, Spain, June 2-6, 2008].

Andalo 2008 *Long-lived structural fluctuations and crystallization of a binary Lennard-Jones mixture.* Presented at XI International Workshop on Complex Systems [Andalo, Italy, March 17-20, 2008].

Sendai 2007 *Volume-energy correlations in the slow degrees of freedom of phospholipid membranes.* Presented at the 5th International Workshop on Complex Systems [Sendai International Center, Sendai, Japan, September 25-28, 2007].

Holderness 2007 *Strong pressure-energy correlations in model liquids.* Presented at The Physics and Chemistry of Liquids (Gordon Conference) [Holderness School, New Hampshir, July 29 - August 3, 2007].

Pisa 2006 *The dynamical Prigogine-Defay ratio: Is the glass transition controlled by one or more order-parameters?* Presented at IV Workshop on Non Equilibrium Phenomena in Supercooled Fluids, Glasses and Amorphous Materials [Pisa, Italy, September 17-22, 2006].

Nyborg Strand 2006 *Molecular Dynamic Simulations of Viscous Toluene.* Presented at the Danish Physical Society Annual Meeting [Nyborg Strand Hotel, Denmark, June 1-2, 2006].

Acknowledgments

In March-April 2007 I spent one month visiting the Francesco Sciortino group at La Sapienza in Rome. I would like to thank them for the hospitality and nice discussions.

In September-November 2007 I visited Peter Harrowell at the School of Chemistry at the University of Sydney, where I also had the pleasure to meet Toby Hudson and Asaph Widmer-Cooper. I really enjoyed the enlightening discussion and warm humor of the Aussies. The study of the crystallisation of the Wahnström binary Lennard-Jones liquid is done in collaboration with Peter Harrowell.

Before handing in the thesis Nicolas P. Bailey and Thomas B. Schrøder read all of the thesis and gave many useful comments and suggestions.

Finally I would like to thank the International Earth Rotation Service for giving an extra second after Jan 1st 00:59:59 2009. In the final phase of writing a thesis some extra time is always welcome.

Contents

Chapter 1

Introduction

The purpose of this chapter is to give a short introduction to the field of supercooled viscous liquids (Section 1.1) and molecular dynamics simulations (Section 1.2). Section 1.3 gives an outline of the remainder of the thesis.

1.1 Supercooled viscous liquids

Imagine we are cooling a liquid as shown in Figure 1.1. Below some temperature T_m the free energy per particle of the crystal μ_{cry} becomes lower than that of the liquid μ_{liq}. According to thermodynamics, the molecules should now form a crystal to lower the free energy. However, making this experiment, in a computer or in the laboratory, the crystal might first form below T_m or never. The liquid is said to be supercooled at $T < T_m$.

To get insight on supercooling, recall classical nucleation theory in its simplest form [Volmer and Weber, 1926, Becker and Doring, 1935]. Imagine that for some reason a spherical crystallite had actually formed in the liquid at $T < T_m$. Let N_c be the number of particles, r_c the radius and $\rho_c = \frac{N_c}{\frac{4}{3}\pi r_c^3}$ the density of the crystallite. The stability of this crystallite is given by the Gibbs free energy G relative to the liquid. Bulk particles in a crystalline environment will give a negative volume contribution; $G_{\text{vol}} = -\frac{4}{3}\pi r_c^3 \rho_c \Delta\mu$ where $\Delta\mu = \mu_{\text{liq}} - \mu_{\text{cry}}$. However, the solid-liquid surface tension γ_∞ will give a positive surface contribution; $G_{\text{surf}} = 4\pi r_c^2 \gamma_\infty$, thereby destabilizing the crystallite. Surface area scales as r_c^2 and volume as r_c^3, so if the crystallite is big enough, the negative volume contribution dominates and the crystallite will grow; $\frac{\partial}{\partial r_c}\Delta G < 0$ for large r_c where $\Delta G = G_{\text{surf}} + G_{\text{vol}}$. However, at some critical size the surface contribution and the volume contribution will balance out. $\frac{\partial}{\partial r_c}\Delta G = 0$, when

$$r_c^* = \frac{2\gamma_\infty}{\rho_c \Delta\mu} \text{ and } \Delta G^* = \frac{16\pi\gamma_\infty^3}{3\rho_c^2(\Delta\mu)^2} \tag{1.1}$$

Crystallites smaller than r_c^* are unstable. The crystallite leading to crystallization is referred to as the critical nucleus. Remember that $\Delta\mu(T_m) \equiv 0$ by definition, thus, the size r_c^* and barrier height ΔG^* of the critical nucleus is infinitely large at the melting temperature. Therefore all liquids can be supercooled since all crystallites are unstable at T_m. If we wait long enough at $T < T_m$ a thermal fluctuation will eventually form the critical nucleus and the
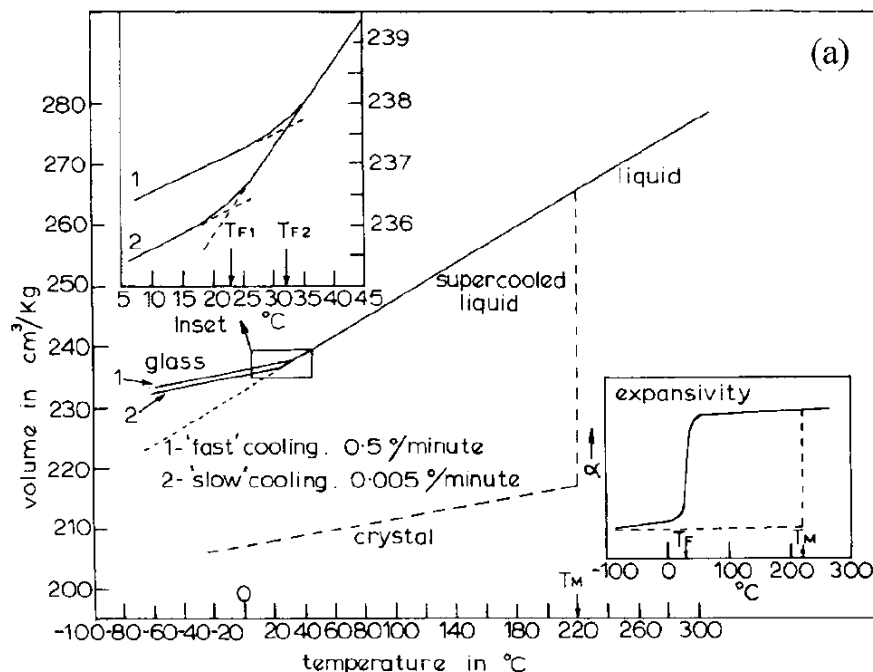
Figure 1.1: Volume of Selenium in different phases. At cooling rates of 0.5 degree per minute and 0.005 degree per minute crystallization is avoided. At these cooling rates, nothing special is observed when passing the melting temperature at $T_m = 220$ °C. Note the change of slope at temperature T_{F1} and T_{F2} enlarge on the upper inset. This is a result of a glass transition. The figure is reprinted from Reference [Dyre, 2006], however, the original figure is from Reference [Owen, 1985] with data from Dzhalilo and Rzaev [1967].

liquid will find its true equilibrium state. However, in the time of an experiment or simulation this might never occur. Therefore, the liquid is said to be in a metastable equilibrium since the liquid behaves as if it was in a true equilibrium. It should be noted that classical nucleation theory is only adequate close to T_m [Debenedetti, 2006].

Now, consider a liquid where crystallization do not occur. As the thermal energy is lowered it becomes more difficult for particles to overcome energy barriers associated with flow events. The liquid becomes highly viscous. If we disturb the system it will take some time for the liquid to find its new (metastable) equilibrium state, characterized by a structural relaxation time τ_α. At some temperature[1], referred to as the glass transition temperature T_g, τ_α will become longer than the time-scales of the experiment or computer simulation. Structure cannot relax, and the liquid falls out of (metastable) equilibrium. The liquid is now in a so-called glassy state as shown in Figures

---

[1]To make T_g well-defined, it is often defined as $\tau_\alpha(T_g) = 100$ seconds. Here we will loosely define T_g as the temperature where we cannot bring the system to its (metastable) equilibrium state.
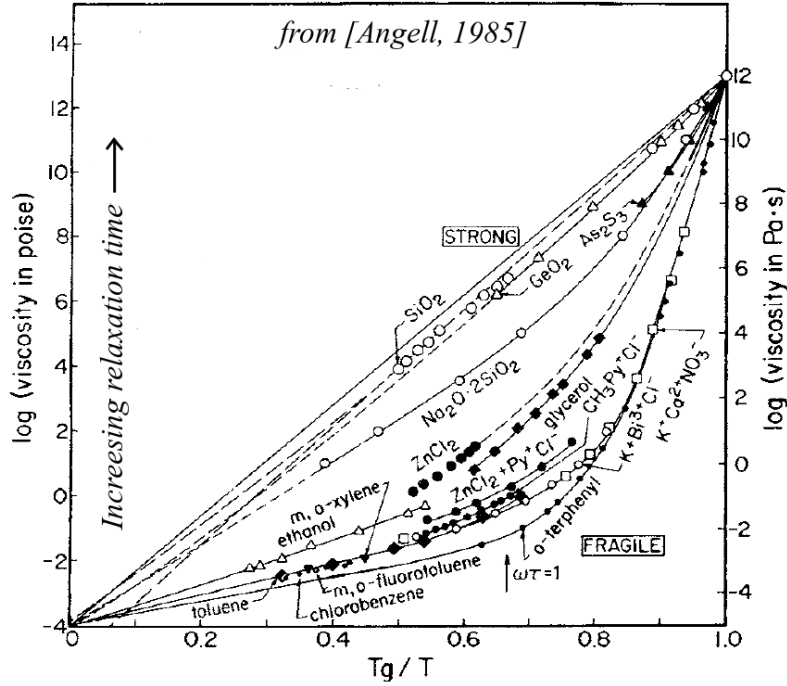
Figure 1.2: Logarithm of viscosity as a function of inverse temperature for several liquids. A straight line in this plot corresponds to an Arrhenius law, Equation 1.2. T_g is defined as $\eta(T_g) = 10^{12}$ Pa·s. According to the Maxwell model [see Dyre, 2006], the relaxation time is given by $\tau_\alpha = \eta/G_\infty$. If assuming that the instantaneous shear modulus G_∞ is constant, then viscosity is proportional to the relaxation time, $\tau_\alpha(T) \propto \eta(T)$. Note that some liquids, like SiO$_2$, follows the Arrhenius law to a good approximation, while others, like o-terphenyl (OTP), have a significant non-Arrhenius growth of structural relaxation. See also Figure 1.8. This figure is originally from Reference [Angell, 1985] (data of heat-capacity is removed from original figure for clarity) and reprinted from [Dyre, 2006].

1.1. The *solid* glass is different from the *solid* crystal, since the structure is not ordered, but has inherited the disordered structure of the liquid.

Let us take a look at the temperature dependency of τ_α. In a situation where there is only one energy barrier E_A, the relaxation time would follow an Arrhenius law [Debenedetti and Stillinger, 2001]

$$\tau_\alpha(T) = \tau_0 \exp\left(\frac{-E_A}{k_B T}\right). \tag{1.2}$$

Figure 1.2 shows (a measure of) relaxations times as a function of inverse temperature for a broad collection of liquids. Structural relaxation of some liquids, like the covalent bonded SiO$_2$, follow this equation to a good approximation. Presumably, E_A is related to breaking bonds needed for flow. Others liquids,

like the van der Waals bonded o-terphenyl (OTP), have a more dramatic increase of τ_α. Apparently, the energy barriers for this kind of liquids increase as the liquid is cooled; $\frac{\partial}{\partial(1/T)} E_A(T) > 0$. Many theoretical descriptions even predict a divergence of $E_A(T)$ at some finite temperature T_0. Experimental data, however, neither confirms nor rejects such a divergence [Hecksher et al., 2008]. Generally, changing volume V will also influence τ_α, so we should write $\tau_\alpha(V,T)$. Explaining the non-Arrhenius behavior of fragile liquids is one of the great puzzles of viscous liquids [Dyre, 2006].

Another great puzzle of viscous liquids relates to how various quantities relax to equilibrium after a disturbance. Let $\Delta A(t) = A(t) - \langle A \rangle$ be the distance to equilibrium of some observable like internal energy, pressure or volume. Again, consider a simple situation where the liquid only have to overcome a single energy barrier to relax. In this scenario relaxation would be exponential,

$$\Delta A(t) = A_0 \exp\left(-\frac{t}{\tau_\alpha}\right) \tag{1.3}$$

However, virtually no liquids behave this way suggesting some distribution of energy barriers.

The studies presented in this thesis utilize molecular dynamics simulations of supercooled viscous liquids. An introduction to this is given in the following section.

1.2 Molecular dynamics simulations

Computers can make an incredible amount of repetitive calculations. For this reason, computational methods play an important role in the field of condensed matter. A popular method is molecular dynamics simulations [ten Wolde and Frenkel, 1998, Allen and Tildesley, 1987]. To illustrate the basic concept of this method, imagine that we want to simulate a liquid of Argon atoms. Our first assumption will be that dynamics can be described using classical mechanics. Next, we need some model of forces between atoms, referred to as the force-field. For simplicity we will assume that Argon atoms only interact pairwise with a force $F_{ij}(r_{ij})$, where r_{ij} is the distance between particle i and j. Imagine we have a box with N particles. We need to consider what to do with the walls of the box. We could put some repulsive interactions at the walls, however, then we would be investigating a liquid close to a wall. For a better simulation of bulk properties we can make use of periodic boundaries as illustrated in Figure 1.3. The result is that there is no wall, although, due to the limited size of the system, there can still be finite size effects.

From an initial configuration of positions and velocities we can integrate the classical equations of motion numerically. A numerical integration consists of a simple repetitive calculation and is therefore ideal for computers. There are numerous algorithms for numerical integrations. A crucial choice is the size of numerical time step, dt^{step}. A large time-step is be preferable, since we are interested in long times. The fastest vibrations, however, set an upper limit for the time step. The longest times of the simulation is determined by the available computer power and the complexity of the system. At present day, a system of 1000 particles can be investigated in a time-window of 10^{-14} seconds to 10^{-4} seconds (Figure 1.7).
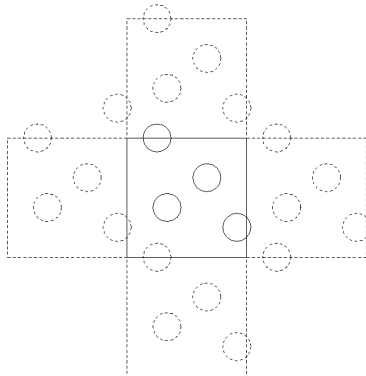
Figure 1.3: Illustration of four particles confined in a box with periodic boundaries. Image boxes are displayed with dashed lines.

In a simulation as presented here the number of particles, volume and total energy are constant. Thus, such a simulation is of the NVE ensemble. Algorithms[2] have been developed to keep temperature and/or pressure constant, making NVT and NpT simulations possible. In long-time simulations a thermostat is preferable since numerical errors make the total energy drift in NVE.

Before we can preform an actual simulation we need to specify a force-field. In the following we will think in terms of pair energy, $U_{ij}(r)$. This is just an other way of writing the force. It is natural to chose to have zero energy at $r_{ij} = \infty$ and therefore $U_{ij}(r) = \int_r^\infty F_{ij}(r)dr$.

Now, let us think of a good expression for $U_{ij}(r)$. Recall that "induced dipole"-"induced dipole" attraction, known as London dispersion forces, act between all atoms [Atkins and de Paula, 2002, or a similar standard textbook]. The pair energy associated with this is $U_{ij}^{\mathrm{London}} \propto -r^{-6}$. Bringing two atoms close together will result in a repulsion since electron-clouds cannot overlap. For this we should choose some function with a steep divergence at $r = 0$. Traditionally $U_{ij}^{\mathrm{rep}} \propto r^{-12}$ is used. Putting this together we obtain the so-called Lennard-Jones potential [Lennard-Jones, 1931],

$$U_{ij}^{\mathrm{LJ}}(r) = 4\varepsilon \left(\left(\frac{\sigma}{r}\right)^{12} - \left(\frac{\sigma}{r}\right)^{6} \right). \tag{1.4}$$

We will refer to this as the Lennard-Jones liquid. Note that ε defines the energy scale, σ the length scale and unit of mass is defined by the mass m of the particles. Dimensionless versions of physical quantities can be defined from these three. As an example, a dimensionless time can be defined as

$$t' = t\sqrt{\frac{\varepsilon}{m\sigma^2}} \tag{1.5}$$

Some good values for Argon are $\varepsilon = 0.997$ kJ/mol, $\sigma = 0.34$ nm and $m = 39.95$ u [van der Spoel et al., 2006]. Using this we have $t = t'2.15$ ps.

---

[2]In the simulations presented in this theses, the Nosé-Hoover thermostat [Nosé, 1984, Hoover, 1985] and the Nosé-Hoover Langevin barostat [Feller et al., 1995] are used.
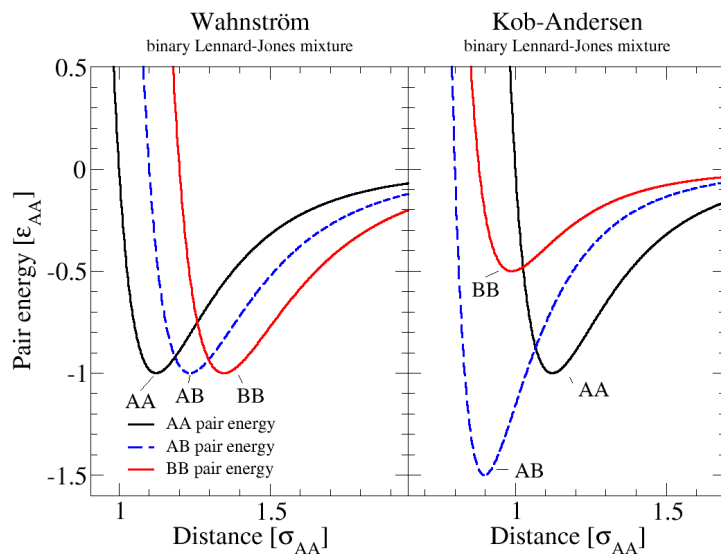
Figure 1.4: Pair potentials of two binary Lennard-Jones mixture; the parameter suggested by Wahnström [1991] and Kob and Andersen [1994]. The parameters for the Wahnström mixture are $\sigma_{BB} = 1.2\sigma_{AA}$, $\sigma_{AB} = 1.1\sigma_{AA}$, $\varepsilon_{AA} = \varepsilon_{AB} = \varepsilon_{BB}$, $m_B = 2m_A$ and $N_A = N_B = 512$ ($\chi_B = 0.5$) in a volume $V = (11.094\sigma_{AA})^3$. The parameters for the Kob-Andersen mixture are $\sigma_{BB} = 0.88\sigma_{AA}$, $\sigma_{AB} = 0.80\sigma_{AA}$, $\varepsilon_{BB} = 0.5\varepsilon_{AA}$, $\varepsilon_{AB} = 1.5\varepsilon_{AA}$, $m_A = m_B$, $N_A = 800$, $N_B = 200$ ($\chi_B = 0.2$) in a volume $V = (9.4\sigma_{AA})^3$. The Kob-Andersen mixture is by far the most well-studied.

The Lennard-Jones liquid can easily form a (defected) face center cubic crystal and it has limited use in the study of supercooled viscous liquids since crystallization will occur before it becomes viscous. Clarke [1979] did, however, investigate the glass transition. Crystallization can be avoided by make more complicated models. It is desirable to keep models as simple as possible, so they are computationally cheap. The following subsection briefly describes the models investigated in this thesis.

1.2.1 Simulated systems

Below is a list of models I have simulated. Where nothing else is noted, simulations where preformed using the Gromacs software package [van der Spoel et al., 2006]. Analysis of the trajectories where done using the Gromacs software package, home-made Octave scripts [http://www.gnu.org/software/octave/] and home-made FORTRAN90 code. Pictures of configurations are made using VMD [Humphrey et al., 1996] assisted with home-made code.

Lennard-Jones liquid: 864 Lennard-Jones particles.

Kob-Andersen binary Lennard-Jones mixture: 800 type A and 200 type B Lennard-Jones particles. The parameters for the three kinds of pair
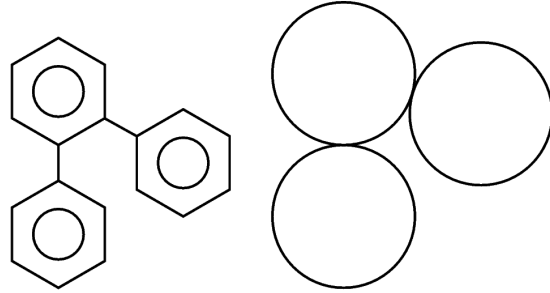
Figure 1.5: The chemical structure of o-terphenyl (OTP), $C_6H_4(C_6H_5)_2$, and a representation of the model suggested by Lewis and Wahnström [1994] where circles represent Lennard-Jones particles. The Lennard-Jones parameters are $\varepsilon = (600 \text{ K})k_B$, $\sigma = 0.483$ nm and $m = 76.768$ u. The center of the Lennard-Jones particles are located in the corners of rigid isosceles triangle with two sides of length σ and one angle of 75°.
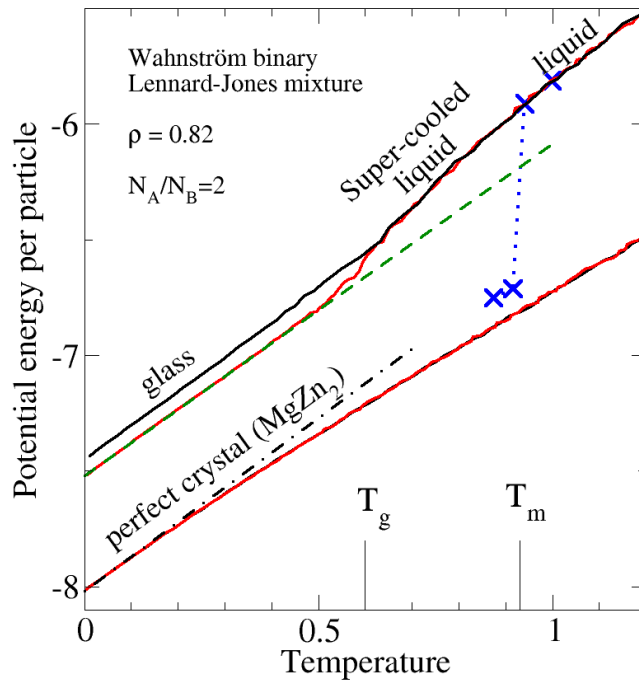
Figure 1.6: The potential energy in different phases of the Wahnström binary Lennard-Jones liquid at $\chi_B = 1/3$. Note that traditionally the $\chi_B = 1/2$ composition is simulated (see Figure 1.4). See Chapter 6 and Paper II for more about the stability of this mixture. Note that the phenomenology is the same as seen in Figure 1.1 for Selenium. Similar phenomenology is found for liquids in general.

Figure 1.7: Mean square displacement, $\langle(\Delta r(t))^2\rangle = \langle(|\vec{r}(t) - \vec{r}(0)|)^2\rangle$, of A and B particles of the Kob-Andersen binary Lennard-Jones mixture. At ultra short times particles have not "felt" each other, and displacements are ballistic, $\langle(\Delta r(t))^2\rangle = (v_m t)^2$ where v_m is the root mean square velocity. At long-times displacements become diffusive, $\langle(\Delta r(t))^2\rangle = 6Dt$, where D is the diffusion constant. At low temperatures, $T < 0.5$, particles become "caged" in the intermediate region.
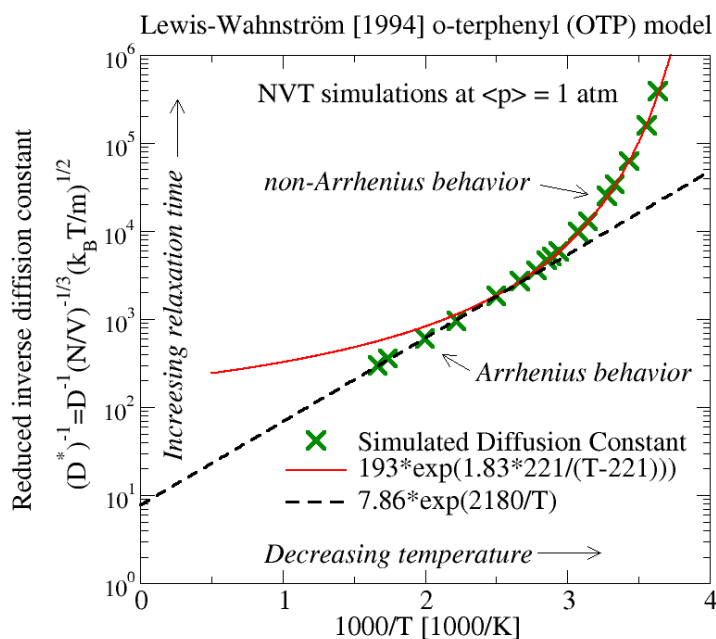
Figure 1.8: Reduced inverse diffusion constant $(D^*)^{-1} = D^{-1}(N/V)^{-1/3}(k_B T/m)^{1/2}$ as a function of inverse temperature in a simulation of the Lewis-Wahnström model of OTP. $(D^*)^{-1}$ relates to some characteristic "diffusion" time. A straight line in this plot corresponds to an Arrhenius law, Equation 1.2. Note that at high temperature $(D^*)^{-1}$ follows an Arrhenius law, but not at lower temperature. A non-Arrhenius behavior at low temperature is also found for experimental data of OTP (see o-terphenyl (OTP) in Figure 1.2).

energies, $U_{AA}^{\mathrm{LJ}}(r)$, $U_{BB}^{\mathrm{LJ}}(r)$, $U_{AB}^{\mathrm{LJ}}(r)$, are $\sigma_{BB} = 0.88\sigma_{AA}$, $\sigma_{AB} = 0.80\sigma_{AA}$, $\varepsilon_{BB} = 0.5\varepsilon_{AA}$, $\varepsilon_{AB} = 1.5\varepsilon_{AA}$. The pair potentials are shown in Figure 1.4. This model was suggested by Kob and Andersen [1994] and is one of the most well-studied model viscous liquids.

Wahnström binary Lennard-Jones mixture: 500 type A and 500 type B Lennard-Jones particles with the interaction parameters $\sigma_{BB} = 1.2\sigma_{AA}$, $\sigma_{AB} = 1.1\sigma_{AA}$, $\varepsilon_{AA} = \varepsilon_{AB} = \varepsilon_{BB}$ and masses $m_B = 2m_A$. The pair potentials are shown in Figure 1.4. This model was suggested by Wahnström [1991].

Lewis-Wahnström OTP model: Lewis and Wahnström [1994] suggested to connect three identical Lennard-Jones particles with rigid bonds as a toy model of o-terphenyl (OTP). The LINCS algorithm [Hess et al., 1997] is used for making rigid bonds (in all the models). See Figure 1.5 for more details about this model.

Asymmetric dumbbells: A system of asymmetric dumbbells as a toy model of toluene, where a phenyl-group, C_6H_5-, and the methyl-group, $-CH_3$

where represented as Lennard-Jones particles.

Seven-site model of toluene: A model of toluene, $C_6H_5CH_3$, were CH_x groups (were x is either 0, 1, or 3) are simulated as Lennard-Jones particles connected by rigid bonds. The UA-OPLS parameter set [Jorgensen et al., 1984] where used for bond lengths and interaction parameters.

SPC/E water: Three-site model of water suggested by Berendsen et al. [1987].

GROMOS methanol: Three-site model of methanol, CH_3OH, where CH_3, O and H are simulated as charged Lennard-Jones spheres. The GROMOS parameter set [van Gunsteren et al., 1996] was used for bond lengths and interaction parameters.

Phospholipid membranes: Seven phospholid membranes where simulated using a modified version of the all-atom CHARMM27 [Foloppe and MacKerell, 2000] parameter set. See Chapter 5, References [Pedersen, 2005, Pedersen et al., 2006, 2007, Sonne et al., 2007], and/or Paper X for more details. As a part of my master thesis [Pedersen, 2005] I simulated one of these membranes, however, the simulations presented in this thesis are conducted by Günther H. Peters (using the NAMD2 program [Kale et al., 1999]).

Model liquids shows the same phenomenology as real liquids. Figures 1.6 to 1.7 exemplifies this. Figure 1.6 shows the potential energy in different phases of the Wahnström binary Lennard-Jones mixture. At the investigated cooling rates of the liquid, crystallization is avoided and a glass transition is observed. Recall that this is the same phenomenology as shown in Figure 1.1.

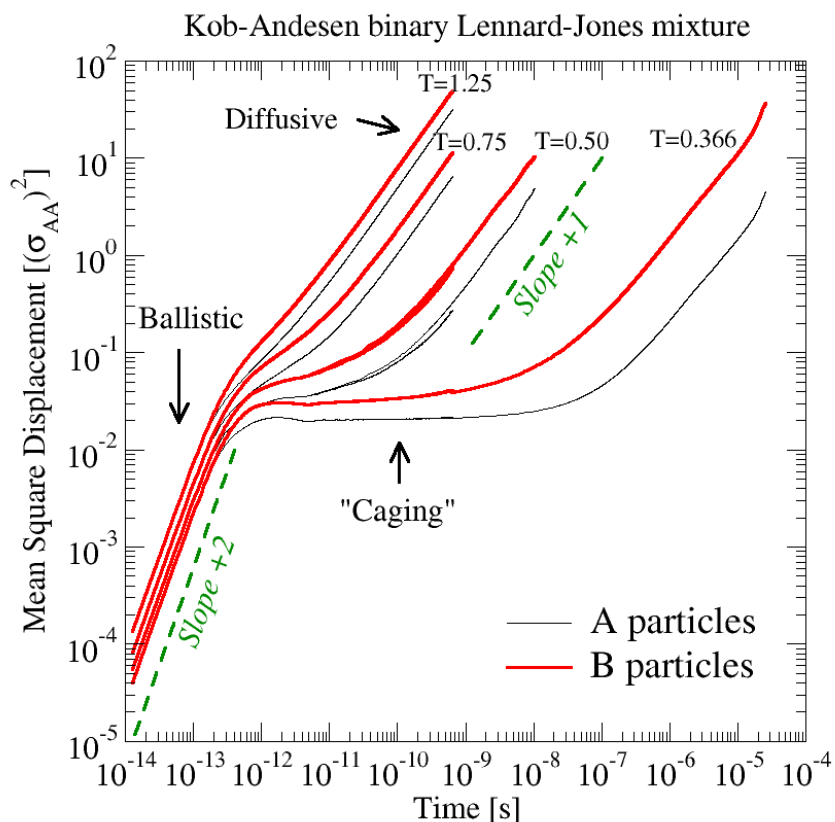Figure 1.7 shows the root mean square displacement $\langle (\Delta r(t))^2 \rangle = \langle (|\vec{r}(t) - \vec{r}(0)|)^2 \rangle$ of particles of the Kob-Andersen Lennard-Jones liquid. At short times displacements are ballistic and at long times they are diffusive. From this last part of the curve, the diffusion constant D can be determined, $\langle (\Delta r(t))^2 \rangle = 6Dt$. At low temperatures an intermediate plateau appears, where particles do not move. At $T = 0.366$ particles are "caged" from 10^{-12} to 10^{-7} seconds (in Argon units).

Figure 1.8 shows the diffusion constant of molecules of the Lewis-Wahnström OTP model at different temperatures. At high-temperatures, the diffusion constant follows an Arrhenius law. However, at low-temperatures, diffusion is clearly non-Arrhenius. This is in good agreement of what is observed for real OTP as seen in Figure 1.2 (labeled o-terphenyl).

1.3 Outline of thesis

In Chapter 2 it is shown that some model liquids exhibit strong correlations in the thermal fluctuations of configurational parts of pressure and energy in the NVT ensemble. Such liquids are referred to as strongly correlating liquids. Chapter 3 explains the origin of the strong correlation. In Chapter 4 it is argued, on the basis of the previous chapters, that strong correlating *viscous* liquids are more simple than viscous liquids in general. This is exemplified by the so-called Progogine-Defay ratio being close to unity (Section 4.1), and scale invariance of structure and dynamics (Section 4.2).

Thermodynamic fluctuations of phospholipid membranes also exhibit strong correlations. These correlations are reported and explained in Chapter 5.

Chapter 6 reports and investigates crystallization from the melt of some of the investigated models. Before the presented study, these models had not been reported to crystallize from the melt. Crystallization of the Wahnström binary Lennard-Jones liquid is investigated in details.

The final chapter is an outlook.

Chapter 2

Strongly correlating liquids

Consider a system of N particles in a fixed volume V. Total energy E is a sum of a kinetic part (kinetic energy) that is only a function of the momenta, $\vec{Q} = \{\vec{q}_1, \vec{q}_2, \ldots, \vec{q}_N\}$, and a configurational part (potential energy) that is only a function of positions, $\vec{R} = \{\vec{r}_1, \vec{r}_2, \ldots, \vec{r}_N\}$;

$$E(\vec{Q}, \vec{R}) = K(\vec{Q}) + U(\vec{R}). \tag{2.1}$$

In the same way, pressure p is a sum of a kinetic and a configurational part,

$$p(\vec{Q}, \vec{R}) = Nk_B T(\vec{Q})/V + W(\vec{R})/V, \tag{2.2}$$

where $T(\vec{Q})$ is the instantaneous temperature. W/V and U are the configurational part of pressure and energy respectively. Note that W is in units of energy. If thermal fluctuations of W and U are strongly correlated in time, this is referred to as a *strongly correlated liquid*. The remainder of this chapter discuss such W-U correlations in model liquids and super critical Argon. The main references for this chapter are Paper III and Paper VIII.

2.1 An example: The Lennard-Jones Liquid

Probably the most well-studied model liquid is the (single component) Lennard-Jones liquid, where particles interact pairwise via the Lennard-Jones potential [Lennard-Jones, 1931]:

$$U_{ij}^{LJ} = 4\varepsilon \left(\left(\frac{\sigma}{r_{ij}} \right)^{12} - \left(\frac{\sigma}{r_{ij}} \right)^6 \right), \tag{2.3}$$

where r_{ij} is the distance between particle i and j (see also Section 1.2). The virial of a system of pairwise interactions particles is

$$W = \frac{1}{3} \sum_{i \neq j} r_{ij} F_{ij} = \sum_{i \neq j} W_{ij} \tag{2.4}$$

where $F_{ij} = -\frac{d}{dr} U_{ij}$ is the force between particle i and j. It is convenient to define a pair virial as

$$W_{ij} = -\frac{r_{ij}}{3} \frac{d}{dr} U_{ij}. \tag{2.5}$$
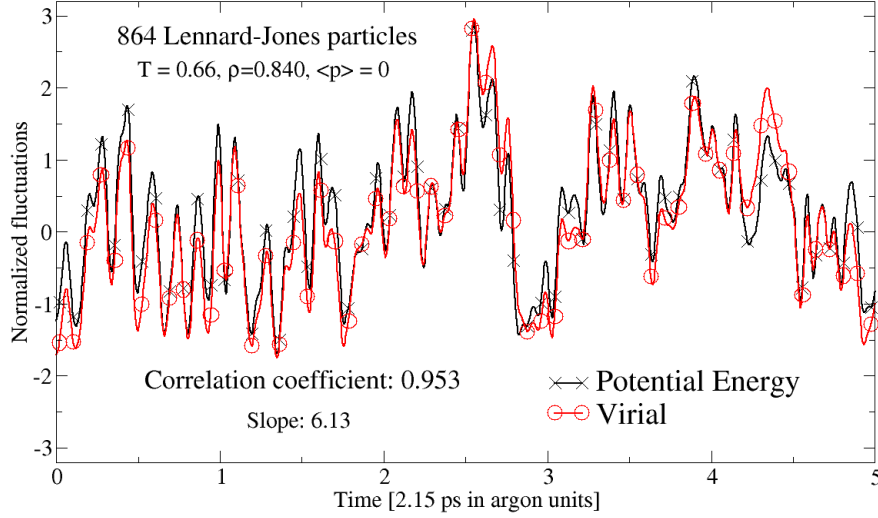
Figure 2.1: Instantaneous normalized fluctuations of virial and potential energy in a single component Lennard-Jones liquid. $W(t)$ and $U(t)$ are strongly correlated. This figure is the same as Figure 1A in Paper III, but for another simulation.

For the Lennard-Jones potential this is

$$W_{ij}^{LJ} = 8\varepsilon \left(2 \left(\frac{\sigma}{r_{ij}} \right)^{12} - \left(\frac{\sigma}{r_{ij}} \right)^{6} \right). \tag{2.6}$$

Figure 2.1 shows a time series of normalized fluctuations (with respect to the standard deviation σ) of virial $W(t)$ and potential energy $U(t)$ in a constant NVT simulation at $T = 0.66$ ($T = 80$ K in Argon units) and $\rho = 0.840$ ($\langle p \rangle = 0$). Virial and potential energy are strongly correlated. This is quantified by the correlation coefficient,

$$R_{WU} \equiv \frac{\langle \Delta W \Delta U \rangle}{\sqrt{\langle (\Delta W)^2 \rangle \langle (\Delta U)^2 \rangle}} = 0.953, \tag{2.7}$$

being close to unity.

Figure 2.2 shows a scatter plot of virial versus potential energy for some more state points. The cigar-form of the scatter-blobs for a given state-point indicates a strong correlation. Note also the constant density path's. The slope of these paths is around 6 ($\pm 10\%$) and the same value as the "slope" of a single state point defined as

$$\gamma_{WU} \equiv \sqrt{\frac{\langle (\Delta W)^2 \rangle}{\langle (\Delta U)^2 \rangle}} \tag{2.8}$$

When pressure is held constant (and not volume), the correlation is weaker.
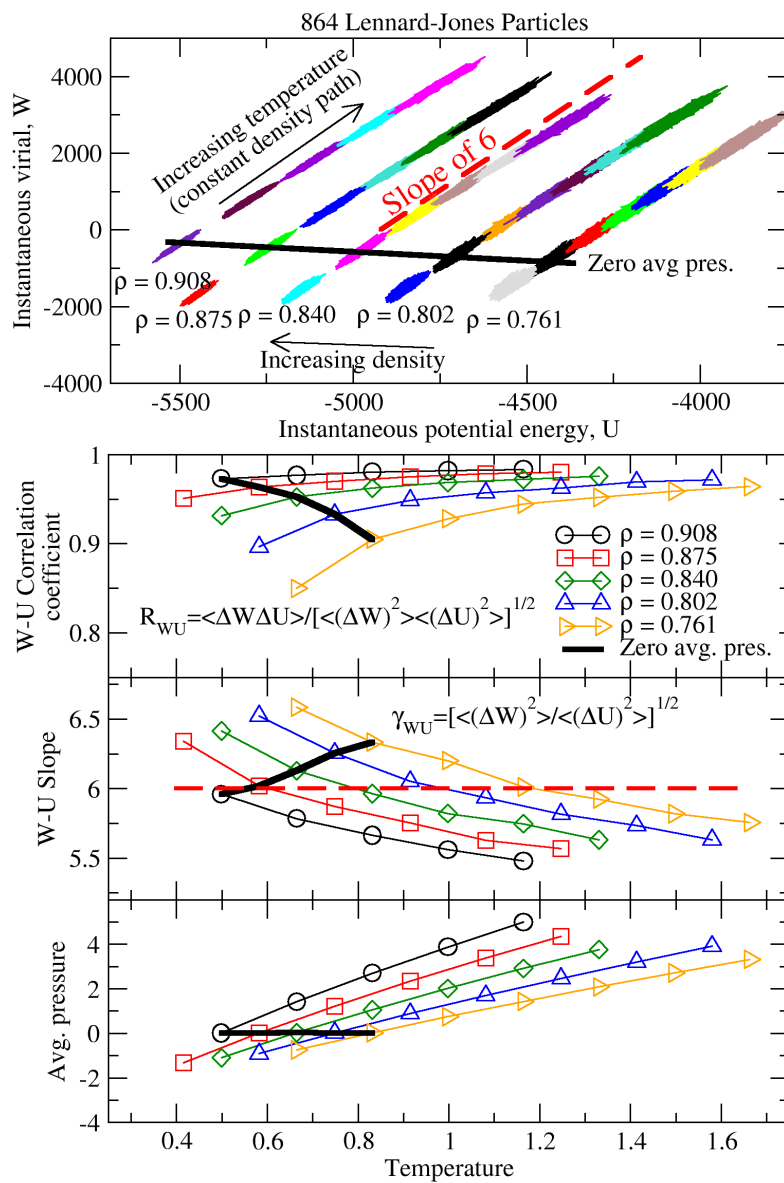
Figure 2.2: Scatter plot of virial and potential energy in a single component Lennard-Jones liquid at different state points. Simulations where done in the NVT ensemble. The lower panels show the W-U correlation coefficient R_{WU} (Equation 2.7), the W-U slope (Equation 2.8) and the average pressure.
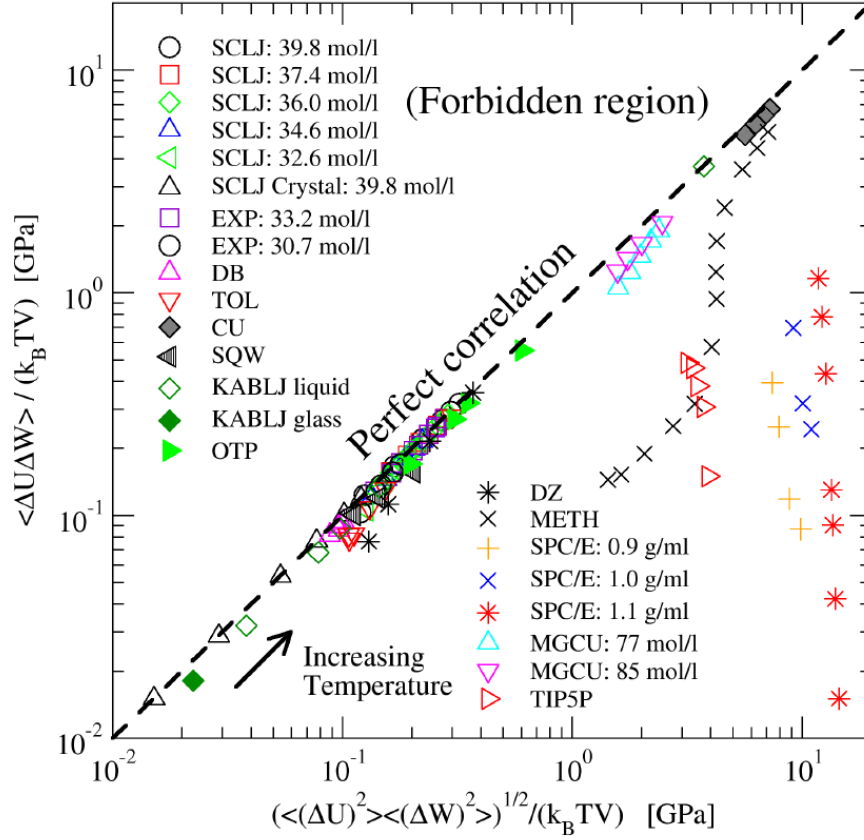
Figure 2.3: *W-U* correlation plot of model liquids. The numerator plotted against the denominator of the correlation coefficient expressed in units of pressure (making them intensive quantities). The diagonal (dashed line) correspond to perfect correlation. Models of van der Waals bonded liquid are close to this line showing strong *W-U* correlations, whereas hydrogen bonded liquids only have weak or no correlation. The simulated systems are the single component Lennard-Jones liquids (SCLJ), a model with exponential repulsion therm (EXP), a asymmetric dumbbell model (DB), model of Toluene using the UA-OPLS parameters (TOL) [Jorgensen et al., 1984], a model of pure Cu with a many body potential (CU) [Jacobsen et al., 1987, 1996], a binary mixture of particles with hard-core repulsion and a square-well attraction (SQW) [Zaccarelli et al., 2002, 2004], a binary Lennard-Jones mixture suggested by Kob and Andersen [1994, 1995a] (KABLJ), a ortho-terphenyl model suggested by Lewis and Wahnström [1994] (OTP), a single component glass former suggested by Dzugutov [1992], a model of methanol using the GROMOS parameters [van Gunsteren et al., 1996], a three-site model of water (SPC/E) [Berendsen et al., 1987], a model of $Mg_{85}Cu_{15}$ [Bailey et al., 2004] and a five-site model of water (TIP5P) [Mahoney and Jorgensen, 2000]. Simulations of SCLJ and EXP where conducted by Thomas B. Schrøder. Simulations of CU, DZ and MGCU where conducted by Nicholas P. Bailey. Simulations of SQW and TIP5P where conducted by Nicolette Gnan. The remaining simulations where conducted by the author, see Section 1.2.1. This figure is the same as Figure 10 in Paper VIII, where simulation details are also given.

2.2   A class of strongly correlating liquids

If strong W-U correlations were only present in the Lennard-Jones liquid, they would not be so interesting. However, other liquids also exhibit strong W-U correlations. Figure 2.3 show the nominator, $\langle \Delta W \Delta U \rangle / (k_B T V)$, versus the denominator, $\sqrt{\langle (\Delta W)^2 \rangle \langle (\Delta U)^2 \rangle} / (k_B T V)$, of the correlation coefficient, in units of pressure to make them intensive quantities, of 13 liquids. In this plot, the diagonal correspond to perfect correlation.

A large group of liquids are strongly correlating. This suggest that there exist a class of strongly correlating liquids (see Sections 3.1, 4.1.3 and 4.2 for more about this conjecture). Note that van der Waals bonded liquids belongs to this class, whereas hydrogen bonded liquids only have weak correlations. The weakening of correlation can be explained by competing interactions. Close to the density maximum of water W and U are uncorrelated, $R_{WU} = 0$. For more about this, see section C in Paper VIII.

2.3   Supercritical Argon

An experimental correlation coefficient of super-critical argon can be calculated[1]: Recall, that for particles with no internal degrees of freedom kinetic parts of pressure and energy is simply that of a mono-atomic ideal gas and that the fluctuation-dissipation theorem relates fluctuations to response functions [Allen and Tildesley, 1987]; For a mono-atomic system we can write

$$\langle (\Delta U)^2 \rangle / k_B T^2 = C_V - \frac{3}{2} N k_B, \tag{2.9}$$

$$\langle (\Delta W)^2 \rangle / k_B T = N k_B T + \langle W \rangle - V K_T + \langle X \rangle \tag{2.10}$$

and

$$\langle \Delta U \Delta W \rangle / k_B T^2 = V \beta_V - N k_B. \tag{2.11}$$

Note, that the so-called "hyper-virial" X [Allen and Tildesley, 1987] goes into the relation between $\langle (\Delta W)^2 \rangle$ and K_T (Eq. 2.10). X is not a thermodynamic quantity and cannot be measured.

Fortunately, it is possible to subtract X out of the equations (with some assumptions), as described in Paper VIII section IIIA. If T_{ref} is the temperature at some reference state-point (along a constant density path) $c_V^{\text{conf}} = c_V - \frac{3}{2} N k_B T$, $\beta_V^{\text{conf}} = \beta_V - N k_B / V$ and $\langle p \rangle^{\text{conf}} = \langle p \rangle - \frac{N k_B T}{V}$ then the correlation coefficient is given by

$$R_{WU} \simeq \sqrt{\frac{B(T) - B(T_{ref})}{A(T) - A(T_{ref})}} \tag{2.12}$$

where

$$A(T) = \langle p \rangle - K_T + \frac{\langle p \rangle^{\text{conf}} \beta_V^{\text{conf}}}{c_V^{\text{conf}}}, \tag{2.13}$$

---

[1]There are two reasons for choosing Argon. 1st: A calculations on lighter noble gasses like Helium should include quantum effects. Here we ignore such quantum effects. 2nd: Heavier noble gasses is known to form compounds indicating that the Lennard-Jones potential is to simple (loosely speaking: the large electron cloud of the heavy noble gasses can make covalent bonds).

and

$$B(T) = T(\beta_V^{\mathrm{conf}})^2/c_V^{\mathrm{conf}}. \tag{2.14}$$

Figure 9 in Paper VIII shows experimental data from the NIST database [Lemmon et al., 2005] of super critical Argon where the diagonal corresponds to perfect correlation. The correlation is strong with a W-U correlation coefficient of 0.96. This show that strongly correlating liquids exist in nature and not just the computer. Equation 2.12 also demonstrate that strongly correlating liquids are more simple than the general case. If we assume $R = 1$, a good approximation for strongly correlating liquids, we can predict a third response function from two others. This is not the general case.

Chapter 3

Origin of strong correlations

In this chapter it is shown that the origin of the strong correlation between virial and energy (in the constant volume ensamble) is a consequence of an effective inverse power-law of the pair-potential. This power-law describes the thermodynamical fluctuations of the NVT ensemble. See also Paper III, Paper VIII and Paper IX. The real pair potential cannot simply be approximated by an inverse power. This would give a wrong equation of state. However, a good approximation is an inverse power-law plus a linear term. The linear term does not contribute (significantly) to fluctuations at fixed volume.

3.1 Effective inverse power-law pair potential

First, consider a soft-sphere liquid [Hoover et al., 1970], where particles interact via an inverse power-law potential:

$$U_{ij}^{\mathrm{pow}} = a r_{ij}^{-n}, \tag{3.1}$$

where n is some exponent and a is a prefactor. As shown in Appendix A.1, potential energy and virial are proportional

$$W^{\mathrm{pow}}(t) = \gamma_{WU}^{\mathrm{pow}} U^{\mathrm{pow}}(t), \tag{3.2}$$

with a proportional constant (or slope) of

$$\gamma_{WU}^{\mathrm{pow}} = n/3. \tag{3.3}$$

Then, recall that the Lennard-Jones potential is a sum of two inverse power-laws, where r^{-12} dominate as short distances. A possible explanation for the correlations could be that the r^{-12} term dominate fluctuations. However, this would give a slope of four, whereas the observed slope is around six. The reason for this is that particles are located close to the minimum, where both r^{-12} and r^{-6} terms play a role (Paper III, [Ben-Amotz and Stell, 2003]). Note, however, that the slope in Figure 2.2 does approach four with increasing pressure (where r^{-12} dominates).

Fluctuations of virial and potential energy (at constant volume) can be described by an effective inverse power-law with an exponent larger than 12. To show this, split the pair energy in an inverse power-law term plus a difference term,

$$U^{\mathrm{LJ}} = U^{\mathrm{pow}} + U^{\mathrm{diff}}. \tag{3.4}$$

19
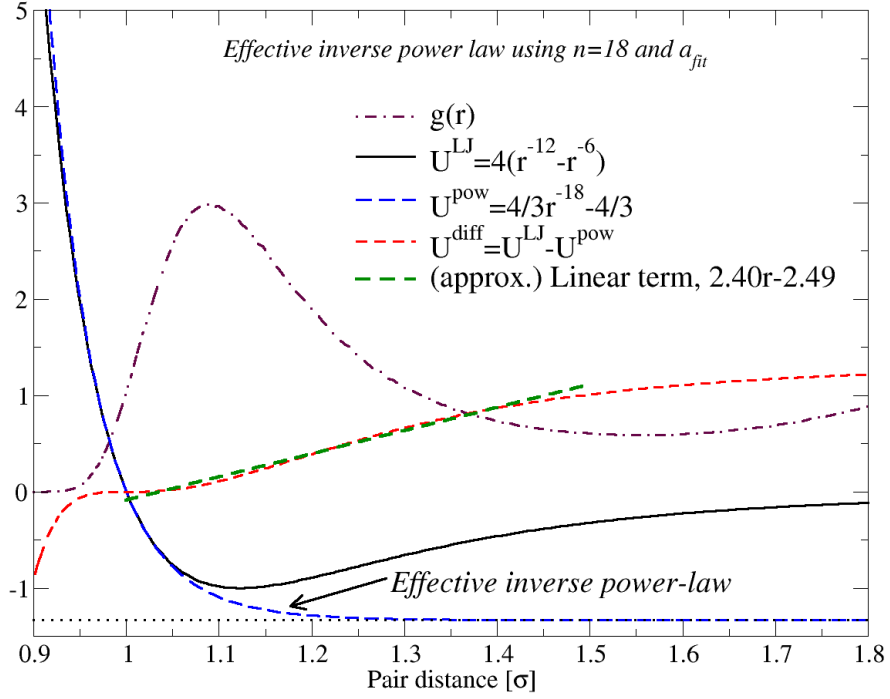
Figure 3.1: Effective inverse power-law $U_{ij}^{\mathrm{pow}} = \frac{4}{3}r^{-18} - \frac{4}{3}$ derived in Appendix A.2. See also Figure 3.5. The definition of the radial distribution function $g(r)$ is given in Section 3.2.

and

$$W^{\mathrm{LJ}} = W^{\mathrm{pow}} + W^{\mathrm{diff}}. \tag{3.5}$$

Then the variance of energy and virial can be written as

$$\langle(\Delta U^{\mathrm{LJ}})^2\rangle = \langle(\Delta U^{\mathrm{pow}})^2\rangle + \langle(\Delta U^{\mathrm{diff}})^2\rangle + 2\langle\Delta U^{\mathrm{pow}}\Delta U^{\mathrm{diff}}\rangle, \tag{3.6}$$

and

$$\langle(\Delta W^{\mathrm{LJ}})^2\rangle = \langle(\Delta W^{\mathrm{pow}})^2\rangle + \langle(\Delta W^{\mathrm{diff}})^2\rangle + 2\langle\Delta W^{\mathrm{pow}}\Delta W^{\mathrm{diff}}\rangle. \tag{3.7}$$

If an effective inverse power-law gives a good description of the fluctuations then

$$\Delta U^{\mathrm{LJ}}(t) \simeq \Delta U^{\mathrm{pow}}(t) \tag{3.8}$$

and

$$\Delta W^{\mathrm{LJ}}(t) \simeq \Delta W^{\mathrm{pow}}(t). \tag{3.9}$$

To quantify "$\simeq$" in the above equations, we can investigate the pow-LJ correlation coefficients

$$R_{U^{\mathrm{pow}},U^{\mathrm{LJ}}} \equiv \frac{\langle\Delta U^{\mathrm{LJ}}\Delta U^{\mathrm{pow}}\rangle}{\sqrt{\langle(\Delta U^{\mathrm{LJ}})^2\rangle\langle(\Delta U^{\mathrm{pow}})^2\rangle}}, \tag{3.10}$$
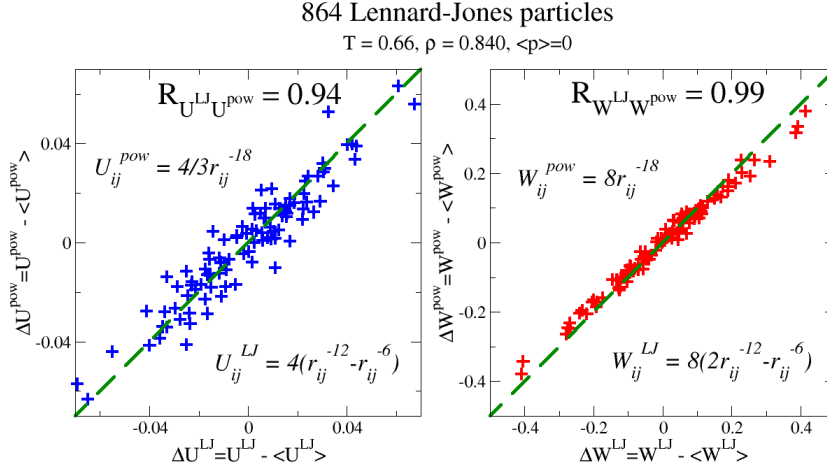
Figure 3.2: The panel on the left shows a scatter plot of ΔU^{pow} versus ΔU^{LJ} (Equation 3.4) and the panel on the right shows ΔW^{pow} versus ΔW^{LJ} (Equation 3.5) of configurations of the Lennard-Jones liquid at $T = 0.66$ and $\rho = 0.840$ ($\langle p \rangle = 0$). The effective inverse power-law describes fluctuations of virial and energy to a good approximation (Equations 3.8 and 3.9).

and

$$R_{W^{\text{pow}}, W^{\text{LJ}}} \equiv \frac{\langle \Delta W^{\text{LJ}} \Delta W^{\text{pow}} \rangle}{\sqrt{\langle (\Delta W^{\text{LJ}})^2 \rangle \langle (\Delta W^{\text{pow}})^2 \rangle}} \tag{3.11}$$

and the amount of variance described by the effective power-law,

$$\gamma^2_{U^{\text{pow}}, U^{\text{LJ}}} \equiv \frac{\langle (\Delta U^{\text{pow}})^2 \rangle}{\langle (\Delta U^{\text{LJ}})^2 \rangle}, \tag{3.12}$$

and

$$\gamma^2_{W^{\text{pow}}, W^{\text{LJ}}} \equiv \frac{\langle (\Delta W^{\text{pow}})^2 \rangle}{\langle (\Delta W^{\text{LJ}})^2 \rangle}. \tag{3.13}$$

If the description is good, all of these should be close to unity.

As a first guess, we will assume that $n = 18$ ($\gamma = 6$) (as the W-U slope on Figure 2.1 suggest), and get a pre-factor a by fitting the inverse-power law to the Lennard-Jones potential by matching 0th, 1st and 2nd derivative as described in Appendix A.2. This give the inverse power-law $U^{\text{pow}}_{ij} = \frac{4}{3}(r_{ij}/\sigma)^{-18}$ shown on Figure 3.1. Figure 3.2 shows that this effective inverse power-law gives a pretty good description of the fluctuations.

In the following, a way to determine the best[1] n and a from fluctuations at one state-point will be given. Figure 3.3 shows Eqs. 3.10–3.13 as a function of n. In some range ($\pm 10\%$) the power-law energy and virial are strongly correlated with the Lennard-Jones ($R_{U^{\text{pow}}, U^{\text{LJ}}} > 0.93$ and $R_{W^{\text{pow}}, W^{\text{LJ}}} > 0.96$) and dominates the fluctuations ($\langle (\Delta U^{\text{LJ}})^2 \rangle \simeq \langle (\Delta U^{\text{pow}})^2 \rangle > \langle (\Delta U^{\text{diff}})^2 \rangle \simeq |\langle \Delta U^{\text{pow}} \Delta U^{\text{diff}} \rangle|$). Both virial and energy fluctuations should be described

---

[1]best: Effective inverse power-law that gives the best description of the fluctuating parts of energy and virial.
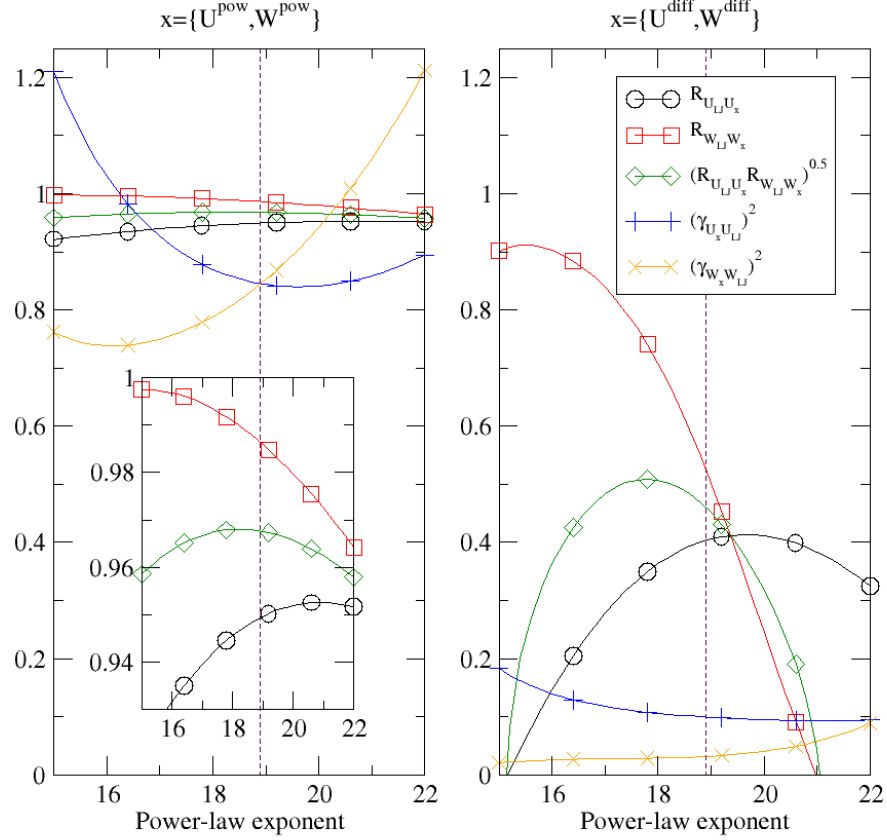
Figure 3.3: Eqs. 3.10 to 3.13 as a function of n (using a_{fit}) of the Lennard-Jones liquids at $T = 0.66$ and $\rho = 0.840$. The *optimization parameter* $\sqrt{R_{U^{\text{pow}},U^{\text{LJ}}}R_{W^{\text{pow}},W^{\text{LJ}}}}$ have maximum, close to $n = 18.9 = 3\sqrt{\frac{\langle(\Delta W)^2\rangle}{\langle(\Delta U)^2\rangle}}$. However, note that $\sqrt{R_{U^{\text{pow}},U^{\text{LJ}}}R_{W^{\text{pow}},W^{\text{LJ}}}}$ is close to unity in the entire investigated region. This suggest that a n not exactly 19.8 works pretty well. Also, note that covariances $\langle\Delta U^{\text{pow}}\Delta U^{\text{diff}}\rangle/\langle(\Delta U^{\text{diff}})^2\rangle = 0.02$ and $\langle\Delta W^{\text{pow}}\Delta W^{\text{diff}}\rangle/\langle(\Delta W^{\text{diff}})^2\rangle = 0.06$ are small at exponent $n = 18.9$.

by the effective inverse power-law (both $R_{U^{\text{pow}},U^{\text{LJ}}}$ and $R_{W^{\text{pow}},W^{\text{LJ}}}$ close to unity). Thus, $\sqrt{R_{U^{\text{pow}},U^{\text{LJ}}}R_{W^{\text{pow}},W^{\text{LJ}}}}$ should be close to unity. Note that this optimization parameter have a maximum close to the exponent calculated from the W-U slope ($n = 3\gamma_{WU} = 18.9$). Thus, the apparent exponent can simply be calculated as

$$n = 3\sqrt{\frac{\langle(\Delta W)^2\rangle}{\langle(\Delta U)^2\rangle}} = 3\gamma_{WU} \tag{3.14}$$

The prefactor a can also be determined from the W and U fluctuations. The a_{fit} calculated in Appendix A.2 worked pretty well, however, a slight increase give a better fit. Figure 3.4 shows that an 8.8% increase gives the best
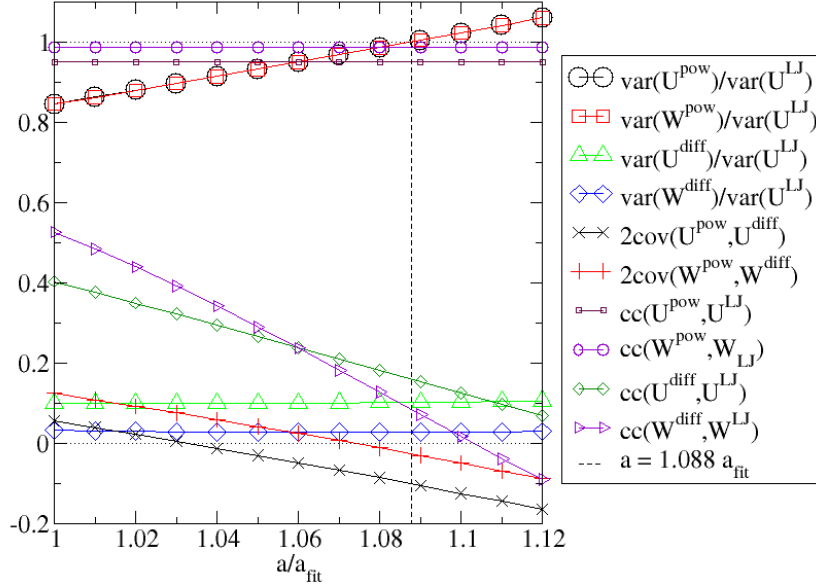
Figure 3.4: Eqs. 3.10 to 3.13 as a function of a/a_{fit} ($n = 18.9$) of the Lennard-Jones liquids at $T = 0.66$ and $\rho = 0.840$. $T = 80$ K and $\langle p \rangle = 0$. At $a_{\mathrm{opt}} = 1.088 a_{\mathrm{fit}} = 1.389$ (dashed line) the variance of $\Delta U^{\mathrm{LJ}}(t)$ equals that of $\Delta U^{\mathrm{LJ}}(t)$ and the variance of $\Delta W^{\mathrm{LJ}}(t)$ equals that of $\Delta W^{\mathrm{LJ}}(t)$. Also, at a_{opt} the variance of $\Delta U^{\mathrm{diff}}(t)$ and $\Delta W^{\mathrm{diff}}(t)$ and the correlation coefficient $R_{U^{\mathrm{LJ}}, U^{\mathrm{diff}}}$ and $R_{W^{\mathrm{LJ}}, W^{\mathrm{diff}}}$ are small.

description. It is possible to match (the magnitude of) both the potential energy and the virial, $\langle (\Delta U^{\mathrm{pow}})^2 \rangle / \langle (\Delta U^{\mathrm{LJ}})^2 \rangle \simeq \langle (\Delta W^{\mathrm{pow}})^2 \rangle / \langle (\Delta W^{\mathrm{LJ}})^2 \rangle \simeq 1$. Note that changing a do not effect the correlation coefficients $R_{U^{\mathrm{pow}}, U^{\mathrm{LJ}}}$ and $R_{W^{\mathrm{pow}}, W^{\mathrm{LJ}}}$.

Figure 3.5 show U_{ij}^{pow} with exponent $n = 18.9$ and $a_{\mathrm{opt}} = 1.088 a_{\mathrm{fit}} = 1.389$. Note that U_{ij}^{diff} of this effective inverse power-law is well approximated by a straight line in the range of the first peak of the radial distribution function, $g(r)$. This will be discussed further in the next section.

So far it is only demonstrated that the effective power-law works for the 6-12 Lennard-Jones liquid. However, in Paper XIII it is argued that a similar fitting can be done for the assymetric dumbell model. Coslovich and Roland [2009] have recently shown that the description also works for the generalized Lennard-Jones potential, $U_{ij}^{\mathrm{gen.LJ}} = (nr^{-m} - mr^{-n})/(m - n)$. It is reasonable that a similar inverse power-law matching can be done in similar systems. Therefore, a good conjecture is that the effective power-law explanation works for van der Waals bonded systems in general. More work is needed to clarify this.

Note that the Lennard-Jones potential cannot simply be replaced by an inverse power-law – only fluctuations (at fixed volume) can be described by a inverse power-law. The Lennard-Jones liquid does not have the same equation of states as the soft-sphere liquid. In the next section will discuss the role of
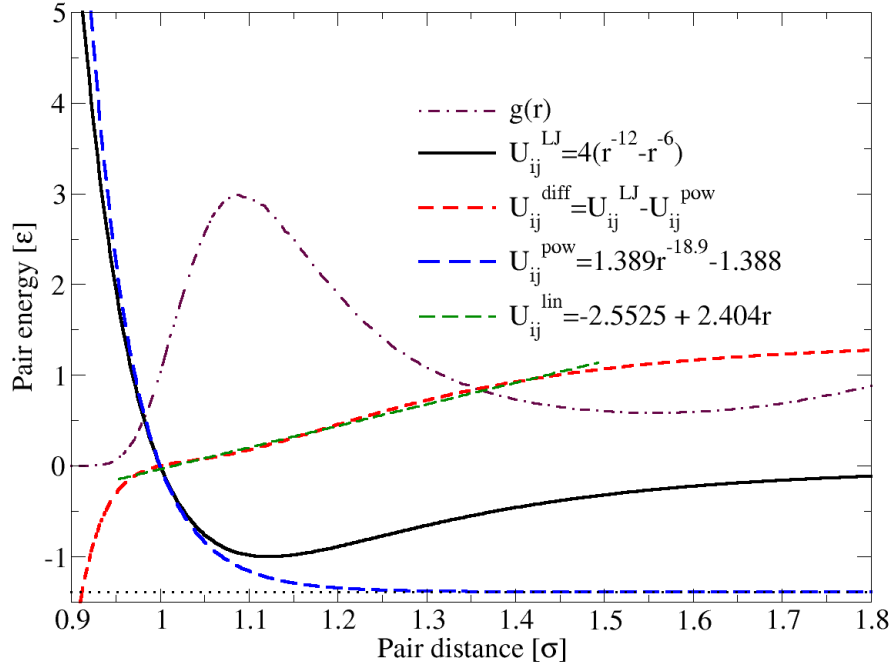
Figure 3.5: The optimal effective inverse power-law of $U_{ij}^{\mathrm{pow}} = 1.389r^{-18.9} - 1.388$ of the Lennard-Jones liquid at the state-point $T = 0.66$ and $\rho = 0.840$. $n = 18.9$ and $a = 1.389$ are calculated from fluctuations as outline in Figure 3.3 and Figure 3.4. The definition of the radial distribution function $g(r)$ is given in Section 3.2.

U^{diff}.

3.2 Approximate inverse power-law plus linear term pair potential

The effective inverse power-law gives a good description of the pair potential at short distances, $r < r_{min}(= 1.12\sigma)$, but not at longer distances, as shown on Figure 3.1. At first glance, it is surprising that the effective power-law does so well after all. Even at zero pressure where particles are located close to the minimum of the Lennard-Jones potential. In the following, it will be discussed why U^{diff} does not contribute to the fluctuations at fixed volume. The whole system, and not just a single pair, has to be taken into account. See also Paper IX section II-D.

Define the instantaneous pair distribution function (or radial distribution function) as[2]

$$g(r,t) = \frac{1}{2N\rho} \sum_{i \neq j} \delta(r - r_{ij}(t)) \tag{3.15}$$

---

[2]$\delta(x)$ is Dirac delta function.

where

$$g(r) = \langle g(r,t) \rangle \tag{3.16}$$

is the traditional pair distribution function [Allen and Tildesley, 1987]. From $g(r,t)$ we can calculate the potential energy at time t as

$$U(t) = (4\pi\rho N/2) \int_0^\infty U_{ij}(r)g(r,t)r^2 dr, \tag{3.17}$$

and

$$\Delta U(t) = (4\pi\rho N/2) \int_0^\infty U_{ij}(r)\Delta g(r,t)r^2 dr, \tag{3.18}$$

where

$$\Delta g(r,t) = g(r,t) - g(r). \tag{3.19}$$

U^{diff}, shown on Figure 3.1, can be approximated with a linear function in the first shell regime (first peak of $g(r)$). The same goes for W^{diff}. The fact that U^{diff} is nearly constant, $\Delta U^{\mathrm{diff}}(t) \simeq 0$, suggests that

$$4\pi\rho N/2 \int_{\mathrm{first\ shell}} r_{ij}\Delta g(r,t)r^2 dr \simeq 0 \tag{3.20}$$

or

$$\int_{\mathrm{first\ shell}} r_{ij}\Delta\rho_b(r,t)r^2 dr \simeq 0 \tag{3.21}$$

where $\rho_b(r,t) = (4\pi\rho N/2)\Delta g(r,t)$ is the bond density. In other words the number of bonds in first shell is constant, and the average first shell bond distance $r_m(t) = \int_{\mathrm{first\ shell}} r\rho_b(r,t)dr$ is constant. This is reasonable for a dense liquid in a fixed volume. Whenever a particle moves it will come closer to some particles and move further away from others – approximately without affecting $r_m(t)$.

If volume is changed we expect an overall change of the bond density, and U^{diff} will change. This is why the $W-U$ scatter plot on Figure 2.2 has constant density paths,

$$W = \gamma_{WU}(U + U_0(\rho)) \tag{3.22}$$

Here, the argumentation of r_m being constant is somewhat imprecise. It is intuitively reasonable, but the "first shell" integral, $\int_{\mathrm{first\ shell}} \ldots dr$, is not well-defined. The following section discuss a one dimensional crystal where a clear argumentat can be made. Note, however, that the reasoning is of the same nature.

3.3   Low temperature limit of crystal

The correlation survives all the way down to the zero temperature limit of the crystal – even at negative pressure (Figure 4 in Paper IX). This low-temperature limit can be explained by approximating the pair potential by a Taylor expansion. In the following we will investigate W-U correlations of a one-dimensional crystal.

Think of a one-dimensional crystal with only nearest neighbor interactions (see also Paper IX section II-B-1). Let N be the number of particles in box of length (or "volume") L. Make the box periodic so particle $N + k$ is a mirror

of particle k. The average pair distance will then be $a = L/N$. For simplicity put a at the minimum of the potential, $U'_{ij}(a = r_m) = 0$, and shift the minimum to zero, $U_{ij}(r_m) = 0$. In the low temperature limit we can make a Taylor expansion of the pair potential, keeping up to the third order in relative displacement. Define

$$S_p \equiv \sum_i^N (r_{i,i+1} - r_m)^p, \tag{3.23}$$

and write energy as (the third order term of energy is explicitly written here, since it goes into the second order term of virial)

$$U = \frac{1}{2}k_2 S_2 + \frac{1}{6}k_3 S_3 + O(S_4), \tag{3.24}$$

and virial as (see Paper IX for details)

$$W = -\frac{1}{3}(k_2 r_m S_1 + (k_2 + \frac{1}{2}k_3 r_m)S_2) + O(S_3), \tag{3.25}$$

where k_p is the p'th derivative of the pair potential at r_m.

The lowest order term of the energy is second order S_2. To second order, W involves both S_1 and S_2, so apparently there is no W–U correlation. However, S_1 vanishes when volume is fixed: Fixed volume implies that $\sum_i^N r_{i,i+1} = Nr_m = L$, and $S_1 = \sum_i^N (r_{i,i+1} - r_m) = \sum_i^N r_{i,i+1} - Nr_m = 0$.

Combining Equations 3.24 and 3.25 (with $S_1 = 0$ and throwing away $O(S_3)$) we recover a W–U correlation,

$$W = -\frac{1}{3}\frac{k_2 + \frac{1}{2}k_3 r_m}{\frac{1}{2}k_2}U. \tag{3.26}$$

For the Lennard-Jones potential (with $r_m = 2^{1/6}\sigma$) the slope is $-\frac{1}{3}\frac{k_2 + \frac{1}{2}k_3 r_m}{\frac{1}{2}k_2} = 6.33$. This is in good agreement with slope found in simulations (see Figure 2.2)[3].

The three dimensional crystal is more complicated (see Paper IX section II-B-2 and II-B-3). Here, the correlation is not exact but the energy-virial correlation is close to unity (Figure in Paper IX) and slope is close to observed six.

Again, note the importance of fixed volume. In the one dimensional crystal the situation is more clear than the effective inverse power-law explanation (and the three dimensional crystal), but are of the same nature. When one bond gets shorter an other must get longer. The volume constrain makes linear terms vanish. That is $S_1 = 0$ or $\int_{\text{first peak}} r\Delta\rho_b(r,t)dr \simeq 0$.

3.4 Weeks-Chandler-Andersen

The reader has perhaps noticed the similarities between the apparent inverse power-law and the celebrated 1971 paper by Andersen, Weeks, and Chandler [1971] (WCA). These authors argue that molecules of a liquid can be thought

---

[3]Traditionally, we think of the low-temperature limit of the crystal as harmonic. However, for the harmonic crystal ($k_3 = 0$) the slope is $-2/3$ and not close to six.

of as hard-core particles ($U_{ij}^{\text{hs}}(r) = \infty$ for $r < r_d$ and $U_{ij}^{\text{hs}}(r) = 0$ elsewhere) with attraction that can be viewed as a perturbation.

The effective inverse power-law plus a linear term agrees with the WCA interpretation, that the repulsive region of the pair potential dominates liquid structure – an important result of WCA-paper. However, in the following chapter it will be demonstrated that an inverse power-law is more useful than a hard-core description. (One can think of a hard-core interactions as a approximation to the effective inverse power-law.)

Chapter 4

Strongly correlating viscous liquids

In this chapter it is demonstrated that strongly correlating *viscous* liquids are more simple than viscous liquids in general.

In the first section, it is argued that the glass-transition of strongly correlating *viscous* liquids is single-parameter in the Prigogine-Defay sense. The references for this section are Paper I, Paper IV, Paper VI and Paper IX. In addition, the section give some simple equations to illustrate possible scenarios of thermodynamic fluctuations and a rethinking of the (classical) Prigogine-Defay ratio Π^{classic}.

In the second section it is shown that strongly correlating viscous liquids have a scale invariant energy landscape. This provides a scaling-law of dynamics (exemplified by the diffusion constant D) and structure (exemplified by the radial distribution function $g(r)$). The references for this section are Paper VII and Paper XIII.

4.1 A single order-parameter of viscous liquids

The classical picture of a single order-parameter description of the glass transition was developed by Davies and Jones [1953a,b]. In these authors' picture, an important number is the so-called Prigogine-Defay ratio [Prigogine and Defay, 1954]. This ratio is calculated from the change of the (static) response function at the glass-transition. If $\Delta c_p = c_p^{\text{liquid}} - c_p^{\text{glass}}$ is the change of the isobaric heat capacity per unit volume, $\Delta \kappa_T = \kappa_T^{\text{liquid}} - \kappa_T^{\text{glass}}$ is the change of isothermal compressibility and $\Delta \alpha_p = \alpha_p^{\text{liquid}} - \alpha_p^{\text{glass}}$ is the change of isobaric expansion coefficient, then the classical Prigogine-Defay ration is defined as[1]

$$\Pi_{pT}^{\text{classic}} = \frac{\Delta c_p \Delta \kappa_T}{T_g (\Delta \alpha_p)^2}. \tag{4.1}$$

In general $\Pi_{pT}^{\text{classic}} \geq 1$ and $\Pi_{pT}^{\text{classic}} = 1$ in the single parameter case. Since then, the topic has been debated in the glass community[2]. Moynihan et al.

---

[1] The superscript "classic" in equation 4.1 is normally not used, but is used here distinguish it from the later defined Progogine-Defay ratios. The subscript pT is to emphasize that this ratio relates the natural response functions of the NpT ensemble - the ensemble preferred in an experimental situation. That is c_p, κ_T and α_p.

[2] See References [Davies and Jones, 1953a,b, DiMarzio, 1974, Goldstein, 1975, Gupta and Moynihan, 1976, Moynihan et al., 1976, Roe, 1977, Moynihan and Gupta, 1978, Lesikar and

[1976] concluded, on the basis of available experimental data, that the ratio typically takes values of $2 < \Pi_{pT}^{\mathrm{classic}} < 4$. The conclusion from this is therefore that in general more than one order-parameter is needed. A collection of ratios available today are compiled in Table 4.1. Note that some Prigogine-Defay ratios are infact close to unity. Table 4.1 is discussed in details in Section 4.1.3.

At this point, I have not explained to the reader what exactly is meant by "a single-order parameter". The reason for this is that Roe [1977], Moynihan and Gupta [1978], Moynihan and Lesikar [1981] realized that the classical Prigogine-Defay ratio is not well-defined. Theoretical predictions solely based on $\Pi_{pT}^{\mathrm{classic}}$ are therefore problematic. The solution to this was a (well-defined) revised Prigogine-Defay ratio. This ratio relates to the frequency dependent response functions of the equilibrium liquid (disregarding the crystal) and is defined as

$$\Pi_{pT}^{\mathrm{linear}} = \frac{[c_p(\omega \to 0) - c_p(\omega \to \infty)][\kappa_T(\omega \to 0) - \kappa_T(\omega \to \infty)]}{T[\alpha_p(\omega \to 0) - \alpha_p(\omega \to \infty)]^2} \qquad (4.2)$$

where $\omega \to \infty$ refers to high-, and $\omega \to 0$ to the low frequency limit. Unfortunately, it is difficult to get good measurements of wide frequency spectra, as needed to get these limits. For this reason no-one has attempted to calculate $\Pi_{pT}^{\mathrm{linear}}$ from experimental data (to the author's knowledge). However, in simulation this can be done as demonstrated by Nielsen [1999] and in Figure 4.3. Ellegaard [2005] showed that $\Pi_{pT}^{\mathrm{linear}}$ can be re-expressed as a single-frequency quantity $\Lambda_{pT}(\omega)$ (see following section), more suited for experiments. This is published in Paper I.

The remainder of this chapter is a newly developed interpretation of "single parameter"-ness, based on $\Lambda_{pT}(\omega)$. In this interpretation, it is clear what is meant by "a single parameter". In the classical understanding it is somewhat unclear what can be learned from a ratio close to unity but not exactly unity. In other words: What should a measured value of $\Pi_{pT}^{\mathrm{clasic}}$ be compared to? Is $\Pi = 1.2$ "significantly larger than unity" as concluded by Takahara et al. [1999]? It will become clear how we should interpret $\Pi_{pT}^{\mathrm{clasic}} > 1$ (Subsection 4.1.3).

4.1.1 Dynamic Prigogine-Defay ratio, $\Lambda(\omega)$

The dynamic Prigogine-Defay ratio $\Lambda_{pT}(\omega)$ is an one-frequency test quantity for single parameter-ness. This was published in Paper I, based on the Ph.D. thesis of Ellegaard [2005]. It is defined from the frequency-dependent response functions. If $c_p(\omega)''$, $\kappa_T''(\omega)$ and $\alpha_p''(\omega)$ are the imaginary parts (at a single frequency) of isobaric heat capacity per unit volume, isothermal compressibility and isobaric expansion coefficient respectively, then

$$\Lambda_{pT}(\omega) \equiv \frac{c_p''(\omega)\kappa_T''(\omega)}{T[\alpha_p''(\omega)]^2}. \qquad (4.3)$$

It is in principle accessible though experiments, although it has not been measured yet. It is not at all trivial to measure frequency dependent response functions. As an example, a resent paper by Christensen et al. [2007] shows that conventional methods to measure frequency-dependent isobaric heat capacity $c_p(\omega)$ fail.

Moynihan, 1980, Moynihan and Lesikar, 1981, Nieuwenhuizen, 1997, 2000, Ellegaard, 2005, Schmelzer and Gutzow, 2006, Pick, 2008] and Paper VI.

Table 4.1: Litterateur values of classical Prigogine-Defay ratios.

Material	Π_{pT}	$\Pi_{pT}^{-1/2}$	Ref.
Pure SiO$_2$ glass	10^3-$2\cdot10^5$	0.03-0.002	a
Glycerol, C$_3$H$_5$(OH)$_3$	9.4	0.33	b
Rubber	8.3	0.33	a
GeO$_2$	6.9±1.3	0.38±0.04	h
16Na$_2$O–10B$_2$O$_3$–74SiO$_2$	4.9	0.45	f
B$_2$O$_3$	4.7	0.46	c/b
0.4Ca·NO$_3$·0.6KNO$_3$	4.5	0.47	c/b
Glucose, OC$_6$H$_7$(OH)$_6$	3.7	0.52	a
16Na$_2$O–10CaO–74SiO$_2$	3.6	0.53	f
Se	2.4	0.65	a/b
Se	2.0	0.71	j
ZrTiCuNiBe	2.4	0.65	e
26Na$_2$O–74SiO$_2$	2.3	0.66	f
Technical glasses	2.0-2.7	0.71-0.61	a
Polyvinylacetate	2.2(1.7)	0.67(0.77)	c/b
n-Propanol, C$_3$H$_7$OH	1.9	0.73	b
Polyvinylchlorid, PVC	1.7	0.77	b
Polystyrene, PS	1.3±0.1 (16)	0.88±0.03 (0.25)	d
OTP(75%)-TPCM(25%)	1.28	0.88	k
OTP(67%)-OPP(33%)	1.20±0.05	0.92±0.02	d
Polystyrene, PS	1.085	0.96	l
Phenoxy	1.03	0.99	g
Polycarbonate	1.02	0.99	g
Polysulfone	0.96	1.02	g
Polyarylate	0.90	1.05	g
Polyisobutene	0.9	1.05	b

Liquids are listed with decreasing classical Prigogine-Defay ratio. As discussed in details in Section 4.1.3 this separates van der Waals bonded liquids, with ratios close to unity, from the rest. References. a: [Nemilov, 1994]; b: [Donth, 1981]; c: [Gupta and Moynihan, 1976]; d: [Takahara et al., 1999]; e: [Samwer et al., 1999]; f: [Wondraczek and Behrens, 2007]; g: [Zoller, 1982]; h: [Dingwell et al., 1993]; i: [Hadac et al., 2007]; j: [Berg and Cooper, 1978]; k: Calculated by Ellegaard [2005] using data from Naoki et al. [1986]; l: [Oels and Rehage, 1977]. Abbreviations: OTP, o-terphenyl: C$_6$H$_4$(C$_6$H$_5$)$_2$; TPCM, triphenylchloromethane: C(C$_6$H$_5$)$_3$Cl; OPP, o-phenylphenol: C$_6$H$_4$(C$_6$H$_5$)OH; Polyvinylacetate: [-CH$_2$(COOCH$_3$)CH-]$_n$; Polyvinylchlorid: [-C(ClH)CH$_2$-]$_n$; Polystyrene: [-CH(C$_6$H$_5$)CH$_2$-]$_n$; Phenoxy: [-CH$_2$CH(OH)CH$_2$O(C$_6$H$_4$)-]$_n$; Polycarbonate: [-C$_2$O(C$_6$H$_4$)C(CH$_3$)$_2$(C$_6$H$_4$)O-]$_n$; Polysulfone: [-(C$_6$H$_4$)SO$_2$(C$_6$H$_4$)O(C$_6$H$_4$)C(CH$_3$)$_2$(C$_6$H$_4$)O-]$_n$; Polyarylate: [-CO(C$_6$H$_4$)COO(C$_6$H$_4$)C(CH$_3$)$_2$(C$_6$H$_4$)O-]$_n$.

In Paper I it is shown that if $\Pi_{pT}^{\text{linear}} = 1$ then $\Lambda_{pT}(\omega) = 1$ at any ω. Such liquids are referred to as "Single parameter liquids". Moreover, if $\Lambda(\omega)$ is unity in one ensemble, then it is unity in all ensembles:

$$1 = \Lambda_{pT}(\omega) = \Lambda_{VT}(\omega) = \Lambda_{pS}(\omega) = \Lambda_{VS}(\omega). \tag{4.4}$$

This is reasonable since is would be peculiar if "single parameter"-ness was ensemble dependent. However, if $\Lambda_{pT}(\omega) > 1$ we cannot say that they are equal. Nevertheless, if one of the ratios is close to unity, the others are likely also to be close to unity, as demonstrated in simulations later.

An equivalent way of expressing "single parameter"-ness is[3]

$$\Delta \bar{p}(t) = \gamma_{pS} \Delta \bar{s}(t) \text{ when controlling } V \text{ and } T \tag{4.5}$$

where the bar indicates fluctuations on some relaxing time-scale. If the relation is exact, the bar is in principle not needed. Later, however, we will discuss a situation where these equations are approximate (replacing "=" with "≃"). Then the bar makes a difference. Again, since "single parameter"-ness must be ensemble independent, it follows that

$$\Delta \bar{V}(t) = \gamma_{VS} \Delta \bar{s}(t) \text{ when controlling } p \text{ and } T, \tag{4.6}$$

$$\Delta \bar{p}(t) = \gamma_{VT} \Delta \bar{T}(t) \text{ when controlling } V \text{ and } S, \tag{4.7}$$

and

$$\Delta \bar{V}(t) = \gamma_{VT} \Delta \bar{T}(t) \text{ when controlling } p \text{ and } S. \tag{4.8}$$

The equations apply when the controlling parameters are held constant. Then the free parameters will fluctuate in a correlated manner (on the relaxing time-scale indicated by the bar). Also, the equations apply to perturbations (in the linear regime). Then relaxation of the free parameters follows the same (scaled) function.

Equations 4.5 to 4.8 answer the question: What is the single parameter? There is only one internal relaxing parameter in the system. Mechanical and thermal relaxation are slaves of this parameter. It is reasonable to speculate that other quantities, like dipole-moment, are also slaves of the single parameter. If dipole-moment is a slave, then dielectric measurements would reflect the "single parameter"-ness. This would make single parameter liquids even more interesting due to the simplicity.

All of the equations in this subsection (Equations 4.3 to 4.8) are equivalent, and any of them can be regarded as the definition of a single parameter liquid. It is easy to show from one of Equations 4.5 to 4.8 that a corresponding $\Lambda_{XY}(\omega)$ is equal to unity. An example is given in next subsection. Showing it the other way, that one of Equations 4.5 to 4.8 can be derived from a cooresponding $\Lambda_{XY}(\omega)$ being unity can also be shown. This is done in Paper I. In the following we will consider Equations 4.3 to 4.8 as the definition of a single parameter liquid. $\Lambda_{XY}(\omega) = 1$ is regarded as a consequence. In future studies this way of thinking is recommended.

---

[3]$s = S/V$ is entropy per unit volume.

4.1.2 Connecting Progogine-Defay ratio to a correlation coefficient

Single parameter liquids and strongly correlating *viscous* liquids are related as discussed in the following. The inverse square-root of the Progogine-Defay ratio equals some correlation coefficient.

This will be demonstrated in the constant VT ensemble. To keep temperature constant, entropy has to be transferred between a heat-bath and the sample: $\Delta S(t) = \Delta q(t)/T$ where q is heat. Since the volume is constant (no $p\Delta V$ work) this heat is seen in the sample as a change of the total energy ΔE and therefore $\Delta E(t) = T\Delta S(t)$. Since we will relate this to computer simulations, where total energy is easy to access, we will write energy instead of entropy.

If $c_V''(\omega)$, $K_T''(\omega)$ and $\beta_V''(\omega)$ are the imaginary parts of the frequency dependent isochoric specific heat capacity per unit volume, isothermal bulk modulus and isochoric pressure coefficient[4] respectively, then the dynamic Prigogine-Defay ratio is (Appendix of Paper I)

$$\Lambda_{VT}(\omega) \equiv -\frac{c_V''(\omega)K_T''(\omega)}{T[\beta_V''(\omega)]^2}. \qquad (4.9)$$

The fluctuation-dissipation theorem [Smit and Frenkel, 2001, Appendix C] connects equilibrium fluctuations to response functions. If $\Delta E(t) = E(t) - \langle E \rangle$, $\Delta p(t) = p(t) - \langle p \rangle$ and $\mathcal{C}_\omega\{f(t)\} = \frac{1}{2\pi}\int f(t)\cos(\omega t)dt$ denotes the cosine transform of $f(t)$, then (Paper IV)

$$c_V''(\omega) = \frac{\omega}{Vk_BT^2}\mathcal{C}_\omega\{\langle\Delta E(0)\Delta E(t)\rangle_{VT}\}, \qquad (4.10)$$

$$K_T''(\omega) = -\frac{\omega}{Vk_BT}\mathcal{C}_\omega\{\langle\Delta p(0)\Delta p(t)\rangle_{VT}\}, \qquad (4.11)$$

$$\beta_V''(\omega) = \frac{\omega}{Vk_BT^2}\mathcal{C}_\omega\{\langle\Delta E(0)\Delta p(t)\rangle_{VT}\}. \qquad (4.12)$$

Combining equation 4.9 to 4.12, $\Lambda_{VT}(\omega)$ can be re-expressed as

$$\Lambda_{VT}(\omega) = \frac{\mathcal{C}_\omega\{\langle\Delta E(0)\Delta E(t)\rangle_{VT}\}\mathcal{C}_\omega\{\langle\Delta p(0)\Delta p(t)\rangle_{VT}\}}{[\mathcal{C}_\omega\{\langle\Delta E(0)\Delta p(t)\rangle_{VT}\}]^2}. \qquad (4.13)$$

For later use, we will also define the frequency-dependent slope as

$$\gamma_{pE}(\omega) = V\sqrt{\frac{\mathcal{C}_\omega\{\langle\Delta p(0)\Delta p(t)\rangle_{VT}\}}{\mathcal{C}_\omega\{\langle\Delta E(0)\Delta E(t)\rangle_{VT}\}}} \qquad (4.14)$$

that can be written (from Equations 4.10 and 4.11) as

$$\gamma_{pE}(\omega) = \sqrt{\frac{-K_T''(\omega)}{Tc_V''(\omega)}}. \qquad (4.15)$$

---

[4]See the Appendix of Paper I for the definition of (all) the frequency-dependent response functions

$\mathcal{C}_\omega(f(t))$ relates to fluctuations of $f(t)$ on a $1/\omega$ time-scale (similar to making a running-average over an $1/\omega$ time-window) and thus,

$$(\Lambda_{VT}(\omega))^{-1/2} = \frac{\mathcal{C}_\omega\{\langle\Delta E(0)\Delta p(t)\rangle_{VT}\}}{\sqrt{\mathcal{C}_\omega\{\langle\Delta E(0)\Delta E(t)\rangle_{VT}\}\mathcal{C}_\omega\{\langle\Delta p(0)\Delta p(t)\rangle_{VT}\}}} \qquad (4.16)$$

is a measure of how correlated p and E are on this time-scale. If we regard Equation 4.5 as our definition of a single parameter liquid, then it follows that $(\Lambda_{VT}(\omega))^{-1/2} = 1$.

In computer simulations, and conceptually, a more convenient way to study slow thermodynamic fluctuations is though time-correlation functions [Hansen and McDonald, 2006] and defining a time-dependent correlation coefficient as

$$R_{pE}(t) \equiv \frac{\langle\Delta E(0)\Delta p(t)\rangle_{VT}}{\sqrt{\langle\Delta E(0)\Delta E(t)\rangle_{VT}\langle\Delta p(0)\Delta p(t)\rangle_{VT}}} \qquad (4.17)$$

and a time-dependent slope

$$\gamma_{pE}(t) = \sqrt{\frac{\langle\Delta p(0)\Delta p(t)\rangle_{VT}}{\langle\Delta E(0)\Delta E(t)\rangle_{VT}}}. \qquad (4.18)$$

From the fluctuation dissipation theorem it follows that this is what could be derived from measurements of step experiments [Smit and Frenkel, 2001].

Let us set-up some equations to illustrate possible scenarios of equilibrium fluctuations. Let $x(t)$ and $y(t)$ be the conjugated variables of the fixed variables X and Y respectively. For simplicity, we will shift and normalize x and y so $\langle x\rangle = \langle y\rangle = 0$ and $\langle x^2\rangle = \langle y^2\rangle = 1$. Imagine that $x(t)$ and $y(t)$ are sums of some hidden independent stochastic Debye processes $f_1(t)$, $f_2(t)$, $s_1(t)$ and $s_2(t)$. They are independent so cross-correlation functions are zero. Let f_1 and f_2 be fast processes, $\langle f_1(0)f_1(t)\rangle = \langle f_2(0)f_2(t)\rangle = \exp(-t)$, and s_1 and s_2 be slow process, $\langle s_1(0)s_1(t)\rangle = \langle s_2(0)s_2(t)\rangle = \exp(-t/100)$. Write $x(t)$ as

$$x(t) = G_{\lambda_x}\lambda_x f_1(t) + G_{\lambda_x}(1-\lambda_x)s_1(t) \qquad (4.19)$$

where λ_x ($0 \leq \lambda_x \leq 1$) determines the relative size of the fast process, and

$$G_\lambda = 1/\sqrt{\lambda^2 + (1-\lambda)^2}, \qquad (4.20)$$

ensures normalization[5], $\langle x^2\rangle = 1$. In addition to f_1 and s_1, let $y(t)$ also depend on f_2 and s_2 to introduce some de-correlation between x and y:

$$\begin{aligned} y(t) &= G_{\lambda_y}G_{\lambda_f}\lambda_y[\lambda_f f_1(t) + (1-\lambda_f)f_2(t)] \\ &+ G_{\lambda_y}G_{\lambda_s}(1-\lambda_y)[\lambda_s s_1(t) + (1-\lambda_s)s_2(t)]. \end{aligned} \qquad (4.21)$$

where λ_y ($0 \leq \lambda_y \leq 1$) determines the relative size of fast process. λ_f ($0 \leq \lambda_f \leq 1$) and λ_s ($0 \leq \lambda_s \leq 1$) determines the amount of correlation on fast and slow time-scales respectively. The time correlation functions for x and y are

$$\begin{aligned} \langle x(0)x(t)\rangle &= G_{\lambda_x}^2\lambda_x^2\langle f_1(0)f_1(t)\rangle \\ &+ G_{\lambda_x}^2(1-\lambda_x)^2\langle s_1(0)s_1(t)\rangle, \end{aligned} \qquad (4.22)$$

---

[5]Since $\langle x^2\rangle = G_{\lambda_x}^2[\lambda_x^2\langle f_1^2\rangle + (1-\lambda_x)^2\langle s_1^2\rangle + 2\lambda_x(1-\lambda_x)\langle f_1 s_1\rangle] = 1$, $\langle f_1^2\rangle = \langle s_1^2\rangle = 1$ and $\langle f_1 s_1\rangle = 0$ then $G_\lambda = 1/\sqrt{\lambda^2 + (1-\lambda)^2}$, Equation 4.20.

Figure 4.1: A possible scenario of thermodynamic fluctuations, Equations 4.19 and 4.21. In the parametrization shown, x and y are strongly correlated on long time-scales, but not on short time-scales. See also Figure 4.2.
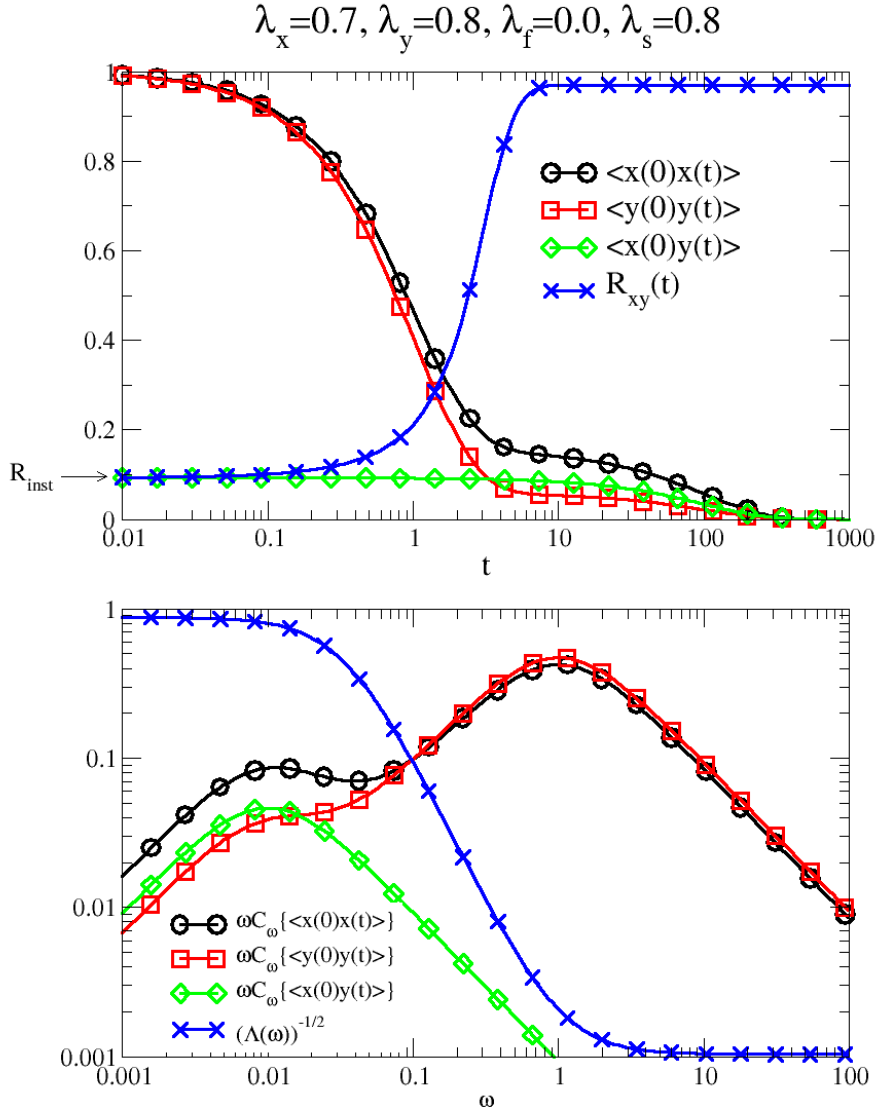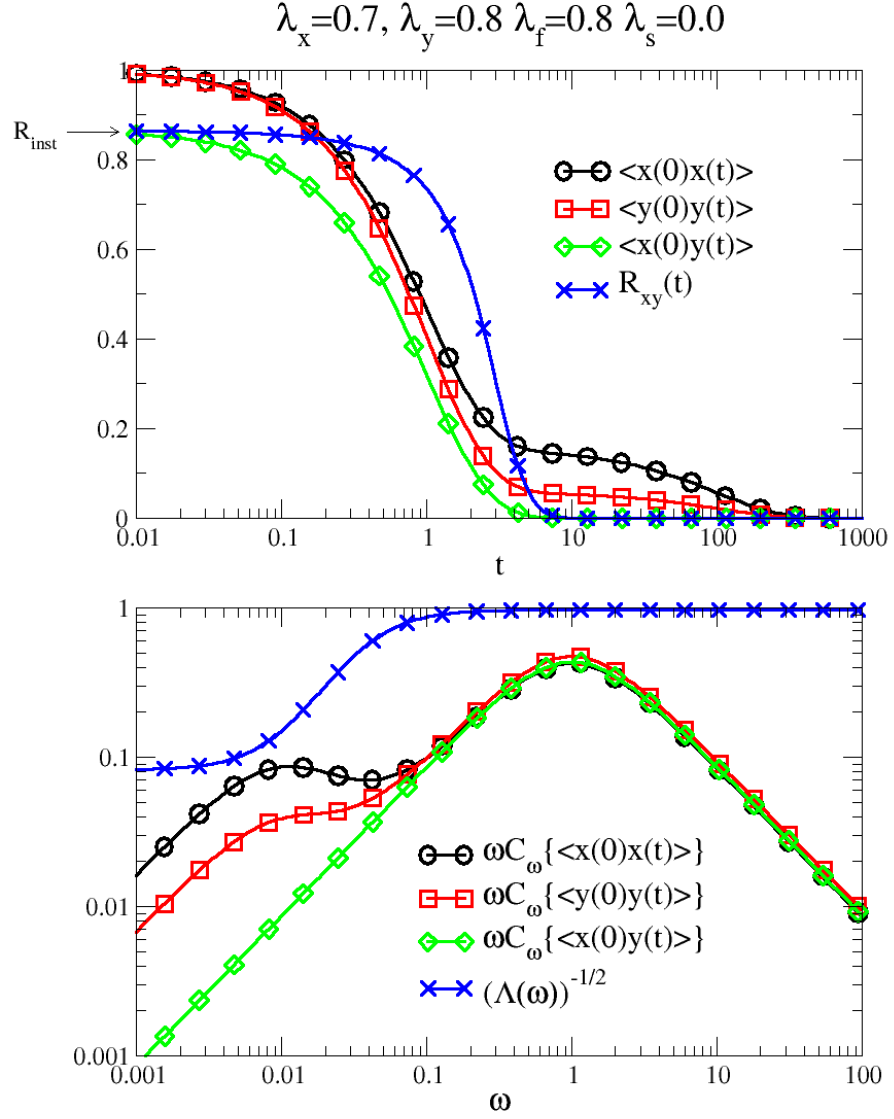
Figure 4.2: A possible scenario of thermodynamic fluctuations, Equations 4.19 and 4.21. In the parametrization shown, x and y are strongly correlated on short time-scales, but not on long time-scales. See also Figure 4.1.

$$
\begin{aligned}
\langle y(0)y(t)\rangle \;=\;& G_{\lambda_y}^2 \lambda_y^2 G_{\lambda_f}^2 \lambda_f^2 \langle f_1(0)f_1(t)\rangle \\
+\;& G_{\lambda_y}^2 \lambda_y^2 G_{\lambda_f}^2 (1-\lambda_f)^2 \langle f_2(0)f_2(t)\rangle \\
+\;& G_{\lambda_y}^2 (1-\lambda_y)^2 G_{\lambda_s}^2 \lambda_s \langle s_1(0)s_1(t)\rangle \\
+\;& G_{\lambda_y}^2 (1-\lambda_y)^2 G_{\lambda_s}^2 (1-\lambda_s) \langle s_2(0)s_2(t)\rangle \quad (4.23)
\end{aligned}
$$

and

$$
\begin{aligned}
\langle x(0)y(t)\rangle \;=\;& G_{\lambda_x} \lambda_x G_{\lambda_y} \lambda_y G_{\lambda_f} \lambda_f \langle f_1(0)f_1(t)\rangle \\
+\;& G_{\lambda_x}(1-\lambda_x) G_{\lambda_y}(1-\lambda_y) G_{\lambda_s} \lambda_s \langle s_1(0)s_1(t)\rangle. \quad (4.24)
\end{aligned}
$$

Since the auto-correlation functions of f_1, f_2, s_1 and s_2 is simply exponential relaxations it is straightforward to get an analytical expression of the time-dependent correlation coefficient $R_{xy}(t)$, Equation 4.17. Moreover, the cosine transform of exponential relaxation is given analytically [Spiegel and Liu, 1999], $\mathcal{C}_\omega\{\exp(-t/\tau)\} = \Im\{\frac{1}{i\omega+1/\tau}\}$, where $\sqrt{-1} = i$ and $\Im$ is the imaginary part. Thus, the dynamic Prigogine-Defay ratio $\Lambda_{XY}(\omega)$, Equation 4.13, also has an analytic expression. Three parametrization are shown on Figures 4.1, 4.2 and 4.5.

Now, consider a strongly correlating viscous liquid (Chapter 2). When $\Lambda_{VT}(\omega)$ is evaluated, fast (picoseconds) kinetic parts of p and E are averaged out. Qualitatively this corresponds to the parametrization of Figure 4.1. Only the configurational parts survive so $\bar{E}(t) = \bar{U}(t)$ and $\bar{p}(t) = \bar{W}(t)/V$ (again, the bar indicates an average). A simple minded guess is therefore that $(\Lambda_{VT}(\omega))^{-1/2}$ is equal to the W-U energy correlation coefficient, R_{WU}. Strictly speaking, we cannot make this connection unless R_{WU} is exactly unity. To demonstrate this, think of $x = W$ and $y = U$ in Figure 4.1. Then the figure illustrates a situation where $(\Lambda_{VT}(\omega))^{-1/2} > R_{WU}$. The opposite situation, $(\Lambda_{VT}(\omega))^{-1/2} < R_{WU}$, is also possible as shown in Figure 4.2 (by changing the parametrization).

A realistic model system, the Kob-Andersen binary Lennard-Jones liquid, show, however, that to a good approximation

$$
R_{pE}(t) \simeq R_{WU} \quad (4.25)
$$

and

$$
(\Lambda_{VT}(\omega))^{-1/2} \simeq R_{WU}, \quad (4.26)
$$

as seen on Figure 4.3 and 4.4. This is a consequence of R_{WU} being close to unity. Moreover, the W-U slope γ_{WU} can to a good approximation be calculated from

$$
\gamma_{pE}(\omega) \simeq \gamma_{WU}, \quad (4.27)
$$

and

$$
\gamma_{pE}(t) \simeq \gamma_{WU}. \quad (4.28)
$$

Before we move on, a final comment should be made. Measurements on viscous liquids typically reveal more than one relaxation processes. Think of a situation where a liquid has a slow α-relaxation and a faster β-relaxation. Imagine that individually they are strongly correlating, but gives different strength to x and y. In other words, they have different slopes. Such a situation is shown on Figure 4.5. Note that in the region where the two processes mix, there is a decrease of correlation. Experimental data of $\Lambda_{pT}(\omega)$ can in this way give some insight about the origin of relaxations.
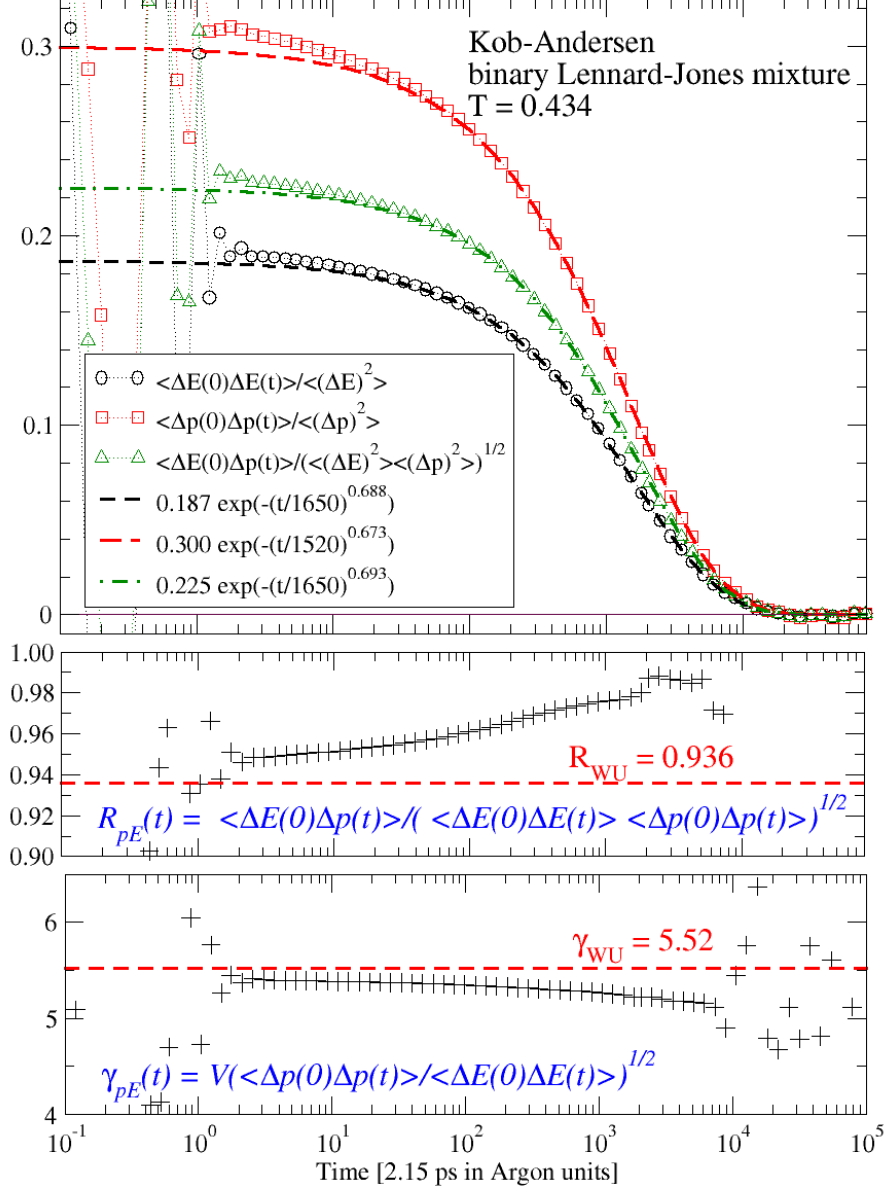
Figure 4.3: Auto- and cross correlation functions of (total) energy and pressure of the Kob-Andersen binary Lennard-Jones liquids at $T = 0.434$. A stretch exponential (fitted at $t > 100$), $A \exp(-(t/\tau)^{-\beta})$, are shown. The linear Prigogine-Defay ratio (Equation 4.2) can be estimated as $\Pi_{VT}^{\text{linear}} \simeq \frac{0.255}{\sqrt{0.187 \cdot 0.300}} = 1.08$ (($\Pi_{VT}^{\text{linear}})^{-1/2} \simeq 0.962$) using the prefactors of the fit. The lower panels shows the time dependent correlation coefficient $R_{pE}(t)$ (Equation 4.17) and the corresponding slope (Equation 4.18). The W-U correlation coefficient $R_{WU} = 0.936$ and W-U slope $\gamma_{WU} = 5.52$ are indicated with dashed lines.
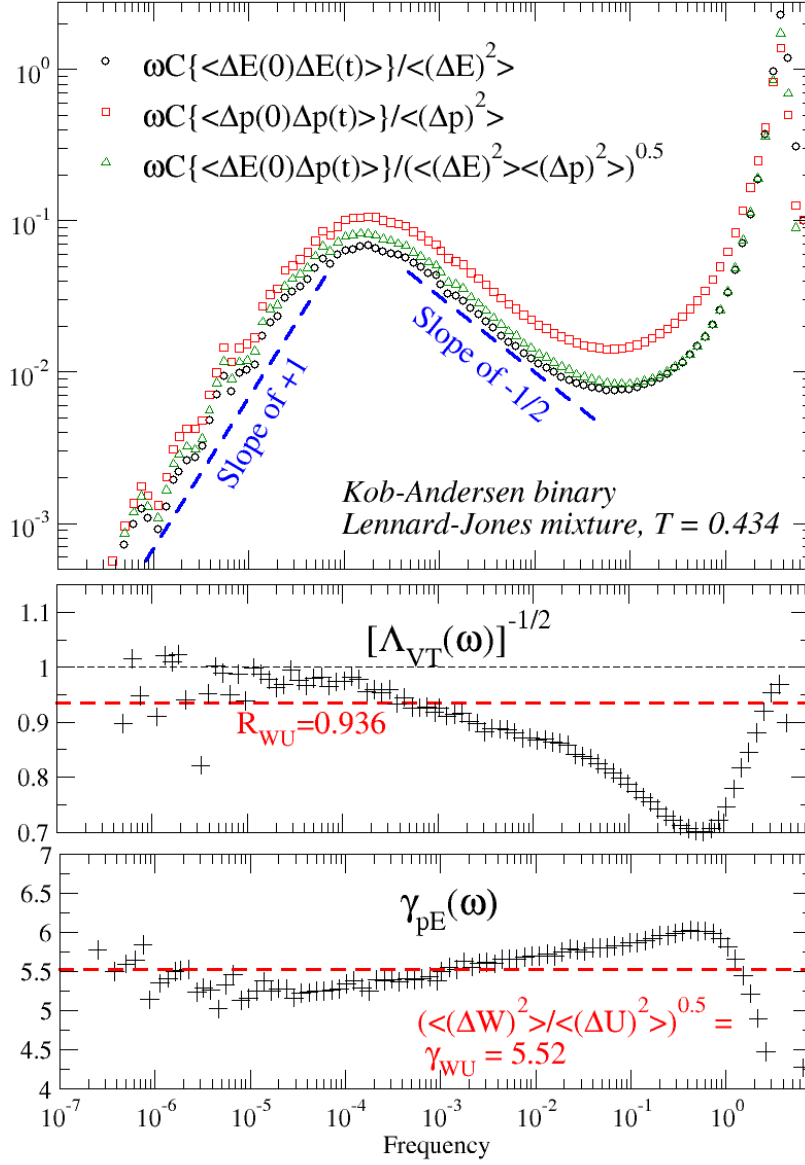
Figure 4.4: Normalized imaginary parts of natural response functions of the NVT ensemble (Equations 4.10 to 4.12) of the Kob-Andersen Lennard-Jones liquids at $T = 0.434$. The peak to the right is partially a consequence of the (artificial) Nosé-Hoover thermostat [Nosé, 1984, Hoover, 1985] and peak on the left is the structural relaxation peak. Note that the left-hand side of the structural relaxation peak has slope $+1$ and the right-hand side has close to slope $-\frac{1}{2}$ (in the log-log representation). This is in good agreement with what is found in experiments [Nielsen et al., 2008] (note that the stretch exponential β, Figure 4.3, is somewhat larger than the limiting slope). The lower panels show the inverse square root of the dynamic Prigogine-Defay ratio (Equation 4.9) and the corresponding slope (Equation 4.14). The instantaneous W-U correlation coefficient $R_{WU} = 0.936$ and slope $\gamma_{WU} = 5.52$ are indicated with red dashed lines.
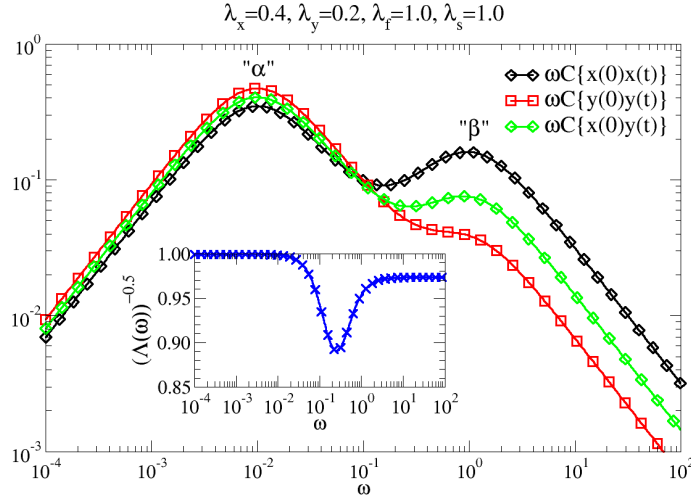
Figure 4.5: A possible scenario of thermodynamic fluctuations, Equations 4.19 and 4.21. Since $\gamma_f = \gamma_s = 1$, the fast and one slow Debye process would give perfect correlation between x and y if they where alone. Since $\gamma_x = 0.4$ is different from $\gamma_x = 0.2$ the slope of the fluctuations are different for the fast and the slow Debye relaxation. The consequence of this is that in the "mixing region" of the two internal Debye relaxations $(\Lambda_{XY}(\omega))^{-1/2}$ have a dip.

4.1.3 Rethinking the classical Prigogine-Defay ratio

As discussed earlier, the classic Prigogine-Defay ratio $\Pi_{pT}^{\mathrm{classic}}$, Equation 4.1 page 29, is not strictly well-defined. However, let us assume that the values of the (static) response functions of the liquid correspond to the $\omega \to 0$ limits and the (static) responses functions of the glass[6] correspond to the $\omega \to \infty$ limits of the frequency-dependent response functions of the equilibrium liquid at T_g. This would make $\Pi_{pT}^{\mathrm{classic}}$ equal to the well-defined linear Prigogine-Defay ratio $\Pi_{pT}^{\mathrm{linear}}$, Equation 4.2 (page 30). Then, the inverse square root of the classical Prigogine-Defay ratio reflects a correlation coefficient,

$$(\Pi_{pT}^{\mathrm{classic}})^{-1/2} \simeq R_{VS}(\text{of slow fluctuations}), \tag{4.29}$$

and

$$(\Pi_{VT}^{\mathrm{classic}})^{-1/2} \simeq R_{pS}(\text{of slow fluctuations}), \tag{4.30}$$

or, as argued in the previous section,

$$(\Pi_{VT}^{\mathrm{classic}})^{-1/2} \simeq R_{WU}. \tag{4.31}$$

This is a novel interpretation of Π^{classic}. Also, the W-U slope can be estimated from the same data as

$$\gamma_{WU} \simeq \gamma_{VT}^{\mathrm{classic}} = \sqrt{\frac{-\Delta K_T}{T \Delta c_V}}. \tag{4.32}$$

---

[6]Since a glass can be prepared in numerous ways, there is no unique value of the glass response functions. How this effects the approximation is a matter of future studies.

Equations 4.31 and 4.32 are verified for the Kob-Andersen binary Lennard-Jones liquid, Figure 4.6. This is an useful approximation, since values of the classical ratio are available in litterateur. A revisit of Π^{classic} enable us to investigating the conjecture of Section 2.2 (page 17). This conjecture speculates that van der Waals bonded liquids are strongly correlating liquids.

First, we investigate Π^{classic} of some model systems. The Kob-Andersen binary Lennard-Jones liquid have a ratio close to unity, Figure 4.6. Clarke [1979] reported $\Pi_{pT}^{\text{classic}} \simeq 1$ for the (single component) Lennard-Jones liquid and Cape and Woodcock [1980] argue that the ratio must be unity in soft-sphere systems (consistent with Chapter 3). These authors noted that this was not in agreement with the wisdom of that time – that Prigogine-Defay ratios typically had values between 2 and 4 [Gupta and Moynihan, 1976]. However, in the light of strongly correlating liquids, a ratio close to unity is expected in all of these model systems. Thus, simulations support the claim that strongly correlating viscous liquids have $\Pi_{pT}^{\text{classic}} \simeq 1$.

Now, let us reexamine the classical Prigogine-Defay found experimentally, Table 4.1. Some $\Pi_{pT}^{\text{classic}}$ are infact close to unity. In Table 4.1 liquids are listed with decreasing $\Pi_{pT}^{\text{classic}}$. Note that the lowest values are for the van der Waals bonded liquids – exactly as it is claimed by the conjecture. As an example, Takahara et al. [1999] have measured $\Pi_{pT}^{\text{classic}} = 1.20 \pm 0.05$ corresponding to a correlation coefficient of $(\Pi_{pT}^{\text{classic}})^{-\frac{1}{2}} = 0.92 \pm 0.02$ for OTP (67%) mixed with OPP (33%). This supports the conjecture that van der Waals bonded liquids are strongly correlating liquids. Unfortunately this the only value of a van der Waals bonded molecular liquid. However, the van der Waals bonded polymers also have $\Pi_{pT}^{\text{classic}}$ close unity.

Another supporting observation relates to n-propanol, with one OH-group, and glycerol with three OH-groups. Both molecules are approximately the same size having a backbone of three carbon atoms. With an increasing number of OH-groups $\Pi_{pT}^{\text{classic}}$ is expected to increase since correlation is destroyed by hydrogen bonds. Indeed $\Pi_{pT}^{\text{classical}}(\text{glycerol}) = 9.4$ is significantly larger than $\Pi_{pT}^{\text{classical}}(\text{n-propanol}) = 1.9$.

There is at present time little interest for $\Pi_{pT}^{\text{classical}}$. Presumably, this is due to the negative result of Gupta and Moynihan [1976]. However, the presented rethinking and revisit of the Prigogine-Defay ratio, demonstrates that interesting information can be extracted from the ratio. As we shall see in the following section the slope γ_{WU} is an important quantity for strongly correlating viscous liquid. This is accessible though equation 4.32. Experimentalists are therefore urged to regain interest in the Prigogine-Defay ratio – both the classical and the more well-defined frequency-dependent version.

4.2 Hidden scale invariance

In this section, in Paper VII and in Paper XIII it is argued that strongly correlating liquids have a hidden scale invariance: State points with the same

$$\Gamma \equiv \rho^{\gamma_s}/T \tag{4.33}$$

have (approximately) the same dynamics and structure (in scaled units). The scaling exponent γ_s is the same as γ_{WU}, however, since γ_{WU} is slightly state
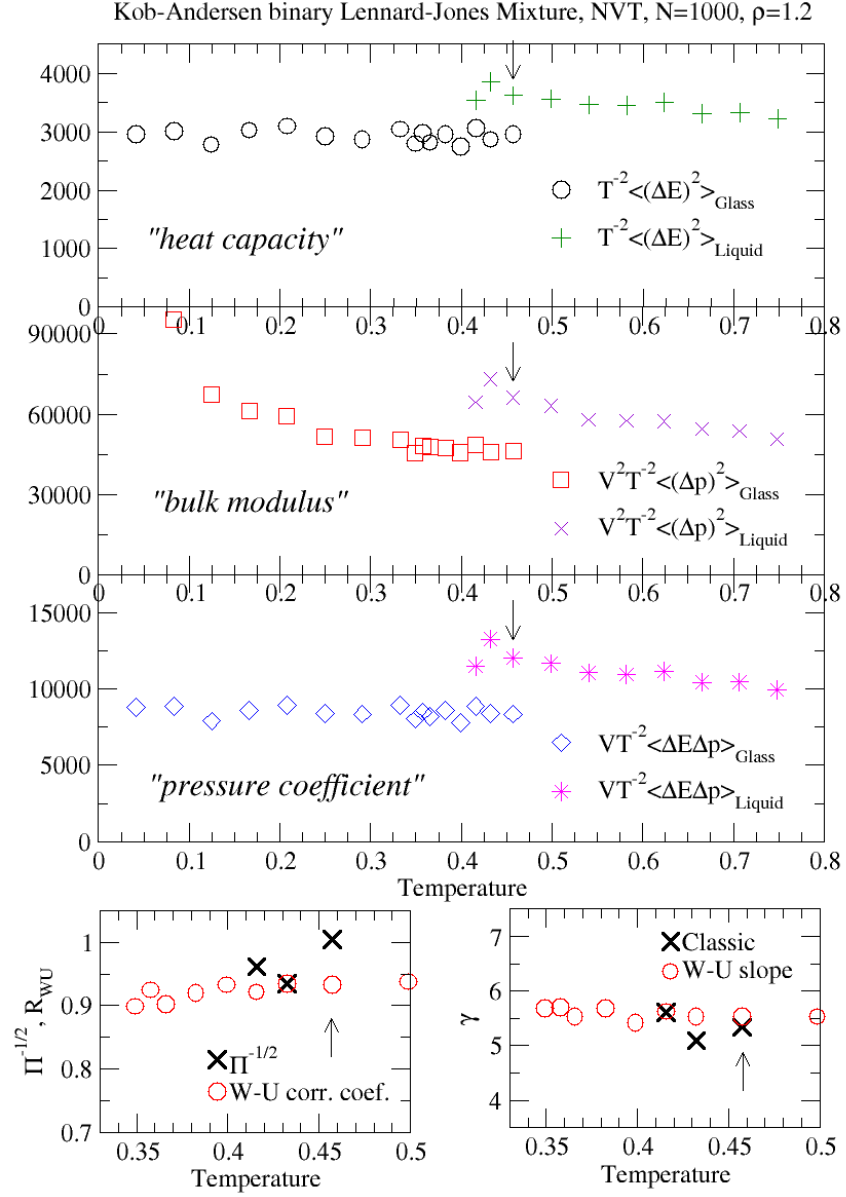
Figure 4.6: Classical approach to obtain the Prigogine-Defay ratio and slope of the Kob-Andersen binary Lennard-Jones liquid. A glass at temperature T was made from a quenched structure (cooled instantaneously to $T = 0$) taken from a configuration in equilibrium at $T = 0.457$ (marked by a arrow). After 500 ps of equilibration, 1000 ps of E and p fluctuations were used to calculate $\langle (\Delta E)^2 \rangle_{\text{Glass}}$, $\langle (\Delta p)^2 \rangle_{\text{Glass}}$ and $\langle \Delta E \Delta p \rangle_{\text{Glass}}$. E and p showed no drift (annealing of the glass) compared to the size of the fluctuations. Within statistical error, the classical approach reproduces the W-U correlation coefficient and W-U slope of instantaneously fluctuations.

42

point dependent, scaling can only be approximate. Nevertheless, as shown below in simulations, γ_s chosen to be the average γ_{WU} of the state points of interest gives good scaling.

The theoretical explanation for hidden scale invariance is as follows: First, recall the work of Hoover and coworkers [Hoover et al., 1970, Hoover and Ross, 1971, Hoover et al., 1971] showing the simplicity of soft-sphere liquids where particles interact pairwise via an inverse power-law,

$$U^{\mathrm{pow}}(r_{ij}) = \varepsilon \left(\frac{r_{ij}}{\sigma} \right)^{-n} . \tag{4.34}$$

In such a systems, physical quantities expressed in units of the characteristic velocity

$$v_s \equiv \sqrt{\frac{k_B T}{m}} \tag{4.35}$$

and the characteristic length

$$l_s \equiv \left(\frac{N}{V} \right)^{-1/3} \tag{4.36}$$

are the same for state points with the same Γ (Equation 4.33) [Hoover et al., 1971]. Thus, in scaled units state points with the same Γ are identical, having the same structure and dynamics. Therefore, soft-sphere liquids are said to have scale invariance.

Now, consider a strongly correlating liquid and recall the origin of the W-U correlation given in Chapter 3. The pair energy can be written as

$$U(r_{ij}) = U^{\mathrm{pow}}(r_{ij}) + b r_{ij} + U^{\mathrm{diff}}(r_{ij}) \tag{4.37}$$

where U^{pow} is referred to as the effective inverse power-law. Let us consider state points with the same Γ in the NVT ensemble. The trajectory at these state points (and in general) is determined by the visited energy surface $U(\vec{R}(t)) = \sum_{\mathrm{pairs}} U(r_{ij})$, where $\vec{R}(t)$ is the $3N$ coordinate vector of the system, $\vec{R}(t) = \{\vec{r}_1(t), \vec{r}_2(t), \ldots, \vec{r}_N(t)\}$. As argued in Chapter 3, $\sum_{\mathrm{pairs}}[br + U^{\mathrm{diff}}(r_{ij})]$ does not fluctuate (at constant volume) and

$$U(\vec{R}(t)) \simeq U^{\mathrm{pow}}(\vec{R}(t)) + U_0(V). \tag{4.38}$$

$U_0(V)$ is only a function of volume V. Assume that U^{pow} is not too state point dependent (γ_{WU} nearly constant). Then, strongly correlating liquids inheritd the scale invariance of structure and dynamics of soft sphere liquids. It should be noted that strongly correlating liquids are not as simple soft-sphere liquids. For soft-sphere liquids the pressure can be related directly to the energy, $\frac{3}{n}(pV/(Nk_BT) - 1) = (E/(Nk_BT) - \frac{3}{2})$ or $\frac{3}{n}W = U$ (Appendix A.1); this is not the case for strongly correlating liquids as disused in Chapter 2 (Figure 2.2 page 15). Nevertheless, scale invariance is found in simulations and experiments as discussed in the following.

Figure 4.7 show the W-U correlation coefficient R_{WU} and the W-U slope γ_{WU} of the Lewis-Wahnström OTP model for a range of state points. Since R_{WU} is close to unity ($0.90 < R_{WU} < 0.93$) this is a strongly correlating liquid. Moreover, the slope γ_{WU} only varies 7% about 7.9 for the investigated
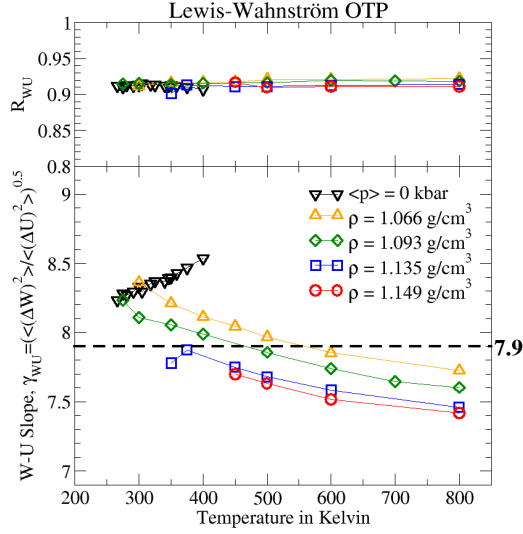
Figure 4.7: W-U correlation coefficient (top) and W-U slope (bottom) of the Lewis-Wahnström OTP model. The correlation is strong $0.90 < R_{WU} < 0.93$ and the slope varies only slightly around 7.9 ($\pm 7\%$).

state points. For comparison, γ_{WU} is about 5.9 with the same spread for the asymmetric dumbbell model (Paper VII and Paper XIII). Therefore, we should expect the Lewis-Wahnström OTP liquid to have scale invariance of structure and dynamics with $\gamma_s = 7.9$.

Figure 4.8 shows the radial distribution function of three selected state points. Two of the state points have same Γ and the same radial distribution function as a function of scaled length $r' = r(N/V)^{1/3}$ (although the scaling is not perfect, see legend of Figure 4.8). Thus structure can be scaled as expected. The third of the shown state points has the same temperature as the first, and the same pressure as the second. However, for this third state point, scaling of structure fails since Γ is different from that of the two other state points. In Paper XIII it is shown that structure of the asymmetric dumbbell model can be scale as well (simulations conducted by Thomas B. Schrøder).

Scaling of dynamics can be investigated though the diffusion constant. Figure 4.9 shows scaling of the reduced (using v_s and l_s defined in Equations 4.35 and 4.36) diffusion constant $D^* = D(N/V)^{1/3}(k_B T/m)^{-1/2}$ [Rosenfeld, 1999, Coslovich and Roland, 2008] of the Lewis-Wahnström OTP model. Scaling of the the asymmetric dumbbell model is shown in Paper VII and Paper XIII. A equivalent scaling of dynamics has been reported experimentally [Tölle, 2001, Dreyfus et al., 2003, Alba-Simionesco et al., 2004, Casalini and Roland, 2004, Roland et al., 2005]. For van der Waals bonded liquids, the structural relaxation is only a function of ρ^{γ_s}/T:

$$\tau_\alpha = g(\rho^{\gamma_s}/T). \tag{4.39}$$

However, before this study, it was not known that $\gamma_s \simeq \gamma_{WU}$ could be calculated from two response function (see previous section). At first, it was believed that
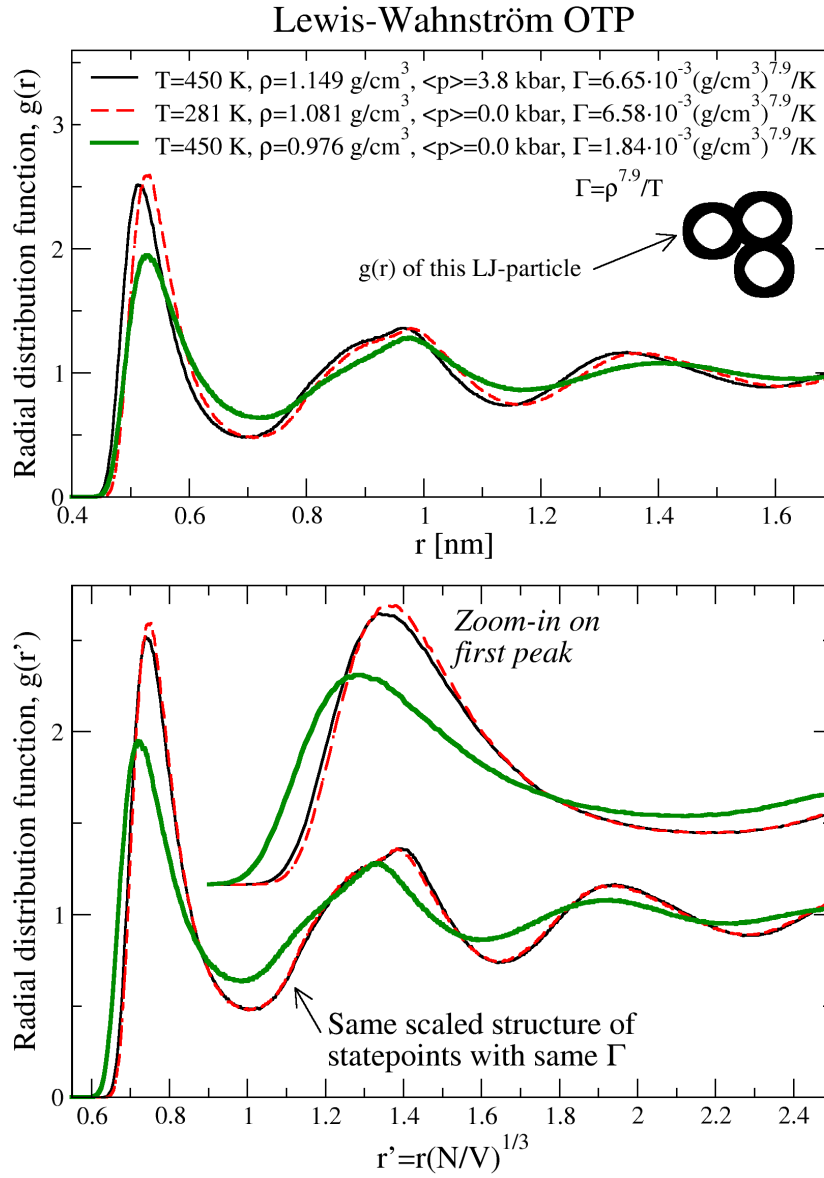
Figure 4.8: The radial distribution function $g(r)$ (top) at three state points of the Lewis-Wahnström OTP model. The definition of $g(r)$ is given in 3.2. In the bottom panel it is shown that when Γ is the same, then the structure is also the same in scaled units. The inset show a zoom-in on the first peak. Note that the scaling is not perfect. This is presumably a consequence of rigid bonds connecting Lennard-Jones particles not scaling.
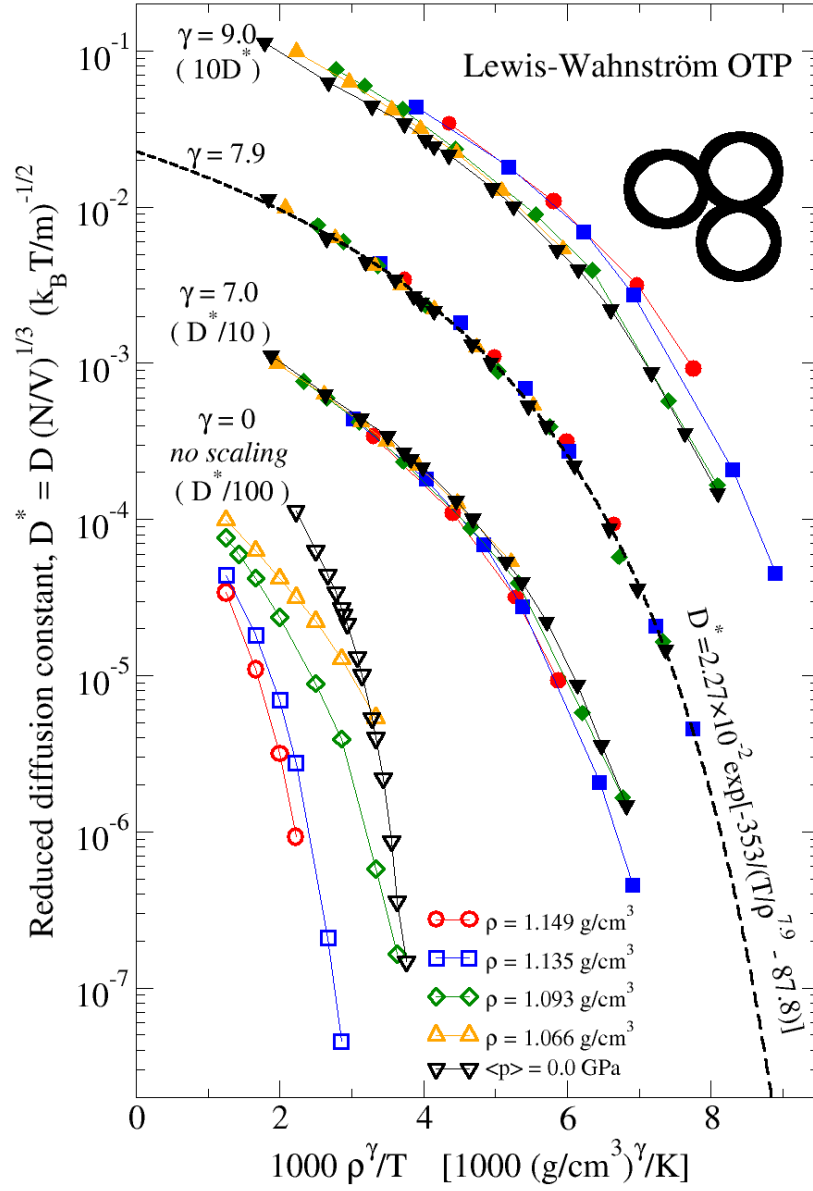
Figure 4.9: Scaling of the reduced diffusion constant of the Lewis-Wahnström OTP model. Note that the scaling works when the scaling exponent equals the W-U slope $\gamma_s = 7.9 \simeq \gamma_{WU}$, see Figure 4.7.

the scaling worked in general for viscous liquids. However, it is now realized that density scaling does not work for hydrogen bonded and covalent bonded liquids [Ferrer et al., 1998, Hensel-Bielowka et al., 2002, Roland et al., 2006, Le Grand et al., 2007, Roland et al., 2008]. This agrees with the theoretical framework given here, since these liquids are not strongly correlating. In Paper VII the failure of scaling for non-strongly correlating liquids is demonstrated by adding charges to the asymmetric dumbbell model (simulations conducted by Thomas B Schrøder).

Finally, it should be noted that Coslovich and Roland [2009] in a resent paper also confirms the theoretical frame work given here in simulations of viscous binary Lennard-Jones mixtures.

Chapter 5

Volume-energy fluctuations of phospholipid membranes

This chapter reports a simulation study of phospholipid membranes. Some membranes have strong correlations between the slow volume and energy fluctuations. The origin of the correlation can be traced to the van der Waals bonded core (the fatty acyl chains). Thus, strong correlations of membranes have the same origin as those of strongly correlating simple liquids (Chapter 3). This demonstrates that complex systems, exemplified by phospholipid membranes, can have properties similar to that of strongly correlating simple liquids (discussed in previous chapters).

Results of this chapter can also be found in Paper V and Paper X.

5.1 Motivation

A phospholipid is an amphiphilic molecule, thus having a hydrophilic and hydrophobic part. In water, phospholipids can self-organize into membranes, where hydrophobic acyl-chains are shielded from water as sketched in Figure 5.1.

Figure 5.2 shows two snapshots of all-atom molecular dynamics simulations of such two phospholipid membranes (details are given later). The acyl-chains are disordered in the membrane to the left, and are ordered in the membrane to the right. Two such phases are also found in nature, and are referred to as the (disordered) L_α and the (ordered) L_β phase [Zhang et al., 1995, Nielsen et al., 2007].

The $L_\beta \rightarrow L_\alpha$ phase transition is seen as a dramatic increase of response functions. Figure 5.3 shows excess (caused by the transition) compressibility $\Delta\kappa_T(T)$, and excess heat capacity $\Delta c_p(T)$ over the $L_\alpha \rightarrow L_\beta$ phase transition of a di-myristoyl-phosphatidyl-choline (DMPC) membrane. As seen in the figure, $\Delta\kappa_T(T)$ and $\Delta c_p(T)$ can be superimposed,

$$\Delta\kappa_T(T) = \frac{(\gamma_{HV})^2 T}{\bar{V}(T)}\Delta c_p(T). \qquad (5.1)$$

Such a proportionality is a natural consequence if

$$\Delta V_i = \gamma_{HV}\Delta H_i \qquad (5.2)$$
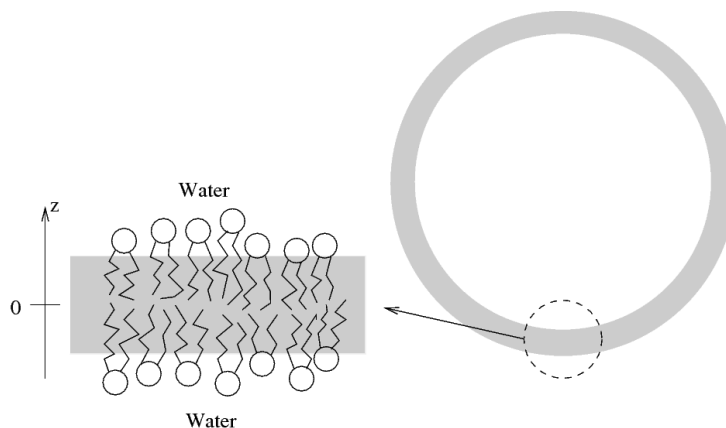
Figure 5.1: Sketch of phospholipids forming a spherical vesicle. Extruded phospholipids form such vesicles. Often phospholipid vesicles serve as a simple model of a biological cell [Alberts et al., 2002]. Hydrophilic head-groups of lipids are drawn as circles, and hydrophobic fatty acyl-chains as lines. The gray area represents a hydrophobic region, separating "in-site" water form "out-site" water. The figure is copied from my master thesis [Pedersen, 2005]. Figure 5.2 show a snap-shot from a simulation of such a phospholipid membrane.
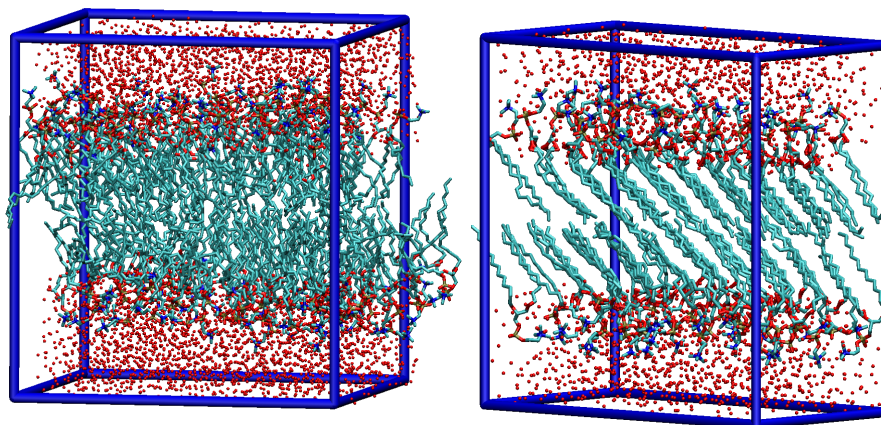
Figure 5.2: Snap-shot from all-atom simulations of two fully-hydrated DMPC membranes. The membrane on the left is in a disordered phase whereas the membrane on the right is in an ordered phase. Hydrogen is not shown for clarity, but is included in the actual simulations. The blue wire-frame indicates the periodic boundary box. This figure can also be found in Paper X.
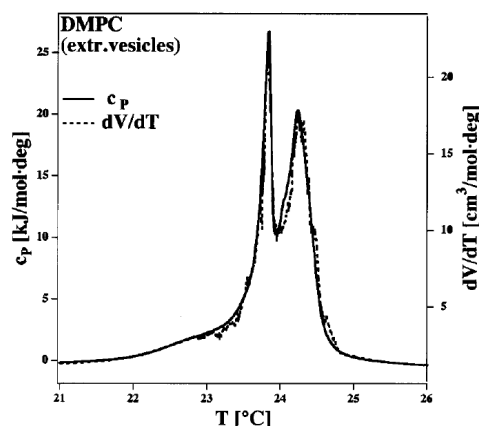
Figure 5.3: Heat capacity and volume expansion coefficient of extruded DMPC vesicles (Figure 5.1) at the phase transition. The two curves can be superimposed, Equation 5.1. This figure is copied from Ebel et al. [2001].

for available micro-states [Ebel et al., 2001, Heimburg, 1998]. Note that this equation is similar to Equations 4.5-4.8 (page 32). This suggests a connection between strongly correlating liquids and membranes. As a part of my master thesis, I simulated phospholipid membranes [Pedersen, 2005, Pedersen et al., 2007] and it was therefore natural to revisit the simulated membranes to investigate the above proportionality.

Before moving on, the importance for biological membranes (where the major constituents are phospholipids), of a proportionality should be mentioned. The conventional wisdom is that nerve signals are carried as electrical signals as formulated in the theory by Hodgkin and Huxley [1952]. However, recently Heimburg and Jackson [2005] showed that biological membranes may carry solitonic sound waves, and subsequently speculated that nerve signals may be carried this way [Heimburg and Jackson, 2007]. An element in the Heimburg-Jackson theory of nerve signals is that enthalpy and volume are correlated in their slow thermal fluctuations.

5.2   A simulation study

The following study includes simulations of seven membranes (simulations conducted by Günther H. Peters). The following abbreviations are used:

DMPC-f: fully hydrated di-myristoyl-phosphatidyl-choline membrane in fluid phase. The initial configuration is taken from Reference [Pedersen et al., 2007].

DMPC-g: fully hydrated di-myristoyl-phosphatidyl-cholin membrane in ordered phase. The initial configuration is built from a configuration in Reference [Venable et al., 2000].

DPPC-f: fully hydrated di-palmitoyl-phosphatidyl-choline membrane in fluid phase. The initial configuration is taken from Reference [Sonne et al., 2007].

DPPC-g: fully hydrated di-palmitoyl-phosphatidyl-choline membrane ordered phase. The initial configuration is built from a configuration in Reference [Venable et al., 2000].

DPPG: fully hydrated di-palmitoyl-phosphatidyl-glycerol membrane in fluid phase with calcium counter ions. Initial configuration is taken from Reference [Pedersen et al., 2006].

DPPS: fully hydrated di-myristoyl-phosphatidyl-serine membrane in fluid phase with calcium counter ions. Initial configuration is taken from Reference [Pedersen et al., 2006].

DMPSH: fully hydrated and protonated di-myristoyl-phosphatidyl-serine membrane in fluid phase. Initial configuration is taken from Reference [Pedersen et al., 2006].

Some simulation details are given in Table 5.1, however, for more details the reader is referred to Paper X and References [Pedersen, 2005, Pedersen et al., 2006, 2007].

It is not feasible to have the simulation temperature at the phase transition and test Equation 5.1 directly since relaxation time of the membrane simply exceeds the simulation time. However, as demonstrated in the following, volume-energy correlations are also present in the fluid and the ordered phase (where "quasi" equilibrium states can be reached).

Figure 5.4 shows a time-series of slow thermal fluctuation of volume and energy (of the DMPC-f membrane). Volume and energy are strongly correlated with a correlation coefficient of

$$R_{\bar{V}\bar{U}} = \frac{\langle \Delta\bar{U}\Delta\bar{V}\rangle}{\sqrt{\langle(\Delta\bar{U})^2\rangle\langle(\Delta\bar{V})^2\rangle}} = 0.77, \qquad (5.3)$$

where the bar indicates an averaging window of $\frac{1}{2}$ ns. This averages out fast fluctuations. If no averaging is done, the correlation coefficient is reduced to $R_{VU} = 0.35$. As seen in the following, this is partially due to fast fluctuations of the water (recall that water is not a strongly correlating liquid as shown in Figure 2.3 page 16).

Table 5.1 list $R_{\bar{V}\bar{U}}$ and Figure 5.5 shows the time-dependent correlation correlation coefficient,

$$R_{VU}(t) = \frac{\langle \Delta U(0)\Delta V(t)\rangle}{\sqrt{\langle\Delta U(0)\Delta U(t)\rangle\langle\Delta V(0)\Delta V(t)\rangle}}, \qquad (5.4)$$

of the seven membranes. Five of the membranes, DMPC-f, DPPC-f, DPPC-g, DMPG and DMPSH, have strong correlations in the slow volume-energy fluctuations with $R_{\bar{V}\bar{U}} \geq 0.75$ and $R_{VU}(t > 0.5 \text{ ns}) > 0.75$. The origin of the correlation can be traced to the hydrophobic (van der Waals bonded) core of the membrane. This can be quantified as done in the following:

First, the atoms are divided into three groups, using the following subscripts:
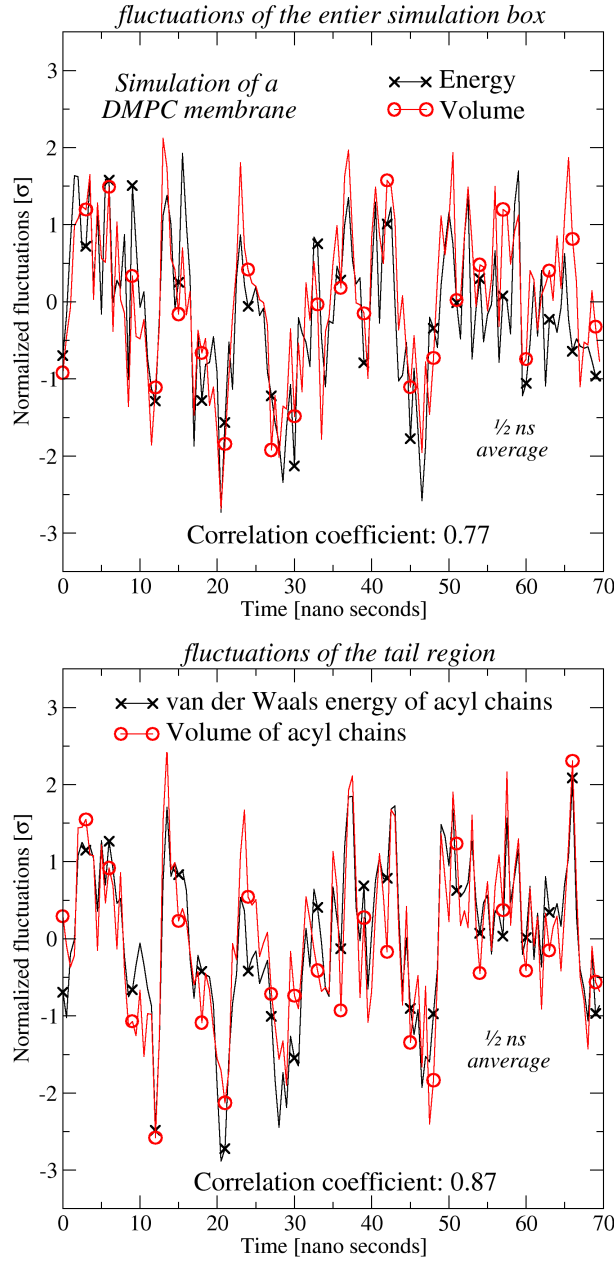
Figure 5.4: The top panel shows normalized fluctuation of volume, $\Delta \bar{V}(t)/\sigma_{\bar{V}}$, and energy, $\Delta \bar{U}(t)/\sigma_{\bar{U}}$ of the DMPC-f membrane. The bar indicates a $\frac{1}{2}$ ns averaging window. $\Delta \bar{V}$ and $\Delta \bar{U}$ are strongly correlated with a correlation coefficient of $R_{\bar{V},\bar{U}} = 0.77$. The bottom panel shows normalized fluctuations of the Voronoi volume of the tail region, $\Delta \bar{V}_t(t)/\sigma_{\bar{V}_t}$, and Lennard-Jones energy of tail-region, $\Delta \bar{U}_t^{\mathrm{LJ}}(t)/\sigma_{U_t^{\mathrm{LJ}}}$. The correlation coefficient is $R_{\bar{V}_t,U_t^{\mathrm{LJ}}} = 0.87$. There figures can also be found in Paper X.

Table 5.1: Overview of simulation details and results

	t_{sim} [ns]	t_{prod} [ns]	N_{lip}	T [K]	$\frac{N_{wat}}{N_{lip}}$	$R_{\bar{V}\bar{U}}$	$\gamma_{\bar{V}\bar{U}}$	$R_{\bar{U}\bar{U}_t}$
DMPC-f	151	121	128	330	33	0.77	6.7	0.82
DMPC-g	65	36	64	286	33	0.47	4.3	0.31
DPPC-f	180	124	72	325	29	0.87	7.1	0.89
DPPC-g	78	48	64	304	33	0.75	4.6	0.71
DMPG	149	49	128	330	33	0.82	5.9	0.80
DMPS	139	49	128	340	36	0.59	5.3	0.64
DMPSH	136	35	128	340	37	0.78	9.2	0.84

t_{sim}: Total simulation time in nanoseconds; t_{prod}: Length of production run in nanoseconds (only membranes in quasi-equilibrium, i.e., with no detectable drift in the area per molecule, were included in the data analysis); N_{lip}: Number of lipid molecules; T: Temperature in Kelvin; N_{wat}/N_{lip}: Number of water molecules per lipid molecule; $R_{\bar{V}\bar{U}}$: Energy-Volume correlation coefficient; $\gamma_{\bar{V}\bar{U}}$: Energy-volume scaling factor in Å^3 mol/kcal; $R_{\bar{U}\bar{U}_t}$: Energy-"Energy of acyl groups" correlation coefficient.
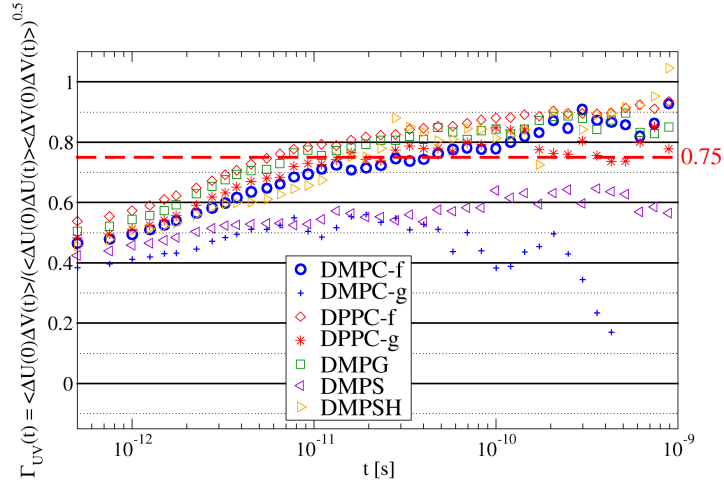
Figure 5.5: Time-dependent correlation function of volume-energy (Equation 5.3. DMPC-f, DPPC-f, DPPC-g, DMPG and DMPSH membranes have strong volume-energy correlation in the slow fluctuations, $R_{VU}(t > 0.5 \text{ ns}) > 0.75$. This figure can also be found in Paper X.
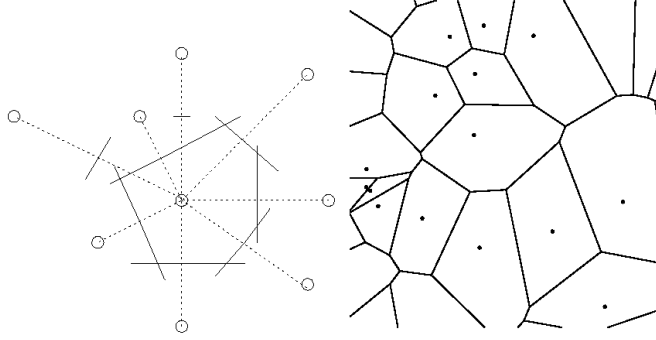
Figure 5.6: The principle of construction of Voronoi polyhedrons [Voronoi, 1908]. For simplicity, a construction in two dimensions is shown. On the left, circles represent particles. The Voronoi polygon of the center atom is drawn with full lines. Points included in this volume have the center particles as the closest particle. The Voronoi polygons of a collection of particles are shown on the right. Note that the Voronoi polygons tile space. The total area is therefore the sum of Voronoi areas. In three dimensions polygons become polyhedra and the total volume is the sum of the Voronoi volumes. This figure is copied from my master thesis [Pedersen, 2005].

t for "tail". Atoms of $-CH_2-$ and $-CH_3$ groups of the fatty acyl-chains. Shown as light blue atoms in Figure 5.2.

h for "head". The remainder of the lipid atoms. As seen in Figure 5.2, these atoms are located in the interface and are in close contact with water.

w for "water". Shown as red spheres in Figure 5.2. Note that water is excluded from the core of the membrane.

The volume of a given region is calculated by summing Voronoi volumes [Voronoi, 1908] of the heavy atoms (excluding hydrogen); $V = V_t + V_h + V_w$. The principle of construction Voronoi polyhedrons are given in Figure 5.6. Also, energy can be split up in three contributions; $U = U_t + U_h + U_w$ where

$$U_x = U_x^{\text{intra}} + \frac{1}{2} \sum_{i\,=\,x} \sum_{j\,=\,\text{all}} U_{ij}^{\text{coul}} + \frac{1}{2} \sum_{i\,=\,x} \sum_{j=\,\text{all}} U_{ij}^{\text{LJ}}, \qquad (5.5)$$

with x either tail, head, or water. U_x^{intra} is the energy of intra-molecular bonds,

$$U_{ij}^{\text{coul}} = q_i q_j / (4\pi\epsilon_0 r_{ij}), \qquad (5.6)$$

is the Coulomb energy of two pairs, and

$$U_{ij}^{\text{LJ}} = 4\varepsilon_{ij}((\sigma_{ij}/r_{ij})^{12} - (\sigma_{ij}/r_{ij})^6) \qquad (5.7)$$

is the Lennard-Jones pair energy.
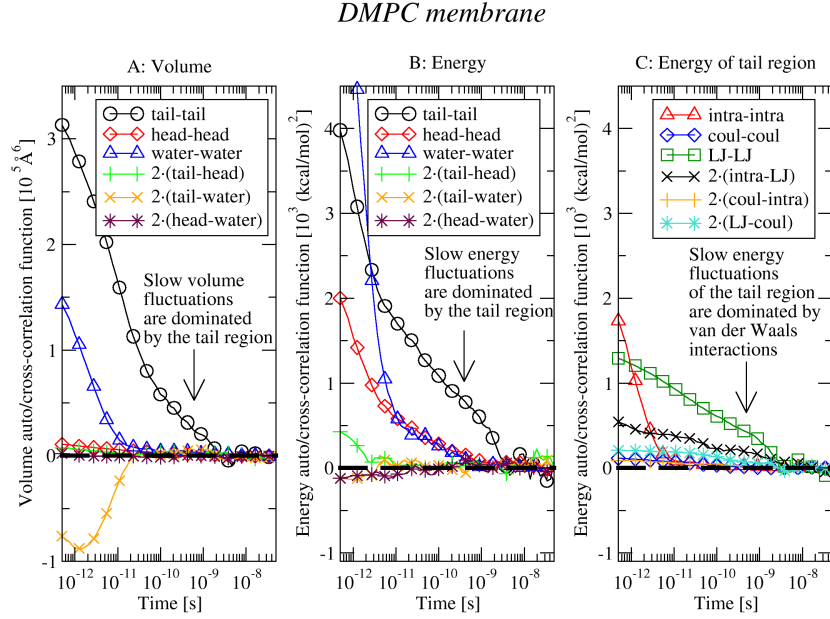
DMPC membrane

Figure 5.7: Terms of equation 5.8 for the DMPC-f membrane. See text after this equation for more details. This figures can also be found in Paper X.

The auto-correlation functions of volume and energy (Equation 5.4), can now be split into six terms:

$$
\begin{aligned}
\langle \Delta \mathcal{V}(0) \Delta \mathcal{V}(t) \rangle \;=\; & \langle \Delta \mathcal{V}_t(0) \Delta \mathcal{V}_t(t) \rangle \\
+\; & \langle \Delta \mathcal{V}_h(0) \Delta \mathcal{V}_h(t) \rangle \\
+\; & \langle \Delta \mathcal{V}_w(0) \Delta \mathcal{V}_w(t) \rangle \\
+\; & 2\langle \Delta \mathcal{V}_t(0) \Delta \mathcal{V}_h(t) \rangle \\
+\; & 2\langle \Delta \mathcal{V}_t(0) \Delta \mathcal{V}_w(t) \rangle \\
+\; & 2\langle \Delta \mathcal{V}_h(0) \Delta \mathcal{V}_w(t) \rangle,
\end{aligned}
\tag{5.8}
$$

with $\mathcal{V}$ either E or V. Figure 5.7 shows the six terms of volume and energy respectively (DMPC-f membrane). The only non-vanishing term of slow ($t \gtrsim \frac{1}{2}$ ns) fluctuations of volume is $\langle \Delta V_t(0) \Delta V_t(t) \rangle$, showing that slow fluctuations of volume are dominated by the tail-region, as expected. Also slow energy fluctuations are dominated by the tail region. However, it should be noted that the contributions to fluctuations from water and head-region are significant. As discussed later, this weakens the (total) volume-energy correlation of a given membrane, explaining that some membranes have stronger $\bar{U}$-$\bar{V}$ correlation than others.

Also, Figure 5.7 shows an additional splitting of the tail-energy in inter-molecular bond energy, Lennard-Jones (or van der Waals) energy and Coulomb energy (similar to that of Equation 5.8). As expected, slow fluctuations are

56

dominated by the Lennard-Jones contribution.

The analysis suggests that the origin of the (total) volume-energy correlation can be traced to the van der Waals bonded tail region:

$$\Delta \bar{V}_t \propto \Delta \bar{U}_t^{LJ},$$
(5.9)

where

$$U_t^{LJ} = \frac{1}{2} \sum_{i=\text{tails}} \sum_{j=\text{all}} U_{ij}^{\text{LJ}}$$
(5.10)

Remember, however, that we throw away some non-vanishing energy terms. Nevertheless, $R_{\bar{V}_t, U_t^{\bar{L}J}} = 0.87$ is larger than $R_{\bar{V}\bar{U}} = 0.78$ strengthens this conclusion. As mentioned earlier, the correlation is weakened by the tail-energy not completely dominating slow fluctuations. To investigate this further, $R_{\bar{U}\bar{U}_t}$ can be used as a measure of how much of the energy fluctuations comes from the tail region. Comparing $R_{\bar{V}\bar{U}}$ with $R_{\bar{U}\bar{U}_t}$, as done in Table 5.1, shows that large values of $R_{\bar{U}\bar{U}_t}$ is followed by $R_{\bar{V}\bar{U}}$ and vice versa.

Finally, a volume-energy scaling factor (or slope) can be calculated from the simulations as

$$\gamma_{\bar{V}\bar{U}} = \sqrt{\frac{\langle (\Delta \bar{V})^2 \rangle}{\langle (\Delta \bar{U})^2 \rangle}}$$
(5.11)

The experimental value (Equations 5.1) is found to be $(7.788 \pm 0.110) \times 10^{-4}$ mL/J $= (5.418 \pm 0.077)$ Å·mol/kcal for DMPC membranes [Ebel et al., 2001]. This roughly agrees with the values calculated in simulations, as seen in Table 5.1. One caveat is that $\gamma_{\bar{V}\bar{U}}$ of the fluid membranes is approximately two times that of the ordered membrane. From the scaling given by Equation 5.1 it is expected that they should be the same. More work is needed to clarify this.

Finally it should be noted that energy and volume generally do not have significant correlation with membrane area or the chain order parameter defined as [Tieleman and Berendsen, 1996]

$$S_{CD} = \left| \left\langle \frac{3}{2} \cos^2(\theta_{CD}) - \frac{1}{2} \right\rangle_{ch} \right|$$
(5.12)

where θ_{CD} is the angle between the membrane normal and the C-H bond of a given methylene group, and $\langle \ldots \rangle_{ch}$ denotes an average over all methylene groups in all chains[1]. Correlation coefficients are listed in Table 5.2.

To conclude this chapter: It has been that demonstrated that a complex system can have properties similar to that of a strongly correlating liquid. Note, the importance of *separation of time-scales*. What happens is that a strongly correlating element of the system dominates fluctuations on some time-scale. In membranes, slow fluctuations of energy and volume are dominated by van der Waals bonded core. Qualitatively this corresponds to what is shown in Figure 4.1 (page 35).

---

[1]Note that usually a static S_{CD} is reported, and for individual methyl-groups. Here a dynamic version is defined.

Table 5.2: Correlation coefficients

	$R_{\bar{V}\bar{U}\bar{V}}$	$\gamma_{\bar{V}\bar{U}}$	$R_{\bar{U}\bar{U}_t}$	$R_{\bar{U}\bar{A}}$	$R_{\bar{V}\bar{A}}$	$R_{\bar{A}\bar{S}_{CD}}$	$R_{\bar{U}\bar{S}_{CD}}$	$R_{\bar{V}\bar{S}_{CD}}$
DMPC-f	0.77	6.7	0.82	0.50	0.57	-0.75	-0.49	-0.54
DMPC-g	0.47	4.3	0.31	0.02	0.05	-0.64	0.12	0.14
DPPC-f	0.87	7.1	0.89	-0.29	-0.36	0.00	-0.61	-0.71
DPPC-g	0.75	4.6	0.71	-0.16	0.12	-0.67	0.09	-0.07
DMPG	0.82	5.9	0.80	0.41	0.40	-0.76	0.01	0.08
DMPS	0.59	5.3	0.64	0.30	0.28	-0.71	0.04	0.20
DMPSH	0.78	9.2	0.84	0.43	0.51	-0.50	0.05	0.14

$R_{\bar{V}\bar{U}}$: Energy-Volume correlation coefficient; $\gamma_{\bar{V}\bar{U}}$: Energy-volume scaling factor in Å^3 mol/kcal; $R_{\bar{U}\bar{U}_t}$: Energy-"Energy of acyl groups" correlation coefficient; $R_{\bar{U}\bar{A}}$: Energy-Area correlation coefficient; $R_{\bar{V}\bar{A}}$: Volume-Area correlation coefficient; $R_{\bar{A}\bar{S}_{CD}}$: Area-"chain order-parameter" correlation coefficient; $R_{\bar{U}\bar{S}_{CD}}$: Energy-"chain order-parameter" correlation coefficient; $R_{\bar{V}\bar{S}_{CD}}$: Volume-"chain order-parameter" correlation coefficient.

Chapter 6

Stability of a binary mixture

Long-time simulations are important for computational studies of viscous liquids. It is now possible to investigate low temperature liquids with several decade of relaxation times. Nowadays, simulation times of 0.1 ms are within reach for a system of 1000 particles, Figure 1.7 (page 8). As shown below, however, some of the standard models used in the computational community of viscous liquids crystallize on these time-scale. Paper II reports crystallization of the Wahnström binary Lennard-Jones liquid [Wahnström, 1991]. Toxværd et al. [2007] report crystallization[1] of the Kob-Andersen Lennard-Jones liquid [Kob and Andersen, 1994, 1995a,b]. Also the ortho-terphenyl model suggested by Lewis and Wahnström [1994] crystallizes as seen in Figure 6.1.

The following sections gives a detailed investigation of the stability of the Wahnström binary Lennard-Jones liquid. A paper including these results are at the moment in the process of being written in collaboration with Peter Harrowell (School of Chemistry, University of Sydney). The stability of the Kob-Andersen Lennard-Jones liquid is only briefly discussed. More details can be found in Paper XI. Crystallization mechanism of the Lewis-Wahnström o-terphenyl model have not been investigated in details. However, the structure of the formed crystal is shown in Figure 6.1.

6.1 The Wahnström binary Lennard-Jones mixture

This mixture was originally suggested by Wahnström [1991] to study viscous liquid dynamics. It consists of two kinds of Lennard-Jones particles, labeled A and B, where the diameter of B particles is $\sigma_{BB}/\sigma_{AA} = 1.2$ that of the A particles. The composition is equivmolar, $N_A = N_B$. See section 1.2.1, Paper II and Figure 1.4 for more details.

---

[1]In the final days before handing in the thesis, it was realized that the force parameters for simulating the Kob-Andesen liquid was implemented wrong. The Lennard-Jones binding energies simulated were $\varepsilon'_{\alpha\beta} = \sigma_{\alpha\beta}\varepsilon_{\alpha\beta}$ where $\sigma_{\alpha\beta}$ and $\varepsilon_{\alpha\beta}$ are the original Kob-Andersen parameters. Thus, the binding energies of BB pairs, $\varepsilon'_{BB} = \sigma_{BB}\varepsilon_{BB} = 0.88 \cdot 0.5 = 0.44$, and AB, $\varepsilon'_{AB} = \sigma_{AB}\varepsilon_{AB} = 0.8 \cdot 1.5 = 1.2$, pairs were reduced. A reduction of the AB binding energy will increase composition fluctuations, and thereby making the system more prone to crystallization. It is therefore still an open question on what time scale the Kob-Andersen mixture will crystallize.
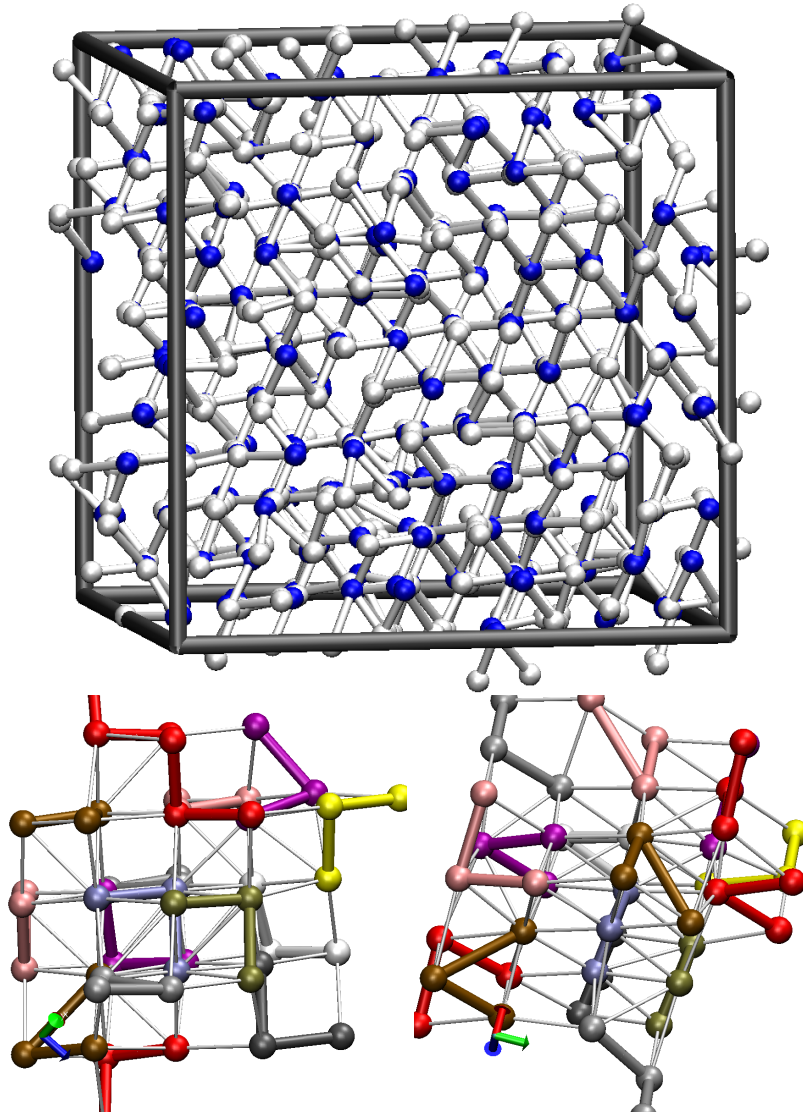
Figure 6.1: Crystal formed spontaneously from the melt of the Lewis-Wahnström o-terphenyl model [Lewis and Wahnström, 1994] (three Lennard-Jones particles placed in a isosceles triangle with an angle of 75°, see Figure 1.5). As seen in the upper part of the figure, all of the 324 molecules are arranged in an ordered structure (center particles are colored blue). A part of crystal viewed from two angles is shown in the lower part of the figure. The gray lines are guidelines for the eye.
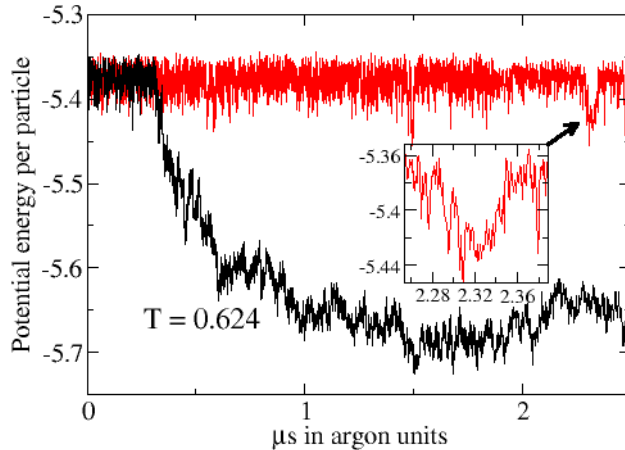
Figure 6.2: Time series of energy in two (selected) simulations of the Wahnström binary Lennard-Jones liquid at $T = 0.624$. The dramatic drop in energy is a consequence of crystallization. The structural relaxation time of the liquid is of the order of a nanosecond.

6.2 The crystal

The Wahnström binary Lennard-Jones mixture can spontaneously form a crystal from the melt. This is seen as a dramatic drop in energy as shown in Figure 6.2. An inspection of particle positions, as done in Figure 6.3, reveals a large crystal with $MgZn_2$ structure[2] (and defects). The $MgZn_2$ structure is not built into the model, and was not, the authors knowledge, predicted. Table 6.2 lists the energy and volume of some close-packed crystal structures. This analysis indeed suggests that the $MgZn_2$ structure is the true ground state.

The crystal is one of the so-called Laves phases that comprise the largest group of inter-metallic phases [Stein et al., 2004, 2005]. Understanding crystallization of a Laves structures is therefore important in its own right. $MgZn_2$ has optimal packing of hard-spheres when the size ratio is $\sigma_B/\sigma_A = \sqrt{3/2} \simeq 1.22$, close to the size ratio $\sigma_B/\sigma_A = 1.2$ of the Wahnström mixture. This close-packing feature of $MgZn_2$ makes crystallization related to packing.

The crystal formed is remarkable on two accounts: i) The AB liquid is off-composition compared to the A_2B crystal. Hence, a significant composition fluctuations must accompani crystal formation. ii) The crystal structure is quite complex, having a unit cell of 12 particles. In the light of this, it is remarkable that the crystal forms at all. This is naturally also the reason why crystallization of this model has not been reported before.

---

[2]$MgZn_2$ structure (C14) have a trigonal, hexagonal unit-cell with $P6_3/mm$ symmetry with six A particles on the h position, two A particles on the a position and four B particles on the f position, where h, a and f are the Wyckoff letters [Pearson, 1972, page 657].
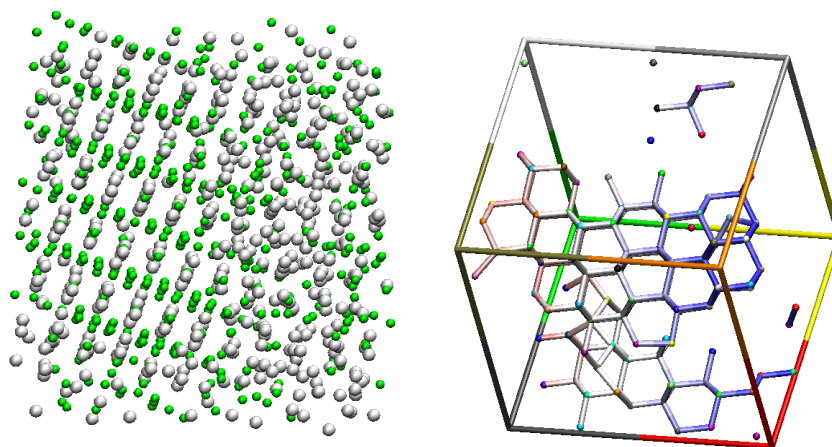
Figure 6.3: Crystal formed spontaneously from the melt of the Wahnström binary Lennard-Jones liquid. B particles are colored white (light gray) and A particles are colored green (dark gray). The coordinates are the quenched structure taken at the last point of the black curve in Figure 6.2. The left hand side of the figure shows the positions of all the particles. The crystal fills roughly half of the box. The remainder of the box is filled with a B-rich liquid since the total composition is AB whereas that of the crystal is A_2B. The structure of the crystal is $MgZn_2$ is shown in Figure 6.5. The right hand side of the figure shows the formed crystal represented as Frank-Kasper bonds (see Figure 6.7). Configurations are rotated for maximum clarity.

6.3 Mechanism of crystallization

First, define the first shell as particles within the first peak of the radial distribution function $g(r)$ using the first minimum as cutoff, as shown in Figure 6.4. Then, define local composition as $\chi_B^{\text{fs}} = Z_B/Z$, where Z_B is the number of B particles, and Z is the total number of particles in the first shell.

Let us take a closer look at the $MgZn_2$ crystal structure shown in Figure 6.5. The smaller A particles have distorted icosahedral first shells with a local composition of $\chi_B^{\text{fs}} = 0.5$. Figure 6.6 shows the distribution of first shell arrangements of the liquids. Note that the most common is of the same kind as the crystal. Coslovich and Pastore [2007] also noted the high abundant of this arrangement. So the local arrangement around A particles is roughly the same in liquid and crystal. On the other hand, crystalline B particles have a first shell that is very different from the liquid. The crystalline B particles have a high coordination of 16 particles and a local composition of $\chi_B^{\text{fs}} = 0.25$. This first shell arrangement is unusual in the liquid (Figure 6.6). Thus, the structural fluctuation leading to crystallization implies a significant change of the first shells of B particles. Note that the composition fluctuation needed is only seen around B particles.

To undertake a study of the rearrangement associated with crystallization, we need to characterize local structure. I have extended the common neighbor

Table 6.1: Energy and packing of Wahnström crystals.

Crystal	V/N $[\sigma_{AA}^3]$	U/N $[\varepsilon_{AA}]$	First shell compositions
Pure A			
FCC†(A)	0.93663	-7.26293	A-12-0
A$_2$B mixture			
(Laves) MgCu$_2$	1.13351	-7.28515	A-6-6 and B-12-4
(Laves) MgZn$_2$	1.13193	-7.29910	A-6-6 and B-12-4
(Laves) MgNi$_2$	1.13275	-7.29179	A-6-6 and B-12-4
MoPt$_2$	1.16593	-6.83436	A-9-5 and B-10-4
MoSi$_2$	1.16594	-6.83429	A-9-5 and B-10-4
AB mixture			
Liquid	1.33341	-5.37896	Figure 6.6
CuAu	1.26577	-6.84244	A-3-8 and B-8-6
FeB	1.26449	-6.84971	A-4-8 and B-8-6
$\frac{3}{4}$MgZn$_2$(A$_2$B)+$\frac{1}{4}$FCC(B)	1.23842	-7.20207	A-6-6, 75% B-12-4 and 25% B-0-12
$\frac{3}{4}$CuZr$_2$(AB$_2$)+$\frac{1}{4}$FCC(A)	1.26088	-6.91559	75% A-4-8, 25% A-12-0 and B-4-9
$\frac{1}{2}$Cu(A)+$\frac{1}{2}$FCC(B)	1.24726	-7.08695	A-12-0 and B-0-12
AB$_2$ mixture			
CuZr$_2$	1.36896	-6.79967	A-4-8 and B-4-9
$\frac{3}{8}$MgZn$_2$(A$_2$B) +$\frac{5}{8}$FCC(B)	1.39815	-7.05651	A-6-6, 37.5% B-12-4 and 62.5% B-4-9
Pure B			
FCC(B)*	1.55788	-6.91096	B-0-12

Energies and volumes were calculated on the basis of NpT simulations of pure crystals: FCC† of A particles, MgCu$_2$, MgZn$_2$, MgNi$_2$, MoPt$_2$, MoSi$_2$, CuAu, FeB, AB$_2$, CuZr$_2$ and a FCC of B particles. Crystals where simulated at $T = 0.624$ and $p = 4.7$ (same as liquid).

All these crystals are stable at this temperature and pressure (in the simulated time interval of some nanoseconds). The candidates for structures where selected from Reference [Kummerfeld et al., 2008] and private correspondence with Toby S. Hudson. Note that at all the investigated compositions, MgZn$_2$ in combination with a pure FCC crystal (A or B) has lowest energy and volume, thus this is a good candidate for the true ground state of the system (of-course, Gibbs free energies are the appropriate quantities to compare). †FCC: face center cubic or Cu. *The energy of the FCC crystals (pure A and pure B) are different although $\varepsilon_{AA} = \varepsilon_{BB}$. The difference is an artifact of the truncation of the potential.
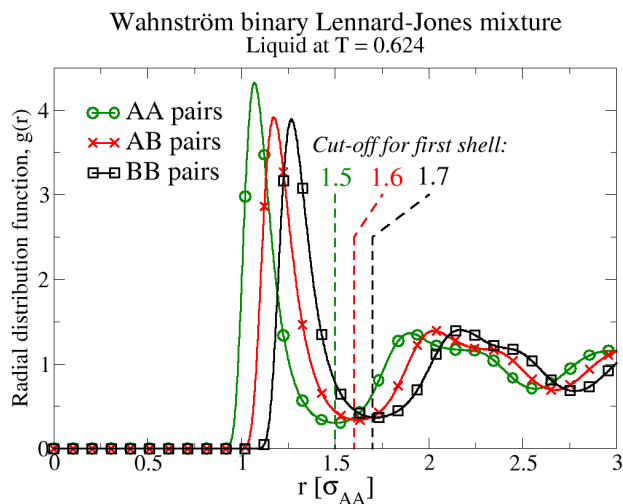
Figure 6.4: Radial distribution function $g(r)$ of the liquid at $T = 0.624$. The first minimum is used as cut-off for when defining particles of the first shell.

analysis suggested by Honeycutt and Andersen [1986] so it takes the two kinds of particles into account: Consider two neighbor particles and their common neighbors as shown in Figure 6.7. Six integers is used to characterize such a (two colored) bi-pyramid graph, $Rn_A n_B s_{AA} s_{AB} s_{BB}$. Where R is the type of neighbor pair so $R = 1$ for AA, $R = 2$ for AB and $R = 3$ for BB, n_A and n_B is the number of A and B common neighbors respectively, and s_{AA}, s_{AB} and s_{BB} is the number of AA, AB and BB contacts amongst common neighbors. We will refer to such a local arrangement as a bond. For later use, the stability of a common neighbor arrangement is measured as the time interval of the first and the last observation. This is referred to as the lifetime. Note that in this time interval a particle can leave the arrangement as long as it returns at a later time.

The crystal is made up of just five types of bonds. Three AA bonds, 114023, 123122 and 132221, an AB bond, 232140, and a BB bond, 360600. In the following the 360600 BB bond will play an important role in the analysis. As seen in Figure 6.5 the MgZn$_2$ crystal structure can be viewed as a hexagonal diamond structure of B particles connected by such bonds. Hence, each B has four 360600-bonds pointing to the corners of a tetrahedron as seen on Figure 6.5. The 360600-tetrahedron is the basic element of all the Laves structures. The difference between the structures is how the 360300-bonds are connected. Such an analysis was the subject of the celebrated work by Frank and Kasper [1958, 1959]. In acknowledgment of their work we will henceforth referrer to 360600 bonds as Frank-Kasper bonds. A Frank-Kasper bond is shown in Figure 6.7.

Let us return to the liquid (at $T = 0.624$). Figure 6.8 shows the average lifetime and abundance of bonds in the liquid. The most common and stable AA and AB bonds are the ones with five bonded common neighbors, $n_A + n_B =$
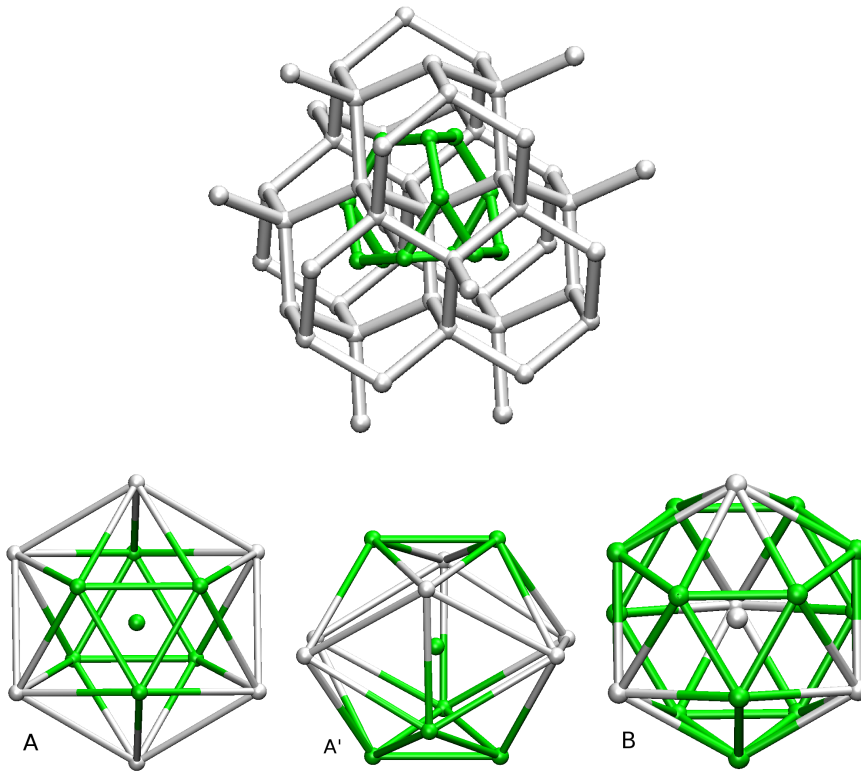
Figure 6.5: The MgZn$_2$ crystal structure of the Wahnström binary Lennard-Jones liquid. The white B particles are arranged in a hexagonal diamond structure, connected with Frank-Kasper bonds (see Figure 6.7). Only first shell green A particles of the central B are shown for clarity. Particles have three kind of first shells shown in the lower part of the figure.

$s_{AA} + s_{AB} + s_{BB} = 5$. These are of the same kind as the bonds of the crystal. This is consistent with the previous conclusion, that the local environment of A particles is similar to that of the crystal. These bonds are not only abundant; they are also the most stable. This is an interesting observation. Some crystal structure is built into the liquid, and, moreover gives stability to the liquid. We will return to this when discussing long-lived structural fluctuations of the liquid, Subsection 6.4.

One BB bond is different from the others, and that is the Frank-Kasper bond (Figure 6.7). As seen in Figure 6.8, there are only about six of these bonds, but when they are there, they are long-lived. The low abundance makes Frank-Kasper bond ideal for investigating the onset of crystallization. Figure 6.9 shows the number of Frank-Kasper bond at the crystallization event and at some points where the liquid experience transient dips in energy. At the onset of crystallization there is, as expected, a large increase of Frank-Kasper bonds. However, also in the meta-stable liquid, large transient clusters of Frank-Kasper bonds appear. If two B particles, having one or more Franks-Kasper bonds, shares A particles, that are a part of these bonds, we will consider the two B
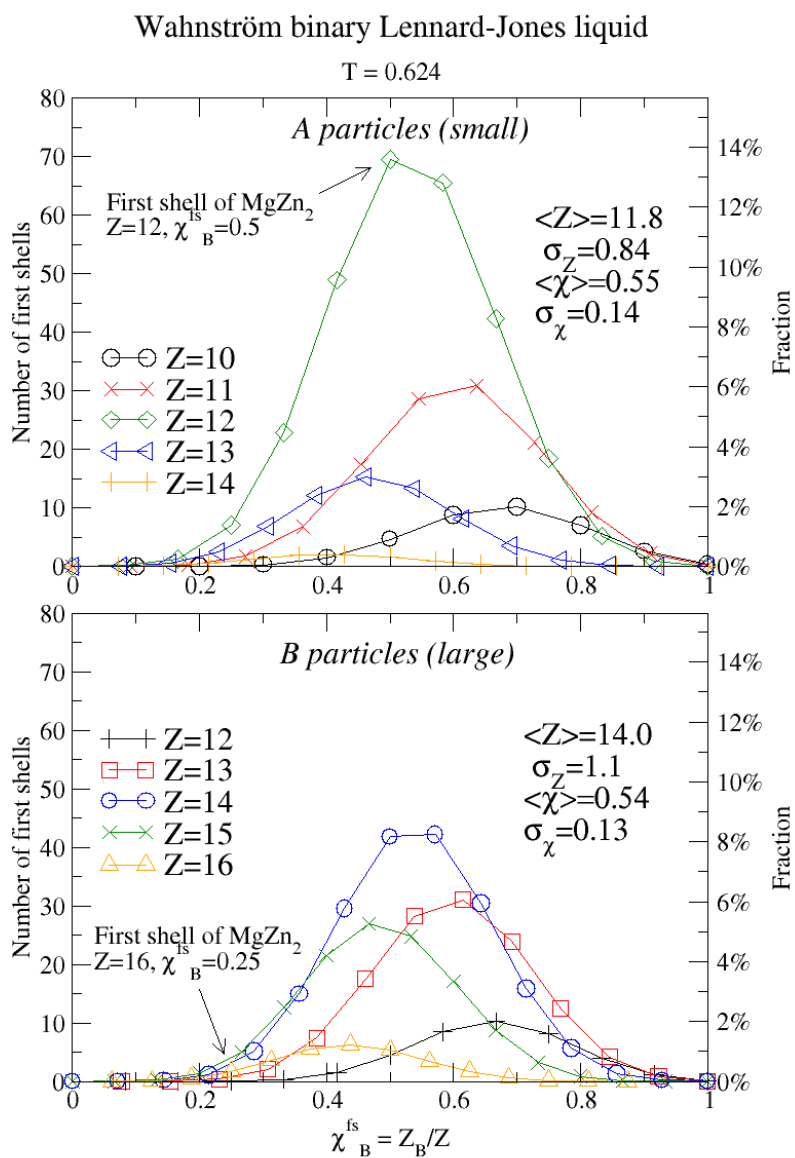
Figure 6.6: Distribution of first shells of Wahnström binary Lennard-Jones liquid. Note that the most frequent first shell of A particles are the same as in the crystal, whereas this is not the case for the B particles.
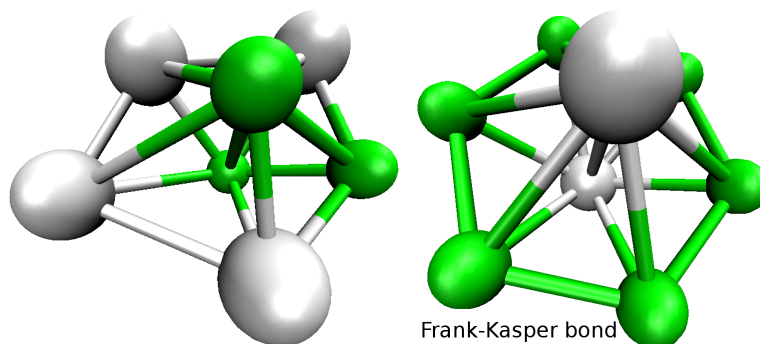
Figure 6.7: Neighboring particles and their common neighbors characterize by six integers, $Rn_A n_B s_{AA} s_{AB} s_{BB}$. The arrangement on the left is a AA pair, $R = 1$, with one common A, $n_A = 1$ and four common B particles, $n_B = 4$. The common neighbors have none AA contacts, $s_{AA} = 0$, two AB contacts, $s_{AA} = 2$, and three BB contacts $s_{BB} = 3$. Thus, this is a 114023-bond. The arrangement on the right is a 360600-bond referred to as a Frank-Kasper bond.

particles to be in the same cluster. Figure 6.10 shows the largest clusters at the transient dips in energy shown in Figure 6.9. Some of the clusters are dense and similar to the crystal, whereas others are open structure not similar to the crystal. Clearly such an open structure hinders crystallization. Also, clusters tend to have (broken) pentagons of Frank-Kasper bonds. This is not a feature of the crystal, and will hinder crystallization. In other words, besides forming the Frank-Kasper bonds, the bonds also have to be arrange in the right way.

The onset of crystallization must be accompanied by a significant composition fluctuation. Figure 6.11 shows the average local composition of B particles with zero to four Frank-Kasper bonds. Note that a substantial part of the composition fluctuation takes place at the formation of just a single Frank-Kasper bond.

We now have a rather complete picture of the crystallization of the Wahnström binary Lennard-Jones liquid. Let us summarize. Local crystalline-like structure of A particles are build into the liquid as distorted icosahedra with $\chi_B^{fs} = 0.5$. However, B particles are not in a local crystalline-like environment. The formation of a Frank-Kasper bond, accompanied by a composition fluctuation sets the onset of a possible crystallization event. A cluster will form, and if it is compact it can continue to grow and eventually lead to non-reversible growth.

6.4 Long-lived structural fluctuations stabilizing the liquid

This section addresses the question: What are the long-lived structural fluctuations stabilizing the metastable liquid? We will address this question by an investigation of the 10% of particles with the longest lifetimes of first shells. Figure 6.12 shows a cluster analysis of these particles. Stable particles are not randomly distributed, but are form extended clusters. With decreasing tem-
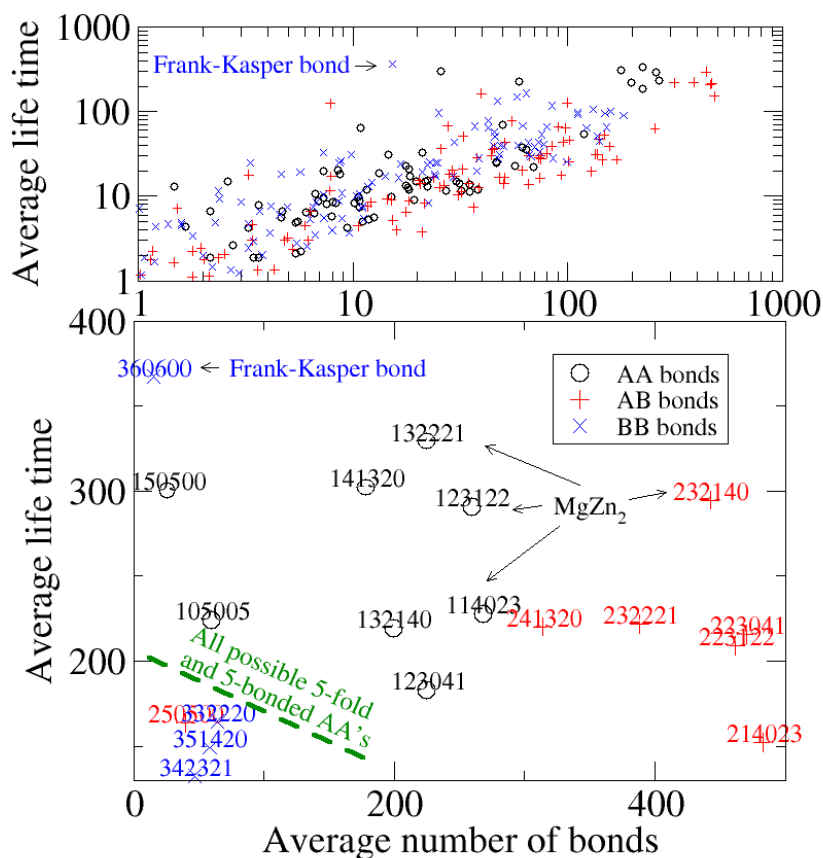
Figure 6.8: Scatter plot of frequency and average lifetime of common neighbor bi-pyramids. See text for more details.

perature the characteristic size of these cluster grow. This is an example of the well-known heterogeneity of viscous liquids [Ediger, 2000].

Figure 6.13 show the first shell distribution of stable particles, relative to the overall distribution. It is possible to identify a particular stable local arrangement: the distorted icosahedra ($Z = 12$) first shells of A particles. Coslovich and Pastore [2007] also note that the frequency of this arrangement grows with decreasing temperature and associated this with the non-Arrhenius growth of the structural relaxation time (although they use a Voronoi construction to investigate neighboring particles, see Figure 5.6). The most stable first shells of B particles are less distinguishable. Nevertheless, a high coordination number tends to give stability. Note that the more crystalline-like the arrangement is, the more stability it gives. In other words, the crystal and the liquid use the same kind of arrangement to get stability. Stability is gained both for the liquid and crystal by the same kind of local packing. This is an interesting observation. Often, properties of the liquid are regarded as disconnected from
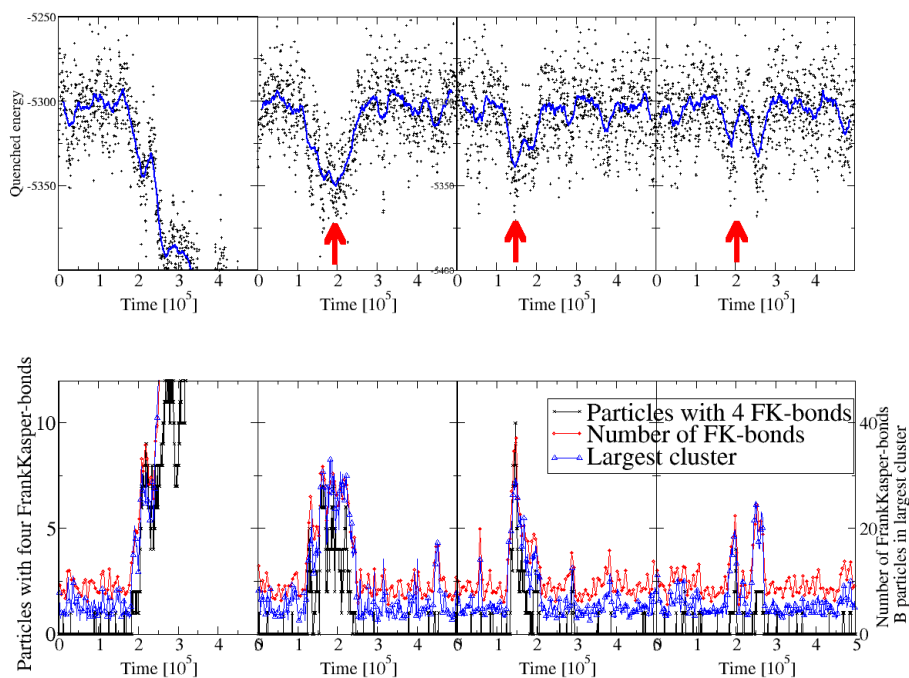
Figure 6.9: The top panels show quenched energy. In Panel 1A the drop in energy is a result of crystallization. In the remaining panels reversible drops in energy are observed. The lower panels show that the drops in energy are accompanied by the formation of extended Frank-Kasper cluster. Clusters at times marked with arrows are shown in Figure 6.10.

the crystal. Here, a connection is demonstrated. The reason why the liquid and crystal can use the same kind of local arrangements is the complexity of the crystal. The locally preferred arrangement can be assembled in many ways, without forming a crystal. The liquid could be said to have "entropic frustration". This phrase is inspired by "geometric frustration", used to explain metastability of the single component Lennard-Jones liquid (in three dimensions[3]). The locally preferred structure of the liquid is a perfect icosahedron. Icosahedra cannot tile space to make a crystal, and the liquid is said to have "geometric frustration" [Sadoc and Mosseri, 1999, Tarjus et al., 2005] (the crystal has the face centered cubic structure). The locally preferred structure of a liquid with entropic frustration can tile space, however, many non-crystal structures can also be build (high entropy). Other systems with some complexity of the crystal could also have entropic frustration.

---

[3]In two dimensions the is no frustration of a single particle liquid. The locally preferred structure is a hexagon. Hexagons can tile space to make a crystal.
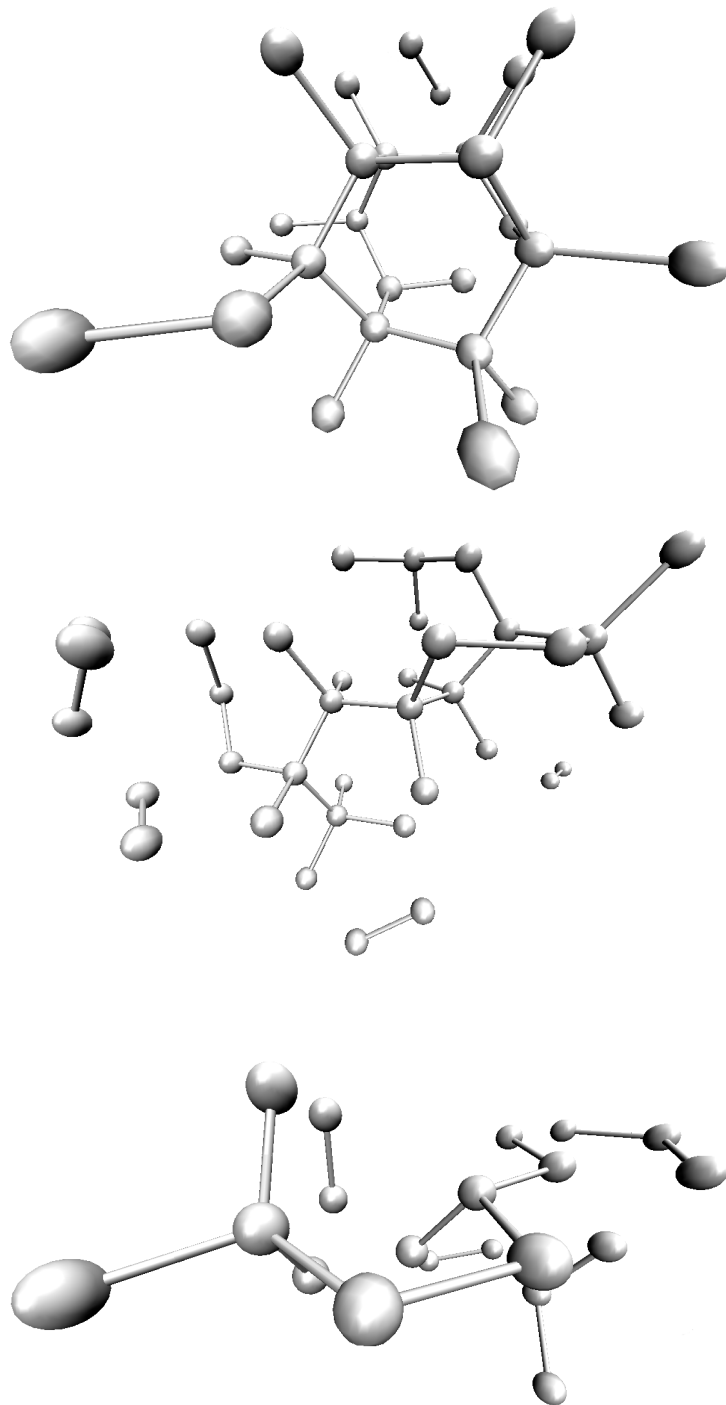
Figure 6.10: Representative transient Frank-Kasper clusters. See the legend of Figure 6.9 for details about the shown clusters. The cluster at the top is dense and similar to the crystal. The middle cluster has a more open structure. Note also the broken pentagon central in the cluster. This is not a feature of the crystal, and will clearly hinder crystallization. The bottom cluster have an even more open structure, not similar to the crystal.
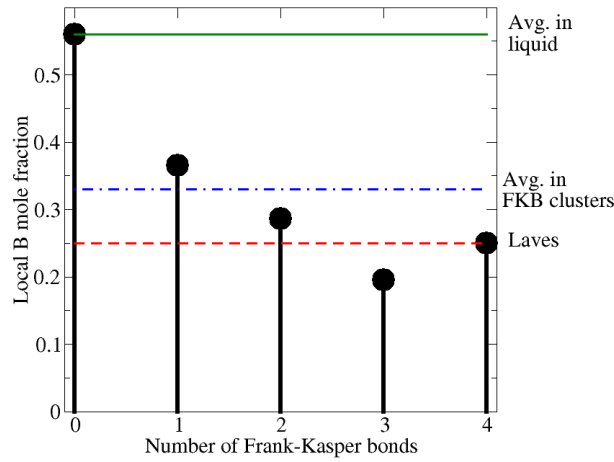
Figure 6.11: Local composition, χ_B^{fs}, of B particles. Note that a large composition fluctuation is associated with the formation of a single Frank-Kasper bond.
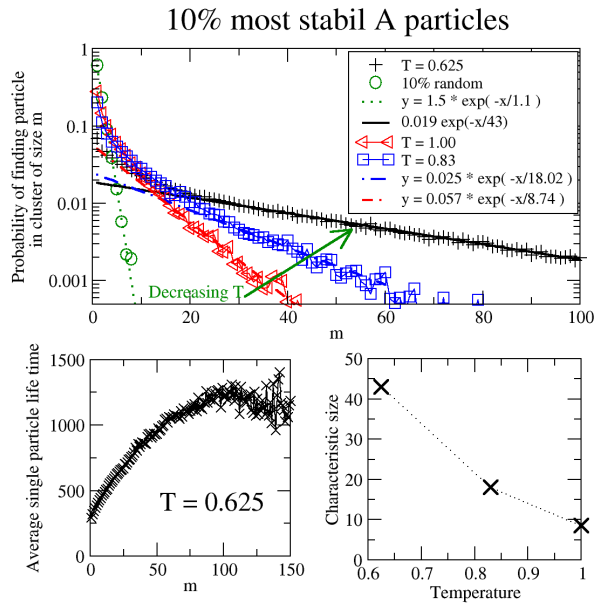
Figure 6.12: Cluster analysis of 10% most long-lived first shells. The top panel shows the cluster distribution at different temperatures. The lower left panel shows that long-lives particles tends to be in large cluster. The lower panel to the right shows that the characteristic cluster size increase when temperature is lowered.
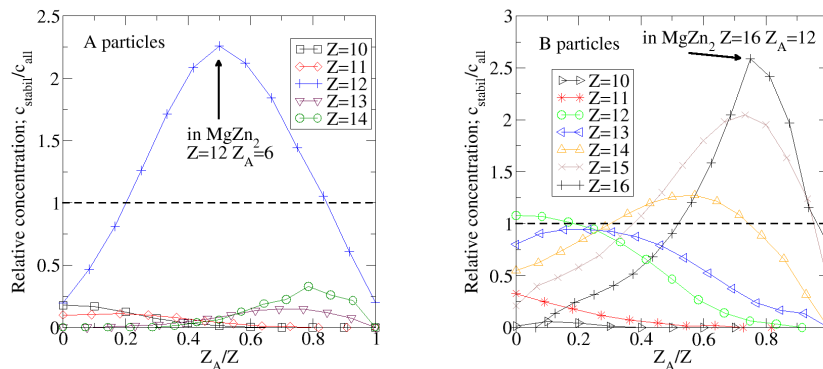
Figure 6.13: First shell of 10% most long-lived first shells. Note that particles with coordination of Z=12 especially stable.

6.5 Kob-Andersen binary Lennard-Jones mixture

The crystallization of the Kob-Andersen binary Lennard-Jones liquid is discussed briefly in the following. The reader is referred to Paper XI for more details.

For both the Wahnström and the Kob-Andersen binary Lennard-Jones liquid the size ratio of particles is about 1.2. However, a difference is that the latter strongly disobeys the Lorentz-Berthelot rule, resulting in a strong AB attraction (see Figure 1.4 on page 6). Usually the Kob-Andersen mixture is simulated at A_4B_1 composition where B refers to the smaller particle[4], but if it is simulated at AB composition it will quickly crystallize in a CsCl structure. Figure 6.14 shows the distribution of first shells of the Kob-Andersen binary Lennard-Jones liquid at the A_4B_1 composition. Note that strong AB attraction reduce composition fluctuations (compare to the Wahnström mixture, Figure 6.6). This prevents the AB crystal from forming at $\chi_B = 0.20$. However, a composition fluctuation can lead to crystallization of A particles in a face centered cubic (FCC) structure as demonstrated by Toxværd et al. [2007, and Paper XI]. Crystallization into a pure FCC crystal of A particles and a mixed CsCl crystal was foreseen by Fernandez and Harrowell [2003]. The FCC crystal is simple with only a single particle in the unit-cell. Thus, the crystal do not have the complexity of the Wahnström binary Lennard-Jones liquid, making the crystallization mechanism simpler.

Crystallization is avoided, if the AA and BB pair potential is truncating at the minimum and leave the AB pair potential untouched (Paper XI, simulations conducted by Søren Toxvaerd). See Paper XI for more details on this.

---

[4]The standard notation is used for classifying small and large particles. For the Wahnström liquid the larger particles are B's and smaller particles are A's. For the Kob-Andersen liquid the standard notation is the opposite so larger particles are A's and smaller particles are B's.
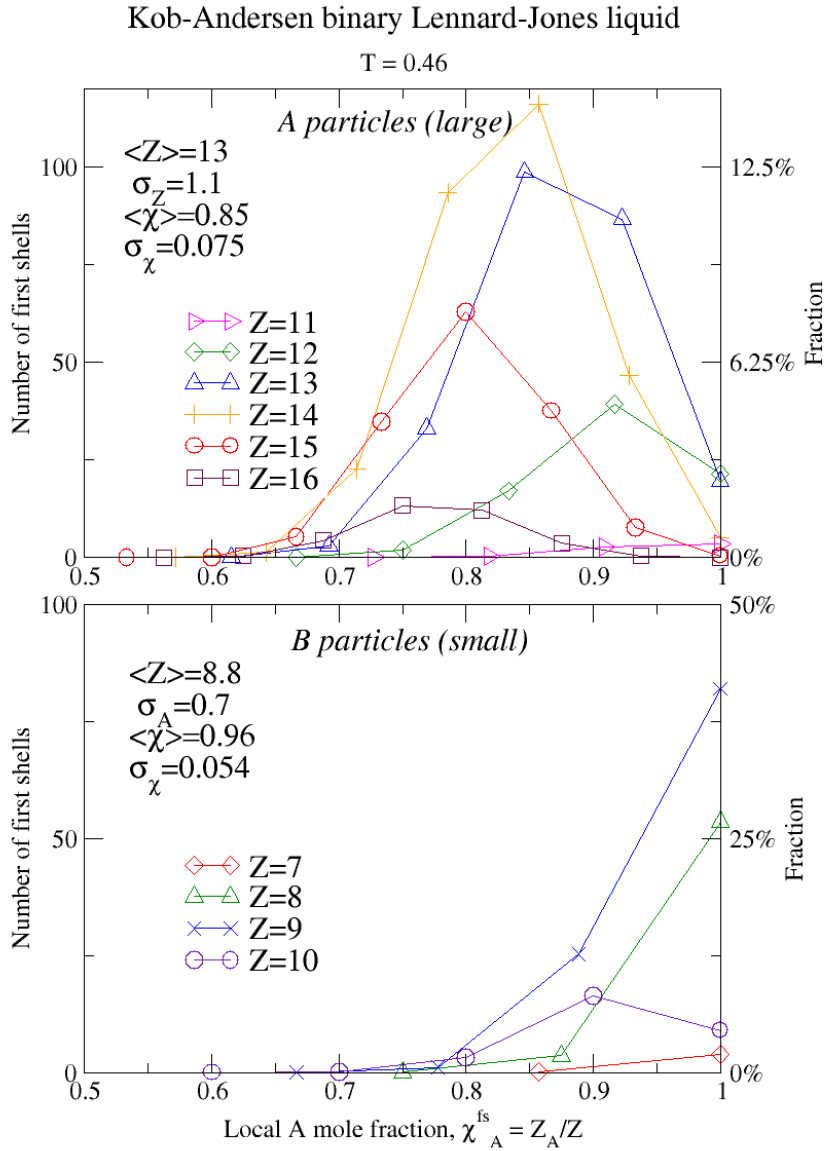
Figure 6.14: First shells of the Kob-Andersen binary Lennard-Jones liquid. Note that local composition fluctuations $\sigma_{\chi_A^{fs}}$ are small compared the Wahnström mixture, Figure 6.6. This is a consequence of strong AB attraction, see text. The most frequent first shells are different from the crystal (CsCl and pure A FCC), see text.

Chapter 7

Outlook

As a summary of the thesis, this chapter provides a list of open questions and future research projects that would be a natural continuation.

A: The model systems investigated (see Figure 2.3 on page 16) in the study of thermodynamic fluctuations do not take quantum effects explicitly into account. First principles molecular dynamics simulations (like the method suggested by Car and Parrinello [1985]), would be valuable to get a better understanding of the thermodynamic correlations of real systems.

B: Strong W-U correlations of the Lennard-Jones liquid are explained by an effective inverse power law (Chapter 3). Paper XIII test and confirms the effective inverse power law explanation for the asymmetric dumbbell model. However, this should also be done for more molecular systems.

C: The revising of the classical Prigogine-Defay ratio supported the conjecture of Section 2.2, that van der Waals bonded liquids are strongly correlating liquids. This raises the question: What other kinds of liquids are strongly correlating? Simulations of the metallic systems Cu and MgCu exhibit correlation coefficients of $R_{WU} = 0.926$ ($T = 2340$ K and $\rho = 125.8$ mol/l) and $R_{WU} = 0.797$ ($T = 650$ K and $\rho = 85$ mol/l) respectively (Paper VIII). The metallic mixture ZrTiCuNiBe has a classic Prigogine-Defay ratio of $\Pi_{pT}^{\text{classic}} = 2.4$, corresponding to a correlation coefficient of $(\Pi_{pT}^{\text{classic}})^{-1/2} = 0.65$. Simulations and experiments can be used to clarify if some metallic systems should be included in the class of strongly correlating liquids.

D: Relaxation of strongly correlating viscous liquids are simpler than that of viscous liquids in general. This has been demonstrated for relaxation of thermodynamic quantities like V, E, p, T. It would be interesting if structural quantities follow the same relaxation. This can be investigated in simulations. In fact, some preliminary studies (data not shown) of the Wahnström binary Lennard-Jones liquid suggest that the number of 12 coordinated A particles, $N_{A^{12}}$, (Section 6.4) follows the (thermodynamic) single parameter. If this is the case, it reasonable to refer to the single parameter as a structural order parameter.

E: Let us assume that $N_{A^{12}}$ follows the (thermodynamic) single parameter. Recall that 12-coordinated A particles were important for the stability of the Wahnström binary Lennard-Jones liquid (Section 6.4). Thus, the single parameter determines how fast the liquid relaxes at a given instant. This may be related to the so-called internal clock of a viscous liquid [Olsen et al., 2008].

F: Values of the static NpT response functions of the glass and liquid at T_g can be found in litterateur for numerous liquids. These values can not only be used to calculate the classical Progogine-Defay ratio (Table 4.1), but also estimate a γ_{WU}-slope (see Subsection 4.1.3 on 40). This estimated γ_{WU} is expected to be equal to γ_s determined from scaling of structural relaxation time (Section 4.2).

G: Figure 4.8 (page 45) shows scaling of the radial distribution function of the Lewis-Wahnström OTP model of two state points with the same Γ. However, the scaling is not perfect as seen in the inset zooming in on the first peak. It is speculated that this is due to intramolecular bonds. This should be investigated further.

H: As discussed in Section 4.1.3, the classical approach of investigating strongly correlating viscous liquids is approximate. Experimentally measured frequency dependent or time dependent response function is a more direct approach. This is an ongoing work of the Glass and Time group.

I: The study of phospholipid membranes demonstrated that strong correlations are present in the slow thermodynamic fluctuations of membranes. One caveat is that $\gamma_{\bar{U}\bar{V}}$ is not the same for the ordered and the disordered phase. This should be investigated further.

J: Other complex systems, where slow dynamics can be traced to a van der Waals bonded region, could have strong thermodynamic correlations (on some time scale). Proteins could be such systems.

K: Chapter 6 reports crystallization of the Lewis-Wahnström OTP model. More work is needed to identify the crystal structure (Figure 6.1) and to undertake a study of the crystallization. A part of this would include defining an orderparameter. Understanding the crystallization mechanism of this one-component system is interesting: Experimentally, OTP shows an interesting mechanics for crystallization close to the glass transition. In the most of the supercooled regime, the growth rate is limited by molecular diffusion. However, Mapes et al. [2006] have reported that close to the glass transition crystal growth is not limited by diffusion, but takes place faster. Apparently, local molecular motion is sufficient for the crystal to form. It is an open question whether the Lewis-Wahnström OTP model exhibits such crystallization mechanism.

L: Investigating the crystallization of the Wahnström binary Lennard-Jones liquid in terms of Frank-Kasper bonds has translated a problem of packing into a problem of forming a network (Section 6.3). However, more work should be made on clarifying which clusters leed to crystallisation and which do not. This investigation may be compared with crystallization of network forming liquids.

Bibliography

C. Alba-Simionesco, A. Cailliaux, A. Alegria, and G. Tarjus. Scaling out the density dependence of the a relaxation in glass-forming polymers. *EUROPHYSICS LETTERS*, 68(1):58–64, OCT 2004. ISSN 0295-5075. doi: 10.1209/epl/i2004-10214-6.

B. Alberts, A. Johnson, J. Lewis, M. Raff, K. Roberts, and P. Walter. *Molecular Biology of the Cell*. Garland, fourth edition, 2002. ISBN 0815332181.

M. P. Allen and D. J. Tildesley. *Computer Simulations of Liquids*. Oxford Science Publications, 1987.

H. C. Andersen, J. D. Weeks, and D. Chandler. Relationship between hard-sphere fluid and fluids with realistic repulsive forces. *Physical Review A: Atomic, Molecular, and Optical Physics*, 4(4):1597, 1971.

C. A. Angell. Relaxations in complex systems. In K. L. Ngai and G. B. Wright, editors, *Strong and fragile liquids*, pages 3–11. U.S. GPO, Washington, D. C., 1985.

P. Atkins and J. de Paula. *Physical Chemistry*. Oxford University Press, 2002.

N. P. Bailey, J. Schiotz, and K. W. Jacobsen. Simulation of Cu-Mg metallic glass: Thermodynamics and structure. *Physical Review B: Condensed Matter and Materials Physics*, 69(14), Apr 2004. ISSN 1098-0121. doi: 10.1103/PhysRevB.69.144205.

R. Becker and W. Doring. Kinetic treatment of germ formation in supersaturated vapour. *Annalen der Physik*, 24(8):719–752, Dec 1935. ISSN 0003-3804.

D. Ben-Amotz and G. Stell. Analytical implementation and critical tests of fluid thermodynamic perturbation theory. *Journal of Chemical Physics*, 119 (20):10777–10788, Nov 22 2003. ISSN 0021-9606. doi: 10.1063/1.1620995.

H. J. C. Berendsen, J. R. Grigera, and T. P. Straatsma. The missing term in effective pair potentials. *Journal of Physical Chemistry*, 91(24):6269–6271, Nov 19 1987. ISSN 0022-3654.

J. I. Berg and A. R. Cooper. Linear Non-Equilibrium Thermodynamic Theory of Glass-Transition Kinetics. *Journal of Chemical Physics*, 68(10):4481–4485, 1978. ISSN 0021-9606.

J. N. Cape and L. V. Woodcock. Glass-transition in a soft-sphere model. *Journal of Chemical Physics*, 72(2):976–985, 1980. ISSN 0021-9606.

R. Car and M. Parrinello. Unified Approach for Molecular-Dynamics and Density-Functional Theory. *Physical Review Letters*, 55(22):2471–2474, 1985. ISSN 0031-9007.

R. Casalini and C. M. Roland. Thermodynamical scaling of the glass transition dynamics. *Physical Review E: Statistical, Nonlinear, and Soft Matter Physics*, 69(6, Part 1), JUN 2004. ISSN 1063-651X. doi: 10.1103/PhysRevE.69.062501.

T. Christensen, N. B. Olsen, and J. C. Dyre. Conventional methods fail to measure c(p)(omega) of glass-forming liquids. *PHYSICAL REVIEW E*, 75 (4, Part 1), Apr 2007. ISSN 1539-3755. doi: 10.1103/PhysRevE.75.041502.

J. H. R. Clarke. Molecular-dynamics studies of glass-formation in the Lennard-Jones model of argon. *Journal of Chemical Society - Faraday Transactions II*, 75(Part 10):1371–1387, 1979. ISSN 0300-9238.

D. Coslovich and G. Pastore. Understanding fragility in supercooled Lennard-Jones mixtures. I. Locally preferred structures. *Journal of Chemical Physics*, 127(12):124504, Sep 28 2007. ISSN 0021-9606. doi: 10.1063/1.2773716.

D. Coslovich and C. M. Roland. Pressure-energy correlations and thermodynamic scaling in viscous Lennard-Jones liquids. *Journal of Chemical Physics*, 130(1):014508, 7 Jan 2009. doi: 10.1063/1.3054635.

D. Coslovich and C. M. Roland. Thermodynamic scaling of diffusion in supercooled Lennard-Jones liquids. *Journal of Physical Chemistry B*, 112(5): 1329–1332, Feb 7 2008. ISSN 1520-6106. doi: 10.1021/jp710457e.

R. O. Davies and G. O. Jones. Thermodynamic and kinetic properties of glasses. *Advances In Physics*, 2(7):370–410, 1953a. ISSN 0001-8732.

R. O. Davies and G. O. Jones. The irreversible approach to equilibrium in glasses. *Proceedings Of The Royal Society Of London Series A: Mathematical And Physical Sciences*, 217(1128):26–42, 1953b.

P. Debenedetti and F. Stillinger. Supercooled liquids and the glass transition. *Nature*, 410(6825):259–267, Mar 8 2001. ISSN 0028-0836.

P. G. Debenedetti. Thermodynamics - When a phase is born. *Nature*, 441 (7090):168–169, May 11 2006. ISSN 0028-0836. doi: 10.1038/441168a.

E. A. DiMarzio. Validity of Ehrenfest relation for a system with more than one order parameter. *Journal of Applied Physics*, 45(10):4143–4145, 1974. ISSN 0021-8979.

D. B. Dingwell, R. Knoche, and S. L. Webb. A volume temperature relationship for liquid GeO_2 and some geophysically relevant derived parameters for network liquids. *Physics and Chemistry of Minerals*, 19(7):445–453, Feb 1993. ISSN 0342-1791.

E.-J. Donth. Der glasübergang. In *Wissenschaftliche Taschenbücher Mathematik-Physik*, volume 271. Akademie-Verlag, Berlin, 1981.

C. Dreyfus, A. Aouadi, J. Gapinski, M. Matos-Lopes, W. Steffen, A. Patkowski, and R. M. Pick. Temperature and pressure study of Brillouin transverse modes in the organic glass-forming liquid orthoterphenyl. *Physical Review E: Statistical, Nonlinear, and Soft Matter Physics*, 68:011204, 2003.

J. C. Dyre. Colloquium: The glass transition and elastic models of glass-forming liquids. *Reviews of Modern Physics*, 78(3):953–972, Jul-Sep 2006. ISSN 0034-6861. doi: 10.1103/RevModPhys.78.953.

S. U. Dzhalilo and K. I. Rzaev. On Phenomenon Of Selenium Vitrification. *Physica Status Solidi*, 20(1):261, 1967. ISSN 0031-8957.

M. Dzugutov. Glass-formation in a simple monatomic liquid with icosahedral inherent local order. *Physical Review A: Atomic, Molecular, and Optical Physics*, 46(6):R2984–R2987, Sep 15 1992. ISSN 1050-2947.

H. Ebel, P. Grabitz, and T. Heimburg. Enthalpy and volume changes in lipid membranes. I. The proportionality of heat and volume changes in the lipid melting transition and its implication for the elastic constants. *Journal of Physical Chemistry B*, 105(30):7353–7360, Aug 2 2001. ISSN 1089-5647. doi: 10.1021/jp010515s.

M. D. Ediger. Spatially heterogeneous dynamics in supercooled liquids. *Annual Review of Physical Chemistry*, 51:99–128, 2000. ISSN 0066-426X.

N. L. Ellegaard. *Energy landscape approaches to the dynamics of supercooled liquids*. PhD thesis, Institut for studiet af Matematik og Fysik samt deres Funktioner i Undervisning, Forskning og Anvendelser (IMFUFA), Roskilde University, Denmark, 2005.

S. E. Feller, Y. H. Zhang, R. W. Pastor, and B. R. Brooks. Constant-Pressure Molecular-Dynamics Simulation - The Langevin Piston Method. *Journal of Chemical Physics*, 103(11):4613–4621, Sep 15 1995. ISSN 0021-9606.

J. R. Fernandez and P. Harrowell. Crystal phases of a glass-forming Lennard-Jones mixture. *Physical Review E: Statistical, Nonlinear, and Soft Matter Physics*, 67(1, Part 1), Jan 2003. ISSN 1063-651X. doi: 10.1103/PhysRevE.67.011403.

M. L. Ferrer, C. Lawrence, B. Demirjian, D. Kivelson, C. Alba-Simionesco, and G. Tarjus. Supercooled liquids and the glass transition: Temperature as the control variable. *Journal of Chemical Physics*, 109(18):8010–8015, Nov 8 1998. ISSN 0021-9606.

N. Foloppe and A. D. MacKerell. All-atom empirical force field for nucleic acids: I. Parameter optimization based on small molecule and condensed phase macromolecular target data. *Journal of Computational Chemistry*, 21 (2):86–104, Jan 30 2000. ISSN 0192-8651.

F. C. Frank and J. S. Kasper. Complex Alloy Structures Regarded as Sphere Packings .1. Definitions and Basic Principles. *Acta Crystallographica*, 11(3): 184–190, 1958. ISSN 0108-7673.

F. C. Frank and J. S. Kasper. Complex Alloy Structures Regarded as Sphere Packing .2. Analysis and Classification of Representative Structures. *Acta Crystallographica*, 12(7):483–499, 1959. ISSN 0108-7673.

M. Goldstein. Validity of Ehrenfest equation for a system with more than one ordering parameter - critique of a paper by Dimarzio. *Journal of Applied Physics*, 46(10):4153–4156, 1975. ISSN 0021-8979.

P. K. Gupta and C. T. Moynihan. Prigogine-Defay ratio for systems with more than one order parameter. *Journal of Chemical Physics*, 65(10):4136–4140, 1976. ISSN 0021-9606.

J. Hadac, P. Slobodian, P. Riha, P. Saha, R. W. Rychwalski, I. Emri, and J. Kubat. Effect of cooling rate on enthalpy and volume relaxation of polystyrene. *Journal of Non-Crystalline Solids*, 353(28):2681–2691, Sep 1 2007. ISSN 0022-3093. doi: 10.1016/j.jnoncrysol.2007.05.017.

J.-P. Hansen and I. McDonald. *Theory of Simple Liquids*. Academic Press, third edition, 2006.

T. Hecksher, A. I. Nielsen, N. B. Olsen, and J. C. Dyre. Little evidence for dynamic divergences in ultraviscous molecular liquids. *Nature Physics*, 4(9): 737–741, Sep 2008. ISSN 1745-2473. doi: 10.1038/nphys1033.

T. Heimburg. Mechanical aspects of membrane thermodynamics. Estimation of the mechanical properties of lipid membranes close to the chain melting transition from calorimetry. *Biochimica et Biophysica Acta, Biomembranes*, 1415(1):147–162, Dec 9 1998. ISSN 0005-2736.

T. Heimburg and A. D. Jackson. On soliton propagation in biomembranes and nerves. *Proceedings of the National Academy of Sciences of the United States of America*, 102(28):9790–9795, Jul 12 2005. ISSN 0027-8424. doi: 10.1073/pnas.0503823102.

T. Heimburg and A. D. Jackson. The thermodynamics of general anesthesia. *Biophysical Journal*, 92(9):3159–3165, May 1 2007. ISSN 0006-3495. doi: 10.1529/biophysj.106.099754.

S. Hensel-Bielowka, M. Paluch, J. Ziolo, and C. M. Roland. Dynamics of sorbitol at elevated pressure. *Journal of Physical Chemistry B*, 106(48): 12459–12463, DEC 5 2002. ISSN 1520-6106. doi: 10.1021/jp0264228.

B. Hess, H. Bekker, H. J. C. Berendsen, and J. G. E. M. Fraaije. LINCS: A linear constraint solver for molecular simulations. *Journal of Computational Chemistry*, 18(12):1463–1472, Sep 1997. ISSN 0192-8651.

A. L. Hodgkin and A. F. Huxley. A Quantitative Description of Membrane Current and its Application to Conduction and Excitation in Nerve. *Journal of Physiology, London*, 117(4):500–544, 1952. ISSN 0022-3751.

J. D. Honeycutt and H. C. Andersen. Small System Size Artifacts in The Molecular-Dynamics Simulation of Homogeneous Crystal Nucleation in Supercooled Atomic Liquids. *Journal of Physical Chemistry*, 90(8):1585–1589, Apr 10 1986. ISSN 0022-3654.

W. G. Hoover. Canonical Dynamics - Equilibrium Phase-Space Distributions. *Physical Review A: Atomic, Molecular, and Optical Physics*, 31(3):1695–1697, 1985. ISSN 1050-2947.

W. G. Hoover and M. Ross. Statistical Theories Of Melting. *Contemporary Physics*, 12(4):339, 1971. ISSN 0010-7514.

W. G. Hoover, M. Roos, K. W. Johnson, D. Henderson, J. A. Barker, and B. C. Brown. Soft-sphere equation of state. *Journal of Chemical Physics*, 52(10):4931, 1970. ISSN 0021-9606.

W. G. Hoover, S. G. Gray, and K. W. Johnson. Thermodynamic Properties of Fluid and Solid Phases force Inverse Power Potentials. *Journal of Chemical Physics*, 55(3):1128, 1971. ISSN 0021-9606.

W. Humphrey, A. Dalke, and K. Schulten. VMD – Visual Molecular Dynamics. *Journal of Molecular Graphics*, 14:33–38, 1996.

K. W. Jacobsen, J. K. Nørskov, and M. J. Puska. Interatomic Interactions In The Effective-Medium Theory. *Physical Review B: Condensed Matter and Materials Physics*, 35(14):7423–7442, May 15 1987. ISSN 0163-1829.

K. W. Jacobsen, P. Stoltze, and J. K. Nørskov. A semi-empirical effective medium theory for metals and alloys. *Surface Science*, 366(2):394–402, Oct 20 1996. ISSN 0039-6028.

W. L. Jorgensen, J. D. Madura, and C. J. Swenson. Optimized intermolecular potential functions for liquid hydrocarbons. *Journal of the American Chemical Society*, 106(22):6638–6646, 1984. ISSN 0002-7863.

L. Kale, R. Skeel, M. Bhandarkar, R. Brunner, A. Gursoy, N. Krawetz, J. Phillips, A. Shinozaki, K. Varadarajan, and K. Schulten. NAMD2: Greater scalability for parallel molecular dynamics. *Journal of Computational Physics*, 151(1):283–312, May 1 1999. ISSN 0021-9991.

W. Kob and H. C. Andersen. Scaling behavior in the β-relaxation regime of a supercooled Lennard-Jones mixture. *Physical Review Letters*, 73(10):1376–1379, Sep 1994. doi: 10.1103/PhysRevLett.73.1376.

W. Kob and H. C. Andersen. Testing mode-coupling theory for a supercooled binary Lennard-Jones mixture I: The van Hove correlation function. *Physical Review E: Statistical, Nonlinear, and Soft Matter Physics*, 51(5):4626–4641, May 1995a. doi: 10.1103/PhysRevE.51.4626.

W. Kob and H. C. Andersen. Testing Mode-Coupling Theory for a Supercooled Binary Lennard-Jones Mixture .2. Intermediate Scattering Function and Dynamic Susceptibility. *Physical Review E: Statistical, Nonlinear, and Soft Matter Physics*, 52(4, Part B):4134–4153, Oct 1995b. ISSN 1063-651X.

J. K. Kummerfeld, T. S. Hudson, and P. Harrowell. The densest packing of AB binary hard-sphere homogeneous compounds across all size ratios. *Journal of Physical Chemistry B*, 112(35):10773–10776, Sep 4 2008. ISSN 1520-6106. doi: 10.1021/jp804953r.

A. Le Grand, C. Dreyfus, C. Bousquet, and R. M. Pick. Scaling of the structural relaxation in simulated liquid silica. *Physical Review E: Statistical, Nonlinear, and Soft Matter Physics*, 75(6, Part 1), Jun 2007. ISSN 1539-3755. doi: 10.1103/PhysRevE.75.061203.

E. W. Lemmon, M. O. McLinden, and D. G. Friend. Thermophysical properties of fluid systems. In P. J. Linstrom and W. G. Mallard, editors, *Chemistry WebBook, NIST Standard Reference Database Number 96*. National Institute of Standards and Technology, Gaithersburg MD, 20899, 2005. URL http://webbook.nist.gov.

J. E. Lennard-Jones. Cohesion. *Proceedings of the Physical Society*, 43(Part 1):461–482, Jan 1931. ISSN 0959-5309.

A. V. Lesikar and C. T. Moynihan. Some relations connecting volume and enthalpy relaxation in the order parameter model of liquids and glasses. *Journal of Chemical Physics*, 72(12):6422–6423, 1980. ISSN 0021-9606.

L. J. Lewis and G. Wahnström. Molecular-dynamics study of supercooled ortho-terphenyl. *Physical Review E: Statistical, Nonlinear, and Soft Matter Physics*, 50(5):3865–3877, Nov 1994. ISSN 1063-651X.

M. W. Mahoney and W. L. Jorgensen. A five-site model for liquid water and the reproduction of the density anomaly by rigid, nonpolarizable potential functions. *Journal of Chemical Physics*, 112(20):8910–8922, May 22 2000. ISSN 0021-9606.

M. Mapes, S. Swallen, and M. Ediger. Self-diffusion of supercooled o-terphenyl near the glass transition temperature. *JOURNAL OF PHYSICAL CHEMISTRY B*, 110(1):507–511, JAN 12 2006. ISSN 1520-6106. doi: 10.1021/jp0555955.

C. T. Moynihan and P. K. Gupta. Order parameter model for structural relaxation in glass. *Journal of Non-Crystalline Solids*, 29(2):143–158, 1978. ISSN 0022-3093.

C. T. Moynihan and A. V. Lesikar. Comparison and analysis of relaxation processes at the glass-transition temperature. *Annals of the New York Academy of Sciences*, 371(Oct):151–169, 1981. ISSN 0077-8923.

C. T. Moynihan, P. B. Macedo, C. J. Montrose, P. K. Gupta, M. A. Debolt, J. F. Dill, B. E. Dom, P. W. Drake, A. J. Easteal, P. B. Elterman, R. P. Moeller, H. Sasabe, and J. A. Wilder. Structural relaxation in vitreous materials. *Annals of the New York Academy of Sciences*, 279(Oct 15):15–35, 1976. ISSN 0077-8923.

M. Naoki, K. Matsumoto, and M. Matsushita. Factors Determining Relaxation-Time and Glass-Transition .2. Triphenylchloromethane Ortho-Terphenyl Mixture. *Journal of Physical Chemistry*, 90(18):4423–4427, Aug 28 1986. ISSN 0022-3654.

S. V. Nemilov. *Thermodynamic and Kinetic Aspects of the Vitreous State*. CRS, London, 1994.

A. I. Nielsen, T. Christensen, B. Jakobsen, K. Niss, N. B. Olsen, R. Richert, and J. C. Dyre. Prevalence of approximate $\sqrt{t}$ relaxation for the dielectric α process in viscous organic liquids. *arXiv*, 0811.1116v1 [cond-mat.soft], 2008. URL http://arxiv.org/abs/0811.1116.

J. K. Nielsen. Linear response theory for thermodynamic properties. *Physical Review E: Statistical, Nonlinear, and Soft Matter Physics*, 60(1):471–481, Jul 1999. ISSN 1063-651X.

L. K. Nielsen, T. Bjornholm, and O. G. Mouritsen. Thermodynamic and real-space structural evidence of a 2D critical point in phospholipid monolayers. *Langmuir*, 23(23):11684–11692, Nov 6 2007. ISSN 0743-7463. doi: 10.1021/la7016352.

T. M. Nieuwenhuizen. Ehrenfest relations at the glass transition: Solution to an old paradox. *Physical Review Letters*, 79(7):1317–1320, Aug 18 1997. ISSN 0031-9007.

T. M. Nieuwenhuizen. Thermodynamic picture of the glassy state. *Journal of Physics: Condensed Matter*, 12(29):6543–6552, Jul 24 2000. ISSN 0953-8984. Workshop on Unifying Concepts in Glass Physics, Trieste, Italy, Sep 15-18, 1999.

S. Nosé. A Molecular-Dynamics Method for Simulations in the Canonical Ensemble. *Molecular Physics*, 52(2):255–268, 1984. ISSN 0026-8976.

H. J. Oels and G. Rehage. Pressure-volume-temperature measurements on atactic polystyrene - thermodynamic view. *Macromolecules*, 10(5):1036–1043, 1977. ISSN 0024-9297.

N. B. Olsen, T. Hecksher, K. Niss, and J. C. Dyre. Physical ageing studied by a device allowing for rapid thermal equilibration. *arXiv.org*, pages arXiv:0811.0994v1 [cond–mat.soft], 2008. URL http://arxiv.org/abs/0811.0994.

A. E. Owen. The glass transition. In N. H. March, R. A. Street, and M. P. Tosi, editors, *Amorphous Solids and The Liquid State*, pages 395–432. Kluwer Academic Publishers Group, 1985.

W. B. Pearson. *The Crystal Chemistry and Physics of Metals and Alloys*. Wiley-Interscience, New York, 1972.

U. R. Pedersen. Strukturelle ændringer af en phospholipidmembran perturberet med n-alkohol undersøgt med md-simuleringer og saxs. Master's thesis, Roskilde University, Postbox 260, DK-4000 Roskilde, Denmark, Dec 2005. In danish. English title: Structural changes of a phospholipidmembran perturbated with n-alcohol investigated by MD-simulations and SAXS.

U. R. Pedersen, C. Leidy, P. Westh, and G. H. Peters. The effect of calcium on the properties of charged phospholipid bilayers. *Biochimica et Biophysica Acta, Biomembranes*, 1758(5):573–582, May 2006. ISSN 0005-2736. doi: 10.1016/j.bbamem.2006.03.035.

U. R. Pedersen, G. H. Peters, and P. Westh. Molecular packing in 1-hexanol-DMPC bilayers studied by molecular dynamics simulation. *Biophysical Chemistry*, 125(1):104–111, Jan 2007. ISSN 0301-4622. doi: 10.1016/j.bpc.2006.07.005.

R. M. Pick. The Prigogine-Defay ratio and the microscopic theory of supercooled liquids. *Journal of Chemical Physics*, 129(12), Sep 28 2008. ISSN 0021-9606. doi: 10.1063/1.2969899.

I. Prigogine and R. Defay. *Chemical thermodynamics*. Longmans, Green and Co, New York, 1954.

R. J. Roe. Thermodynamics of glassy state with multiple order parameters. *Journal of Applied Physics*, 48(10):4085–4091, 1977. ISSN 0021-8979.

C. M. Roland, S. Hensel-Bielowka, M. Paluch, and R. Casalini. Supercooled dynamics of glass-forming liquids and polymers under hydrostatic pressure. *Reports on Progress in Physics*, 68(6):1405–1478, Jun 2005. ISSN 0034-4885. doi: 10.1088/0034-4885/68/6/R03.

C. M. Roland, S. Bair, and R. Casalini. Thermodynamic scaling of the viscosity of van der Waals, H-bonded, and ionic liquids. *Journal of Chemical Physics*, 125(12), Sep 28 2006. ISSN 0021-9606. doi: 10.1063/1.2346679.

C. M. Roland, R. Casalini, R. Bergman, and J. Mattsson. Role of hydrogen bonds in the supercooled dynamics of glass-forming liquids at high pressures. *Physical Review B: Condensed Matter and Materials Physics*, 77(1), Jan 2008. ISSN 1098-0121. doi: 10.1103/PhysRevB.77.012201.

Y. Rosenfeld. A quasi-universal scaling law for atomic transport in simple fluids. *Journal of Physics: Condensed Matter*, 11(28):5415–5427, Jul 19 1999. ISSN 0953-8984.

J. F. Sadoc and R. Mosseri. *Geometric Frustration*. Cambridge University Press, 1999.

K. Samwer, R. Busch, and W. L. Johnson. Change of compressibility at the glass transition and Prigogine-Defay ratio in ZrTiCuNiBe alloys. *Physical Review Letters*, 82(3):580–583, Jan 18 1999. ISSN 0031-9007.

J. W. P. Schmelzer and I. Gutzow. The prigogine-defay ratio revisited. *Journal of Chemical Physics*, 125(18), Nov 14 2006. ISSN 0021-9606. doi: 10.1063/1.2374894.

B. Smit and D. Frenkel. *Understanding Molecular Simulation: from Algorithms to Applications*. Academic Press; 2nd edition (October 15, 2001), second edition, 2001.

J. Sonne, M. O. Jensen, F. Y. Hansen, L. Hemmingsen, and G. H. Peters. Reparameterization of all-atom dipalmitoylphosphatidylcholine lipid parameters enables simulation of fluid bilayers at zero tension. *Biophysical Journal*, 92(12):4157–4167, Jun 2007. ISSN 0006-3495. doi: 10.1529/biophysj.106.087130.

M. R. Spiegel and J. Liu. Mathematical handbook of formulars and tables. In *Schaum's Outline Series*. McGraw-Hill, 2nd edition, 1999.

F. Stein, M. Palm, and G. Sauthoff. Structure and stability of Laves phases. Part I. Critical assessment of factors controlling Laves phase stability. *Intermetallics*, 12(7-9, Sp. Iss. SI):713–720, Jul-Sep 2004. ISSN 0966-9795. doi: 10.1016/j.intermet.2004.02.010.

F. Stein, A. Palm, and G. Sauthoff. Structure and stability of Laves phases part II - structure type variations in binary and ternary systems. *Intermetallics*, 13(10):1056–1074, Oct 2005. ISSN 0966-9795. doi: 10.1016/j.intermet.2004.11.001.

S. Takahara, M. Ishikawa, O. Yamamuro, and T. Matsuo. Structural relaxations of glassy polystyrene and o-terphenyl studied by simultaneous measurement of enthalpy and volume under high pressure. *Journal of Physical Chemistry B*, 103(5):792–796, Feb 4 1999. ISSN 1089-5647.

G. Tarjus, S. A. Kivelson, Z. Nussinov, and P. Viot. The frustration-based approach of supercooled liquids and the glass transition: a review and critical assessment. *Journal of Physics: Condensed Matter*, 17(50):R1143–R1182, Dec 21 2005. ISSN 0953-8984. doi: 10.1088/0953-8984/17/50/R01.

P. R. ten Wolde and D. Frenkel. Computer simulation study of gas-liquid nucleation in a Lennard-Jones system. *Journal of Chemical Physics*, 109 (22):9901–9918, Dec 8 1998. ISSN 0021-9606.

D. P. Tieleman and H. J. C. Berendsen. Molecular dynamics simulations of a fully hydrated dipalmitoyl phosphatidylcholine bilayer with different macroscopic boundary conditions and parameters. *Journal of Chemical Physics*, 105(11):4871–4880, Sep 15 1996. ISSN 0021-9606.

A. Tölle. Neutron scattering studies of the model glass former ortho-terphenyl. *Reports on Progress in Physics*, 64(11):1473–1532, Nov 2001. ISSN 0034-4885.

S. Toxværd, T. B. Schrøder, and J. C. Dyre. Crystallization of the Kob-Andersen binary Lennard-Jones liquid. *arXiv*, 0712.0377v2 [cond-mat.soft], Dec 2007. URL http://arxiv.org/abs/0712.0377.

D. van der Spoel, E. Lindahl, B. Hess, A. R. van Buuren, E. Apol, P. J. Meulenhoff, D. P. Tieleman, A. L. Sijbers, K. A. Feenstra, R. van Drunen, and H. J. Berendsen. *GROMACS user manual version 3.3*, 2006. URL www.gromacs.org.

W. F. van Gunsteren, S. R. Billeter, A. A. Eising, P. H. Hunenberger, P. Kruger, A. E. Mark, W. R. P. Scott, and I. G. Tironi. *Biomolecular simulation: The GROMOS96 manual and user guide*. vdf Hochschulverlag AG an der ETH Zurich and BIOMOS b.v., Zurich, Groningen, 1996.

R. M. Venable, B. R. Brooks, and R. W. Pastor. Molecular dynamics simulations of gel (L-beta I) phase lipid bilayers in constant pressure and constant surface area ensembles. *Journal of Chemical Physics*, 112(10):4822–4832, Mar 8 2000. ISSN 0021-9606.

M. Volmer and A. Weber. Germ-formation in oversaturated figures. *Zeitschrift für Physikalische Chemie–Stochiometrie und Verwandtschaftslehre*, 119(3/4): 277–301, Mar 1926. ISSN 0372-8501.

G. Voronoi. New parametric applications concerning the theory of quadratic forms - second announcement. *Journal für die Reine und Angewandte Mathematik*, 134:198–287, 1908.

G. Wahnström. Molecular-Dynamics Study of a Supercooled 2-Component Lennard-Jones System. *Physical Review A: Atomic, Molecular, and Optical Physics*, 44(6):3752–3764, Sep 15 1991. ISSN 1050-2947.

L. Wondraczek and H. Behrens. Molar volume, excess enthalpy, and Prigogine-Defay ratio of some silicate glasses with different (P,T) histories. *Journal of Chemical Physics*, 127(15), Oct 21 2007. ISSN 0021-9606. doi: 10.1063/1.2794745.

E. Zaccarelli, G. Foffi, K. A. Dawson, S. V. Buldyrev, F. Sciortino, and P. Tartaglia. Confirmation of anomalous dynamical arrest in attractive colloids: A molecular dynamics study. *Physical Review E: Statistical, Nonlinear, and Soft Matter Physics*, 66(4, Part 1), Oct 2002. ISSN 1063-651X. doi: 10.1103/PhysRevE.66.041402.

E. Zaccarelli, F. Sciortino, and P. Tartaglia. Numerical study of the glass-glass transition in short-ranged attractive colloids. *Journal of Physics: Condensed Matter*, 16(42, Sp. Iss. SI):S4849–S4860, Oct 27 2004. ISSN 0953-8984. doi: 10.1088/0953-8984/16/42/004. Workshop on Structural Arrest Transitions in Colloidal Systems with Short-Range Attractions, Messina, ITALY, DEC 17-20, 2003.

R. T. Zhang, W. J. Sun, S. Tristramnagle, R. L. Headrick, R. M. Suter, and J. F. Nagle. Critical Fluctuations in Membranes. *Physical Review Letters*, 74(14):2832–2835, Apr 3 1995. ISSN 0031-9007.

P. Zoller. A study of the pressure-volume-temperature relationships of four related amorphous polymers: Polycarbonate, polyarylate, phenoxy, and polysulfone. *Journal of Polymer Science, Part B: Polymer Physics*, 20:1453–1464, 1982. doi: 10.1002/pol.1982.180200811.

Appendix A

Calculations

A.1 Energy-pressure correlations in a soft-sphere liquid

In soft-sphere liquid where particles interact via a inverse power-law potential [1];

$$U_{ij}^{pow} = a_{ij} r_{ij}^{-n}. \tag{A.1}$$

where r_{ij} is the distance between particle i and j, and $a_{i,j}$'s and b are constants. The total potential energy of a system of N particles is

$$U^{pow} = \sum_{i>j}^{N} U_{ij}^{pow} \tag{A.2}$$

The virial is given by

$$W = \frac{1}{3} \sum_{ih} r_{ij} F_{ij} \tag{A.3}$$

where

$$F_{ij} = -\frac{d}{dr} U_{ij} = n a_{ij} r_{ij}^{-n} \tag{A.4}$$

is the force between particle i and j. Thus, virial is proportional to potential energy,

$$W^{pow}(t) = \gamma_{WU}^{pow} U^{pow}(t), \tag{A.5}$$

with a proportionality constant of

$$\gamma_{WU}^{pow} = n/3. \tag{A.6}$$

A.2 Fitting inverse power-law to the generalized Lennard-Jones potential

At distance r_s ($r_s < 1$) we can fit and inverse power-law plus a constant,

$$U_{ij}^{pow} = a r^{-p} + c, \tag{A.7}$$

---

[1]Note that we here uses index ij on the prefactor a_{ij} for the sake of generality. So perfect correlation goes for a poly-disperse system as well as a mono-disperse.

to the generalized Lennard-Jones potential (having a global minimum of -1 at $r = 1$),

$$U_{ij}^{LJ} = (nr^{-m} - mr^{-n})/(m - n), \tag{A.8}$$

by matching pair energy (U_{ij}), virial ($W_{ij} = -r\frac{d}{dr}U_{ij}$) and hyper-virial ($X_{ij} = -r\frac{d}{dr}W_{ij}$). First, put $\frac{X_{ij}^{\text{LJ}}(r_s)}{W_{ij}^{\text{LJ}}(r_s)} = \frac{X_{ij}^{\text{pow}}(r_s)}{W_{ij}^{\text{pow}}(r_s)}$ and isolate the exponent,

$$p = (mr_s^{-m} - nr_s^{-n})/(r_s^{-m} - r_s^{-n}). \tag{A.9}$$

Then put $W_{ij}^{\text{LJ}}(r_s) = W_{ij}^{\text{pow}}(r_s)$ and isolate the pre-factor,

$$a = mn(r_s^{-m} - r_s^{-n})/[(m - n)pr_s^{-p}]. \tag{A.10}$$

Finaly put $U_{ij}^{\text{LJ}}(r_s) = U_{ij}^{\text{pow}}(r_s)$ to get the constant,

$$c = (nr_s^{-m} - mr_s^{-n})/(m - n) - ar_s^{-p}. \tag{A.11}$$

If p is known and not r_s, then isolate r_s from equation A.9,

$$r_s = [(n - p)/(m - p)]^{1/(n-m)}. \tag{A.12}$$

The inverse power-law fitted to the standard Lennard-Jones potential (with $m = 12$ and $n = 6$) at the characteristic distance $r_s = 2^{-1/6}$ where $U_{ij}^{LJ}(r_s) = 0$ is

$$U_{ij}^{pow} = \frac{1}{6}r^{-18} + \frac{4}{3}. \tag{A.13}$$

Rescaling the Lennard-Jones potential to get the minimum to $2^{1/6}$ ($r' = 2^{1/6}r$) we get

$$U_{ij}^{pow} = \frac{4}{3}r'^{-18} + \frac{4}{3} \tag{A.14}$$

shown on Figure 3.1 page 20.

Appendix B

Papers

Single-order-parameter description of glass-forming liquids: A one-frequency test

Niels L. Ellegaard, Tage Christensen, Peder Voetmann Christiansen, Niels Boye Olsen, Ulf R. Pedersen, Thomas B. Schrøder, and Jeppe C. Dyre
DNRF Centre "Glass and Time," IMFUFA (27), Department of Sciences, Roskilde University, Postbox 260, DK-4000 Roskilde, Denmark

Thermoviscoelastic linear-response functions are calculated from the master equation describing viscous liquid inherent dynamics. From the imaginary parts of the frequency-dependent isobaric specific heat, isothermal compressibility, and isobaric thermal expansion coefficient, we define a "linear dynamic Prigogine-Defay ratio" $\Lambda_{Tp}(\omega)$ with the property that if $\Lambda_{Tp}(\omega) = 1$ at one frequency, then $\Lambda_{Tp}(\omega)$ is unity at all frequencies. This happens if and only if there is a single-order-parameter description of the thermoviscoelastic linear responses via an order parameter (which may be nonexponential in time). Generalizations to other cases of thermodynamic control parameters than temperature and pressure are also presented. © *2007 American Institute of Physics.*
[DOI: 10.1063/1.2434963]

I. INTRODUCTION

A famous result of classical glass science is that if a glass-forming liquid is described by a single-order-parameter, the Prigogine-Defay ratio is unity. Recall that if Δc_p is the difference between liquid and glass isobaric specific heat per unit volume at the glass transition temperature T_g, $\Delta \kappa_T$ the similar liquid-glass difference of isothermal compressibilities, and $\Delta \alpha_p$ the difference of isobaric thermal expansion coefficients, the Prigogine-Defay ratio Π is defined[1–3] by

$$\Pi = \frac{\Delta c_p \Delta \kappa_T}{T_g (\Delta \alpha_p)^2}. \tag{1}$$

Both experimentally and theoretically the following inequality was established early on: $\Pi \geq 1$.[1–9] The vast majority of reported Π's are significantly larger than unity,[10] and for decades the consensus has been that—possibly with a few exceptions[11,12]—a single-order parameter is not sufficient for describing glass-forming liquids.

The above picture came about as follows. The glass transition is a freezing of configurational degrees of freedom. If kinetic aspects are ignored, the glass transition has the appearance of a second-order phase transition in the Ehrenfest sense with continuity of volume and entropy, but discontinuity of their thermodynamic derivatives. If the "order parameters" (numbers characterizing the structure) are denoted by $z_1, \ldots, z_k$, these are frozen in the glass phase. In the equilibrium liquid phase the order parameters depend on pressure and temperature, a dependence that is determined by minimizing Gibbs free energy $G(T, p, z_1, \ldots z_k)$: $\partial G / \partial z_i = 0$.[3] In the classical papers by Davies and Jones from the 1950s[1,2] it was shown that within this framework one always has $\Pi \geq 1$ and that $\Pi = 1$ if there is just a single-order parameter. The simplest dynamics for the approach to equilibrium for the order parameters $\dot{z}_i = -\Lambda_i \partial G / \partial z_i$ imply exponential decays for each order parameter for small perturbations from

equilibrium. Under this assumption, in the case of just one order parameter any quantity relaxes exponentially to equilibrium after a small disturbance. Exponential relaxations of the macroscopic variables are seldom observed, although there is evidence that relaxation is often intrinsically exponential so that the nonexponential behavior comes from a distribution of exponential relaxations.[13–15] This reflects dynamic heterogeneity. Historically the fact that macroscopic relaxations are nonexponential was often taken as confirming the conventional wisdom that one order parameter is rarely not enough.—Besides the reported Prigogine-Defay ratios being almost always significantly larger than unity, a further classical argument for the necessity of more than one order parameter is the following:[16] If structure were characterized by a single-order parameter, glasses with the same index of diffraction would also have all other physical properties identical, which is not the case. This does not rule out the possibility that a single-order parameter is sufficient to describe the linear thermoviscoelastic response of the viscous liquid phase, however, and it is this possibility we shall inquire into in the present paper.

Because kinetic aspects cannot be ignored, the glass transition is not a phase transition. Thus, there is no exact T_g and strictly speaking the Π of Eq. (1) is not well defined. This is because the properties of a glass depend to some extent on the cooling history; moreover, extrapolations from the glass phase are somewhat ambiguous because glass properties change slightly with time. Thus the changes in specific heat, etc., found by extrapolating glass and liquid specific heats from below and above, respectively, to T_g (Ref. 17) are not rigorously well defined. This weakens the generally accepted conclusion that in the vast majority of cases there must be more than one order parameter.

The problem of making the Prigogine-Defay ratio rigorously well defined is solved by referring exclusively to linear-response experiments on the equilibrium viscous liq-

uid phase.[16,18,19] In viscous liquids, thermodynamic coefficients are generally frequency dependent, $c_p = c_p(\omega)$, etc. The high-frequency limits reflect glassy behavior where relaxations do not have enough time to take place, corresponding to "frozen" structure. Thus for the equilibrium viscous liquid phase at any given temperature T one redefines Eq. (1) to be the "linear Prigogine-Defay ratio" given[16,18,19] by

$$\Pi = \frac{[c_p(\omega \to 0) - c_p(\omega \to \infty)][\kappa_T(\omega \to 0) - \kappa_T(\omega \to \infty)]}{T[\alpha_p(\omega \to 0) - \alpha_p(\omega \to \infty)]^2}. \tag{2}$$

Descriptions of viscous liquids and the glass transition by means of one or more order parameter were actively discussed in the 1970s.[16,18–22] Since the Π of Eq. (1) is not well defined and since there are no measurements of the linear Prigogine-Defay ratio of Eq. (2), the question of one or more order parameters remains open.[23,24] In our view, there are a number of reasons to take seriously the possibility that some glass-forming liquids may be described by a single order parameter: (1) In early computer simulations Clarke reported Prigogine-Defay ratios close to one for a 216 particle Lennard-Jones model of Argon.[25] This is not a highly viscous liquid, but recent extensive simulations by Sciortino and coworkers of viscous liquids confirmed this scenario by showing that structural relaxations for small temperature changes are basically controlled by a single parameter (e.g., the volume).[26–29] (2) Experiments monitoring loss peak frequency and loss maximum of the Johari-Goldstein dielectric beta relaxation process upon temperature jumps revealed a striking correlation between these two quantities, a correlation which is difficult to explain unless structure is parametrized by a single-order parameter.[30] In these experiments the relaxation of beta process properties is controlled by the alpha relaxation time. This is to be expected because the alpha time is the structural relaxation time, but it is highly nontrivial that alpha and beta relaxations correlate in equilibrium viscous liquids, as shown recently by Böhmer and coworkers;[31] this may be taken as a further indication that a single order parameter controls the behavior. (3) Experiments studying dielectric relaxation under varying temperature and pressure conditions showed that the shape of the alpha loss peak as quantified by the stretching exponent β depends only on the loss peak frequency.[32] This could be a consequence of there being just one order parameter, determining both alpha relaxation time and stretching. (4) Finally, we would like to mention theoretical works suggesting that the Prigogine-Defay ratio may be unity in some cases.[23,33,34] More speculatively, in our opinion it would not be too surprising if there is just one order parameter for liquids where time-temperature superposition applies accurately, because in these liquids linear relaxations appear to be particularly simple with a generic $\omega^{-1/2}$ high-frequency decay of, e.g., the dielectric and mechanical alpha loss peaks.[35,36]

The wide-frequency measurements required to determine Π of Eq. (2) will probably be difficult to perform in the foreseeable future. There are, in fact, no measurements of all three required frequency-dependent thermoviscoelastic linear-response functions. Work at our laboratory indicates that such measurements are possible,[37] but only over a limited frequency range. This motivates a search for an alternative to the linear Prigogine-Defay ratio. In this article, we introduce a "linear dynamic Prigogine-Defay ratio" (where the double prime indicates the imaginary part of the corresponding frequency-dependent linear-response function):

$$\Lambda_{Tp}(\omega) = \frac{c_p''(\omega)\kappa_T''(\omega)}{T_0(\alpha_p''(\omega))^2}. \tag{3}$$

Based on the description of viscous liquid dynamics in terms of Markovian inherent dynamics, in Secs. II and III we prove that $\Lambda_{Tp}(\omega) = 1$ if and only if the linear Prigogine-Defay ratio [Eq. (2)] is unity. This happens if and only if there is a single, generally nonexponential order parameter. Moreover, it is proved that if $\Lambda_{Tp}(\omega) = 1$ at one frequency, this is true at all frequencies. In Sec. IV we investigate the matter in a thermodynamic approach and prove that in this framework the existence of a single-order parameter implies that $\Lambda_{Tp}(\omega) = 1$ at all frequencies. In the Appendix it is shown that $\Lambda_{Tp}(\omega)$ is just one out of a family of four linear dynamic Prigogine-Defay ratios larger than or equal to one, which equal unity if and only if there is a single order parameter.

II. RESPONSE MATRIX FOR MARKOVIAN INHERENT DYNAMICS

Adopting the energy landscape approach to viscous liquid dynamics[38] we model the liquid (henceforth: "system") by the inherent dynamics consisting of jumps between the potential energy minima.[29,39–41] This description is believed to be realistic in the highly viscous phase where there is a clear separation between the vibrational time scales (in the picosecond range) and the (alpha) relaxation time scale—the time scale of interest here. If the system has N potential energy minima, an ensemble of similar systems is described by a vector of probabilities $\mathbf{P} = (P_1, P_2, \ldots, P_N)$, where P_n denotes the fraction of systems vibrating around energy minimum n. If $G_n(T, p)$ denotes the vibrational Gibbs free energy of minimum n, the $\mathbf{P}$-dependent Gibbs free energy is defined[39] by

$$G(T, p, \mathbf{P}) = \sum_n P_n(G_n(T, p) + k_B T \ln P_n). \tag{4}$$

Via the standard thermodynamic identities the $\mathbf{P}$-dependent entropy S and volume V are given by

$$S(T, p, \mathbf{P}) = -\sum_n P_n\left(\frac{\partial G_n}{\partial T} + k_B \ln P_n\right),$$

$$V(T, p, \mathbf{P}) = \sum_n P_n \frac{\partial G_n}{\partial p}. \tag{5}$$

It is convenient to introduce the notation $\mathbf{X} = (T, -p)$ for the controlled ("input") variables and $\mathbf{Q} = (S, V)$ for the induced responses ("output"). Thus

$$Q_\alpha = -\frac{\partial G}{\partial X_\alpha}, \quad \alpha = 1, 2. \tag{6}$$

The equilibrium probability distribution is found by minimizing $G(T, p, \mathbf{P})$ under the constraint $\Sigma_n P_n = 1$; this leads[42] to the well-known canonical probabilities (where $G(T, p)$ is the Gibbs free energy of Eq. (4) evaluated at the equilibrium probabilities)

$$P_n^{eq}(T, p) = \exp\left(-\frac{G_n(T, p) - G(T, p)}{k_B T}\right). \tag{7}$$

Inherent dynamics consist of transitions between minima.[41] The inherent dynamics are modeled as a Markov process; thus the probabilities obey a standard master equation[43]

$$\dot{P}_n = \sum_m W_{nm} P_m. \tag{8}$$

The rate matrix W and the equilibrium probability distribution P_n^{eq} both depend on T and p, and for all n one has

$$\sum_m W_{nm}(T, p) P_m^{eq}(T, p) = 0. \tag{9}$$

In the following the variables T and p are assumed to vary slightly from their average values T_0 and p_0 as arbitrary externally-controlled functions of time, resulting in small changes of S and V. Examining perturbations around the reference state $\mathbf{X}_0 = (T_0, -p_0)$ it is convenient to introduce the notation $W_{nm}^0 \equiv W_{nm}(T_0, p_0)$ and $P_n^0 \equiv P_n^{eq}(T_0, p_0)$. If δ denotes perturbations from the reference state, $P_n(t) = P_n^0 + \delta P_n(t)$, etc., Eq. (8) implies to first order

$$\delta \dot{P}_n = \sum_m (W_{nm}^0 \delta P_m + \delta W_{nm} P_m^0). \tag{10}$$

Since $\delta(\Sigma_m W_{nm} P_m^{eq}) = 0$ [Eq. (9)], one has $\Sigma_m \delta W_{nm} P_m^0 = -\Sigma_m W_{nm}^0 \delta P_m^{eq}$. When this is substituted into Eq. (10) we get

$$\delta \dot{P}_n = \sum_m W_{nm}^0 (\delta P_m - \delta P_m^{eq}). \tag{11}$$

Next, we expand δP_m^{eq} in terms of δX_α. Equations (5) and (7) imply[44] (where $\beta = 1, 2$ and $\delta_{\beta 1}$ is the Kronecker delta symbol)

$$\frac{\partial \ln P_m^{eq}}{\partial X_\beta} = \frac{1}{k_B T}\left(\frac{\partial Q_\beta}{\partial P_m} - Q_\beta + \delta_{\beta 1} k_B\right). \tag{12}$$

Thus to lowest order

$$\delta P_m^{eq} = \frac{P_m^0}{k_B T_0}\left[\left(\frac{\partial Q_1}{\partial P_m} - Q_1 + k_B\right)\delta X_1 + \left(\frac{\partial Q_2}{\partial P_m} - Q_2\right)\delta X_2\right]. \tag{13}$$

Inserting this into Eq. (11) and utilizing Eq. (9) we arrive at the following "equation of motion" for the probabilities when temperature and pressure vary slightly as arbitrary functions of time [$\delta X_\beta \equiv \delta X_\beta(t)$]:

$$\delta \dot{P}_n = \sum_m W_{nm}^0 \left(\delta P_m - \frac{1}{k_B T_0} \sum_\beta P_m^0 \frac{\partial Q_\beta}{\partial P_m} \delta X_\beta\right). \tag{14}$$

Consider now a harmonic linear perturbation of the system. In relaxing systems like glass-forming liquids the ordinary thermodynamic response functions are frequency dependent and complex. Writing $T(t) = T_0 + \text{Re}(\delta T \, e^{i\omega t})$ and $p(t) = p_0 + \text{Re}(\delta p \, e^{i\omega t})$, the oscillations of S and V are similarly described by $S(t) = S_0 + \text{Re}(\delta S \, e^{i\omega t})$ and $V(t) = V_0 + \text{Re}(\delta V \, e^{i\omega t})$. If δP_n and δX_β denote the (complex) frequency-dependent amplitudes, in steady state Eq. (14) implies that

$$\sum_n (W_{ln}^0 - i\omega\delta_{ln})\delta P_n = \frac{1}{k_B T_0}\sum_{m,\beta} W_{lm}^0 P_m^0 \frac{\partial Q_\beta}{\partial P_m}\delta X_\beta. \tag{15}$$

For $\omega > 0$ we solve Eq. (15) by defining (where I is the identity matrix)

$$A_{nm}(\omega) = \frac{1}{k_B T_0}\sum_l (W^0 - i\omega I)_{nl}^{-1} W_{lm}^0 P_m^0, \tag{16}$$

leading to the following equation for the frequency-dependent complex probability amplitudes:

$$\delta P_n = \sum_{m,\beta} A_{nm}(\omega)\frac{\partial Q_\beta}{\partial P_m}\delta X_\beta. \tag{17}$$

In order to calculate the thermoviscoelastic linear-response functions we first define $J_{\alpha\beta}^\infty = (\partial Q_\alpha / \partial X_\beta)$. This symmetric 2×2 matrix gives the instantaneous (glassy) linear response because it determines the variations of S and V when the probabilities P_n are frozen.[39] Next, we expand the frequency-dependent complex amplitudes δQ_α to get

$$\delta Q_\alpha = \sum_n \frac{\partial Q_\alpha}{\partial P_n}(T_0, p_0)\delta P_n + \sum_\beta J_{\alpha\beta}^\infty \delta X_\beta. \tag{18}$$

Here and henceforth, for any function f the notation $f(T_0, p_0)$ for a variable that also depends on the probabilities $\mathbf{P}$ signifies that f is evaluated at the equilibrium probabilities [Eq. (7)]. When Eq. (17) is inserted into Eq. (18), we get

$$\delta Q_\alpha = \sum_\beta J_{\alpha\beta}(\omega)\delta X_\beta, \tag{19}$$

where

$$J_{\alpha\beta}(\omega) = J_{\alpha\beta}^\infty + \sum_{m,n} \frac{\partial Q_\alpha}{\partial P_n}(T_0, p_0) A_{nm}(\omega)\frac{\partial Q_\beta}{\partial P_m}(T_0, p_0). \tag{20}$$

Since $A_{nm}(\omega \to \infty) = 0$ it follows that $J_{\alpha\beta}(\omega \to \infty) = J_{\alpha\beta}^\infty$, justifying the notation.

We proceed to show that the 2×2-matrix $J_{\alpha\beta}(\omega)$ is symmetric. Introducing the matrix Y_{nm} defined by

$$Y_{nm} = (P_n^0)^{-1/2} W_{nm}^0 (P_m^0)^{1/2}, \tag{21}$$

the detailed-balance requirement implies that Y is symmetric.[43,45] For later use we note that Y is negative semidefinite:[43] For all vectors x one has $\langle x|Y|x\rangle \leq 0$. Moreover, equality applies if and only if $x \propto (P^0)^{1/2}$; the latter property of Y expresses "ergodicity," i.e., the assumption about the master equation that all states are connected by some sequence of transitions. We define a diagonal matrix R by

$$R_{nm} = (P_n^0)^{1/2} \delta_{nm} \tag{22}$$

and note that $W^0 = RYR^{-1}$. This implies that

$$
\begin{aligned}
A(\omega) &= \frac{1}{k_B T_0}(W^0 - i\omega I)^{-1} W^0 R^2 \\
&= \frac{1}{k_B T_0}(R(Y - i\omega I)R^{-1})^{-1} RYR \\
&= \frac{1}{k_B T_0} R(Y - i\omega I)^{-1} YR. \tag{23}
\end{aligned}
$$

Since Y and R are both symmetric, it follows that $A(\omega)$ is symmetric. Thus by Eq. (20) the 2×2 matrix $J_{\alpha\beta}(\omega)$ is symmetric.

The $J_{\alpha\beta}(\omega)$ matrix determines the frequency-dependent thermoviscoelastic linear response defined as follows: If $c_p(\omega)$ denotes the isobaric heat capacity per unit volume, $\alpha_p(\omega)$ the isobaric thermal-expansion coefficient, and $\kappa_T(\omega)$ the isothermal bulk compressibility, the complex frequency-

dependent coefficients δT, δp, δS, and δV are related by the following matrix (the symmetry of which reflects the symmetry of $J_{\alpha\beta}(\omega)$):

$$
\begin{pmatrix} \delta S \\ \delta V \end{pmatrix} = V_0 \begin{pmatrix} c_p(\omega)/T_0 & \alpha_p(\omega) \\ \alpha_p(\omega) & \kappa_T(\omega) \end{pmatrix} \begin{pmatrix} \delta T \\ -\delta p \end{pmatrix}. \tag{24}
$$

Whenever there is time-reversal invariance, the (dc, i.e., zero-frequency) symmetry implied by a Maxwell relation translates into (ac) Onsager reciprocity, a well-known result.[43,45]

III. LINEAR DYNAMIC PRIGOGINE-DEFAY RATIO

We proceed to calculate the linear Prigogine-Defay ratio of Eq. (2) from the expression for the frequency-dependent linear response functions. Since $A_{nm}(\infty) = 0$, we find by inserting Eq. (20) into Eq. (2) [with $T = T_0$ and where $\partial S / \partial P_n \equiv \partial S / \partial P_n(T_0, p_0)$ and $\partial V / \partial P_n \equiv \partial V / \partial P_n(T_0, p_0)$ but "(T_0, p_0)" is left out for brevity]

$$\Pi = \frac{\left(\sum_{m,n} \dfrac{\partial S}{\partial P_n} A_{nm}(0) \dfrac{\partial S}{\partial P_m} \right)\left(\sum_{m,n} \dfrac{\partial V}{\partial P_n} A_{nm}(0) \dfrac{\partial V}{\partial P_m} \right)}{\left(\sum_{m,n} \dfrac{\partial S}{\partial P_n} A_{nm}(0) \dfrac{\partial V}{\partial P_m} \right)^2}. \tag{25}$$

Next we reason in a way analogous to that of Davies and Jones[2] based on the Cauchy-Schwartz inequality. This inequality is the well-known mathematical theorem that if a real symmetric matrix $\mathbf{B}$ is positive or negative semidefinite, the following applies: For any vectors x and y one has $\langle x|\mathbf{B}|y\rangle^2 \leq \langle x|\mathbf{B}|x\rangle\langle y|\mathbf{B}|y\rangle$, and for nonzero x and y equality applies if and only if a number γ exists such that $x - \gamma y \in N(\mathbf{B})$ where $N(\mathbf{B})$ is the kernel (null space) of $\mathbf{B}$. The matrix $A(0)$ is positive semidefinite and the kernel of $A(0)$ is the one-dimensional linear subspace spanned by the vector $(1, \ldots, 1)$.[46] This implies that $\Pi \geq 1$ and that $\Pi = 1$ if and only if there are constants γ and c such that the following equations apply for all n (compare Refs. 2, 5, and 47):

$$\frac{\partial V}{\partial P_n}(T_0, p_0) = \gamma \frac{\partial S}{\partial P_n}(T_0, p_0) + c. \tag{26}$$

For reasons given in the next section this situation is referred to as the single-order-parameter case.

As mentioned in the Introduction, the linear Prigogine-Defay ratio of Eq. (2) is difficult to measure. Instead we propose to consider the "linear dynamic Prigogine-Defay ratio" defined in Eq. (3). When Eq. (20) is inserted into this we find

$$\Lambda_{Tp}(\omega) = \frac{\left(\sum_{m,n} \dfrac{\partial S}{\partial P_n} A_{nm}''(\omega) \dfrac{\partial S}{\partial P_m} \right)\left(\sum_{m,n} \dfrac{\partial V}{\partial P_n} A_{nm}''(\omega) \dfrac{\partial V}{\partial P_m} \right)}{\left(\sum_{m,n} \dfrac{\partial S}{\partial P_n} A_{nm}''(\omega) \dfrac{\partial V}{\partial P_m} \right)^2}. \tag{27}$$

Because the matrix $A''(\omega)$ is negative semidefinite for all $\omega > 0$,[46] the Cauchy-Schwartz inequality implies that $\Lambda_{Tp}(\omega) \geq 1$. Again, equality applies if and only if a number γ exists such that the vector with nth component $\partial V / \partial P_n - \gamma \partial S / \partial P_n$ is in the kernel of the matrix $A''(\omega)$, which is the one-dimensional space spanned by the vector $(1, \ldots, 1)$.[46] Thus for all $\omega > 0$ the equation $\Lambda_{Tp}(\omega) = 1$ is mathematically equivalent to Eq. (26), and $\Lambda_{Tp}(\omega) = 1$ is equivalent to $\Pi = 1$.

In particular, if $\Lambda_{Tp}(\omega)$ is unity at one frequency, $\Lambda_{Tp}(\omega)$ is unity for all frequencies—and this happens precisely when $\Pi = 1$.

IV. WHY $\Pi = 1$ CORRESPONDS TO A SINGLE ORDER PARAMETER

We define the order parameter ε by

$$\delta\varepsilon(t) = \sum_n \frac{\partial S}{\partial P_n}(T_0, p_0)\delta P_n(t). \tag{28}$$

Combining Eq. (28) with Eqs. (18) and (26) we find that in any linear experiment (thus calculating to lowest order) S and V are functions of T, p, and $\delta\varepsilon$ (where $J_{12}^\infty = J_{21}^\infty$)

$$\delta S(t) = \delta\varepsilon(t) + J_{11}^\infty \delta T(t) - J_{12}^\infty \delta p(t),$$
$$\delta V(t) = \gamma\delta\varepsilon(t) + J_{21}^\infty \delta T(t) - J_{22}^\infty \delta p(t). \tag{29}$$

The situation described by these equations is more general than the single-order parameter model of Prigogine and Meixner,[3,48] because Eq. (29) allows for an order parameter with nonexponential dynamics. The common physics, however, are that besides T and p one single number determines both entropy and volume fluctuations. In the present approach ε might well have a memory of the thermal prehistory.

By the definition we shall adopt here, the single-order-parameter situation applies whenever Eq. (29) is obeyed for some variable $\delta\varepsilon$. In the last section we proved that if $\Lambda_{Tp}(\omega) = 1$ applies at one frequency, then Eq. (29) follows. We proceed to show that conversely, if Eq. (29) applies for some order parameter ε, then $\Lambda_{Tp}(\omega) = 1$ for all ω. To prove this, consider a situation with periodically varying temperature and pressure fields. In steady state δS, δV, and $\delta\varepsilon$ vary periodically with complex amplitudes $\delta S(\omega)$, $\delta V(\omega)$, and $\delta\varepsilon(\omega)$. According to Eq. (29) these amplitudes are given by (for any ω)

$$\delta S(\omega) = \delta\varepsilon(\omega) + J_{11}^\infty \delta T(\omega) - J_{12}^\infty \delta p(\omega),$$
$$\delta V(\omega) = \gamma\delta\varepsilon(\omega) + J_{21}^\infty \delta T(\omega) - J_{22}^\infty \delta p(\omega). \tag{30}$$

In the case where only temperature varies, comparing to Eq. (24) shows that the following two equations apply:

$$\frac{V_0}{T_0}c_p(\omega) = \left(\frac{\delta S(\omega)}{\delta T(\omega)}\right)_p = \left(\frac{\delta\varepsilon(\omega)}{\delta T(\omega)}\right)_p + J_{11}^\infty,$$
$$V_0\alpha_p(\omega) = \left(\frac{\delta V(\omega)}{\delta T(\omega)}\right)_p = \gamma\left(\frac{\delta\varepsilon(\omega)}{\delta T(\omega)}\right)_p + J_{21}^\infty. \tag{31}$$

Since the J^∞'s are real numbers, we have

$$\gamma\frac{c_p''(\omega)}{T_0} = \alpha_p''(\omega). \tag{32}$$

Similarly, if only pressure varies Eqs. (30) and (24) imply

$$V_0\alpha_p(\omega) = -\left(\frac{\delta S(\omega)}{\delta p(\omega)}\right)_T = -\left(\frac{\delta\varepsilon(\omega)}{\delta p(\omega)}\right)_T + J_{12}^\infty,$$
$$V_0\kappa_T(\omega) = -\left(\frac{\delta V(\omega)}{\delta p(\omega)}\right)_T = -\gamma\left(\frac{\delta\varepsilon(\omega)}{\delta p(\omega)}\right)_T + J_{22}^\infty; \tag{33}$$

thus

$$\gamma\alpha_p''(\omega) = \kappa_T''(\omega). \tag{34}$$

Eliminating γ by combining Eqs. (32) and (34) yields $\Lambda_{Tp}(\omega) = 1$ for any ω. Note that in the case of one order

parameter the imaginary ("loss") parts of all three response functions are proportional.

The above line of reasoning can be repeated for different choices of input and output variables. Altogether there are four different natural (linear) dynamic Prigogine-Defay ratios as demonstrated in the Appendix; here it is also shown that the requirement of positive dissipation implies that no dynamic Prigogine-Defay ratio can be smaller than unity.

V. CONCLUDING REMARKS

The original Prigogine-Defay ratio of Eq. (1) is not rigorously well defined. The "linear" Prigogine-Defay ratio of Eq. (2) *is* well defined, but requires measurements of thermoviscoelastic response functions over many decades of frequency. There are still no methods for measuring a complete set of these response functions. Hopefully such measurements are possible in the near future, but realistically they will initially only cover a few decades.[37] This motivates the one-frequency criterion proposed and developed mathematically in this article: If the linear dynamic Prigogine-Defay ratio is unity at one frequency, this quantity is unity at all frequencies and a single-order parameter description applies. Conversely, if a single-order parameter description applies, the dynamic Prigogine-Defay ratio is unity at all frequencies. If this happens, the imaginary parts of the three linear response functions of Eq. (24) are proportional. As shown in the Appendix, these results all generalize to the three other natural choices of input and output variables. These are strict mathematical statements; in practice one cannot determine whether or not the dynamic Prigogine-Defay ratio is precisely one. What one can do is test how close to unity is this quantity. We expect that a single-parameter description is a good approximation whenever the dynamic Prigogine-Defay ratio is close to unity. Note that if there are several relaxation processes with well-separated time scales, it is possible that some of these are well described by a single-order parameter, though not perfectly, whereas others are not. In this case the frequency-dependent one-parameter test developed here in principle would be useful although, as mentioned already, it will probably not be possible in the foreseeable future to determine all three required response functions over wide frequency ranges.

In the present paper we referred to the $\Lambda_{Tp} = 1$ situation as that of a single, generally nonexponential order parameter. As emphasized by Goldstein,[5] however, due to a mathematical equivalence it is really a matter of taste whether one prefers instead to refer to a situation of several order parameters obeying a mathematical constraint [in our case Eq. (26)]. It is not possible *a priori* to estimate how restrictive or unlikely it is that Eq. (26) applies; only experiment can settle this question. It should be noted, though, that there is a simple physical interpretation of the single-order parameter case: In the approximation where each inherent state is regarded as a potential energy minimum with a harmonic potential, via Eqs. (5) and (7), Eq. (26) is equivalent to $V_n = \alpha_1 E_n + \alpha_2$ where V_n is the inherent state volume and E_n the inherent state energy (potential energy minimum). Thus there is a single-order parameter if and only if inherent state vol-

ume correlates perfectly and linearly with inherent state energy (in practice: for the dominant fluctuations at a given temperature). It is expected that this condition is obeyed to a good approximation if and only if the dynamic Prigogine-Defay ratio is close to unity.

ACKNOWLEDGMENTS

APPENDIX: GENERALIZATIONS TO OTHER CONTROL VARIABLES

Standard thermodynamics give rise to a number of (dc) linear-response coefficients. If the thermodynamic variables of interest are T, p, S, V, there are 24 coefficients of the form $(\partial a / \partial b)_c$ with a, b, and c chosen among T, p, S, V.[49] These coefficients form 12 pairs that are trivially related by inversion [e.g., $(\partial a / \partial b)_c = 1/(\partial b / \partial a)_c$]. As is well known, the 12 coefficients are not all independent, but related by various Maxwell relations (given below). There are the following eight basic linear-response coefficients (where the specific heats are per unit volume and the last three coefficients have no generally accepted names):

isochoric specific heat: $c_V \equiv \dfrac{T}{V}\left(\dfrac{\partial S}{\partial T}\right)_V$;

isobaric specific heat: $c_p \equiv \dfrac{T}{V}\left(\dfrac{\partial S}{\partial T}\right)_p$;

isothermal compressibility: $\kappa_T \equiv -\dfrac{1}{V}\left(\dfrac{\partial V}{\partial p}\right)_T$;

adiabatic compressibility: $\kappa_S \equiv -\dfrac{1}{V}\left(\dfrac{\partial V}{\partial p}\right)_S$;

$$(A1)$$

isobaric expansion coefficient:

$$\alpha_p \equiv \frac{1}{V}\left(\frac{\partial V}{\partial T}\right)_p = -\frac{1}{V}\left(\frac{\partial S}{\partial p}\right)_T ;$$

"adiabatic contraction coefficient: "

$$\alpha_S \equiv -\frac{1}{V}\left(\frac{\partial V}{\partial T}\right)_S = \frac{1}{V}\left(\frac{\partial S}{\partial p}\right)_V ;$$

"isochoric pressure coefficient: "

$$\beta_V \equiv \left(\frac{\partial p}{\partial T}\right)_V = \left(\frac{\partial S}{\partial V}\right)_T ;$$

"adiabatic pressure coefficient: "

$$\beta_S \equiv \left(\frac{\partial p}{\partial T}\right)_S = \left(\frac{\partial S}{\partial V}\right)_p .$$

Consider harmonically varying scalar thermal and mechanical perturbations of equilibrium for a small volume element. "Small" here means that its linear dimensions are much smaller than both the heat diffusion length and the sound wavelength corresponding to the frequency under consideration, implying that the perturbations may be regarded as homogeneous over the small volume element. Let $\delta T(\omega)$, $\delta p(\omega)$, $\delta s(\omega)$, $\delta v(\omega)$ denote the complex amplitudes of perturbations varying with time as $\propto \exp(i\omega t)$ and define the intensive variables $v \equiv V/V_0$ and $s \equiv S/V_0$ where V_0 is the equilibrium volume. If small perturbations around temperature T_0 are considered, following Eq. (A1) one defines the following complex frequency-dependent linear-response quantities (where according to the so-called correspondence principle[50] all thermodynamic relations survive and the Maxwell relations become Onsager reciprocity relations[48]):

isochoric specific heat: $c_V(\omega) \equiv T_0\left(\dfrac{\delta s(\omega)}{\delta T(\omega)}\right)_V$;

isobaric specific heat: $c_p(\omega) \equiv T_0\left(\dfrac{\delta s(\omega)}{\delta T(\omega)}\right)_p$;

isothermal compressibility: $\kappa_T(\omega) \equiv -\left(\dfrac{\delta v(\omega)}{\delta p(\omega)}\right)_T$;

adiabatic compressibility: $\kappa_S(\omega) \equiv -\left(\dfrac{\delta v(\omega)}{\delta p(\omega)}\right)_S$;

$$(A2)$$

isobaric expansion coefficient:

$$\alpha_p(\omega) \equiv \left(\frac{\delta v(\omega)}{\delta T(\omega)}\right)_p = -\left(\frac{\delta s(\omega)}{\delta p(\omega)}\right)_T ;$$

"adiabatic contraction coefficient: "

$$\alpha_S(\omega) \equiv -\left(\frac{\delta v(\omega)}{\delta T(\omega)}\right)_S = \left(\frac{\delta s(\omega)}{\delta p(\omega)}\right)_V ;$$

"isochoric pressure coefficient: "

$$\beta_V(\omega) \equiv \left(\frac{\delta p(\omega)}{\delta T(\omega)}\right)_V = \left(\frac{\delta s(\omega)}{\delta v(\omega)}\right)_T ;$$

"adiabatic pressure coefficient: "

$$\beta_S(\omega) \equiv \left(\frac{\delta p(\omega)}{\delta T(\omega)}\right)_S = \left(\frac{\delta s(\omega)}{\delta v(\omega)}\right)_p .$$

The general procedure now works as follows. Let $(\delta X(\omega), \delta Y(\omega))$ denote the amplitudes of two periodically varying thermodynamic variables considered as control variables and $(\delta Z(\omega), \delta W(\omega))$ the remaining two periodically varying variables. The relationship between the two sets of variables generally takes the form

$$\begin{pmatrix} \delta Z(\omega) \\ \delta W(\omega) \end{pmatrix} = \begin{pmatrix} a_{11}(\omega) & a_{12}(\omega) \\ a_{21}(\omega) & a_{22}(\omega) \end{pmatrix} \begin{pmatrix} \delta X(\omega) \\ \delta Y(\omega) \end{pmatrix}. \tag{A3}$$

In the case of a single order parameter ε—compare to Eq. (30)—we can write (where the 2×3-matrix is real and frequency independent)

$$\begin{pmatrix} \delta Z(\omega) \\ \delta W(\omega) \end{pmatrix} = \begin{pmatrix} a_{11}^\infty & a_{12}^\infty & b_1 \\ a_{21}^\infty & a_{22}^\infty & b_2 \end{pmatrix} \begin{pmatrix} \delta X(\omega) \\ \delta Y(\omega) \\ \delta \varepsilon(\omega) \end{pmatrix}. \tag{A4}$$

Comparing to Eq. (A3), when Y does not vary we get

$$\left. \begin{array}{l} a_{11}(\omega) = a_{11}^\infty + b_1 \left(\dfrac{\delta \varepsilon(\omega)}{\delta X(\omega)} \right)_Y \\[2mm] a_{21}(\omega) = a_{21}^\infty + b_2 \left(\dfrac{\delta \varepsilon(\omega)}{\delta X(\omega)} \right)_Y \end{array} \right\} \Rightarrow \dfrac{a_{21}''(\omega)}{a_{11}''(\omega)} = \dfrac{b_2}{b_1} \equiv \gamma_{XY}, \tag{A5}$$

and when X does not vary

$$\left. \begin{array}{l} a_{12}(\omega) = a_{12}^\infty + b_1 \left(\dfrac{\delta \varepsilon(\omega)}{\delta Y(\omega)} \right)_X \\[2mm] a_{22}(\omega) = a_{22}^\infty + b_2 \left(\dfrac{\delta \varepsilon(\omega)}{\delta Y(\omega)} \right)_X \end{array} \right\} \Rightarrow \dfrac{a_{22}''(\omega)}{a_{12}''(\omega)} = \dfrac{b_2}{b_1} = \gamma_{XY}. \tag{A6}$$

In principle there are six different choices of control variables. Below we treat the four natural cases where the input variables consist of one from the (S, T) "energy bond"[51,52] and one from the $(-p, V)$ energy bond, and similarly for the output variables. In each case the signs are chosen to make the response matrix symmetric. Via Eqs. (A5) and (A6) in each of the four cases the three imaginary (loss) parts of the relevant linear-response functions are proportional. The four cases are detailed below, where the explicit amplitude frequency dependence is left out for simplicity of notation.

1. Control variables δT and $-\delta p$

This case was considered in the main paper, but is included here for completeness

$$\begin{pmatrix} \delta s \\ \delta v \end{pmatrix} = \begin{pmatrix} c_p(\omega)/T_0 & \alpha_p(\omega) \\ \alpha_p(\omega) & \kappa_T(\omega) \end{pmatrix} \begin{pmatrix} \delta T \\ -\delta p \end{pmatrix}. \tag{A7}$$

Applying Eqs. (A5) and (A6) to this we get

$$\frac{T_0 \alpha_p''(\omega)}{c_p''(\omega)} = \gamma_{Tp} = \frac{\kappa_T''(\omega)}{\alpha_p''(\omega)}, \tag{A8}$$

and thus

$$\Lambda_{Tp}(\omega) \equiv \frac{c_p''(\omega)\kappa_T''(\omega)}{T_0[\alpha_p''(\omega)]^2} = 1. \tag{A9}$$

2. Control variables δs and δv

$$\begin{pmatrix} \delta T \\ -\delta p \end{pmatrix} = \begin{pmatrix} T_0/c_V(\omega) & -1/\alpha_S(\omega) \\ -1/\alpha_S(\omega) & 1/\kappa_S(\omega) \end{pmatrix} \begin{pmatrix} \delta s \\ \delta v \end{pmatrix}. \tag{A10}$$

Applying Eqs. (A5) and (A6) to this we get

$$-\frac{(1/\alpha_S(\omega))''}{(T_0/c_V(\omega))''} = \gamma_{SV} = -\frac{(1/\kappa_S(\omega))''}{(1/\alpha_S(\omega))''} \tag{A11}$$

and thus

$$\Lambda_{SV}(\omega) \equiv \frac{(T_0/c_V(\omega))''(1/\kappa_S(\omega))''}{[(1/\alpha_S(\omega))'']^2} = 1. \tag{A12}$$

3. Control variables δs and $-\delta p$

$$\begin{pmatrix} \delta T \\ -\delta v \end{pmatrix} = \begin{pmatrix} T_0/c_p(\omega) & -1/\beta_S(\omega) \\ -1/\beta_S(\omega) & -\kappa_S(\omega) \end{pmatrix} \begin{pmatrix} \delta s \\ -\delta p \end{pmatrix}. \tag{A13}$$

Applying Eqs. (A5) and (A6) to this we get

$$-\frac{(1/\beta_S(\omega))''}{(T_0/c_p(\omega))''} = \gamma_{Sp} = \frac{\kappa_S''(\omega)}{(1/\beta_S(\omega))''} \tag{A14}$$

and thus

$$\Lambda_{Sp}(\omega) \equiv -\frac{(T_0/c_p(\omega))''\kappa_S''(\omega)}{[(1/\beta_S(\omega))'']^2} = 1. \tag{A15}$$

4. Control variables δT and δv

$$\begin{pmatrix} \delta s \\ -\delta p \end{pmatrix} = \begin{pmatrix} c_V(\omega)/T_0 & -\beta_V(\omega) \\ -\beta_V(\omega) & -1/\kappa_T(\omega) \end{pmatrix} \begin{pmatrix} \delta T \\ -\delta v \end{pmatrix}. \tag{A16}$$

Applying Eqs. (A5) and (A6) to this we get

$$-\frac{T_0 \beta_V''(\omega)}{c_V''(\omega)} = \gamma_{TV} = \frac{(1/\kappa_T(\omega))''}{\beta_V''(\omega)} \tag{A17}$$

and thus

$$\Lambda_{TV}(\omega) \equiv -\frac{c_V''(\omega)(1/\kappa_T(\omega))''}{T_0[\beta_V''(\omega)]^2} = 1. \tag{A18}$$

For each case we showed above that, if there is a single-order parameter, the dynamic Prigogine-Defay ratio is unity. Below we proceed to prove that, conversely, if one of the dynamic Prigogine-Defay ratios is unity at some frequency, then this dynamic Prigogine-Defay ratio is unity at all frequencies and there is a single-order parameter. In particular, if one dynamic Prigogine-Defay ratio is unity at one frequency, all dynamic Prigogine-Defay ratios are unity at all frequencies.

In the periodic situation the dissipation is proportional to $\text{Im}[\delta T(\omega)\delta s^*(\omega) - \delta p(\omega)\delta v^*(\omega)]$.[48,53] The requirement of positive dissipation implies that all four dynamic Prigogine-Defay ratios are larger than or equal to unity; this follows by considering the special case of in-phase input variables in which case it is easy to show that the determinant of the imaginary response matrix must be non-negative to have positive dissipation. If one of the dynamic Prigogine-Defay ratios is unity at some frequency ω, the determinant of the imaginary part of the corresponding response matrix is zero. This implies that there is an eigenvector of the imaginary response matrix with zero eigenvalue. Thus the dynamic Prigogine-Defay ratio is unity if and only if a thermodynamic cycle exists with zero dissipation. It follows that, if in one of cases 2–4 the dynamic Prigogine-Defay ratio is unity

at frequency ω, then $\Lambda_{Tp}(\omega)=1$. This implies that $\Lambda_{Tp}(\omega)=1$ at all frequencies (Sec. III), and that there is a single order parameter ε such that S and V are given by Eq. (29). These equations are easily rewritten to give the required output variables in terms of the input variables and ε. This implies that the relevant dynamic Prigogine-Defay ratio is unity at all frequencies, and that all other dynamic Prigogine-Defay ratios are also unity at all frequencies.

[1] R. O. Davies and G. O. Jones, Proc. R. Soc. London, Ser. A **217**, 26 (1952).

[2] R. O. Davies and G. O. Jones, Adv. Phys. **2**, 370 (1953).

[3] I. Prigogine and R. Defay, *Chemical Thermodynamics* (Longman, London, 1954).

[4] M. Goldstein, J. Chem. Phys. **39**, 3369 (1963).

[5] M. Goldstein, in *Modern Aspects of the Vitreous State*, edited by J. D. Mackenzie (Butterworths Scientific, London, 1964), Vol. 3, p. 90.

[6] C. A. Angell and W. Sichina, Ann. N.Y. Acad. Sci. **279**, 53 (1976).

[7] S. Brawer, *Relaxation in Viscous Liquids and Glasses* (American Ceramic Society, Columbus, OH, 1985).

[8] S. V. Nemilov, *Thermodynamic and Kinetic Aspects of the Vitreous State* (CRC, Boca Raton, FL, 1995).

[9] E. Donth, *The Glass Transition* (Springer, Berlin, 2001).

[10] C. T. Moynihan, P. B. Macedo, C. J. Montrose, C. J. Montrose, P. K. Gupta, M. A. DeBolt, J. F. Dill, B. E. Dom, P. W. Drake, A. J. Easteal, P. B. Elterman, R. P. Moeller, H. Sasabe, and J. A. Wilder, Ann. N.Y. Acad. Sci. **279**, 15 (1976).

[11] H.-J. Oels and G. Rehage, Macromolecules **10**, 1036 (1977).

[12] P. Zoller, J. Polym. Sci., Polym. Phys. Ed. **20**, 1453 (1982).

[13] H. Wendt and R. Richert, Phys. Rev. E **61**, 1722 (2000).

[14] R. Böhmer, G. Diezemann, G. Hinze, and E. Rössler, Prog. Nucl. Magn. Reson. Spectrosc. **39**, 191 (2001).

[15] R. Richert and S. Weinstein, Phys. Rev. Lett. **97**, 095703 (2006).

[16] R.-J. Roe, J. Appl. Phys. **48**, 4085 (1977).

[17] I. M. Hodge, J. Non-Cryst. Solids **169**, 211 (1994).

[18] C. T. Moynihan and P. K. Gupta, J. Non-Cryst. Solids **29**, 143 (1978).

[19] C. T. Moynihan and A. V. Lesikar, Ann. N.Y. Acad. Sci. **371**, 151 (1981).

[20] E. A. DiMarzio, J. Appl. Phys. **45**, 4143 (1974).

[21] M. Goldstein, J. Appl. Phys. **46**, 4153 (1975).

[22] A. V. Lesikar and C. T. Moynihan, J. Chem. Phys. **72**, 6422 (1980).

[23] Th. M. Nieuwenhuizen, Phys. Rev. Lett. **79**, 1317 (1997).

[24] M. R. H. Javaheri and R. V. Chamberlin, J. Chem. Phys. **125**, 154503 (2006).

[25] J. H. R. Clarke, J. Chem. Soc., Faraday Trans. 2 **75**, 1371 (1979).

[26] E. La Nave, S. Mossa, and F. Sciortino, Phys. Rev. Lett. **88**, 225701 (2002).

[27] M. S. Shell, P. G. Debenedetti, E. L. Nave, and F. Sciortino, J. Chem. Phys. **118**, 8821 (2003).

[28] S. Mossa and F. Sciortino, Phys. Rev. Lett. **92**, 045504 (2004).

[29] F. Sciortino, J. Stat. Mech.: Theory Exp. 2005, P05015.

[30] J. C. Dyre and N. B. Olsen, Phys. Rev. Lett. **91**, 155703 (2003).

[31] R. Böhmer, G. Diezemann, B. Geil, G. Hinze, A. Nowaczyk, and M. Winterlich, Phys. Rev. Lett. **97**, 135701 (2006).

[32] C. M. Roland, S. Hensel-Bielowka, M. Paluch, and R. Casalini, Rep. Prog. Phys. **68**, 1405 (2005).

[33] R. J. Speedy, J. Phys. Chem. B **103**, 4060 (1999).

[34] J. Wu, J. Appl. Polym. Sci. **71**, 143 (1999).

[35] N. B. Olsen, T. Christensen, and J. C. Dyre, Phys. Rev. Lett. **86**, 1271 (2001).

[36] B. Jakobsen, K. Niss, and N. B. Olsen, J. Chem. Phys. **123**, 234511 (2005).

[37] T. Christensen *et al.*, to be published.

[38] M. Goldstein, J. Chem. Phys. **51**, 3728 (1969).

[39] R. G. Palmer, Adv. Phys. **31**, 669 (1982).

[40] F. H. Stillinger and T. A. Weber, Phys. Rev. A **28**, 2408 (1983).

[41] T. B. Schrøder, S. Sastry, J. C. Dyre, and S. C. Glotzer, J. Chem. Phys. **112**, 9834 (2000).

[42] The relation $\partial G/\partial P_n = \text{const}$ leads to $G_n + k_B T \ln P_n^{\text{eq}} + k_B T = \text{const}$. Insert this into Eq. (4) to find $G_n + k_B T \ln P_n^{\text{eq}} = G$, then isolate P_n^{eq} to get the desired result.

[43] N. G. Van Kampen, *Stochastical Processes in Physics and Chemistry* (North Holland, Amsterdam, 1981).

[44] We have $\partial \ln P_m^{\text{eq}}/\partial T = [-1/k_B T](\partial(G_m-G)/\partial T - (G_m-G)/T) = (1/k_B T) \times (\partial S/\partial P_m - S + k_B)$ and $\partial \ln P_m^{\text{eq}}/\partial(-p) = [-1/k_B T_0][\partial(G_m-G)/\partial(-p)] = (1/k_B T_0)(\partial V/\partial P_m - V)$.

[45] L. E. Reichl, *A Modern Course in Statistical Physics*, 2nd ed. (Wiley, New York, 1998).

[46] If the eigenvalues of Y are denoted by λ_k with corresponding eigenvectors e_k, there are $N-1$ negative eigenvalues and one zero eigenvalue.[43] Equation (23) implies that for any vector x we have $\langle x|A(\omega)|x\rangle = (1/k_B T_0)\Sigma_{\lambda_k<0}\langle Rx|e_k\rangle\langle e_k|Rx\rangle\lambda_k/(\lambda_k - i\omega)$ (where the sum is restricted to the $N-1$ negative eigenstates). Letting $\omega \to 0$ we find that $\langle x|A(0)|x\rangle \geq 0$, showing that $A(0)$ is positive semidefinite. For the imaginary part, we find that $\langle x|A''(\omega)|x\rangle = (1/k_B T_0)\Sigma_{\lambda_k<0}\langle Rx|e_k\rangle\langle e_k|Rx\rangle\lambda_k\omega/(\lambda_k^2 + \omega^2) \leq 0$ whenever $\omega > 0$; thus $A''(\omega)$ is negative semidefinite. In both cases, equality applies if and only if the vector Rx lies in the one-dimensional eigenspace of Y corresponding to the zero eigenvalue. Thus equality applies if and only if $(Rx)_n \propto (P_n^0)^{1/2}$, or $x \propto (1, \ldots, 1)$.

[47] P. K. Gupta and C. T. Moynihan, J. Chem. Phys. **65**, 4136 (1976).

[48] J. Meixner and H. G. Reik, in *Principen der Thermodynamik und Statistik*, edited by S. Flügge, Handbuch der Physik, Vol. 3 (Springer, Berlin, 1959), p. 413.

[49] J. I. Berg and A. R. Cooper, J. Chem. Phys. **68**, 4481 (1978).

[50] R. M. Christensen, *Theory of Viscoelasticity*, 2nd ed. (Academic, New York, 1982).

[51] G. F. Oster, A. S. Perelson, and A. Katchalsky, Q. Rev. Biophys. **6**, 1 (1973).

[52] D. C. Mikulecky, *Applications of Network Thermodynamics to Problems in Biomedical Engineering* (New York University, New York, 1993).

[53] J. Bataille and J. Kestin, J. Non-Equil. Thermodyn. **4**, 229 (1979).

Crystallization of the Wahnström Binary Lennard-Jones Liquid

Ulf R. Pedersen, Nicholas P. Bailey, Jeppe C. Dyre and Thomas B. Schrøder

DNRF Centre "Glass and Time", IMFUFA, Department of Sciences,
Roskilde University, Postbox 260, DK-4000 Roskilde, Denmark

(Dated: February 5, 2008)

We report observation of crystallization of the glass-forming binary Lennard-Jones liquid first used by Wahnström [G. Wahnström, Phys. Rev. A **44**, 3752 (1991)]. Molecular dynamics simulations of the metastable liquid on a timescale of microseconds were performed. The liquid crystallized spontaneously. The crystal structure was identified as $MgZn_2$. Formation of transient crystallites is observed in the liquid. The crystallization is investigate at different temperatures and compositions. At high temperature the rate of crystallite formation is the limiting factor, while at low temperature the limiting factor is growth rate. The melting temperature of the crystal is estimated to be $T_m = 0.93$ at $\rho = 0.82$. The maximum crystallization rate of the A_2B composition is $T = 0.60 \pm 0.02$.

The use of computer models of liquids has played an important role for understanding glass forming-liquids. Computationally undemanding models are attractive, since long simulation times are important. Further more, the model does not have to be specific since the glass transition is universal. A simple model for molecular interactions is the the famous Lennard-Jones pair potential, $U_{ij}(r_{ij}) = 4\varepsilon((r_{ij}/\sigma_{ij})^{12} - (r_{ij}/\sigma_{ij})^6)$. It is not possible to investigate a single component Lennard-Jones liquid close to the glass transition since the structural relaxation time is of the same order as the crystallization time. This can be avoided by using a binary Lennard-Jones liquid where the liquid consists of two kind of particles with differend radii σ_{ij} and binding energy ε_{ij} [1, 2]. In 1991 Wahnström suggested parameters for a binary Lennard-Jones liquid in order to investigate the metastable undercooled liquid [1]. In the following years the model has been used by several others as a standard liquid [3, 4, 5, 6, 7, 8, 9, 10].

Increasing computer power expands the time scale that can be simulated. On a time scale of microseconds, the Wahnström liquid is no longer meta-stable, but crystallizes. In this paper we report observations of formations of crystallites and growth. It is possible to investigate a liquid, a highly viscous metastable liquid, a glass and crystallization within the same model. There is a separation of phonons, structural relaxation, formation of crystallites, and crystal growth in time.

The classical understanding of the crystallization process is as follows [11]. Crystallization consists of two events: formation of a critical crystallite and subsequent growth. The free energy of a crystallite (below the melting temperature) consists of a positive surface part and a negative volume part. Crystallites below a critical size are unstable since the surface part will dominate. When a crystallite is above the critical size, the volume part will dominate, and the crystallite will grow.

We have performed molecular dynamics simulations of the binary Lennard-Jones liquid suggested by Wahn-ström [1]. Particles interact via the Lennard-Jones pair potential. The system consists of two types of particles labelled A and B. Energy is reported in units of ε_{AA}, length in units of σ_{AA}, mass in units of m_A, temperature in units of $T = \varepsilon_{AA}/k_B$, and time in units of $t^* = \sigma_{AA}\sqrt{m_{AA}/\varepsilon_{AA}}$. Type B particles have a larger radius than type A particles, $\sigma_{BB} = \frac{6}{5}\sigma_{AA}$ and $\sigma_{AB} = \frac{1}{2}(\sigma_{BB} + \sigma_{AA}) = 1.1\sigma_{AA}$ and twice the mass, $m_B = 2m_A$. All binding energies are equal, $\varepsilon_{AA} = \varepsilon_{BB} = \varepsilon_{AB}$.

We define Argon units such that A particles may be considered to be Argon molecules; $\varepsilon_{AA} = 1$ kJ/mol, $\sigma_{AA} = 0.34$ nm $m_A = 40$ g/mol, $\varepsilon_{AA}/k_B = 120.27$ K and $t^* = 2.15$ ps.

The simulations were performed using Gromacs software [12]. A switch function from $2.0\sigma_{AA}$ to $3.5\sigma_{AA}$ was used to make potential go smoothly to zero at $3.5\sigma_{AA}$. Periodic boundaries were imposed. The Verlet velocity integrator with a time step of $0.01t^*$ were used. The temperature was held constant using the Nosé-Hoover thermostat [13]. The density were $N/V = 0.75\sigma_{AA}^{-3}$ and $N_A = N_B = 512$. This is the same density and N_A/N_B ratio as originally used by Wahnström [1], but twice the size. We also performed simulations with $N_A = 2N_B$ and a density of $0.82\sigma_{AA}^{-3}$. The program VMD was used for visualization [14].

Fig. 1 shows the potential energy per particle as a function of time for independent samples at $T = 0.624$ and $T = 0.599$. The composition was AB. At $T = 0.624$ the total simulation time covers 15 μs or in the order of $10^4\tau_\alpha$ structural relaxation times. One of the samples show a dramatic drop in energy due to crystallization. Crystallization is a rare event at this temperature but more common at the lower temperature. The samples that do not crystallize show some transient drops in energy. This can be explained as formation of small crystallites. This was confirmed by a common neighbor analysis (data not shown) [15].

The bottom panel on Fig. 1 show the quenched structure of the crystallized sample. A crystal with a few
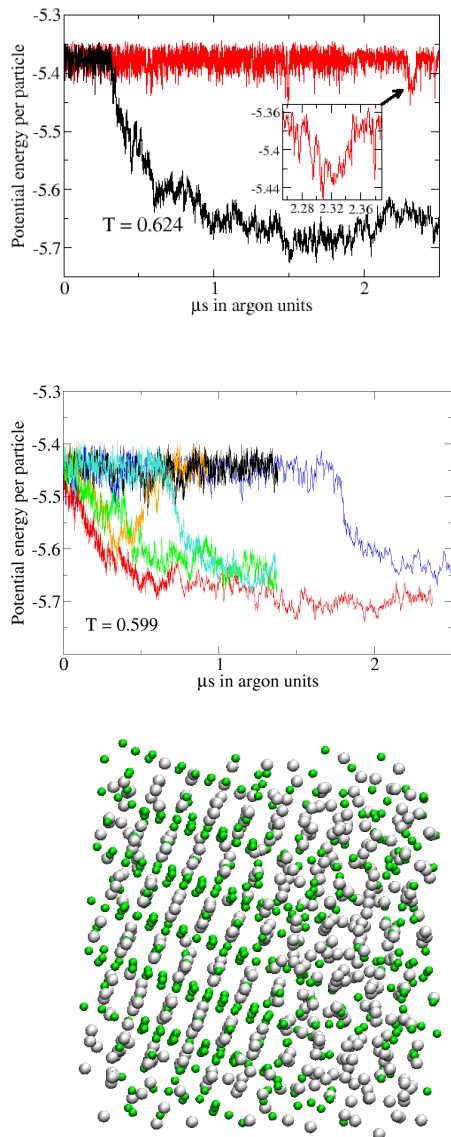
FIG. 1: The two top panels show the potential energy per particle as a function of time for independent runs at two temperatures with $N_A = N_B = 512$. Several of the samples show a dramatic drop in energy due the growth of crystallites. At $T = 0.624$ the total simulation time of liquid is $t = 13$ μs (we made nine samples, not all data are shown), but only one sample crystallizes. The inset on the top panel shows a transient drop in energy which can be identified as temporary formation of a crystallite. At $T = 0.599$ crystallization happens more often. The bottom panel the quenched structure of the crystallized sample at $T = 0.624$. Type A particles are green (dark gray) and type B particles are white (light gray). A crystal has formed with $N_A/N_B \simeq 2$, see Fig. 2. The excess B particles and some A particles form a liquid in the remained of the box. It was not possible to crystallize the whole sample within 4.5 μs.
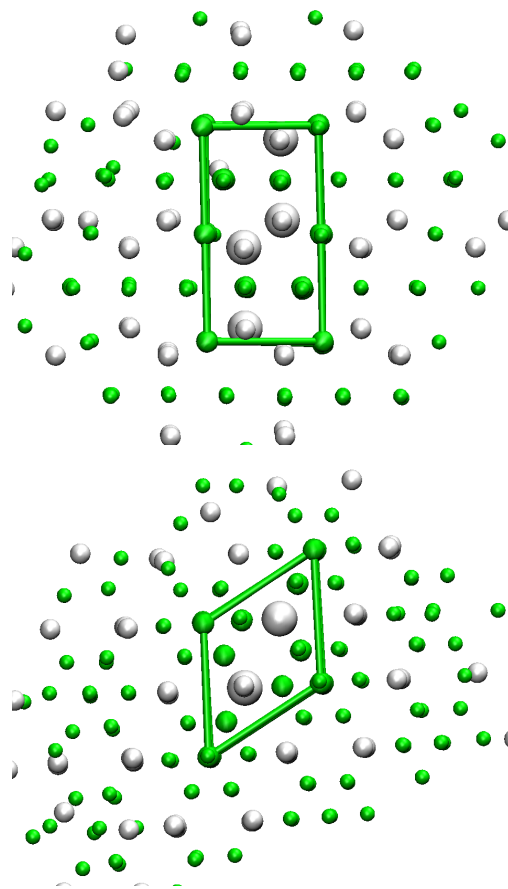
FIG. 2: Part of crystal seen from different perspectives. The outline of a trigonal, hexagonal unit cell is sketched. Type A particles are colored in green (dark gray) and type B particles in white (light gray). The crystal structure is $MgZn_2$ (C14) with $P6_3/mmc$ symmetry. There are 6 type A particles on the h position, 2 on the a position and 4 type B particles on the f position (where h, a and f are Wyckoff letters) [16].

defects has formed. It fills half the box, while the rest of the box is occupied by liquid. The crystal consists of more type A than type B particles so that $N_A/N_B \simeq 2$, whereas the liquid mainly consists of type B particles.

Fig. 2 shows a part of the crystal seen from different perspectives. A unit cell is sketched. The crystal structure is identified as the hexagonal $MgZn_2$ Laves structure. This is a close packing structure for the A_2B composition with $\sigma_B/\sigma_A = \sqrt{3}/\sqrt{2} \simeq 1.22$ [17]. This is in good agreement with the parameters used.

Fig. 3 shows simulations of a perfect crystal in an orthorhombic cell with 864 type A and 432 type B particles. The density was $\rho = 0.82$. The crystal was heated
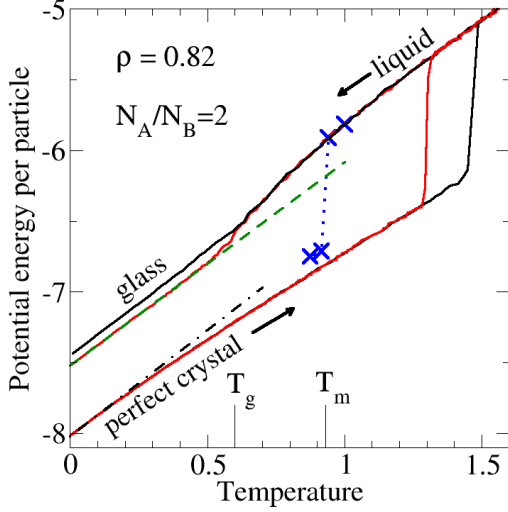
FIG. 3: The lower line shows the potential energy per particle during heating of a perfect crystal. The heating rates were 2.2×10^4 K/μs and 2.2×10^2 K/μs in Argon units. At $T = 1.3$ and $T = 1.5$ respectively the crystal melted. The systems were then cooled at the same rates. The liquids undergoes a glass transition at $T_g \simeq 0.6$ (depending on cooling rate). The dashed line is a linear fit to the glass data with a slope of 1.44. A partially melted crystal (approximately 90% crystal) was instantaneously cooled and kept at constant temperature T' for 30 ns. The ×'s mark the final energy at different T' temperatures. From this data, the melting temperature was estimated to be $T_m = 0.93 \pm 0.02$. The dash-dot line have a slope of 3/2 corresponding to a classical harmonic crystal.

FIG. 4: Potential energy per particle during simulations of metastable liquids at $T = \{0.625, 0.583\}$, $\rho = 0.82$, $N_A = 1024$ and $N_B = 512$. Four independent samples are shown at each temperature. Six of the eight samples crystallizes. At $T = 0.625$ the limiting factor is the formation rate of crystallites, while growth rate is the limiting factor at $T = 0.583$.

at constant density from zero temperature with a rate of $\frac{dT}{dt} = 4 \times 10^{-4}$ and $\frac{dT}{dt} = 4 \times 10^{-6}$. At $T = 1.3$ and $T = 1.5$ respectively the crystal melted. We expect the crystal to be over-heated at these temperatures. The melting temperature T_m was estimated by simulating a partially melted sample (approximately 90% of the volume were crystal) at constant temperature T' for 30 ns. The sample melted when $T' > T_m = 0.93 \pm 0.02$ and partially recrystallized when $T' < T_m$.

The liquid made from the melted crystal was cooled with a rate of $\frac{dT}{dt} = -4 \times 10^{-4}$ and $\frac{dT}{dt} = -4 \times 10^{-6}$. At T_m the sample did not crystallize, but became super-cooled. At $T_g \simeq 0.6$ the sample passed though a glass transition (slightly dependent on cooling rate).

In order to investigate the crystallization properties at the A$_2$B composition further, we performed simulations of the super-cooled liquid at constant temperature with

$N = 1536$ and $\rho = 0.82$. Fig. 4 shows the potential energy per particle as a function of time at $T = 0.624$ and $T = 0.582$. We used several independent samples. At the high temperature two out of four sample show a dramatic drop in energy. Here, the limiting factor for crystallization is the formation of a critical crystallite. When a critical crystallite have formed, the rest of the sample crystallizes fast. At the low temperature all four samples have formed a critical crystallite at $t \simeq 0$ but the growth rate is slow. From simulations at several temperatures the maximum crystallization rate was estimated to $T = 0.60 \pm 0.02$ (data not shown).

In summary, we show for the first time that the Wahnström binary Lennard-Jones liquid undergoes crystalliza-

tion when the metastable liquid is simulated for a time of $10^4\tau_a$ close to the glass transition. The crystal structure is identified as MgZn$_2$. This crystal is rather complex, but can form even when the composition is $N_A = N_B$. The melting temperature of the crystal (at the A$_2$B composition and $\rho = 0.82$) is $T_m = 0.93 \pm 0.02$. The maximum crystallization rate of the sample is $T = 0.60 \pm 0.02$.

----

[1] G. Wahnström, Phys. Rev. A **44**, 3752 (1991)

[2] W. Kob and H. C. Andersen, Phys. Rev. Lett. **73**, 1376 (1994).

[3] D. Coslovich and G. Pastore, Europhysics letters **75**, 784 (2006)

[4] N. Lacevic and S. C. Glotzer, J. Phys. Chem. B **108**, 19623 (2004)

[5] F. Albano, N. Lacevic, M. L. Falk and S. C. Glotzer, Matrials science and engineering A **375**, 671 (2004)

[6] N. Lacevic, F. W. Starr, T. B. Schrøder and S. C. Glotzer, J. Chem. Phys. **119**, 7372 (2003)

[7] N. Lacevic and S. C. Glotzer, J. Phys.: Condens. Matter **15**, 2437 (2003)

[8] T. B. Schrøder, S. Sastry, J. C. Dyre and S. C. Glotzer, J. Chem. Phys. **112**, 9834 (2000)

[9] S. Sastry, P. G. Debenedetti, F. H. Stillinger FH, T. B. Schrøder, J. C. Dyre and S. C. Glotzer, Physica A **270**, 301 (1999)

[10] S. Fujiwara, F. Yonezawa, Phys. Rev. **54**, 644 (1996)

[11] S. Balibar and F. Caupin, C. R. Physique **7**, 988 (2006)

[12] E. Lindahl, B. Hess and D. van der Spoel, J. Mol. Mod. **7**, 306 (2001);H. J. C. Berendsen, D. van der Spoel and R. van Drunen, Comp. Phys. Comm. **91**, 43 (1995)

[13] S. A. Nosé, Mol. Phys. **52**, 255 (1984);W. G. Hoover, Phys. Rev. A **31**, 1695 (1985)

[14] W. Humphrey, A. Dalke and K. Schulten, J. Molec. Graphics **14**, 33 (1996)

[15] J. D. Honeycutt and H. C. Andersen, J. Phys. Chem. **91**, 4950 (1987)

[16] W. B. Pearson, The Crystal Chemistry and Physics of Metals and Alloys, (Wiley-Interscience, New York, 1972) p. 657

[17] E. Parthé, Zeitscrift für Kristallographie **115**, 52 (1961)

Strong Pressure-Energy Correlations in van der Waals Liquids

Ulf R. Pedersen, Nicholas P. Bailey, Thomas B. Schrøder, and Jeppe C. Dyre

DNRF Centre "Glass and Time," IMFUFA, Department of Sciences, Roskilde University, Postbox 260, DK-4000 Roskilde, Denmark
(Received 29 August 2007; revised manuscript received 21 November 2007; published 3 January 2008)

Strong correlations between equilibrium fluctuations of the configurational parts of pressure and energy are found in computer simulations of the Lennard-Jones liquid and other simple liquids, but not for hydrogen-bonding liquids such as methanol and water. The correlations that are present also in the crystal and glass phases reflect an effective inverse power-law repulsive potential dominating fluctuations, even at zero and slightly negative pressure. In experimental data for supercritical argon, the correlations are found to be approximately 96%. Consequences for viscous liquid dynamics are discussed.

For any macroscopic system thermal fluctuations are small and apparently insignificant. Their significance, however, was pointed out by Einstein, who showed that for any system in equilibrium with its surroundings, the specific heat is determined by the magnitude of the energy fluctuations. This result may be generalized, and it has long been well understood that linear-response quantities are determined by equilibrium fluctuations of suitable quantities [1–3]. One expects few new insights to come from studies of fluctuations in equilibrated systems. We here report strong correlations between instantaneous pressure and energy equilibrium fluctuations in one of the most studied models in the history of computer simulation, the Lennard-Jones liquid, as well as for other van der Waals liquids. These findings have significant consequences, in particular, for the dynamics of highly viscous liquids.

Using molecular dynamics [4,5], fluctuations were studied for $N = 864$ particles interacting via the Lennard-Jones (LJ) pair potential [6] $\phi_{LJ}(r) = 4\epsilon[(\sigma/r)^{12} - (\sigma/r)^6]$ in the NVT ensemble [7], where r is the distance between two particles. The configurational contribution to the instantaneous pressure defines the instantaneous virial $W(t)$ by [4] $p(t)V = Nk_BT(t) + W(t)$. Figure 1(a) shows normalized instantaneous equilibrium fluctuations of $W(t)$ and the potential energy $U(t)$ for a simulation at zero average pressure. The two quantities correlate strongly. To study the correlations systematically, temperature was varied at five different densities. The results are summarized in Fig. 1(b), plotting instantaneous virial versus instantaneous potential energy, with each color representing equilibrium fluctuations at one particular temperature and density. The figure reveals strong W, U correlations with correlation coefficients mostly above 0.9; see Table I. The results at a given density form approximate straight lines. The data include slightly negative pressure conditions, as well as three instances of the crystallized liquid (lower left corner).

For any system with pairwise interactions $W(t) = -\sum_{i<j} r_{ij}(t)\phi'[r_{ij}(t)]/3$ [2,4]. Perfect W, U correlation applies if $\phi(r) = ar^{-n} + \phi_0$ in which case $\Delta W(t) = (n/3)\Delta U(t)$, where $\Delta W(t) \equiv W(t) - \langle W \rangle$, etc. An obvious

first guess is therefore that the strong correlation directly reflects the r^{-12} term in the LJ potential. That is not correct because the exponent $n = 12$ implies a slope of $\gamma = 4$ of the lines in Fig. 1(b); the observed slope is $\gamma = 6$ ($\pm 10\%$, see Table I), corresponding to effective inverse power-law exponents $n \approx 18$. The repulsive core of the LJ potential ($r < 2^{1/6}\sigma$), however, can be well approximated by $\phi_{pow}(r) = ar^{-n} + \phi_0$, with an exponent n considerably *larger* than 12 [8,9]. If one requires that the 0th, 1st, and 2nd derivatives of the two potentials agree at $r = r_0$, one finds $n(r_0) = 6 + 12/[2 - (r_0/\sigma)^6]$. Thus, $n(\sigma) = 18$, whereas $n(0.969\sigma) = 16.2$ (this is where $\phi_{LJ} = \epsilon$).

To directly test whether the fluctuations are well described by an inverse power-law potential, we proceeded as follows. A large number of configurations from the simulation of the zero-pressure state point in Fig. 1(a) were stored. This time series of configurations was analyzed by splitting the potential energy into two terms: $U(t) = U_{pow}(t) + U_{rest}(t)$, where $U_{pow}(t) \equiv \sum_{i<j} \phi_{pow}[r_{ij}(t)]$, i.e., the potential energy if the interatomic potential were an inverse power law. Comparing $U_{pow}(t)$ and $U(t)$ it was found that the fluctuations were nearly identical, $\Delta U_{pow}(t) \approx \Delta U(t)$, with a correlation coefficient of 0.94. Applying the same procedure to the virial, we found $\Delta W_{pow}(t) \approx \Delta W(t)$ with a correlation coefficient of 0.99. These results prove that the repulsive core of the LJ potential dominates fluctuations, even at zero and slightly negative pressure, *and* that at a given state point it is well described by an inverse power-law potential. The fact that the repulsive forces dominate the physics—here the fluctuations—confirms the philosophy of the well-known Weeks, Chandler, Andersen approximation [10].

It should be stressed that our approach is *not* to choose a particular inverse power law and analyze the results in terms of it. In fact, for an exact inverse power-law potential all data points in Fig. 1(b) would fall on the same line [$W(t) = \frac{n}{3}U(t)$]. Instead, we simply study the equilibrium fluctuations at each state- point and find strong W, U correlations, which in turn can be explained by an effective inverse power law dominating the *fluctuations*. The effective inverse power law exponent is weakly state-point
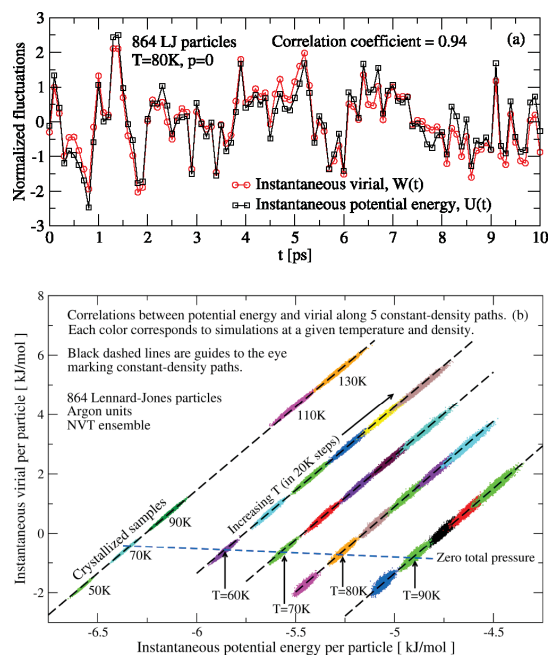
PHYSICAL REVIEW LETTERS

TABLE I. The correlation coefficient, R, and the slope $\gamma \equiv \sqrt{\langle(\Delta W)^2\rangle/\langle(\Delta U)^2\rangle}$ along an isochore, an isotherm, and an isobar for the Lennard-Jones liquid.

$\rho = 34.6$ mol/l	60 K	80 K	100 K	1000 K
R	0.900	0.939	0.953	0.997
γ	6.53	6.27	6.08	4.61
$T = 130$ K	32.6 mol/l	36.0 mol/l	39.8 mol/l	
R	0.945	0.974	0.987	
γ	6.06	5.71	5.40	
$p = 0.0$ GPa	60K	70K	80K	90K
R	0.965	0.954	0.939	0.905
γ	6.08	6.17	6.27	6.52

FIG. 1 (color). Results from equilibrium molecular dynamics simulations of 864 particles interacting via the Lennard-Jones potential studied in the *NVT* ensemble where "argon units" were used ($\sigma = 0.34$ nm, $\epsilon = 0.997$ kJ/mol). (a) Normalized fluctuations at $T = 80$ K and zero average pressure (density = 34.6 mol/l) of the virial, W, $\Delta W(t)/\sqrt{\langle(\Delta W)^2\rangle}$, and of the potential energy, $\Delta U(t)/\sqrt{\langle(\Delta U)^2\rangle}$. The equilibrium fluctuations of virial and potential energy are strongly correlated, as quantified by the correlation coefficient: $R \equiv \langle\Delta W\Delta U\rangle/\sqrt{\langle(\Delta W)^2\rangle\langle(\Delta U)^2\rangle} = 0.94$, where averages are over the full length of the simulation (10 ns) after 10 ns of equilibration. (b) Configurational parts of pressure and energy—virial versus potential energy—for several state points of the Lennard-Jones liquid. Each color represents simulations at one particular state point where each data point marks instantaneous values of virial and potential energy from a 10ns simulation. The black dashed lines mark constant density paths with the highest density to the upper left (densities: 39.8, 37.4, 36.0, 34.6, 32.6 mol/l). State points on the blue dashed line have zero average total pressure. The plot includes three crystallized samples (lower left corner).

dependent, and the above explanation is consistent with the qualitative trends seen in Table I: Increasing temperature along an isochore or increasing density along an isotherm results in stronger correlation and smaller slopes, corresponding to a numerically smaller apparent exponent. This reflects particles approaching closer to each other, and thus r_0 decreasing [$n(r_0)$ decreasing] and the inverse power law being an even better approximation to the LJ potential close to r_0. We do find that $\gamma \to 4$ ($n \to 12$) at high temperatures and/or densities as expected, but only under quite extreme conditions; see Table I. Along an isobar there

is competition between the effects of density and temperature. Our results show that the density effect dominates: the correlation increases with *decreasing* temperature. This, incidentally, is the limit of interest when studying highly viscous liquids (see below).

In order to investigate how general the W, U correlations are, several other systems were studied. If $W(t)$ and $U(t)$ are perfectly correlated ($R = 1$), the following identity applies: $\langle\Delta W\Delta U\rangle^2 = \langle(\Delta W)^2\rangle\langle(\Delta U)^2\rangle$. Figure 2 summarizes our simulations in a plot where the diagonal corresponds to perfect correlation and the y variable by the fluctuation-dissipation theorem equals T times the configurational pressure coefficient $[(T/V)(\partial W/\partial T)_V]$. Liquids with strong W, U correlations ($R > 0.9$) include: (1) A liquid with exponential short-range repulsion; (2) the Kob-Andersen binary Lennard-Jones liquid [11]; (3) a liquid consisting of asymmetric "dumbbell" type molecules (two unlike Lennard-Jones spheres connected by a rigid bond [12]); (4) a seven-site united-atom model of toluene [13]. The last three liquids are examples of good glass formers that can be cooled to high viscosity without crystallizing. Liquids not showing strong W, U correlations are methanol [14] and SPC/E water [15]; in these models the instantaneous potential energy has contributions from both LJ interactions ($U_{LJ}(t)$) and Coulomb interactions ($U_C(t)$). Since the Coulomb interaction is an inverse power law with $n = 1$, the corresponding contribution to the instantaneous virial is given by $W_C(t) = U_C(t)/3$, i.e., perfect correlation. For the LJ interaction of SPC/E water we find $\Delta W_{LJ}(t) \approx 6\Delta U_{LJ}(t)$ with correlations coefficients above 0.9. Since the proportionality constants are different, however, the *sums* of the contributions do not correlate very well. In fact, close to the density maximum of water we find that $W(t)$ and $U(t)$ are uncorrelated. For methanol $\Delta W(t)$ and $\Delta U(t)$ correlate well at such high temperatures that the LJ interactions completely dominate (≈ 3000 K).

Do strong pressure-energy correlations have consequences accessible by experiment? In the following we demonstrate how it is possible to test for strong W, U correlations in systems where the kinetic contribution to the isochoric heat capacity is known, exemplified by experimental data for supercritical argon. From the definition of R, utilizing

three fluctuation formulas [4] it is straightforward to show [16] (where c_V^{conf} and β_V^{conf} are the configurational parts of the isochoric heat capacity per volume and pressure coefficient, respectively, and K_T is the isothermal bulk modulus) that

$$T(\beta_V^{\text{conf}})^2/c_V^{\text{conf}} = R^2(p - K_T + \langle X \rangle/V). \qquad (1)$$

Here $X = \sum_{i<j} rw'(r_{ij})/9$ is the so-called "hypervirial" where $w(r) = r\phi'(r)$. This quantity cannot be determined experimentally [4], so we apply an approximation. For an exact power-law potential, one has $X = (n/3)W$, which, however, is not expected to be a good approximation since the apparent power law depends on the state point. In the vicinity of a given reference state point, however, one expects $[X - X_{\text{ref}}] \approx (n/3)[W - W_{\text{ref}}]$ along an isochore
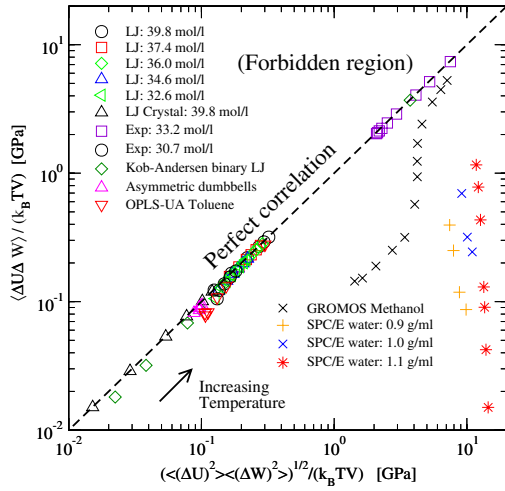

FIG. 2 (color online). $\langle \Delta W \Delta U \rangle/(k_B TV)$ plotted as a function of $(\langle(\Delta W)^2\rangle\langle(\Delta U)^2\rangle)^{1/2}/(k_B TV)$ for several liquids. If the correlation is perfect $(R = 1)$ the data fall on the diagonal. The region above the diagonal corresponds to $R > 1$ and is thus forbidden. LJ: Lennard-Jones results from the simulations reported in Fig. 1. Similar results were found in the NVE ensemble, for larger samples, and using Langevin dynamics (results not shown). Exp: 500 particles interacting via a pair potential with exponential repulsion; $U(r) = \frac{\epsilon}{8}[6e^{-14(r/\sigma-1)} - 14(\sigma/r)^6]$, simulated with Metropolis dynamics. Kob-Andersen binary LJ: The Kob-Andersen binary Lennard-Jones liquid, $N = 1000$ [11]. This includes data for the less-viscous liquid, the highly viscous liquid, as well as the glass. Asymmetric dumbbell: 512 asymmetric "dumbbell" molecules [12]. OPLS-UA Toluene: A 7-site united-atom model of toluene, $N = 1000$ [13]. GROMOS Methanol: 512 methanol molecules [14]. SPC/E water: 4142 SPC/E water molecules [15]. Except for the two systems with Coulomb interactions (Methanol and water), all systems studied have strong correlations between fluctuations in virial and potential energy; correlation coefficients are above 0.9 for all state points shown, except those with negative pressure, where they are slightly smaller. The correlation coefficients increase with increasing density and temperature.

(confirmed by our simulations). Using this approximation and assuming that R is roughly constant, we can test for strong W, U correlations. Figure 3 shows experimental data for supercritical argon covering the temperature range 200–660 K at three different densities [17], showing that W and U correlate 96% in this case. The apparent power-law exponents, $n = 3\beta_V^{\text{conf}}/c_V^{\text{conf}}$ [16] varies from 13.2 to 15.8, decreasing with increasing temperature and density. The inset shows that the argon data do *not* follow the prediction following from an exact inverse power-law potential [16,18] [Eq. (1) with $R = 1$ and $X = (n/3)W$]; thus the W, U correlations show that such an effective power-law description applies to a good approximation only for the *fluctuations*. This is analogous to the situation for the Lennard-Jones liquid: The equation of state is poorly described by that following from an inverse power-law potential (see, e.g., [19]), although the fluctuations are well described by this.

A different class of systems where it is possible to test for strong W, U correlations experimentally is highly viscous liquids [12,20]. These are characterized by a clear separation of time scales between the fast vibrational degrees of freedom on the picosecond time scale and the much slower configurational degrees of freedom on the second or hour time scale, depending on temperature [21–27]. Suppose a highly viscous liquid has perfectly correlated W, U fluctuations. When W and U are time averaged
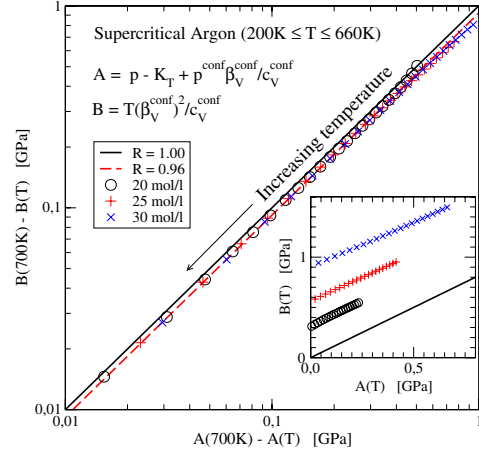
FIG. 3 (color online). Data for supercritical argon at 3 different densities covering the temperature range 200–660K [17] showing a W, U correlation of 96% [$K_T \equiv -V(\partial p/\partial V)_T$, $p^{\text{conf}} \equiv p - Nk_BT/V = W/V$, $\beta_V^{\text{conf}} \equiv (\partial p/\partial T)_V - Nk_B/V$, and $c_V^{\text{conf}} \equiv C_V/V - (3/2)Nk_B/V$]. The full line corresponds to perfect correlation between virial and potential energy [16]. The inset shows the prediction for an exact inverse power-law interatomic potential (full line): $B(T) = A(T)$. The poor fit shows that the fact that *fluctuations* are well described by an effective inverse power law does not imply that this is the case also for the equation of state.

over, say, one tenth of the liquid relaxation time [12], they still correlate 100%. Since the kinetic contribution to pressure is fast, the time-averaged pressure equals the time average of W/V plus a constant. Similarly, the time-averaged energy equals the time-averaged potential energy plus a constant. Thus the fluctuations of the time-averaged W and U are the slowly fluctuating parts of pressure and energy, so these slow parts will also correlate 100% in their fluctuations. This is the single ''order'' parameter scenario of Ref. [20]. In this case, knowledge of just one of the eight fundamental frequency-dependent thermoviscoelastic response functions implies knowledge of them all [20] (except for additive constants [28]). This constitutes a considerably simplification of the physics of glass-forming liquids. Unfortunately, there are few reliable data for the frequency-dependent thermoviscoelastic response functions [29]. Based on the results presented above we predict the existence of a class of ''strongly correlating viscous liquids'' where just one frequency-dependent thermoviscoelastic response function basically determines all. Our simulations suggest that the class of strongly correlating liquids includes van der Waals liquids, but not network liquids like water or silica. This is consistent with the findings of De Michele *et al.* [30].

Very recently Coslovich and Roland studied diffusion constants D in highly viscous binary Lennard-Jones mixtures at varying pressure and temperature [31]. Their data follow the ''density scaling'' expression $D = F(\rho^\gamma/T)$ [32], and they showed convincingly that the exponent γ reflects the effective inverse power law of the repulsive core. In view of these findings, we conjecture that strongly correlating viscous liquids obey density scaling, and vice versa. If this conjecture is confirmed, by virtue of their simplicity the class of strongly correlating liquids provides an obvious starting point for future theoretical works on the highly viscous liquid state.

[1] L. D. Landau and E. M. Lifshitz, *Statistical Physics* (Pergamon, London, 1980), Part 1.

[2] J. P. Hansen and I. R. McDonald, *Theory of Simple Liquids*, (Academic, New York, 1986), 2nd ed.

[3] L. E. Reichl, *A Modern Course in Statistical Physics* (Wiley, New York, 1998), 2nd ed.

[4] M. P. Allen and D. J. Tildesley, *Computer Simulation of Liquids* (Oxford Science Publications, Oxford, 1987).

[5] H. J. C. Berendsen, D. van der Spoel, and R. van Drunen, Comput. Phys. Commun. **91**, 43 (1995); E. Lindahl, B. Hess, and D. van der Spoel, J. Mol. Model. **7**, 306 (2001).

[6] J. E. Lennard-Jones, Proc. Phys. Soc. London **43**, 461 (1931).

[7] S. A. Nosé, J. Chem. Phys. **81**, 511 (1984); W. G. Hoover, Phys. Rev. A **31**, 1695 (1985).

[8] H. S. Kang, C S. Lee, T. Ree, and F. H. Ree, J. Chem. Phys. **82**, 414 (1985).

[9] D. Ben-Amotz and G. J. Stell, J. Chem. Phys. **119**, 10 777 (2003).

[10] J. D. Weeks, D. Chandler, and H. C. Andersen, J. Chem. Phys. **54**, 5237 (1971).

[11] W. Kob and H. C. Andersen, Phys. Rev. Lett. **73**, 1376 (1994).

[12] U. R. Pedersen, T. Christensen, T. B. Schrøder, and J. C. Dyre, cond-mat/0611514 [Phys. Rev. E (to be published)].

[13] W. L. Jorgensen, J. D. Madura, and C. J. Swenson, J. Am. Chem. Soc. **106**, 6638 (1984).

[14] W. R. P. Scott, P. H. Hunenberger, I. G. Tironi, J. Phys. Chem. A **103**, 3596 (1999).

[15] H. J. C. Berendsen, J. R. Grigera, and T. P. Straatsma, J. Chem. Phys. **91**, 6269 (1987).

[16] See EPAPS Document No. E-PRLTAO-100-033802 for detailing method for analyzing experimental data for supercritical argon. For more information on EPAPS, see http://www.aip.org/pubservs/epaps.html.

[17] E. W. Lemmon, M. O. McLinden, and D. G. Friend, ''Thermophysical Properties of Fluid Systems'' in *NIST Chemistry WebBook, NIST Standard Reference Database Number 69*, edited by P. J. Linstrom and W. G. Mallard (NIST, Gaithersburg, MD, 2005), http://webbook.nist.gov.

[18] J. N. Cape and L. V. Woodcock, J. Chem. Phys. **72**, 976 (1980); M. Baus and J.-P. Hansen, Phys. Rep. **59**, 1 (1980); J. D. Weeks, Phys. Rev. B **24**, 1530 (1981).

[19] J. K. Johnson, J. A. Zollweg, and K. E. Gubbins, Mol. Phys. **78**, 591 (1993).

[20] N. L. Ellegaard, T. Christensen, P. V. Christiansen, N. B. Olsen, U. R. Pedersen, T. B. Schrøder, and J. C. Dyre, J. Chem. Phys. **126**, 074502 (2007).

[21] W. Kauzmann, Chem. Rev.. **43**, 219 (1948).

[22] S. Brawer, *Relaxation in Viscous Liquids and Glasses* (Amer. Ceramic Soc., Columbus, OH, 1985).

[23] C. A. Angell, K. L. Ngai, G. B. McKenna, P. F. McMillan, and S. W. Martin, J. Appl. Phys. **88**, 3113 (2000).

[24] P. G. Debenedetti and F. H. Stillinger, Nature (London) **410**, 259 (2001).

[25] F. Sciortino, J. Stat. Mech. (2005) P05015.

[26] K. Binder and W. Kob, *Glassy Materials and Disordered Solids: An Introduction to their Statistical Mechanics* (World Scientific, Singapore, 2005).

[27] J. C. Dyre, Rev. Mod. Phys. **78**, 953 (2006).

[28] More precisely, knowledge of one response function implies knowledge of any other except for two real numbers giving the low- and high-frequency limits, respectively.

[29] T. Christensen, N. B. Olsen, and J. C. Dyre, Phys. Rev. E **75**, 041502 (2007).

[30] C. De Michele, P. Tartaglia, and F. Sciortino, J. Chem. Phys. **125**, 204710 (2006).

[31] D. Coslovich and C. M. Roland, arXiv:0709.1090.

[32] C. Alba-Simionesco, A. Cailliaux, A. Alegria, and G. Tarjus, Europhys. Lett. **68**, 58 (2004); R. Casalini and C. M. Roland, Phys. Rev. E **69**, 062501 (2004); C. M. Roland, S. Hensel-Bielowka, M. Paluch, and R. Casalini, Rep. Prog. Phys. **68**, 1405 (2005).

Feasibility of a single-parameter description of equilibrium viscous liquid dynamics

Ulf R. Pedersen, Tage Christensen, Thomas B. Schrøder, and Jeppe C. Dyre

DNRF centre "Glass and Time," IMFUFA, Department of Sciences, Roskilde University, Postbox 260, DK-4000 Roskilde, Denmark

(Received 24 November 2006; revised manuscript received 22 April 2007; published 15 January 2008)

Molecular dynamics results for the dynamic Prigogine-Defay ratio are presented for two glass-forming liquids, thus evaluating the experimentally relevant quantity for testing whether metastable-equilibrium liquid dynamics is described by a single parameter to a good approximation. For the Kob-Andersen binary Lennard-Jones mixture as well as for an asymmetric dumbbell model liquid, a single-parameter description works quite well. This is confirmed by time-domain results where it is found that energy and pressure fluctuations are strongly correlated on the α time scale in the constant-volume, constant-temperature ensemble; similarly, energy and volume fluctuations correlate strongly in the constant-pressure, constant-temperature ensemble.

The physics of viscous liquids approaching the glass transition continue to attract attention [1]. Basic problems like the origins of nonexponential relaxations and non-Arrhenius viscosities are still actively debated. A question that is not currently actively debated is whether a single "order" parameter is enough to describe glass-forming liquids and the glass transition [2]. For more than 30 years the consensus has been that with few exceptions more than one parameter is required, a conclusion that appears scarcely surprising given the complexity of glass-forming liquids [3–9]. In glass science "order" parameters traditionally refer to numbers characterizing the structure of the glassy phase, but we emphasize from the outset that this paper deals with the metastable equilibrium viscous liquid phase above the glass transition.

The prevailing paradigm of glass science regarding "order" parameters may be summarized as follows [1–9]. If Δc_p is the drop in isobaric specific heat per volume going from liquid to glass, $\Delta \kappa_T$ and $\Delta \alpha_p$ are the same changes in isothermal compressibility and isobaric thermal expansion coefficient, respectively, and T_g is the glass transition temperature, the Prigogine-Defay ratio Π is defined by

$$\Pi = \frac{\Delta c_p \Delta \kappa_T}{T_g (\Delta \alpha_p)^2}. \tag{1}$$

Davies and Jones in 1952 proved that if there is just one "order" parameter, then $\Pi = 1$ [4]. In their formulation, if a liquid is described by a single parameter, its linear relaxations are all simple exponentials [4]. The vast majority of reported Prigogine-Defay ratios obey $\Pi > 1$ [10]. Following Davies and Jones this is consistent with the observation that linear relaxations are virtually never exponential. The case for requiring more than one parameter got further support from the classical crossover experiment of Kovacs [11] as well as from several other experiments, all showing that glass structure cannot be completely characterized by a single number [12,13].

Part of this conventional wisdom may be challenged, though. First, note that Π is not strictly well defined. This is because to evaluate Δc_p, etc., one must extrapolate measurements in the glass phase into the liquid region, but the glass phase is not unique, it relaxes with time, and moreover extrapolations are not mathematically uniquely defined. Second, as shown by Goldstein [5] and Moynihan and Lesikar [14], but perhaps not generally appreciated, it is possible to have liquids with $\Pi = 1$ described by a single parameter with nonexponential dynamics.

Although it has been conclusively demonstrated that not all aspects of glass structure can be described by a single number [1–9], this does not rule out the possibility that a single parameter is sufficient for describing a more limited range of phenomena—e.g., the linear thermoviscoelastic properties of a glass-forming liquid [15–17]. It is this possibility we inquire into below, where all simulations were performed in metastable equilibrium with no reference to the glassy phase.

Experiments carried out the last few years by Richert and Weinstein [18], Ngai *et al.* [19], and our group [20] indicate that a single-parameter description in fact may be appropriate for some situations. The motivation of the present work is a paper from 2004 by Mossa and Sciortino who simulated aging of a molecular model of ortho-terphenyl [21]. For small temperature steps they found that the location of the aging system in configuration space can be traced back to equilibrium states, implying that [21] "a thermodynamic description based on one additional parameter can be provided" for cases of nonlinear relaxations fairly close to equilibrium. This suggests studying the (metastable) equilibrium viscous liquid itself in order to investigate whether—and how—"one-parameter-ness" may be reflected in the *equilibrium fluctuations*.

A single-parameter description of the metastable-equilibrium liquid dynamics by definition applies in the following situation [17]. Suppose a linear-response experiment is performed where "input" infinitesimal temperature and pressure variations $\delta T(t)$ and $\delta p(t)$ are imposed on the liquid and "output" infinitesimal entropy and volume variations $\delta S(t)$ and $\delta V(t)$ are observed. Since highly viscous liquids exhibit time-scale separation between the fast (vibrational) degrees of freedom and the much slower (relaxational) degrees of freedom, in general one expects that each of the outputs may be written as instantaneous couplings to the inputs plus a relaxing contribution—the latter being a standard linear convolution integral involving the previous temperature and pressure histories. By definition, if the two relaxing contributions are proportional, the liquid is described
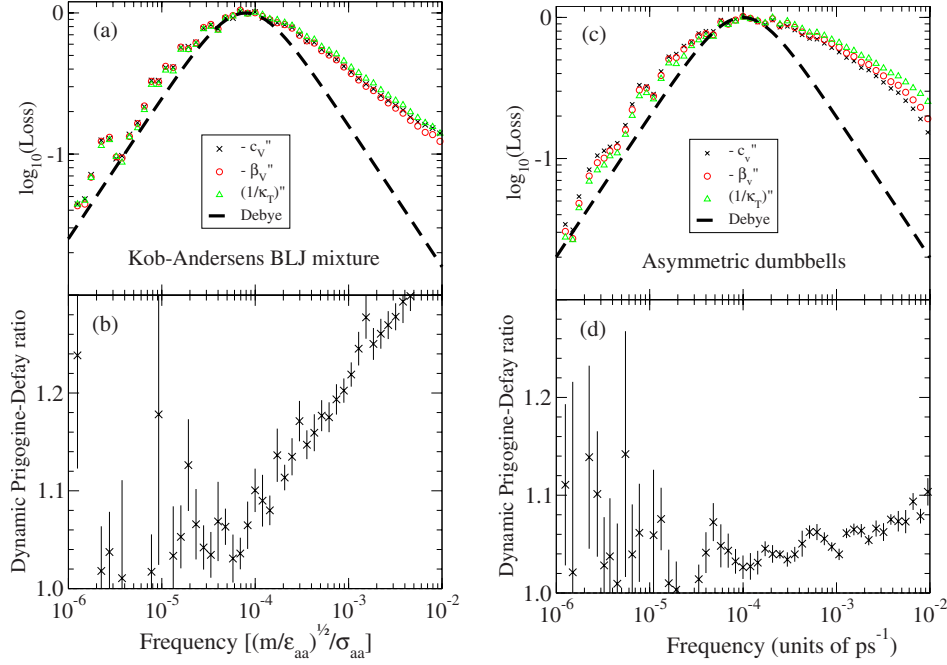
FIG. 1. (Color online) (a) shows the imaginary parts (scaled to maximum value) of $-c_v(\omega)$, $-\beta_v(\omega)$, and $1/\kappa_T(\omega)$ for the Kob-Andersen binary Lennard-Jones (BLJ) 80-20 mixture [27]; (c) shows the same for a system of asymmetric dumbbells [28]. The dashed lines indicate Debye relaxation with relaxation times $\tau_\alpha = 2000 \; \sigma_{aa}\sqrt{m/\epsilon_{aa}}$ and $\tau_\alpha = 1600$ ps, respectively. (b) and (d) show the corresponding dynamic Prigogine-Defay ratios, Eq. (2). For both systems the total simulation time covers more than $10^4 \tau_\alpha$.

by a single parameter [17]. In other words, a single-parameter description applies whenever a variable $\delta\epsilon$ exists such that

$$\delta S(t) = \gamma_1 \, \delta\epsilon(t) + J_{11}^\infty \, \delta T(t) - J_{12}^\infty \, \delta p(t),$$

$$\delta V(t) = \gamma_2 \, \delta\epsilon(t) + J_{21}^\infty \, \delta T(t) - J_{22}^\infty \, \delta p(t). \tag{2}$$

In Ref. [17] it was proved that for any stochastic dynamics a single-parameter description applies if and only if the following "dynamic Prigogine-Defay ratio", that is always larger than one, is unity at all frequencies:

$$\Lambda_{Tp}(\omega) = \frac{c_p''(\omega) \kappa_T''(\omega)}{T[\alpha_p''(\omega)]^2}. \tag{3}$$

Here the double primes denote the imaginary part of the response function. Furthermore, it was proved that if the dynamic Prigogine-Defay ratio is unity at one frequency, it is unity at all frequencies. Unfortunately, the relevant frequency-dependent thermoviscoelastic response functions are difficult to measure—in fact, no reliable measurements appear yet to exist. This single-frequency criterion should be useful for the interpretation of experiment, since it is likely that the first measurements will cover only a limited frequency range. In real experiments one can, of course, never prove that a number is unity, but it seems reasonable to assume that the closer the dynamic Prigogine-Defay ratio is to

unity, the more accurate a single-parameter description is.

There is no simple physical interpretation of the parameter $\delta\epsilon$ except that it controls both entropy and volume relaxations. There is no reason to believe that $\delta\epsilon$ gives a complete characterization of the molecular structure in the way "order" parameters of traditional glass science are supposed to do. Despite this severe limitation it is not obvious that glass-forming liquids exist that to a good approximation are described by a single parameter. Recent results studying thermal fluctuations of less-viscous liquids give rise to optimism, though: For a number of model liquids [22]—including the standard Lennard-Jones system—the potential energy and the virial correlate better than 90% in their thermal equilibrium fluctuations. Recall that the virial when divided by volume is the contribution to pressure from the molecular interactions—i.e., in addition to the ever-present ideal-gas contribution deriving from the kinetic degrees of freedom, $Nk_B T/V$. This strong virial-energy correlation is not surprising at high pressure where the repulsive part of the potential dominates. The correlation, however, applies even at densities where the pressure is slightly negative [22] which is less obvious *a priori*, the reason being that the fluctuations are dominated by particle-particle close encounters, even at zero and negative pressure.

The observed strong virial potential energy correlations do not depend significantly on viscosity. For highly viscous liquids, because of the time-scale separation, one expects

that the slow (relaxing) contributions to pressure are given by the virial and that the slow contributions to energy come from the potential energy. Thus these variables should be highly correlated in their slow equilibrium fluctuations for systems similar to those studied in Ref. [22]. This suggests that to a good approximation a single, relaxing parameter controls both quantities, in which case it is obvious to expect that Eq. (2) may apply as well.

To test this the dynamic Prigogine-Defay ratio was evaluated for two viscous liquid model systems by computer simulation. The test requires that three frequency-dependent thermoviscoelastic response functions must be evaluated. For simulations carried out at constant temperature and volume (the *NVT* ensemble) the relevant response functions are the isochoric specific heat per unit volume c_v, the isothermal compressibility κ_T, and the isochoric pressure coefficient $\beta_v \equiv (\partial p / \partial T)_V$. These quantities enter the *NVT* dynamic Prigogine-Defay ratio [17] via

$$\Lambda_{TV}(\omega) = -\frac{c_v''(\omega)[1/\kappa_T(\omega)]''}{T[\beta_v''(\omega)]^2}. \quad (4)$$

The fluctuation-dissipation (FD) theorem [23–26] implies that the above linear-response functions may be determined from the equilibrium fluctuations of energy (E) and pressure (p) as follows. If $\Delta E(t) \equiv E(t) - \langle E \rangle_{V,T}$, $\Delta p(t) \equiv p(t) - \langle p \rangle_{V,T}$ and $\mathcal{C}_\omega\{f(t)\}$ denotes the cosine transform of $f(t)$ at frequency ω, according to the FD theorem

$$\Lambda_{TV}(\omega) = \frac{\mathcal{C}_\omega\{\langle \Delta E(0)\Delta E(t)\rangle_{V,T}\}\mathcal{C}_\omega\{\langle \Delta p(0)\Delta p(t)\rangle_{V,T}\}}{[\mathcal{C}_\omega\{\langle \Delta E(0)\Delta p(t)\rangle_{V,T}\}]^2}. \quad (5)$$

If energy and pressure fluctuations correlate perfectly, one has $\Delta E(t) \propto \Delta p(t)$ and consequently $\Lambda_{TV}(\omega)=1$ at all frequencies. Equation (5) suggests that the dynamic Prigogine-Defay ratio tests how well the two relevant quantities (here energy and pressure) correlate on the time scale defined by the frequency, as sort of a time-scale-dependent inverse correlation coefficient squared.

Figure 1(a) shows the frequency dependence of the imaginary parts of the three linear-response functions for the standard Kob-Andersen binary Lennard-Jones 80-20 mixture [27]. The three response functions are very similar, and all exhibit the characteristic asymmetry toward higher frequencies observed for real glass-forming liquids. Figure 1(b) shows the dynamic Prigogine-Defay ratio; as mentioned, this number is unity if and only if the three imaginary parts are strictly proportional [17]. This is not the case, but the ratio is fairly close to unity in the frequency range of the main (α) process. Thus in the range of frequencies one decade above and below the loss-peak frequency—the "α-relaxation range"—the ratio stays below 1.2. In accordance with the above interpretation of $\Lambda_{TV}(\omega)$ this indicates that on time scales in the α-relaxation range energy and pressure have a correlation coefficient that is larger than 0.9.

We also simulated a highly viscous single-component molecular liquid. This is a system of "asymmetric dumbbell" molecules defined as two Lennard-Jones spheres of different radii held together by a rigid bond [28]. As shown in Figs. 1(c) and 1(d) the imaginary parts of the response functions
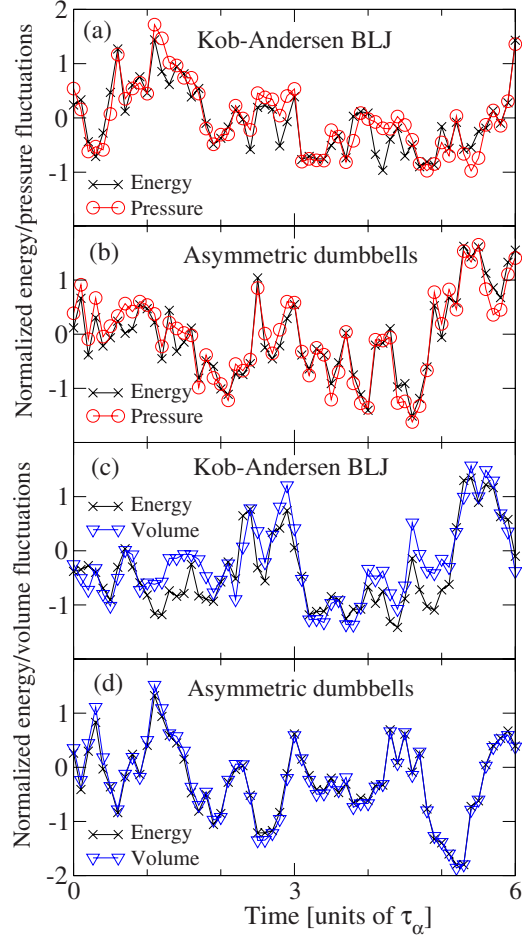
FIG. 2. (Color online) (a) and (b) Fluctuations of energy and pressure in the *NVT* ensemble for the Kob-Andersen binary Lennard-Jones mixture [27] and the asymmetric dumbbell system [28]. Each point represents an average over a time interval of $0.1\tau_\alpha$ where τ_α is defined as the inverse loss-peak frequency [Figs. 1(a) and 1(c)]. Energy and pressure fluctuations are highly correlated, showing that a single-order-parameter description is a good approximation. (c) and (d) Fluctuations of energy and volume in the *NpT* ensemble at the same state points as (a) and (b), respectively.

are similar and the dynamic Prigogine-Defay ratio stays below 1.06 in the α-relaxation region.

The results in Fig. 1 show that a class of viscous liquids exists where the dynamic Prigogine-Defay ratio is close to unity. This is consistent with earlier computer simulations of the (poorly defined) standard Prigogine-Defay ratio Π [Eq. (1)] for a few systems, showing that this quantity is often close to unity [29,30]. In Figs. 2(a) and 2(b) we plot energy and pressure equilibrium fluctuations as functions of time for both systems. In order to focus on fluctuations in the α-time

range, both pressure and energy were averaged over one-tenth of τ_α (defined as the inverse loss-peak frequency), corresponding to focusing on the inherent dynamics [31] appropriate for understanding the viscous behavior. As expected, the correlations are strong. Both systems were also simulated at constant temperature and pressure. Here energy and volume show similarly strong correlations [Figs. 2(c) and 2(d)]. Thus the appropriateness of a single-parameter description is not ensemble dependent.

To summarize, it has been shown that it is possible to investigate the single-parameter question by monitoring thermal equilibrium fluctuations. The dynamic Prigogine-Defay ratio provides a convenient test quantity for this, a quantity that is also relevant for experiment because it refers to one single frequency. Several questions are still unanswered. For instance, it is not known whether there is any link to fragility; one traditionally expects strong liquids to be single-parameter systems and fragile liquids to require a multiple-parameter description. The findings of Ref. [22], however, indicate that network liquids are *not* well described by a single parameter in the above sense, whereas purely van der Waals liquids are. Clearly, more work is needed to clarify this and other issues, and we hope that the results presented here serve to encourage the physics and glass communities to once again address the old question: one or more "order" parameters?

---

[1] W. Kauzmann, Chem. Rev. **43**, 219 (1948); G. Harrison, *The Dynamic Properties of Supercooled Liquids* (Academic Press, New York, 1976); S. Brawer, *Relaxation in Viscous Liquids and Glasses* (American Ceramic Society, Columbus, OH, 1985); C. A. Angell, K. L. Ngai, G. B. McKenna, P. F. McMillan, and S. W. Martin, J. Appl. Phys. **88**, 3113 (2000); C. Alba-Simionesco, C. R. Acad. Sci., Ser. IV Phys. Astrophys. **2**, 203 (2001); P. G. Debenedetti and F. H. Stillinger, Nature (London) **410**, 259 (2001); W. Kob, in *Slow Relaxations and Nonequilibrium Dynamics in Condensed Matter*, Proceedings of the Les Houches Summer School of Theoretical Physics, 2002, edited by J.-L. Barrat, M. Feigelman, J. Kurchan, and J. Dalibard (Springer, Berlin, 2004), Session LXXVII, p. 199; J. C. Dyre, Rev. Mod. Phys. **78**, 953 (2006).

[2] In glass science the term "order parameters" is traditionally used for numbers that in conjunction with pressure and temperature completely characterize a glass—i.e., the molecular structure. In order to avoid confusion with the use of the term in connection with critical phenomena, it may be prudent to just speak of "parameters" or "order" parameters.

[3] I. Prigogine and R. Defay, *Chemical Thermodynamics* (Longman, London, 1954).

[4] R. O. Davies and G. O. Jones, Proc. R. Soc. London, Ser. A **217**, 26 (1952); R. O. Davies and G. O. Jones, Adv. Phys. **2**, 370 (1953).

[5] M. Goldstein, in *Modern Aspects of the Vitreous State*, edited by J. D. Mackenzie (Butterworths Scientific, London, 1964), Vol. 3, p. 90.

[6] C. A. Angell and W. Sichina, Ann. N. Y. Acad. Sci. **279**, 53 (1976).

[7] I. Gutzow and J. Schmelzer, *The Vitreous State: Thermodynamics, Structure, Rheology, and Crystallization* (Springer, Berlin, 1995).

[8] S. V. Nemilov, *Thermodynamic and Kinetic Aspects of the Vitreous State* (CRC Press, Boca Raton, FL, 1995).

[9] E. Donth, *The Glass Transition* (Springer, Berlin, 2001).

[10] C. T. Moynihan *et al.*, Ann. N.Y. Acad. Sci. **279**, 15 (1976).

[11] A. J. Kovacs, Fortschr. Hochpolym.-Forsch. **3**, 394 (1963).

[12] R.-J. Roe, J. Appl. Phys. **48**, 4085 (1977).

[13] G. W. Scherer, *Relaxations in Glass and Composites* (Academic, New York, 1986).

[14] C. T. Moynihan and A. V. Lesikar, Ann. N. Y. Acad. Sci. **371**, 151 (1981).

[15] Th. M. Nieuwenhuizen, Phys. Rev. Lett. **79**, 1317 (1997).

[16] R. J. Speedy, J. Phys. Chem. B **103**, 8128 (1999).

[17] N. L. Ellegaard, T. Christensen, P. V. Christiansen, N. B. Olsen, U. R. Pedersen, T. B. Schrøder, and J. C. Dyre, J. Chem. Phys. **126**, 074502 (2007).

[18] R. Richert and S. Weinstein, Phys. Rev. Lett. **97**, 095703 (2006).

[19] K. L. Ngai, R. Casalini, S. Capaccioli, M. Paluch, and C. M. Roland, J. Phys. Chem. B **109**, 17356 (2005).

[20] J. C. Dyre and N. B. Olsen, Phys. Rev. Lett. **91**, 155703 (2003).

[21] S. Mossa and F. Sciortino, Phys. Rev. Lett. **92**, 045504 (2004); see also S. Mossa, E. La Nave, F. Sciortino, and P. Tartaglia, Eur. Phys. J. B **30**, 351 (2002).

[22] U. R. Pedersen, N. Bailey, T. B. Schrøder, and J. C. Dyre, Phys. Rev. Lett. **100**, 015701 (2008).

[23] N. G. van Kampen, *Stochastical Processes in Physics and Chemistry* (North-Holland, Amsterdam, 1981).

[24] L. E. Reichl, *A Modern Course in Statistical Physics*, 2nd ed. (Wiley, New York, 1998).

[25] J. K. Nielsen and J. C. Dyre, Phys. Rev. B **54**, 15754 (1996).

[26] J. K. Nielsen, Phys. Rev. E **60**, 471 (1999).

[27] The Kob-Andersen binary Lennard-Jones 80-20 mixture was set up [W. Kob and H. C. Andersen, Phys. Rev. Lett. **73**, 1376 (1994)] with $N=1000$, $V=(9.4\sigma_{aa})^3$. The temperature was held constant at $T=0.474$ $\epsilon_{aa}k_B^{-1}$ using the Nosé-Hoover thermostat [S. A. Nosé, Mol. Phys. **52**, 255 (1984); W. G. Hoover, Phys. Rev. A **31**, 1695 (1985)]. The simulations were carried out using GROMACS software [H. J. C. Berendsen, D. van der Spoel, and R. van Drunen, Comput. Phys. Commun. **91**, 43 (1995); E. Lindahl, B. Hess, and D. van der Spoel, J. Mol. Model. **7**, 306 (2001)]. The total time covers more than 10^7 Lennard-Jones time units ($\sigma_{aa}\sqrt{m/\epsilon_{aa}}$).

[28] A system consisting of 512 asymmetric dumbbell molecules modeled as two Lennard-Jones spheres connected by a rigid bond was simulated. The dumbbells were parametrized to mimic toluene. A large sphere (mimicking a phenyl group) was

taken from the Wahnström ortho-terphenyl model [L. J. Lewis and G. Wahnström, Phys. Rev. E **50**, 3865 (1994)] with the parameters m_p=77.106 u, σ_p=0.4963 nm, and ϵ_p=5.726 kJ/mol. A small sphere (mimicking a methyl group) was taken from UA-OPLS [W. L. Jorgensen, J. D. Madura, and Carol J. Swenson, J. Am. Chem. Soc. **106**, 6638 (1984)] having m_m=15.035 u, σ_m=0.3910 nm, and ϵ_m=0.669 44 kJ/mol. The bonds were kept rigid using the LINCS algorithm [B. Hess, H. Bekker, H. J. C. Berendsen, and J. G. E. M. Fraaije, J. Comput. Chem. **18**, 1463 (1997)] with a bond length of d=0.29 nm. The volume was V=77.27 nm^3 giving an average pressure of approximately 1 atm. The temperature was held constant at T=130 K using the Nosé-Hoover thermostat. The simulations were carried out using GROMACS software.

[29] C. A. Angell, J. H. R. Clarke, and L. V. Woodcock, Adv. Chem. Phys. **48**, 397 (1981).

[30] D. Morineau, G. Dosseh, R. J. M. Pellenq, M. C. Bellissent-Funel, and C. Alba-Simionesco, Mol. Simul. **20**, 95 (1997).

[31] T. B. Schrøder, S. Sastry, J. C. Dyre, and S. C. Glotzer, J. Chem. Phys. **112**, 9834 (2000).

Volume-Energy Correlations in the Slow Degrees of Freedom of Computer-Simulated Phospholipid Membranes

Ulf R. Pedersen*, Günther H. Peters†, Thomas B. Schrøder*, and Jeppe C. Dyre*

*DNRF Centre "Glass and Time," IMFUFA, Department of Sciences, Roskilde University, Postbox 260, DK-4000 Roskilde, Denmark
†Center for Membrane Biophysics (MEMPHYS), Department of Chemistry, Technical University of Denmark, DK-2800 Lyngby, Denmark

Abstract. Molecular dynamics simulations of phospholipid membranes reveals striking correlations between equilibrium fluctuations of volume and energy on the nanosecond time-scale. Volume-energy correlations have previously been observed experimentally at the phase transition between the L_α phase and the L_β phase, but not in the fluid L_α phase. The correlations are investigated in four membranes, with correlation coefficients ranging between 0.81 and 0.89. An experimentally single parameter test is proposed.

Keywords: Molecular dynamics simulation, Phospholipid membrane, Single parameter description
PACS: 05.40.-a, 64.60.Cn, 68.05.Cf

Biological membranes are an essential part of living cells. They not only act as passive barrier between outside and inside, but play an active role in various biological mechanisms. The major constituent of biological membranes are phospholipids. Pure phospholipid membranes often serve as a models for the more complex biological membranes. Close to physiological temperatures membranes undergo a transition from the fluid L_α phase (often referred to as the biologically relevant phase) to an ordered gel phase L_β. In the melting regime, at the transition temperature T_m, the response functions such as heat-capacity, volume expansion coefficient and area expansion coefficient increase dramatically. Also, the characteristic time for the collective degrees of freedom increases and becomes longer than milliseconds. Heimburg et. al. found that the response functions are connected so a single function describes the temperature dependence of all of them. Experiments indeed shows that heat capacity and volume expansion coefficient of DMPC can be superimposed at T_m [1] (see also [2, 3]).

The fluctuation-dissipation (FD) theorem connects response functions to equilibrium fluctuations. The isobaric heat capacity c_p can be calculated from enthalpy fluctuations as follows: $c_p = \langle (\Delta H)^2 \rangle / (Vk_BT^2)$, where $\langle ... \rangle$ is an average in the constant temperature and pressure ensemble and Δ is deviation from the average value. Similarly, volume fluctuations are connected to the isothermal volume compressibility by the expression $\kappa_T = \langle (\Delta V)^2 \rangle / (Vk_BT)$. If the response functions were described by a single parameter, fluctuations are also described by a single parameter [1, 4] and the microstates were connected via the relation $\Delta H_i = \gamma^{vol} \Delta V_i$. At constant pressure this relation applies if and only if

$\Delta E_i = \gamma^{vol} \Delta V_i$ (where E is energy), which is the relation investigated below. This situation is referred to as a that of a single-parameter description [4]. A single-parameter description applies to a good approximation for several models of van der Waals bonded liquids as well as for experimental super-critical argon [5].

Molecular dynamics simulation is not a good method for investigate the "single parameter"-ness of membranes at T_m, since the relaxation time for collective motions exceeds typical simulation times. However, we show below that a single parameter description is not only feasible at the phase transition, but also in the fluid L_α phase approaching T_m. We discusss how this can be tested in experiments.

It is not trivial that a single parameter is sufficient. Simulations of water and methanol show no "single parameter"-ness, since competing interactions destroy the correlation. Contributions to volume and energy fluctuations from hard core repulsion compete with directional hydrogen bonds [5]. Membranes are complex anisotropic systems and one cannot give an a priori reason for why volume and energy should be correlated.

A membrane may be perturbated via three thermodynamic energy bonds. A change of the enthalpy dH can be written as a contribution from a thermal bond, a mechanical volume bond and mechanical lateral (or area) energy bond, $dH = dE + pdV + \Pi dA$ where E is internal energy, p is pressure, V is volume, Π is surface tension of the membrane and A is the membrane area. The natural ensemble to consider is the constant T, p and Π ensemble since water will act as a reservoir. If a single parameter controls the microstates, for all states i one would have $\Delta E_i = \gamma^{vol} \Delta V_i = \gamma^{area} \Delta A_i$ where the γ's are constants.
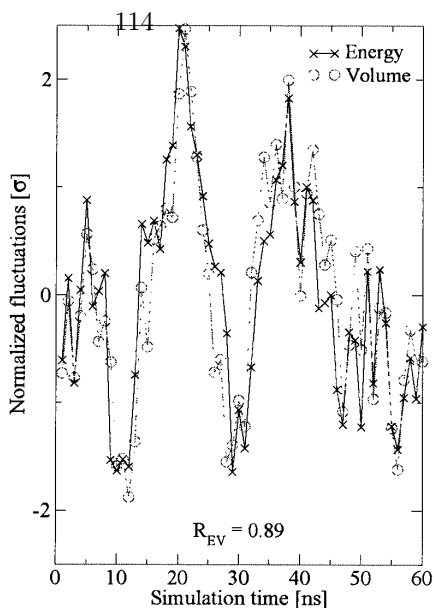
FIGURE 1. (Color online) Normalized fluctuations of energy (×) and volume (○) for a DMPC membrane at 310 K. Each data point represents a 1 ns average. Energy and volume are correlated with a correlation coefficient of $R = 0.89$.

FIGURE 2. (Color online) Time correlation functions of potential energy C_{EE} (×), total volume C_{VV} (○), membrane area C_{AA} (△) and cross correlation between energy and volume C_{EV} (◇). Time correlation for membrane areas are scaled by a factor 0.2. Panel A shows data for a DMPC membrane at 330 K and panel B for a DMPC membrane at 310 K. The inset (C) displays $\Gamma = C_{EV}/\sqrt{C_{EE}C_{VV}}$ at 310 K (○) and 330 K (×). Γ approaches unity at $t \simeq 1$ ns meaning that volume and energy become strongly correlated on this timescale. Color online.

In general, the microstates may of course be controlled by several parameters. An interesting question is how many parameters are sufficient to describe the membrane thermodynamics to a good approximation. This question is addressed below by investigating molecular-dynamics simulations of different phospholipid membranes.

An overview of the simulated systems is found in table 1. The simulated systems include different head groups (both charged and zwitterions) and temperatures. All simulations was carried out in the constant pressure, temperature ensemble. The membranes are fully hydrated and in the fluid L_α phase. The simulations were performed using the program NAMD [6] and a modified version of CHARMM27 all hydrogen parameter set [7, 8]. More simulation details have previously been published [8, 9].

Striking correlations between time-averaged equilibrium fluctuations of volume and energy on the nanosecond time-scale of a DMPC membrane at 310 K are shown on Figure 1. If $\overline{E(t)}$ is the energy averaged over 1 nanosecond and $\overline{V(t)}$ is the volume averaged over 1 nanosecond then

$$\Delta\overline{E(t)} \simeq \gamma^{vol}\Delta\overline{V(t)} \tag{1}$$

where $\gamma^{vol} = \sigma_E/\sigma_V$ is a constant, σ is the standard deviation and Δ is difference from the thermo-

dynamical average value. Equivalent results are found for the remaining membranes. Table 1 shows correlation coefficients between volume and energy, $R = \langle\Delta\overline{E}\Delta\overline{V}\rangle/\sqrt{\langle(\Delta\overline{E})^2\rangle\langle(\Delta\overline{V})^2\rangle}$ ranging between 0.81 and 0.89.

The correlation depends on the time scales considered. This can be investigated by evaluating $\Gamma(t) = C_{EV}(t)/\sqrt{C_{EE}(t)C_{VV}(t)}$ where $C_{AB}(t) = \langle\Delta A(\tau)\Delta B(\tau+t)\rangle/\sqrt{\langle(\Delta A)^2\rangle\langle(\Delta B)^2\rangle}$ is a time correlation function. $\Gamma(t) = 0$ implies that energy at time τ is uncorrelated with volume at time $t + \tau$ whereas $\Gamma(t)$ close to unity implies strong correlation. $\Gamma(t)$ is plotted in the inset of figure 2. At short time (picoseconds) Γ is around 0.5 but approaches unity at $t \simeq 1$ ns.

The "single parameter"-ness between volume and energy is connected to the experimental finding of Heimburg et. al. [1] since the slow collective degrees of freedom (at $t > 1$ ns) are the same ones which give rise to the dramatic changes of the response functions at T_m. There are some indications of this. Figure 2 shows time correlation functions of energy, volume and membrane area of

TABLE 1. Data from simulations of fully hydrated phospholipid membranes of 1,2-Dimyristoyl-sn-Glycero-3-Phosphocholine (DMPC), 1,2-Dimyristoyl-sn-Glycero-3-Phospho-L-Serine with sodium as counter ion (DMPS-Na) and hydrated DMPS (DMPSH). The columns lists temperature, correlation coefficient between volume and energy, average lateral area per lipid, simulation time in equilibrium (used in data analysis) and total simulation time.

	T [K]	R	A_{lip} [Å^2]	t [ns]	t_{tot} [ns]
DMPC	310	0.885	53.1	60	114
DMPC	330	0.806	59.0	50	87
DMPS-Na	340	0.835	45.0	22	80
DMPSH	340	0.826	45.0	40	77

DMPC membranes at 330 K and 310 K. The time constant and the magnitude of the slow fluctuations increase when the the temperature is decreased. γ^{vol} in equation 1 is 9.3×10^{-4} cm^3/J. This is the same order of magnitude as $\gamma^{vol} = 7.721 \times 10^{-4}$ cm^3/J calculated from experimental data of $C_p(T)$ and $\kappa_T^{vol}(T)$ at T_m [1].

Both the volume and energy time correlation functions show a two step relaxation at 310 K for DMPC (Figure 2B). As temperature is lowered toward T_m the separation is expected to be more significant. It makes sense to divide the dynamics into two separated processes, a fast and a slow collective process. Our simulations suggest that slow degrees of freedom can be described by a single parameter.

To see the "single parameter"-ness of the L_α phase, the fast degrees of freedom have to be filtered out. Experiments must deal with macroscopic samples where fluctuations are small and difficult to measure (the relative fluctuations scales as $1/\sqrt{N}$ where N is the number of molecules). It is therefore difficult to do the same analysis as we have done here. It is easier to measure response functions.

Fast fluctuations can be filtered out by measuring frequency dependent response functions. The slow collective degrees of freedom will show as a separate peak. The frequency dependent Prigogine-Defay ratio $\Lambda_{Tp}(\omega)$ has been suggested as a test quantity for "single parameter"-ness [4]. If $c_p''(\omega)$, $\kappa_T''(\omega)$ and $\alpha_p''(\omega)$ are the imaginary parts of the isobaric specific heat capacity per volume, isothermal compressibility and isobaric expansion coefficient respectively then

$$\Lambda_{Tp}(\omega) = \frac{c_p''(\omega)\kappa_T''(\omega)}{T_0[\alpha_p''(\omega)]^2}. \qquad (2)$$

In general $\Lambda_{Tp} \geq 1$ and only have the value of unity if a single parameter describes the fluctuations. $1/\sqrt{\Lambda_{Tp}}$ can be related to a correlation coefficient.

In summary, we found strong volume-energy correlations of the slow collective degrees of freedom in molecular dynamics simulations of different phospholipid membranes in the L_α phase. An experimental test was suggested.

ACKNOWLEDGMENTS

REFERENCES

1. T. Heimburg, *Biochim. Biophys. Acta* **1415**, 147–162 (1998).
2. T. Heimburg, and A. D. Jackson, *Proc. Natl. Acad. Sci.* **102**, 9790–9795 (2005).
3. H. Ebel, P. Grabitz, and T. Heimburg, *J. Phys. Chem. B* **105**, 7353–7360 (2001).
4. N. L. Ellegaard, T. Christensen, P. V. Christiansen, N. B. Olsen, U. R. Pedersen, T. B. Schrøder, and J. C. Dyre, *J. Chem. Phys.* **126**, 074502-1–074502-8 (2007).
5. U. R. Pedersen, T. Christensen, T. B. Schrøder, and J. C. Dyre, *arXiv.org cond-mat/0611514* (2006).
6. J. C. Phillips, R. Braun, W. Wang, J. Gumbart, E. Tajkhorshid, E. Villa, C. Chipot, R. D. Skeel, L. Kale, and K. Schulten, *J. Comput. Chem.* **26**, 1781–1802 (2005).
7. N. Foloppe, and A. D. MacKerell, *J. Comput. Chem.* **21**, 86–104 (2000).
8. U. R. Pedersen, C. Leidy, P. Westh, and G. H. Peters, *Biochim. Biophys. Acta* **1758**, 573–582 (2006).
9. U. R. Pedersen, G. H. Peters, and P. Westh, *Biophysical Chemistry* **125**, 104–111 (2007).

Glass-forming liquids: one or more 'order' parameters?

Nicholas P Bailey, Tage Christensen, Bo Jakobsen, Kristine Niss, Niels Boye Olsen, Ulf R Pedersen, Thomas B Schrøder and Jeppe C Dyre

DNRF Centre 'Glass and Time', IMFUFA, Department of Sciences, Roskilde University, Postbox 260, DK-4000 Roskilde, Denmark

Abstract
We first summarize the classical arguments that the vast majority of glass-forming liquids require more than one 'order' parameter for their description. Critiques against this conventional wisdom are then presented, and it is argued that the matter deserves to be reconsidered in the light of recent experimental developments. Out of the eight basic thermoviscoelastic frequency-dependent response functions, there are generally three independent functions. For stochastic dynamics we show that there are only two independent response functions; for this case it is shown how analytic continuation may be utilized to express the third response functions in terms of two others. Operational criteria are presented for the linear thermoviscoelasticity being described by a single 'order' parameter, in which case there is just one independent thermoviscoelastic response function. It is shown that a description with a single 'order' parameter applies to a good approximation whenever thermal equilibrium fluctuations of fundamental variables like energy and pressure are strongly correlated. Results from computer simulations showing that this is the case for a number of simple glass-forming liquids, as well as a few exceptions, are briefly presented. Finally, we briefly discuss a new conjecture according to which experiments at varying temperature and pressure follow the density scaling expression for the relaxation time, $\tau = F(\rho^x/T)$ (ρ and T are density and temperature), if and only if the liquid is 'strongly correlating', i.e., to a good approximation is described by a single 'order' parameter.

(Some figures in this article are in colour only in the electronic version)

1. Introduction

The question whether one 'order' parameter is sufficient for describing glass structure attracted considerable interest among glass scientists in the period 1950–1980. The question was thoroughly discussed in particular in the 1970s [1–6] leading to clarifications of a number of theoretical questions. Since then, based on experimental evidence the consensus has been that one 'order' parameter is rarely enough.

The term 'order parameter' was commonly used in the glass community before the term in the 1960s became commonly known in the physics community where it took on a somewhat different meaning. In connection with critical phenomena and the theory of second order phase transitions, renormalization, etc, 'order parameters' reflect the relevant Lie group symmetry and determine the relevant part of the free energy within a Ginzburg–Landau expansion of the free energy. In order not to confuse the issue it is probably a good idea to change the wording, so below we refer to *'order' parameters* or occasionally just *parameters*.

The present paper summarizes and extends recent works making the case that the question of how many 'order' parameters are sufficient deserves to be reconsidered. In section 2 we briefly summarize the classical viewpoint, in section 3 critiques against it are presented, in section 4 the more restricted well-defined case of linear thermoviscoelasticity is presented, in section 5 thermoviscoelasticity in complete generality is discussed, in section 6 we show that in any stochastic description of the dynamics there are only two independent response functions, section 7 treats the single-parameter case where there is just one independent thermoviscoelastic response function, in section 8 the

118   *B. Papers*

J. Phys.: Condens. Matter **20** (2008) 244113   N P Bailey *et al*

new concept of a 'dynamic' Prigogine–Defay ratio, which tests 'one-parameter-ness' by reference to single-frequency thermoviscoelastic measurements, is presented. Section 9 presents a few computer simulations showing that several systems indeed are well described by only a single parameter, section 10 discusses a recent conjecture stating that the single-parameter liquids are precisely those that obey density scaling for the results of high-pressure experiments. Finally, section 11 gives a brief summary.

2. The conventional wisdom: one parameter is seldom enough

The standard 'order' parameter theory of glass science was developed by Davies and Jones in the 1950s [7, 8]. This theory idealizes the glass transition and treats it as a genuine phase transition. In the liquid the 'order' parameters are functions of pressure and temperature, whereas they are frozen in the glass phase. If Δc_p is the difference between liquid and glass isobaric specific heat per unit volume at the glass transition temperature T_g, $\Delta\kappa_T$ the liquid–glass difference of isothermal compressibilities, and $\Delta\alpha_p$ the liquid–glass difference of isobaric thermal expansion coefficients, the Prigogine–Defay ratio Π is defined [7–9] by

$$\Pi = \frac{\Delta c_p \Delta\kappa_T}{T_g \left(\Delta\alpha_p\right)^2}. \tag{1}$$

Within the Davies–Jones framework one can prove [7, 8] that $\Pi \geqslant 1$, an inequality that has been confirmed in many experiments on quite diverse glass-forming liquids [10–13]. If there is just a single 'order' parameter, one has $\Pi = 1$. Although there are glass-forming polymers where $\Pi = 1$ within experimental uncertainty [14, 15], the vast majority, if not all, glass-forming liquids have $\Pi > 1$ (typically: $2 < \Pi < 5$) [2]. If simple first order dynamics are adopted, the case of a single parameter implies an exponential decay towards equilibrium after external disturbances [1–8]. This is rarely observed, a fact that traditionally was seen as a confirmation of the conventional wisdom that more than one parameter is required.

A further classical argument for one parameter not being enough is the well-known fact that glass properties are not uniquely defined by, e.g., the density, as one would expect if there is just one parameter [3, 11]. For instance, one can prepare glasses with same index of refraction, but different electrical conductivity. This point was beautifully illustrated in Kovacs' classical crossover experiments [11, 16].

In summary: the observed Prigogine–Defay ratios are almost always significantly larger than unity, relaxations are almost always non-exponential, and glass properties are not just a function of density. This altogether makes a convincing case for there generally being a need for more than one parameter, a conclusion that also appears natural given the complexities of glass-forming liquids and glass structure. Based on this, with few exceptions (e.g., [17–20]), the matter has not been actively discussed for long time.

3. Questioning the conventional wisdom

The first point to be noted is that the question of one or more 'order' parameters is not really well defined in the classical approach, because the glass transition is not a phase transition. The fact that the glass transition is a dynamic phenomenon— a gradual falling out of equilibrium that inevitably takes place whenever inherent relaxation times become longer than experimental times—is well known and well understood. This weakens the classical theory where one regards the glass transition as a freezing-in process taking place at a particular temperature [21].

A related conceptual problem is that the Π of equation (1) is not strictly well defined. The changes in specific heat, etc, from liquid to glass are not well defined because of two facts: (1) these changes are found by extrapolating the liquid and glass properties, respectively, to the transition region. The glass transition temperature, however, is not strictly well defined because the glass transition is not a phase transition. (2) The glass phase is not well defined—and it relaxes continuously—in principle making any measured property in the glass phase a function of time. Many researchers would argue that, while this is correct in principle, these effects are minor and not sufficiently important to reduce the observed Prigogine–Defay ratios to unity. We take a more purist viewpoint, however, and believe that concepts that are not well defined should be avoided in a scientific description.

Recent experiments monitoring ageing of a glass at temperatures around T_g indicate that in some cases the deviations from equilibrium may be quantified in terms of a single parameter. One example is a study where the characteristics of the dielectric Johari–Goldstein beta loss peak were used to monitor structural relaxations taking place on the alpha timescale [22, 23]. To keep things simple only beta loss-peak frequency and beta maximum loss were monitored, thus providing two numbers that depend on structure and temperature. For both sorbitol [22] and tripropylene glycol [23] it was found that at any given temperature these two numbers correlate linearly. Thus even after a complex thermal history, when returning back to some given temperature, beta loss-peak frequency and loss maximum always lie on a line characterizing that temperature. An example of this is provided in figure 1 showing loss-peak frequency and maximum loss for the Johari–Goldstein beta process of tripropylene glycol during a temperature cycling around T_g. If the structure were characterized by more than one order parameter, there is no reason why such a correlation should hold. On the other hand, if structure is characterized by a single parameter, at any given temperature the two quantities must correlate, and for fairly small deviations from equilibrium this correlation would appear approximately linear (in linear as well as in log–log plots).

Other dielectric experiments also indicate that a single structural parameter may be sufficient in some cases. Thus studying the shape of the alpha loss peak as quantified by the exponent of the best-fit stretched exponential function, it has been shown for a number of liquids [24] that when both temperature and pressure are varied, the shape depends only of
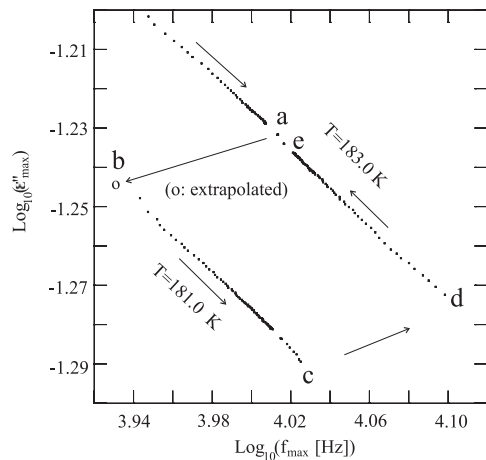
Paper VI   119

J. Phys.: Condens. Matter **20** (2008) 244113   N P Bailey *et al*

Figure 1. Temperature-jump experiment for tripropylene glycol monitored via the beta loss-peak frequency and loss-peak maximum [23]. These two numbers depend on structure, and their relaxation monitors structural relaxation (known to take place on the alpha timescale). Starting at 185.0 K temperature was first lowered to 183.0 K and kept there for 84 h. Then temperature was changed to 181.0 K where it was kept for 140 h. Thereafter temperature was changed back to 183.0 K and kept there for another 140 h. The fact that the beta loss-peak frequency and loss maximum correlate at any given temperature, also after jumping to 181.0 K and back go 183.0 K, indicates that the structure controlling the beta relaxation is described by a single parameter.

the loss-peak frequency. A simple explanation of this would be that there is just a single structural parameter, because if that were the case, this parameter would determine both loss-peak frequency and loss-peak shape and consequently these two quantities would automatically correlate.

Richert and Weinstein from a study of the nonlinear dielectric response on glycerol showed that, although the dielectric and thermal relaxation times vary throughout the liquid, they are locally closely correlated [25]. Again, if there is just one parameter determining all properties, one would expect that this parameter may fluctuate in space, but locally determine both dielectric and thermal relaxation time.

More evidence comes from computer simulations. In a model of ortho-terphenyl Mossa and Sciortino [26] studied ageing for fairly small temperature steps that were, however, large enough to be well outside the linear regime. The simulations showed that in configuration space the location of the ageing system can be traced back to equilibrium states. The authors summarized their findings by stating that for nonlinear relaxations close to equilibrium 'a thermodynamic description based on one additional parameter can be provided.'

There seems to be a general understanding in the glass community that there is one 'order' parameter if and only if the Prigogine–Defay ratio is unity, which happens if and only if relaxations are simple exponentials. This is not correct, however, and not what one finds from reading the classical papers carefully. Goldstein in his 1964 review, for instance, noted that in some situations with several parameters that

are mathematically constrained by several constraints, the Prigogine–Defay ratio may be unity. In this situation 'it is really a matter of taste' [27] whether one prefers to speak of many (constrained) parameters or of a single *generally non-exponential* 'order' parameter. Thus the observation of non-exponential relaxations does not imply that there must be more than one parameter.

In 2006 Schmelzer and Gutzow revisited the Prigogine–Defay ratio and the question of the number of 'order' parameters [20]. Assuming just a single parameter the dynamics of which follow the classical framework of the thermodynamics of irreversible processes, they argued that the standard Prigogine–Defay ratio (obtained by extrapolating from glass and liquid to T_g) nevertheless is larger than unity. This result seriously questions the prevailing understanding of the glass community reviewed above, and it emphasizes the need for further work.

The first one should do in reconsidering the 'order' parameter question is to make sure that the problem is well defined. As mentioned, the standard Prigogine–Defay ratio Π of equation (1) is not well defined. As became clear in the 1970s [3, 4, 6], it is possible to define a version of Π that is well defined. This is done by referring exclusively to properties of the equilibrium viscous liquid phase and its linear responses. In this phase thermodynamic properties are generally frequency dependent, and the high-frequency limits correspond to glassy behaviour where structural relaxations do not take place. If $c_p(\omega)$ is the frequency-dependent isobaric specific heat per unit volume [28], etc, this leads to the following rigorous definition of the Prigogine–Defay ratio for the metastable equilibrium viscous liquid at any temperature T:

$$\Pi = \{[c_p(\omega \to 0) - c_p(\omega \to \infty)]$$
$$\times [\kappa_T(\omega \to 0) - \kappa_T(\omega \to \infty)]\}$$
$$\times \{T[\alpha_p(\omega \to 0) - \alpha_p(\omega \to \infty)]^2\}^{-1}. \tag{2}$$

4. Linear thermoviscoelasticity

From now on we turn the focus exclusively to the metastable liquid phase with no reference to the glass phase. This limits the discussion compared to what is standard in glass science, but has the advantage of making all concepts rigorously well defined. Linear thermoviscoelasticity deals with the frequency dependence of thermodynamic properties and their coupling to frequency-dependent mechanical properties. It is understood that, in principle, only infinitesimal perturbations are applied, thus ensuring linearity. In the simplest (isotropic) theory there are two fundamental 'energy bonds,' a thermal and a mechanical. An energy bond has an 'effort' variable and a 'displacement' variable [29–31]. The thermal energy bond is characterized by entropy S as the displacement variable and temperature T as the effort, for the mechanical energy bond the displacement variable is the volume V and the effort is the negative pressure, $-p$. The product of the effort and the differential displacement variable gives the energy transferred into the system from its surroundings. Thus the two energy bonds (figure 2) simply express the well-known fundamental identity $dE = T\,dS - p\,dV$.
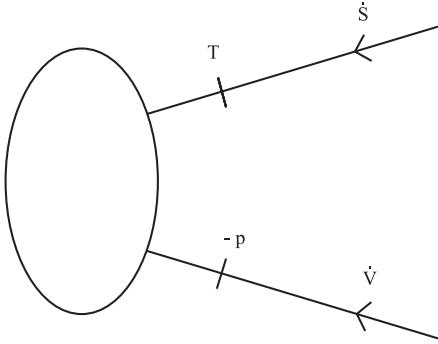
Figure 2. The two fundamental energy bonds [31] for a system described by standard thermodynamics. One energy bond is thermal; here the 'effort' is temperature T and the displacement variable is the entropy S; thus if $\dot{S} \equiv dS/dt$ is the entropy flux into the system, the rate of energy transferred into the system is $T\dot{S}$. The second energy bond is mechanical; here the effort is negative pressure $-p$ and the displacement variable is the volume V; if $\dot{V}$ is the volume flux into the system, the rate of energy transferred into the system is $-p\dot{V}$.

For infinitesimal perturbations around equilibrium with angular frequency ω, if one imagines controlling the effort variables and measuring displacement changes, and if the usual complex notation is adopted where, e.g., $T(t) = T_0 + \delta T(t)$ with $\delta T(t) = \mathrm{Re}[\delta T \exp(i\omega t)]$, linearity is expressed in the following relation where δs is entropy change per unit volume and δv is relative volume change:

$$\begin{pmatrix} \delta s(\omega) \\ \delta v(\omega) \end{pmatrix} = \begin{pmatrix} c_p(\omega)/T & \alpha_p(\omega) \\ \alpha_p(\omega) & \kappa_T(\omega) \end{pmatrix} \begin{pmatrix} \delta T(\omega) \\ -\delta p(\omega) \end{pmatrix}. \quad (3)$$

The response matrix is sometimes termed the thermal compliance matrix. Its symmetry expresses Onsager reciprocity, reflecting the fundamental fact that there is time reversibility on the microscopic level [32, 33].

5. The completely general case: three independent thermoviscoelastic response functions

How many independent thermoviscoelastic response functions exist? From the four variables, entropy, temperature, volume and pressure, one may choose any two as 'control' variables. Usually, one chooses one control variable from each energy bond. There are thus four natural choices of control ('input') variables, the two remaining are the measured ('output') variables. For each choice there is one response matrix as in equation (3) [34]. These four matrices are all symmetric by Onsager reciprocity, leaving 12 frequency-dependent response functions. These are not independent, however; if one matrix is known, the three others are easily calculated from it by isolating the output variables in question on the left-hand sides of two equations. Thus there are only the *three* independent response functions, for instance those of equation (3).

The above statement is true in complete generality. Papers by Moynihan and others of the 1970s showed, however, that in the 'order' parameter description there are really only *two*

independent response functions [1, 4, 35] (see also [36]). The formula for calculating the third response function in terms of the two others involves analytic continuation (next section). The situation is analogous to that of the Kramers–Kronig relation which allows one to calculate the imaginary part of a response function in terms of its real part, but only if the latter is known at all frequencies.

6. The general stochastic case: two independent thermoviscoelastic response functions

In this section we summarize the master equation description of viscous liquid dynamics [34, 37, 38] and show that it implies that there are just two independent response functions. More precisely, it is shown that knowledge of $c_p(\omega)$ and $\alpha_p(\omega)$ at all frequencies allows one to calculate $\kappa_T(\omega)$ except for an overall additive constant giving the high-frequency limit. This is equivalent to the above-mentioned result derived long ago [1, 3, 36], but now in a setting that is explicitly consistent with statistical mechanics.

In a master equation there are states and stochastic transitions between the states. A complete description is provided by the set of probabilities $\{P_n\}$ that the system is in state n. This is an ensemble description making it possible to calculate all properties, including the entropy. Following [34] we shall think of each state as an inherent state in the sense of Stillinger and Weber [39] (i.e., a potential energy minimum in configuration space), but other state interpretations are also possible. Each state has the vibrational Gibbs free energy $G_n(T, p)$. The ensemble Gibbs free energy that includes the probability dependence is given [34, 38] by

$$G(T, p, \{P_n\}) = \sum_n P_n(G_n(T, p) + k_\mathrm{B}T \ln P_n). \quad (4)$$

From this one finds the ensemble volume and entropy by the usual thermodynamic relations $V = \partial G/\partial p$ and $S = -\partial G/\partial T$.

The master equation dynamics are given by first order equations in time that are mathematically similar to those of the classical 'order' parameter description of glass science:

$$\dot{P}_n = \sum_m W_{nm} P_m. \quad (5)$$

The main difference to the 'order' parameter description is the constraint $\sum_n P_n = 1$ and that the present formalism ensures consistency with statistical mechanics.

The rate matrix W depends on T and p and changes slightly when these variables are perturbed by small time-dependent variations. The same applies for the equilibrium probabilities, $P_n^{\mathrm{eq}} \propto \exp[-G_n(T, p)/k_\mathrm{B}T]$. According to the principle of detailed balance, which ensures consistency with statistical mechanics as well as time-reversal invariance, the equilibrium probabilities [32, 33] obey

$$W_{nm}(T, p)P_m^{\mathrm{eq}}(T, p) = W_{mn}(T, p)P_n^{\mathrm{eq}}(T, p). \quad (6)$$

Here temperature and pressure may be arbitrary functions of time. For periodic infinitesimal perturbations from

Paper VI   121

J. Phys.: Condens. Matter **20** (2008) 244113   N P Bailey *et al*

equilibrium the dynamics are perturbed via the transition matrix's dependence on pressure and temperature. The equilibrium probabilities at $p = p_0$ and $T = T_0$ are denoted by P_n^0 and the transition matrix at this state point is denoted by W^0.

If Q_1 is entropy and Q_2 volume, solving the resulting system of equations leads [34] to the following expression for the compliance matrix of equation (3) (where $\frac{\partial Q_\alpha}{\partial P_m}$ and $\frac{\partial Q_\beta}{\partial P_m}$ are evaluated at (T_0, p_0), the matrix $A(\omega)$ is defined by $A(\omega) \equiv (W^0 - \mathrm{i}\omega)^{-1} W^0 P^0$, $\alpha, \beta = 1, 2$):

$$J_{\alpha\beta}(\omega) = J_{\alpha\beta}^\infty + \sum_{m,n} \frac{\partial Q_\alpha}{\partial P_n} A_{nm}(\omega) \frac{\partial Q_\beta}{\partial P_m}. \qquad (7)$$

Note that $A(\omega) \to 0$ for $\omega \to \infty$; thus $J_{\alpha\beta}(\omega) \to J_{\alpha\beta}^\infty$ for $\omega \to \infty$. Introducing the matrix $Y_{nm} \equiv (P_n^0)^{-\frac{1}{2}} W_{nm}^0 (P_m^0)^{\frac{1}{2}}$, the detailed balance requirement equation (6) implies that Y is symmetric. In terms of Y, the matrix $A(\omega)$ is given [34] by $A(\omega) = RY(Y - \mathrm{i}\omega)^{-1} R$ where $R_{nm} = (P_n^0)^{\frac{1}{2}} \delta_{nm}$. Thus for the relaxing part of the compliance matrix $\Delta J = J - J^\infty$, if ∂Q_α is the vector whose n th component is $\partial Q_\alpha / \partial P_n(T_0, p_0)$, one has [34]

$$\Delta J_{\alpha\beta}(\omega) = \langle R\partial Q_\alpha | \frac{Y}{Y - \mathrm{i}\omega} | R\partial Q_\beta \rangle. \qquad (8)$$

Adopting the standard 'ergodicity' assumption that all states are connected by some path of intermediate states, the matrix Y has a one-dimensional eigenspace corresponding to the eigenvalue zero whereas all other eigenvalues are negative [32, 33]. If the eigenvectors of Y corresponding to all the negative eigenvalues are denoted by $|\psi_j\rangle$ with corresponding eigenvalue $-1/\tau_j$, equation (8) implies

$$\Delta J_{\alpha\beta}(\omega) = \sum_j \langle R\partial Q_\alpha | \psi_j \rangle \langle \psi_j | R\partial Q_\beta \rangle \frac{-1/\tau_j}{-1/\tau_j - \mathrm{i}\omega}. \qquad (9)$$

Since $(-1/\tau_j)/(-1/\tau_j - \mathrm{i}\omega) = 1/(1 + \mathrm{i}\omega\tau_j)$, changing to a continuous notation equation (9) becomes

$$\Delta J_{\alpha\beta}(\omega) = \int_0^\infty \frac{g_\alpha(\tau) g_\beta(\tau)}{1 + \mathrm{i}\omega\tau} \, \mathrm{d}\tau, \qquad (10)$$

where the functions $g_\alpha(\tau)$ are real, but not necessarily positive.

By reference to the theory of analytic functions we show below that not all three functions of the compliance matrix are independent. This is intuitively obvious already from the fact that the *three* compliance functions are determined by the *two* functions $g_1(\tau)$ and $g_2(\tau)$. More precisely the argument goes as follows. The three compliance functions $\Delta J_{\alpha\beta}(\omega)$ are analytic. Knowledge of such a function at all real, positive frequencies by analytic continuation uniquely determines the function in the complex plane. Equation (10) shows that there is a branch cut along the positive imaginary frequency axis. Given that $\Delta J_{\alpha\beta}(\omega) \to 0$ for $\omega \to \infty$, the pole distribution on the branch cut uniquely determines the compliance function. More specifically, equation (10) implies that

$$\Delta J_{22}(\omega) = \int_0^\infty \lim_{\omega' \to \mathrm{i}/\tau} \left\{ (1 + \mathrm{i}\omega'\tau) \frac{\Delta J_{12}^2(\omega')}{\Delta J_{11}(\omega')} \right\}$$
$$\times \frac{1}{1 + \mathrm{i}\omega\tau} \, \mathrm{d}\tau. \qquad (11)$$

Thus knowledge of $\Delta c_p(\omega)$ and $\Delta\alpha_p(\omega)$ at all real, positive frequencies implies knowledge of $\Delta\kappa_T(\omega)$. Similarly, knowledge of $\Delta\kappa_T(\omega)$ and $\Delta\alpha_p(\omega)$ at all real, positive frequencies implies knowledge of $\Delta c_p(\omega)$.

7. The single-parameter case: one independent thermoviscoelastic response function

The compliance matrix $J_{\alpha\beta}(\omega)$ reflects both the relaxing responses (completely characterized by $\Delta J(\omega)$) and the instantaneous responses given by the high-frequency limits. Switching to the time domain, if the relaxing responses of the two energy bonds are always proportional, i.e., controlled by a common variable $\delta\varepsilon(t)$, the entropy and volume responses per unit volume are given by expressions of the form

$$\delta s(t) = \gamma_1 \delta\varepsilon(t) + J_{11}^\infty \delta T(t) - J_{12}^\infty \delta p(t)$$
$$\delta v(t) = \gamma_2 \delta\varepsilon(t) + J_{21}^\infty \delta T(t) - J_{22}^\infty \delta p(t). \qquad (12)$$

We refer to this situation as that of a single 'order' parameter [34] and proceed to show following [34] that in this case there is basically just one compliance function. Note that no reference is made to the properties of the glassy state.

For periodically varying fields equation (12) implies

$$\delta s(\omega) = \gamma_1 \delta\varepsilon(\omega) + J_{11}^\infty \delta T(\omega) - J_{12}^\infty \delta p(\omega)$$
$$\delta v(\omega) = \gamma_2 \delta\varepsilon(\omega) + J_{21}^\infty \delta T(\omega) - J_{22}^\infty \delta p(\omega). \qquad (13)$$

The ε-parameter may be expanded to first order as follows:

$$\delta\varepsilon(\omega) = \Lambda_1(\omega)\delta T(\omega) - \Lambda_2(\omega)\delta p(\omega). \qquad (14)$$

Substituting equation (14) into (13) and using the symmetry of the compliance matrix leads to the identity $\gamma_1\Lambda_2(\omega) + J_{12}^\infty = \gamma_2\Lambda_1(\omega) + J_{21}^\infty$. For the imaginary parts this implies

$$\frac{\Lambda_1''(\omega)}{\gamma_1} = \frac{\Lambda_2''(\omega)}{\gamma_2}. \qquad (15)$$

When two analytical functions both with branch cuts on the positive imaginary axis of the complex ω-plane have same imaginary part, they are identical except for an overall additive constant. The latter is zero, because the fact that the two functions give the *relaxing* part of the responses implies that they both go to zero for $\omega \to \infty$. Thus $\Lambda_1(\omega) \propto \Lambda_2(\omega)$. By considering the constant pressure and constant temperature cases it now follows easily from equations (13) and (14) that $\Delta J_{11}(\omega) \propto \Delta J_{12}(\omega) \propto \Delta J_{22}(\omega)$, or:

$$\Delta c_p(\omega) \propto \Delta\alpha_p(\omega) \propto \Delta\kappa_T(\omega). \qquad (16)$$

In conclusion, in the case of a single 'order' parameter (equation (12)) there is basically just one independent thermoviscoelastic response function, i.e., knowledge of one of them implies knowledge of the two others except for the overall additive constants giving their high-frequency limits.

8. 'Dynamic' Prigogine–Defay ratio: a single-parameter test

In principle, in order to test experimentally whether or not a single 'order' parameter suffices, one measures the three response functions of the compliance matrix to test whether the relaxing parts are proportional (equation (16)). This, however, requires wide-frequency measurements of the thermoviscoelastic response functions, and there are yet no measurements of all three thermoviscoelastic response functions on a glass-forming liquid. (Even the isobaric frequency-dependent specific heat $c_p(\omega)$ has not yet been measured reliably [28]. The problem is that, because frozen-in stresses relax on the same timescale that the enthalpy relaxes, establishing truly isobaric conditions is difficult and in most experimental set-ups the stress tensor is not diagonal.)

Even when methods have been developed for measuring the compliance matrix of equation (3), one may still expect that initial measurements cover only a rather limited dynamic range. This leads to the question: is it still possible to test the single-parameter conjecture equation (12)? This question was discussed in a recent publication [34] where it was shown that, in fact, measurements at one single frequency are enough to test the single-parameter conjecture. Of course, one can never *prove* that a single-parameter description is correct in an absolute sense—it is all a matter of investigating *how good* such a description is. In the above-mentioned recent paper [34] it was shown that a 'dynamic' Prigogine–Defay ratio $\Lambda_{Tp}(\omega) \geqslant 1$ exists with the property that, if this quantity is unity at one frequency, it is unity at all frequencies—which happens if and only if a single-parameter description applies. The dynamic Prigogine–Defay ratio is given by the imaginary parts of the three thermoviscoelastic response functions [34] as follows:

$$\Lambda_{Tp}(\omega) = \frac{c_p''(\omega)\kappa_T''(\omega)}{T_0(\alpha_p''(\omega))^2}. \tag{17}$$

In order to minimize uncertainties measurements should preferably be taken at a frequency around the alpha loss-peak frequency, because only here the imaginary parts are significantly different from zero. We expect that if $\Lambda_{Tp}(\omega)$ is close to unity in the main relaxation region (e.g., below 1.1), a single-parameter description applies to a good approximation.

9. Results from computer simulations

Recently thermal equilibrium fluctuations were studied in computer simulations of various liquids [40, 41]. In many cases it was found that in constant temperature and volume simulations (the so-called NVT ensemble) pressure and energy fluctuations correlate strongly. More accurately, this applies for the *configurational* parts of pressure and energy, the 'virial' and the potential energy. (The kinetic parts of pressure and energy—the ideal gas pressure at the given density and temperature, and the kinetic energy—trivially correlate 100%, but with a different proportionality constant.) As an example, figure 3 shows the thermal fluctuations of virial and potential energy for a standard Lennard-Jones liquid.
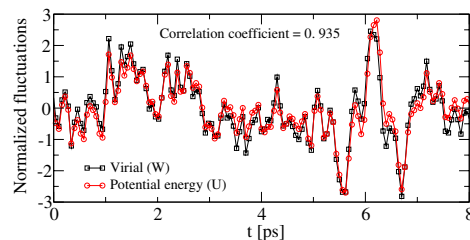
Figure 3. Thermal equilibrium fluctuations of potential energy and viral (the configurational part of pressure) for a standard Lennard-Jones liquid [41]. The fact that these two quantities correlate strongly shows that, as regards the configurational degrees of freedom, a single-parameter description is quite good for the thermoviscoelastic behaviour. For highly viscous liquids the timescale separation between the slow configurational degrees of freedom and the remaining implies that these correlations (that we have also seen, e.g., in simulations of the highly viscous Kob–Andersen binary Lennard-Jones mixture) implies that the three thermoviscoelastic response functions are basically identical.

As shown in [34], liquids for which these quantities correlate strongly in their fluctuations are well described by a single order parameter. Intuitively this may be understood by reference to equation (12) considered without perturbations ($\delta T(t) = \delta p(t) = 0$) which, if assumed to describe also the *fluctuations*, shows that entropy and volume fluctuations are 100% correlated. Thus one expects that the dynamic Prigogine–Defay ratio is close to unity for such 'strongly correlating liquids'. Figure 4 shows that strongly correlating liquids include the Lennard-Jones liquid as well as a number of other glass-forming liquids. Water and methanol are interesting exceptions that do not show strong correlations between virial and potential energy fluctuations (figure 5); thus for these two hydrogen-bonding liquids a single-parameter description does not apply.

10. A conjecture: strongly correlating liquids obey density scaling and vice versa

The last five years large amounts of data on the behaviour of glass-forming liquids under pressure have been published. The motivation is that by not just varying temperature, but pressure as well, much more information may be learned about these systems. Generally, the liquid relaxation time τ, which is basically the Maxwell relaxation time or the inverse alpha loss-peak frequency, depends strongly on both temperature and pressure, increasing with lowering temperature or raised pressure. This is not surprising. A new and significant finding [42–44], however, is that if ρ is the density, many liquids obey 'thermodynamic' or 'density' scaling, i.e., the function $\tau(T, p)$ may be written

$$\tau = F\left(\frac{\rho^x}{T}\right). \tag{18}$$

Both the function F and the exponent x depend on the liquid in question. This expression has mainly been tested on glass-forming molecular liquids, the systems that are most easily

Paper VI   123

J. Phys.: Condens. Matter **20** (2008) 244113   N P Bailey *et al*

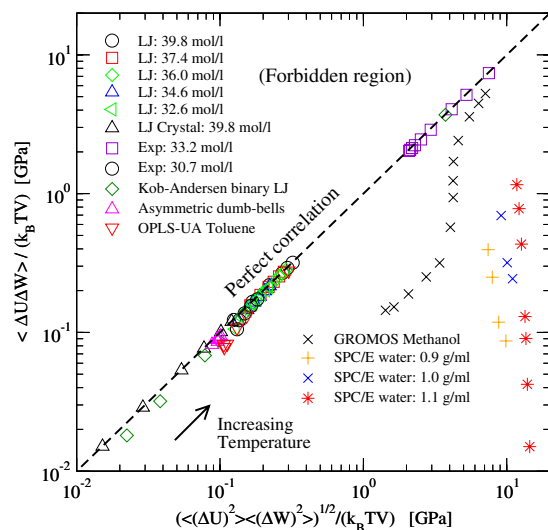**Figure 4.** Correlation coefficient between virial (volume times the configurational part of the pressure) and potential energy thermal equilibrium fluctuations for a number of liquids evaluated by computer simulations [41]. The liquids represented are: LJ: standard Lennard-Jones, exp: monatomic liquid with exponential repulsive forces, dumb-bell: a molecule model of two atoms of unlike size, BLJ: the Kob–Andersen binary Lennard-Jones liquid, methanol, and SPC/ *E* water. The last two are hydrogen bonding and do not show significant correlations; the other liquids do. It has been argued that virial and potential energy give the slowly fluctuating parts of the pressure and energy [41]; thus whenever the former quantities correlate strongly, to a good approximation the liquid may be regarded as described by a single parameter.

Figure 5. Correlation coefficients for a number of glass-forming liquids between virial and potential energy thermal equilibrium fluctuations as function of temperature (in reduced units). The liquids represented are: LJ: standard Lennard-Jones, exp: monatomic liquid with exponential repulsive forces, dumb-bell: a molecule model of two atoms of unlike size, BLJ: the Kob–Andersen binary Lennard-Jones liquid, methanol, and SPC/ *E* water. The figure shows the same systems as those of figure 4 studied by computer simulations. The two hydrogen-bonding liquids, water and methanol, show poor correlation, the remaining systems are all strongly correlating. For the latter the correlation even increases as temperature rises; this is because at high temperature the particles approach each other more in collisions than at low temperatures and the inverse power law description of the works better the closer the particles are.

accessible. For hydrogen-bonding liquids like glycerol or sorbitol the x's initially reported were anomalously small [44], but it now appears that the reason is that density scaling does not work very well for hydrogen-bonding liquids [45].

Recently, Coslovich and Roland presented computer simulations of binary Lennard-Jones type systems where the exponent of the repulsive term of the potential varied, taking the values 8, 12, 24, and 36 [46]. Such systems may be cooled to low temperatures where the viscosity is very large, without crystallizing. Their simulation results obey the density scaling expression equation (18), which by itself is an interesting finding. Even more interesting is the fact that the exponent x appears to be one third of the effective exponent describing the approximate power law of the potential. For the standard binary Lennard-Jones case, for instance, this latter exponent is not 12 as naively expected, but a number close to 18 depending on the precise choice of fitting criteria [41].

In [41] some of the present authors previously found that there are strong energy–pressure correlations whenever the repulsive part of the interaction is well described by an inverse power law. Since this seems also to be the criterion for a liquid obeying density scaling (equation (18)), an obvious conjecture is [41] that: *A glass-forming liquid is strongly correlating if and only if it obeys density scaling.* Two liquids that in computer simulations were not strongly

correlating are water and methanol [41], and we surmise that hydrogen-bonding liquids generally are not strongly correlating. The argument is that the existence of 'competing interactions' (van der Waals forces as well as the directional hydrogen bonds) destroy significant correlations, implying that hydrogen-bonding liquids are not well described by a single 'order' parameter. This is consistent with the finding that hydrogen-bonding liquids do not obey density scaling [45].

If this conjecture is correct, by virtue of their simplicity the class of strongly correlating liquids provides an obvious starting point for theories for viscous liquids and glass formation. It would be obvious to further conjecture that also covalently bonding liquids are not strongly correlating, again due to the directional nature of the bonds. Many of these systems have fairly low fragility. Low-fragility liquids are traditionally thought to be simple (e.g., have to almost exponential relaxations if the liquid is almost Arrhenius). We here conjecture almost the opposite, namely that many high-fragility liquids in a certain sense are simpler than many low-fragility liquids. Note that this simplicity, however, does not relate to the degree of non-exponentiality: both strongly correlating and 'complex' liquids may have close to exponential relaxations; there is no obvious correlation between the degree of non-exponentiality and how strongly correlating a liquid is.

11. Summary and final remarks

We have argued that the old discussion of one or more 'order' parameters deserves to be revitalized. There are

124   *B. Papers*

J. Phys.: Condens. Matter **20** (2008) 244113   N P Bailey *et al*

indications that at least some glass formers may be well described by a single order parameter as regards their linear thermoviscoelasticity. It is important to emphasize that no claim is made that the molecular structure is completely characterized by a single number. We now have an experimentally useful criterion for whether or not a single-parameter description is accurate. Computer simulations confirm that some model liquids are well described by a single parameter; these liquids are referred to as 'strongly correlating'. Since hydrogen-bonding liquids do not show these correlations, we expect that liquids with directional bonding are not well described by a single parameter, whereas van der Waals bonded liquids are. Thus it is conjectured that for van der Waals liquids the relaxing parts of the three thermoviscoelastic response functions of equation (3) are all proportional, whereas for hydrogen-bonding liquids this is conjectured not to be the case. This prediction can be tested once methods have been developed to measure the full thermoviscoelastic compliance matrix.

Acknowledgment

References

[1] Gupta P K and Moynihan C T 1976 *J. Chem. Phys.* **65** 4136
[2] Moynihan C T *et al* 1976 *Ann. New York Acad. Sci.* **279** 15
[3] Roe R-J 1977 *J. Appl. Phys.* **48** 4085
[4] Moynihan C T and Gupta P K 1978 *J. Non-Cryst. Solids* **29** 143
[5] Lesikar A V and Moynihan C T 1980 *J. Chem. Phys.* **72** 6422
[6] Moynihan C T and Lesikar A V 1981 *Ann. New York Acad. Sci.* **371** 151
[7] Davies R O and Jones G O 1952 *Proc. R. Soc.* **217** 26
[8] Davies R O and Jones G O 1953 *Adv. Phys.* **2** 370
[9] Prigogine I and Defay R 1954 *Chemical Thermodynamics* (London: Longman)
[10] Brawer S 1985 *Relaxation in Viscous Liquids and Glasses* (Columbus, OH: American Ceramic Society)
[11] Scherer G W 1986 *Relaxations in Glass and Composites* (New York: Academic)
[12] Gutzow I and Schmelzer J 1995 *The Vitreous State* (Berlin: Springer)
[13] Donth E 2001 *The Glass Transition* (Berlin: Springer)
[14] Oels H-J and Rehage G 1977 *Macromolecules* **10** 1036
[15] Zoller P 1982 *J. Polym. Sci. Polym. Phys. Ed.* **20** 1453
[16] Kovacs A J 1963 *Fortschr. Hochpolym.-Forsch.* **3** 394
[17] Nieuwenhuizen Th M 1997 *Phys. Rev. Lett.* **79** 1317
[18] Samwer K, Busch R and Johnson W L 1999 *Phys. Rev. Lett.* **82** 580
[19] Javaheri M R H and Chamberlin R V 2006 *J. Chem. Phys.* **125** 154503
[20] Schmelzer J W P and Gutzow I 2006 *J. Chem. Phys.* **125** 184511
[21] Simon F 1931 *Z. Anorg. Allg. Chem.* **203** 219
[22] Olsen N B 1998 *J. Non-Cryst. Solids* **235** 399
[23] Dyre J C and Olsen N B 2003 *Phys. Rev. Lett.* **91** 155703
[24] Ngai K L, Casalini R, Capaccioli S, Paluch M and Roland C M 2005 *J. Phys. Chem. B* **109** 17356
[25] Richert R and Weinstein S 2006 *Phys. Rev. Lett.* **97** 095703
[26] Mossa S and Sciortino F 2004 *Phys. Rev. Lett.* **92** 045504
     see also Mossa S, La Nave E, Sciortino F and Tartaglia P 2002 *Eur. Phys. J. B* **30** 351
[27] Goldstein M 1964 *Modern Aspects of the Vitreous State* vol 3, ed J D Mackenzie (London: Butterworths Scientific) p 90
[28] Christensen T, Olsen N B and Dyre J C 2007 *Phys. Rev. E* **75** 041502
[29] Oster G F, Perelson A S and Katchalsky A 1973 *Q. Rev. Biophys.* **6** 1
[30] Mikulecky D C 1993 *Applications of Network Thermodynamics to Problems in Biomedical Engineering* (New York: New York University)
[31] Christiansen P V 2005 *Energy Bond Graphs* (*IMFUFA text No. 440*) Roskilde
[32] Van Kampen N G 1981 *Stochastical Processes in Physics and Chemistry* (Amsterdam: North-Holland)
[33] Reichl L E 1998 *A Modern Course in Statistical Physics* 2nd edn (New York: Wiley)
[34] Ellegaard N L, Christensen T, Christiansen P V, Olsen N B, Pedersen U R, Schrøder T B and Dyre J C 2007 *J. Chem. Phys.* **126** 074502
[35] Berg J I and Cooper A R Jr 1978 *J. Chem. Phys.* **68** 4481
[36] Meixner J and Reik H G 1959 *Principen der Thermodynamik und Statistik* (*Handbuch der Physik*) vol 3, ed S Flügge (Berlin: Springer) p 413
[37] Sciortino F 2005 *J. Stat. Mech.* P05015
[38] Palmer R G 1982 *Adv. Phys.* **31** 669
[39] Stillinger F H and Weber T A 1983 *Phys. Rev. A* **28** 2408
[40] Pedersen U R, Christensen T, Schrøder T B and Dyre J C 2008 *Phys. Rev. E* **77** 011201
[41] Pedersen U R, Bailey N, Schrøder T B and Dyre J C 2008 *Phys. Rev. Lett.* **100** 015701
[42] Alba-Simionesco C, Cailliaux A, Alegria A and Tarjus G 2004 *Europhys. Lett.* **68** 58
[43] Casalini R and Roland C M 2004 *Phys. Rev. E* **69** 062501
[44] Roland C M, Hensel-Bielowka S, Paluch M and Casalini R 2005 *Rep. Prog. Phys.* **68** 1405
[45] Grzybowski A, Grzybowski K, Ziolo J and Paluch M 2006 *Phys. Rev. E* **74** 041503
[46] Coslovich D and Roland C M 2008 *J. Phys. Chem.* B at press

Density scaling as a property of strongly correlating viscous liquids

Thomas B. Schrøder, Ulf R. Pedersen, and Jeppe C. Dyre
DNRF Centre "Glass and Time," IMFUFA, Department of Sciences,
Roskilde University, Postbox 260, DK-4000 Roskilde, Denmark
(Dated: June 2, 2008)

We address a recent conjecture according to which the relaxation time τ of a viscous liquid obeys density scaling ($\tau = F(\rho^\gamma/T)$ where ρ is density) if the liquid is "strongly correlating," i.e., has almost 100% correlation between equilibrium virial and potential-energy fluctuations [Pedersen *et al.*, PRL **100**, 011201 (2008)]. Computer simulations of two model liquids - an asymmetric dumbbell model and the Lewis-Wahnström OTP model - confirm the conjecture and demonstrate that the scaling exponent γ can be accurately predicted from equilibrium fluctuations.

PACS numbers: 64.70.P-

Understanding the glass transition depends on understanding the preceding highly viscous liquid phase, where the relaxation time upon cooling approaches and exceeds seconds [1]. Increasing the pressure also leads to much slower relaxations. The study of glass-forming liquids under high pressure has recently become popular, and many data are now available on the properties of the alpha and beta processes, etc., under pressure. If the density is ρ and T is temperature, the last few years have shown that for many highly viscous liquids the (alpha) relaxation time follows the scaling expression

$$\tau = F(\rho^\gamma/T) . \tag{1}$$

The state of this rapidly developing field as of 2005 was summarized in the review Ref. [2] by Roland *et al.* that presented data for more than 50 liquids and polymers.

Equation (1) defines what is referred to as thermodynamic or density scaling. Density scaling is a recent discovery that, following pioneering works by Tölle and Dreyfus *et al.* [3, 4], was proposed as a general principle in 2004 in papers by Alba-Simionesco and co-workers and by Casalini and Roland [5, 6]. The former authors demonstrated data collapse at varying temperature and density following a more general expression than Eq. (1) used by the latter authors.

Dreyfus and co-workers found $\gamma = 4$ for ortho-terphenyl (OTP) and argued that this could be linked to the r^{-12} repulsive term of the Lennard-Jones potential. It turned out, however, that $\gamma = 4$ is not a special exponent [2], leaving the question of the microscopic interpretation of γ open. Coslovich and Roland very recently addressed this by computer simulations of binary Lennard-Jones like liquids where the exponent of the repulsive part of the potential took the values $8, 12, 24, 36$ [7]. These model systems obey density scaling and the exponent γ is to a good approximation $1/3$ of the exponent characterizing the effective power law of the repulsive core of the potential, as expected for an exact inverse power-law potential [7] (see also Ref. [8]).

Recently, simulations of the thermal equilibrium fluctuations of pressure, energy, and volume in different ensembles revealed that these quantities correlate strongly for a number of model systems [9, 10]. For instance, in the NVT ensemble (i.e., constant volume and temperature) the following systems are "strongly correlating" in the sense that they show more than 90% correlation between virial (the non-kinetic part of the pressure) and potential energy: The standard Lennard-Jones liquid, a liquid with exponential short-range repulsion, the Kob-Andersen binary Lennard-Jones liquid, a seven-site united-atom model of toluene, and the model system studied below consisting of asymmetric "dumb-bell" type molecules. The correlations derive from the repulsive core of the intermolecular potential that, interestingly, dominate fluctuations even at zero and slightly negative pressure [10, 11]. For the standard Lennard-Jones liquid the repulsive core is approximately described by a repulsive r^{-18} term [10, 12]. The exponent of the approximate power law depends weakly on state point.

In view of the fact that both density scaling and the strong correlations reflects an effective inverse power-law of the repulsive core of the potential, the following conjecture was proposed in Ref. [10]: A viscous liquid is strongly correlating if and only if it obeys density scaling to a good approximation. There is evidence indirectly supporting this: Highly viscous liquids with strong hydrogen bonds are not strongly correlating because of the "competing interactions" [10], and these liquids also do not obey density scaling very well [2, 13, 14]. In the present publication simulations are presented that supports the conjecture and strengthens it by adding: *For strongly correlating viscous liquids density scaling is obeyed with a scaling exponent γ that can be determined from thermal equilibrium virial and potential energy fluctuations.* This amounts to the simplest possible assumption; that it is the same part of the potential that dominates equilibrium fluctuations and flow dynamics.

We performed NVT molecular dynamics simulations [15] of 512 asymmetric dumbbell molecules consisting of pairs of Lennard-Jones (LJ) spheres connected by rigid bonds. The dumbbells were parameterized to mimic toluene [19]. Charges of $\pm q$ (specified below) were ap-
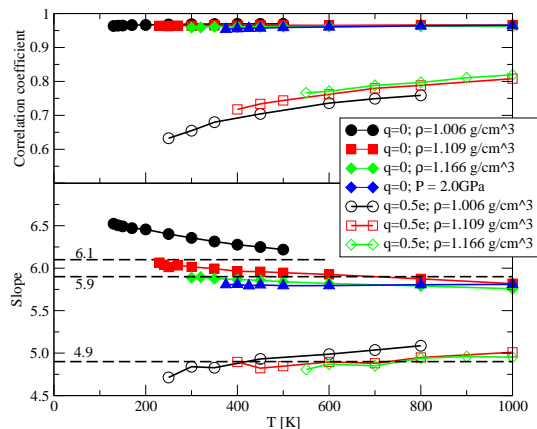
FIG. 1: Results from equilibrium molecular dynamics simulations of 512 asymmetric dumbbell molecules with, respectively, a strong dipole moment ($q = 0.5e$, open symbols, three isochores), and zero dipole moment ($q = 0e$, filled symbols, three isochores and an isobar). (a) Correlation coefficients, $R \equiv \langle \Delta W \Delta U \rangle / \sqrt{\langle \Delta W^2 \rangle \langle \Delta U^2 \rangle}$. (b) The 'slopes', $\gamma \equiv \sqrt{\langle (\Delta W)^2 \rangle / \langle (\Delta U)^2 \rangle}$.

plied to the LJ spheres. The model was simulated with two charges: i) $q = 0$ corresponding to the simulations done in Refs. [9] and [10]. This version of the model is a "strongly correlating viscous liquid". ii) $q = 0.5e$ (e being the elementary charge) resulting in a dipole moment of 7.0D, i.e., almost 20 times stronger than in toluene, and almost 4 times stronger than water. The purpose of using such a large value of q was to break the correlations and thus to have a version of the model that is *not* strongly correlating.

If the virial is denoted by W, and U is the potential energy, $\Delta W(t) \equiv W(t) - \langle W \rangle$ and $\Delta U(t) \equiv U(t) - \langle U \rangle$, where $\langle ... \rangle$ indicates thermal average. The correlation coefficient is defined by $R \equiv \langle \Delta W \Delta U \rangle / \sqrt{\langle \Delta W^2 \rangle \langle \Delta U^2 \rangle}$. R is plotted for a several state points in Fig. 1(a). For $q = 0$ (filled symbols) all investigated state points have $R > 0.95$. For $q = 0.5e$ (open symbols) the correlation coefficient is significantly smaller; the Coulomb interactions do indeed break the correlations as expected [10].

We define $\gamma \equiv \sqrt{\langle (\Delta W)^2 \rangle / \langle (\Delta U)^2 \rangle}$. If $R \approx 1$ it follows that $\Delta W(t) \approx \gamma \Delta U(t)$ in their instantaneous fluctuations [10], and consequently we refer to γ as the 'slope'. According to our conjecture, the slope γ is also the scaling exponent in Eq. (1). In Fig. 1(b) we show the slopes for all investigated state points. For $q = 0$ (filled symbols) there is a small, but significant dependence on density and temperature. Thus if the conjecture is correct, density scaling can not be exact: To apply density scaling a single value of γ is needed, but the γ we get from the fluc-
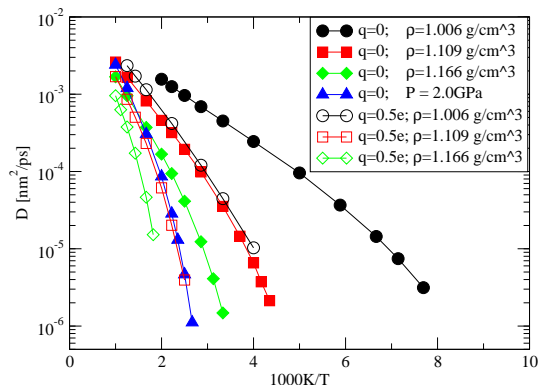
FIG. 2: Arrhenius plot of the diffusion coefficient, D, for the asymmetric dumbbell model.

tuations depends slightly on the state point [10]. In the following we consider for $q = 0$ two values of the scaling exponent: the slope averaged over all state points with $q = 0$; $\gamma = 6.1$, and the slope averaged over the three data sets with the smallest slopes for $q = 0$ ($\rho = 1.109$ g/cm^3, $\rho = 1.166$ g/cm^3 and P=2.0GPa); $\gamma = 5.9$, i.e., the 'best' compromise if we chose to ignore the $\rho = 1.006$ g/cm^3 isochore. For $q = 0.5e$ the slopes are less density dependent with a mean value $\gamma = 4.9$.

In the following we apply density scaling to the diffusion coefficient estimated from the long-time behavior of the mean-square displacement, $\langle \Delta r^2(t) \rangle$, of the large spheres (the "phenyl group") [22]. The diffusion coefficients for all state points studied are given in Fig. 2.

Following Coslovich and Roland [7] we apply density scaling to the reduced diffusion coefficient, $D^* \equiv (N/V)^{1/3}(k_B T/m)^{-1/2}D$ where m is the mass of the molecules. In Fig. 3(a) D^* is plotted for $q = 0$ as a function of $1000\rho^\gamma/T$ with four different values of γ. Clearly, density scaling works neither with $\gamma = 7.0$ or $\gamma = 5.0$. Comparing the scaling with $\gamma = 6.1$ to the data without scaling (filled symbols in Fig. 2), we find here good data collapse; by far most of the density dependence is captured by the density scaling with $\gamma = 6.1$. With $\gamma = 5.9$ the data collapse is even better for three of the data sets, whereas one data set deviates slightly from the master curve comprised of these three sets. This is the isochore $\rho = 1.006$ g/cm^3, i.e., the one that was ignored when choosing $\gamma = 5.9$ (Fig. 1(b)).

The conclusion drawn from Fig. 3 is two-fold: i) Density scaling is approximate (as discussed above) - for a larger region of state points scaling will be less perfect. ii) For a given range of state points, the scaling exponent can be found by studying equilibrium fluctuations.

In Fig. 4 the reduced diffusion coefficients D^* for $q = 0.5e$ are plotted as a function of $1000\rho^\gamma/T$ with three
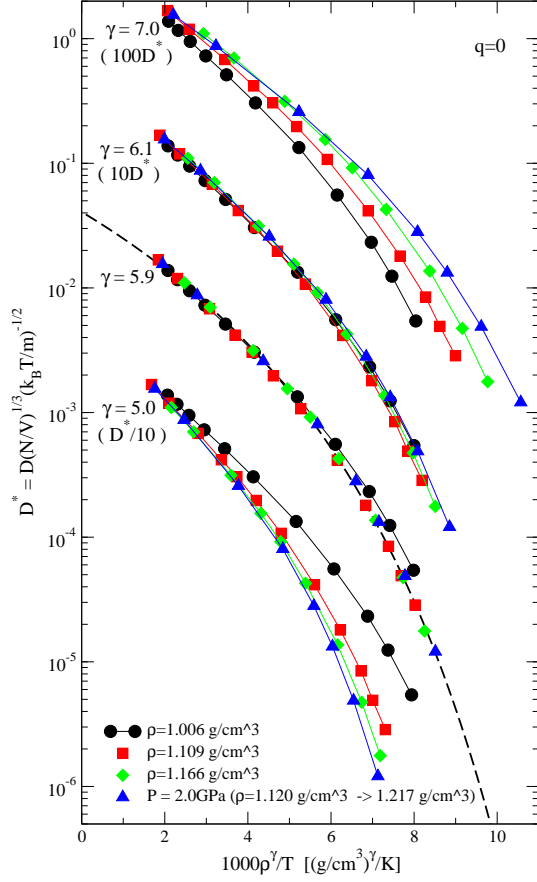
FIG. 3: The reduced diffusion coefficient, D^* $\equiv$ $(N/V)^{1/3}(k_BT/m)^{-1/2}D$, for the asymmetric dumbbell model with $q = 0$ scaled according to Eq. (1), with four different scaling exponents: $\gamma = 7.0$ (Upper set of curves, D^* multiplied by 100), $\gamma = 6.1$ (Second set of curves, D^* multiplied by 10), $\gamma = 5.9$ (Third set of curves), and $\gamma = 5.0$ (Lower set of curves, D^* divided by 10). As a guide to the eye, the equation $D^* = 4.07 \times 10^{-2} \exp\left(-462/(T/\rho^{5.9} - 60.8)\right)$ is plotted as a fit to the three collapsing curves for $\gamma = 5.9$.

FIG. 4: The reduced diffusion coefficient, D^* $\equiv$ $(N/V)^{1/3}(k_BT/m)^{-1/2}D$, for the asymmetric dumbbell model with $q = 0.5e$ scaled according to Eq. (1), with three different scaling exponents: $\gamma = 6.0$ (Upper set of curves, D^* multiplied by 10), $\gamma = 4.9$ (Middle set of curves), and $\gamma = 4.0$ (Lower set of curves, D^* divided by 10).

different values of γ. The value $\gamma = 4.9$ chosen from the equilibrium fluctuations (Fig. 1(b)), is found to be a reasonable scaling exponent. However, as conjectured, the data collapse achieved is inferior to that for the strongly correlating version of the model ($q = 0$).

To test the generality of our findings, we repeated the analysis for the Lewis-Wahnström OTP model (LW-OTP) [15, 23] (see also Refs. [24] and [25]). The results achieved for this model (Fig. 5) are qualitatively similar to the results for the asymmetric dumbbell model with $q = 0$; (i) LW-OTP is strongly correlating ($0.91 < R <$

0.92) [26], (ii) the slope is slightly state point dependent, (iii) choosing the average slope as scaling exponent γ gives good data collapse.

In summary, we have presented numerical evidence for the conjecture that density scaling is a property of strongly correlating viscous liquids. For the two strongly correlating models investigated density scaling applies with a scaling exponent that can be accurately predicted from the equilibrium fluctuations. This represents a step forward in the theoretical understanding of density scaling. In particular, the scaling exponent γ should no longer be regarded as an empirical fitting parameter. In computer simulations γ can be estimated directly from the equilibrium fluctuations. Via the fluctuation dissipation theorem the equilibrium fluctuations determine the frequency-dependent linear thermoviscoelastic response functions - this fact provides a possible future route for independent experimental estimation of the scaling exponent γ [9, 27].
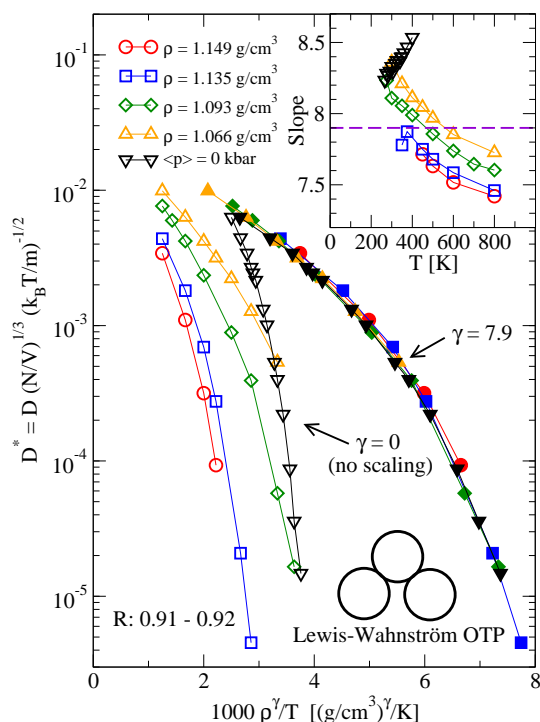
FIG. 5: The reduced diffusion coefficient, $D^* \equiv (N/V)^{1/3}(k_BT/m)^{-1/2}D$, for LW-OTP [23]. For the zero pressure isobar the densities covers the interval 1.008 g/cm^3 to 1.089 g/cm^3 Filled symbols: D^* scaled according to Eq. (1) with $\gamma = 7.9$ chosen from the slopes (inset). Open symbols: D^* plotted without scaling ($\gamma = 0$).

[1] W. Kauzmann, Chem. Rev. **43**, 219 (1948); G. Harrison, *The Dynamic Properties of Supercooled Liquids* (Academic, New York, 1976); S. Brawer, *Relaxation in viscous liquids and glasses* (American Ceramic Society, Columbus, OH, 1985); I. Gutzow and J. Schmelzer, *The Vitreous State: Thermodynamics, Structure, Rheology, and Crystallization* (Springer, Berlin, 1995); M. D. Ediger, C. A. Angell, and S. R. Nagel, J. Phys. Chem. **100**, 13200 (1996); C. A. Angell, K. L. Ngai, G. B. McKenna, P. F. McMillan, and S. W. Martin, J. Appl. Phys. **88**, 3113 (2000); C. Alba-Simionesco, C. R. Acad. Sci. Paris (Ser. IV) **2**, 203 (2001); P G. Debenedetti and F. H. Stillinger, Nature **410**, 259 (2001); K. Binder and W. Kob, *Glassy Materials and Disordered Solids: An Introduction to their Statistical Mechanics* (World Scientific, Singapore, 2005); F. Sciortino, J. Stat. Mech., P05015 (2005); J. C. Dyre, Rev. Mod. Phys. **78**, 953 (2006).

[2] C. M. Roland, S. Hensel-Bielowka, M. Paluch, and R. Casalini, Rep. Prog. Phys. **68**, 1405 (2005).

[3] A. Tölle, Rep. Prog. Phys. **64**, 1473 (2001).

[4] C. Dreyfus, A. Aouadi, J. Gapinski, M. Matos-Lopes, W. Steffen, A. Patkowski, R. M. Pick, Phys. Rev. E **68**, 011204 (2003).

[5] C. Alba-Simionesco, A. Cailliaux, A. Alegria, and G. Tarjus, Europhys. Lett. **68**, 58 (2004).

[6] R. Casalini and C. M. Roland, Phys. Rev. E **69**, 062501 (2004).

[7] D. Coslovich and C. M. Roland, J. Phys. Chem. B **112**, 1329 (2008).

[8] C. De Michele, F. Sciortino, and A. Coniglio, J. Phys.: Cond. Mat. **16** L489 (2004).

[9] U. R. Pedersen, T. Christensen, T. B. Schrøder, and J. C. Dyre, Phys. Rev. E **77**, 011201 (2008).

[10] U. R. Pedersen, N. P. Bailey, T. B. Schrøder, and J. C. Dyre, Phys. Rev. Lett. **100**, 015701 (2008).

[11] N. P. Bailey, U. R. Pedersen, N. Gnan, T. B. Schrøder, and J. C. Dyre, In preperation.

[12] D. Ben-Amotz and G. J. Stell, J. Chem. Phys. **119**, 10777 (2003).

[13] A. Grzybowski, K. Grzybowska, J. Ziolo, and M. Paluch, Phys. Rev. E **74**, 041503 (2006),

[14] C. M. Roland, R. Casalini, R. Bergman, and J. Mattsson, Phys. Rev. B **77**, 012201 (2008).

[15] NVT simulations were carried out using Gromacs software [16] using the Nosé-Hoover thermostat [17]. Molecules were kept rigid using the LINCS [18] algorithm.

[16] Berendsen, H. J. C., van der Spoel, D. & van Drunen, R. *Comp. Phys. Comm.* **91**, 43 (1995); Lindahl, E., Hess, B. & van der Spoel, D. *J. Mol. Mod.* **7**, 306 (2001).

[17] S. A. Nosé, Mol. Phys. **52**, 255 (1984); W. G. Hoover, Phys. Rev. A **31**, 1695 (1985).

[18] B. Hess, H. Bekker, H. J. C. Berendsen and J. G. E. M. Fraaije, J. Comp. Chem. **18**, 1463 (1997).

[19] The large LJ sphere mimicking the phenyl group is similar to the one in the Lewis-Wahnström OTP model [20] with the parameters $m_p = 77.106$ u, $\sigma_p = 0.4963$ nm and $\epsilon_p = 5.726$ kJ/mol. A small sphere mimicking the methyl group was taken from UA-OPLS [21] with $m_m = 15.035$ u, $\sigma_m = 0.3910$ nm and $\epsilon_m = 0.66944$ kJ/mol. Bond length: $d = 0.29$ nm. The interaction between unlike particles is governed by the Lorentz-Berthelot mixing rules.

[20] G. Wahnström and L. J. Lewis, Physica A **201**, 150 (1993) L. J. Lewis and G. Wahnström, Phys. Rev. E **50**, 3865 (1994).

[21] W. L. Jorgensen, J. D. Madura and Carol J. Swenson, J. Am. Chem. Soc. **106**, 6638 (1984).

[22] All state points were simulated for at least the time t_{10}, where $\left\langle \Delta r^2(t_{10}) \right\rangle = 10$nm^2, i.e. on average the large spheres moved at least $6\sigma_p$ during the simulations. Equilibration runs were performed for at least the time t_{10}.

[23] $N = 324$ molecules consisting of three LJ particles (with $\sigma = 0.483$ nm, $\varepsilon = 600$ K$k_B \simeq 4.989$ kJ/mol and $m = 76.768$ u) placed in the corners of a rigid isosceles triangle with two sides of length $\sigma = 0.483$ nm and one angle of $75°$ [20]. LJ potentials were cut at $r_c = 2.5\sigma$ using a shift function [16] with $r_1 = 2.3\sigma$. At the end of long simulations (0.1 μs to 5μs), the system crystallized at several state points (data not included in analysis): $T \leq 400$ K at $\rho = 1.149$ g/ml, $T \leq 400$ K at $\rho = 1.135$ g/ml, $T \leq 350$ K at $\rho = 1.135$ g/ml, and $T \leq 260$ K at $\rho = 1.093$ g/ml ($\langle p \rangle = 0$ kbar).

[24] S.-H. Chong and F. Sciortino, Phys. Rev. E **69**, 051202

5

(2004).

[25] G. Tarjus, D. Kivelson, S. Mossa, and C. Alba-Simionesco, J. Chem. Phys. **120** 6135 (2004).

[26] At zero pressure we find $R < 0.9$ for $T > 400K$. Except for exact soft-spheres, the "strongly correlating"-property holds only for a region of state points [10].

[27] N. L. Ellegaard, T. Christensen, P. V, Christiansen, N. B. Olsen, U. R. Pedersen, T. B. Schrøder, and J. C. Dyre, J. Chem. Phys. **126**, 074502 (2007).

Pressure-energy correlations in liquids. I. Results from computer simulations

Nicholas P. Bailey,[a)] Ulf R. Pedersen, Nicoletta Gnan, Thomas B. Schrøder, and Jeppe C. Dyre
DNRF Center "Glass and Time," IMFUFA, Department of Sciences, Roskilde University,
P.O. Box 260, DK-4000 Roskilde, Denmark

We show that a number of model liquids at fixed volume exhibit strong correlations between equilibrium fluctuations of the configurational parts of (instantaneous) pressure and energy. We present detailed results for 13 systems, showing in which systems these correlations are significant. These include Lennard-Jones liquids (both single- and two-component) and several other simple liquids, neither hydrogen-bonding liquids such as methanol and water, nor the Dzugutov liquid, which has significant contributions to pressure at the second nearest neighbor distance. The pressure-energy correlations, which for the Lennard-Jones case are shown to also be present in the crystal and glass phases, reflect an effective inverse power-law potential dominating fluctuations, even at zero and slightly negative pressure. An exception to the inverse power-law explanation is a liquid with hard-sphere repulsion and a square-well attractive part, where a strong correlation is observed, but only after time averaging. The companion paper [N. P. Bailey *et al.*, J. Chem. Phys. **129**, 184508 (2008)] gives a thorough analysis of the correlations, with a focus on the Lennard-Jones liquid, and a discussion of some experimental and theoretical consequences. © *2008 American Institute of Physics.* [DOI: 10.1063/1.2982247] [Two typos on pages 1 and 2 corrected]

I. INTRODUCTION

Physicists are familiar with the idea of thermal fluctuations in equilibrium. They also know how to extract useful information from them, using linear response theory.[1–4] These methods started with Einstein's observation that the specific heat in the canonical ensemble is determined by the magnitude of energy fluctuations. In any thermodynamic system some variables are fixed and some fluctuate. The magnitude of the variances of the latter, as well as their mutual covariances, determines the thermodynamic "response" parameters.[1] For example, in the canonical (*NVT*) ensemble, pressure p and energy E fluctuate; the magnitude of pressure fluctuations is related to the isothermal bulk modulus $K_T \equiv -V(\partial p/\partial V)_T$, that of the energy fluctuations to the specific heat at constant volume $c_V \equiv T(\partial S/\partial T)_V$, while the covariance $\langle \Delta p \Delta E \rangle$ is related[4] to the thermal pressure coefficient $\beta_V \equiv (\partial p/\partial T)_V$. If the latter is nonzero, it implies a degree of correlation between pressure and energy fluctuations. There is no obvious reason to suspect any particularly strong correlation, and to the best of our knowledge none has ever been reported. However, in the course of investigating the physics of highly viscous liquids by computer simulation, we noted strong correlations between pressure and energy equilibrium fluctuations in several model liquids, also in the high temperature, low-viscosity state. These included the most studied of all computer liquids, the Lennard-Jones system. Surprisingly, these strong correlations survive crystallization, and they are also present in the glass phase. "Strong" here and henceforth means a correlation coefficient of order

0.9 or larger. In this paper we examine several model liquids and detail which systems exhibit strong correlations and which do not. In the companion paper[5] (referred to as Paper II) we present a detailed analysis of the correlations for the single-component Lennard-Jones (SCLJ) system, and discuss some consequences.

Specifically, the fluctuations that are in many cases strongly correlated are those of the configurational parts of pressure and energy. The (instantaneous) pressure p and energy E have contributions both from particle momenta and positions as follows:

$$p = Nk_B T(\mathbf{p}_1, \ldots, \mathbf{p}_N)/V + W(\mathbf{r}_1, \ldots, \mathbf{r}_N)/V,$$
$$E = K(\mathbf{p}_1, \ldots, \mathbf{p}_N) + U(\mathbf{r}_1, \ldots, \mathbf{r}_N), \tag{1}$$

where K and U are the kinetic and potential energies, respectively. Here $T(\mathbf{p}_1, \ldots, \mathbf{p}_N)$ is the "kinetic temperature,"[4] proportional to the kinetic energy per particle. The configurational contribution to pressure is the virial W, which is defined[4] by

$$W = -\frac{1}{3}\sum_i \mathbf{r}_i \cdot \nabla_{\mathbf{r}_i} U, \tag{2}$$

where $\mathbf{r}_i$ is the position of the ith particle. Note that W has dimension energy. For a pair interaction we have

---
a)Electronic mail: nbailey@ruc.dk.

129, 184507-1
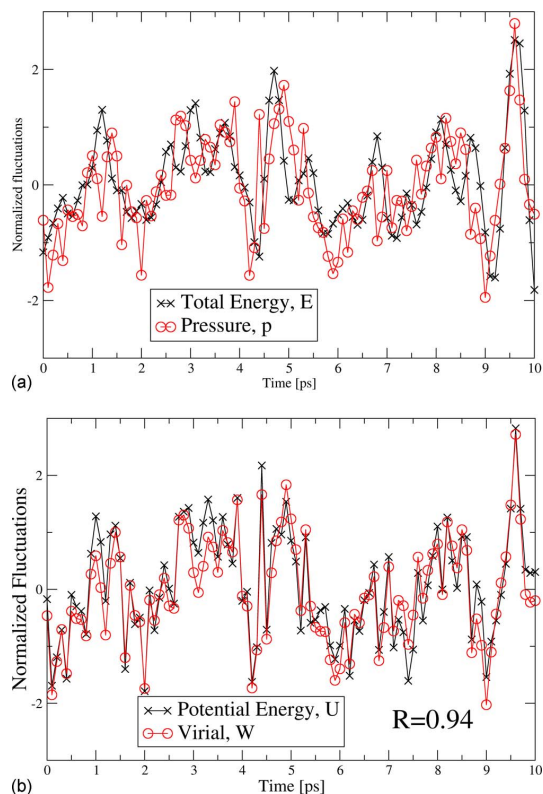
FIG. 1. (Color online) Equilibrium fluctuations of (a) pressure p and energy E and (b) virial W and potential energy U, in a single-component Lennard-Jones system simulated in the *NVT* ensemble at $\rho = 34.6$ mol/1 and $T = 80$ K (argon units). The time-averaged pressure was close to zero (1.5 MPa). The correlation coefficient R between W and U is 0.94, whereas the correlation coefficient is only 0.70 between p and E. Correlation coefficients were calculated over the total simulation time (10 ns).

$$U_{\text{pair}} = \sum_{i<j} v(r_{ij}), \tag{3}$$

where r_{ij} is the distance between particles i and j and $v(r)$ is the pair potential. The expression for the virial [Eq. (2)] becomes[4]

$$W_{\text{pair}} = -\frac{1}{3}\sum_{i<j} r_{ij} v'(r_{ij}) = -\frac{1}{3}\sum_{i<j} w(r_{ij}), \tag{4}$$

where for convenience we define

$$w(r) \equiv r v'(r). \tag{5}$$

Figure 1(a) shows normalized instantaneous values of p and E, shifted and scaled to have zero mean and unit variance, as a function of time for the standard SCLJ liquid, while Fig. 1(b) shows the corresponding fluctuations of W and U. We quantify the degree of correlation by the standard correlation coefficient R, defined by
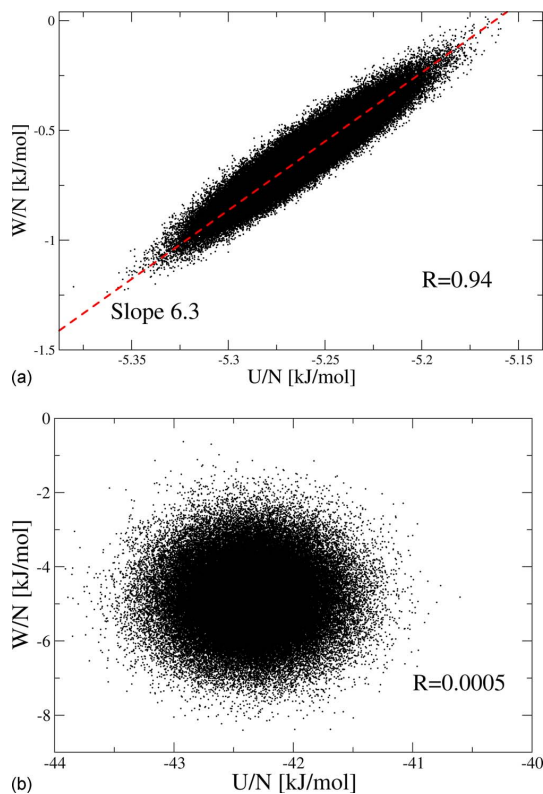
FIG. 2. (Color online) (a) Scatter plot of instantaneous virial W and potential energy U from the simulation of Fig. 1. The dashed line is a guide to the eyes, with a slope determined by the ratio of standard deviations of W and U [Eq. (7)]. (b) Example of a system with almost no correlation between W and U: TIP5P water at $T = 12.5$ °C and density of 1007.58 kg/m³ (*NVT*). This system has Coulomb, in addition to Lennard-Jones, interactions.

$$R = \frac{\langle \Delta W \Delta U \rangle}{\sqrt{\langle (\Delta W)^2 \rangle}\sqrt{\langle (\Delta U)^2 \rangle}}. \tag{6}$$

Here the angle brackets $\langle \ \rangle$ denote thermal averages while Δ denotes deviation from the average value of the given quantity. The correlation coefficient is ensemble dependent, but our main focus—the $R \to 1$ limit—is not. Most of the simulations reported below were carried out in the *NVT* ensemble. Another important characteristic quantity is the "slope" γ, which we define as the ratio of standard deviations as follows:

$$\gamma \equiv \frac{\sqrt{\langle (\Delta W)^2 \rangle}}{\sqrt{\langle (\Delta U)^2 \rangle}}. \tag{7}$$

Considering the "total" quantities, p and E [Fig. 1(a)], there is some correlation; the correlation coefficient is 0.70. For the configurational parts, W and U, on the other hand [Fig. 1(b)], the degree of correlation is much higher, $R = 0.94$ in this case. Another way to exhibit the correlation is a scatter plot of W against U, as shown in Fig. 2(a).

Is this correlation surprising? Actually, there are some interatomic potentials for which there is a 100% correlation

Paper VIII

133

184507-3   Pressure-energy correlations in liquids. I.

J. Chem. Phys. **129**, 184507 (2008)

between virial and potential energy. If we have a pair potential of the form $v(r) \propto r^{-n}$, an inverse power law, then $w(r) = -nv(r)$ and $W_{\text{pair}} = (n/3)U_{\text{pair}}$, holds exactly. In this case the correlation is 100% and $\gamma = n/3$.

Conversely, suppose a system is known to be governed by a pair potential and that there is 100% correlation between W and U. We can write both U and W at any given time t as integrals over the instantaneous radial distribution function defined[4] as

$$g(r,t) \equiv \frac{2}{N\rho} \sum_{i<j} \delta(r - r_{ij}(t))/(4\pi r^2), \tag{8}$$

from which

$$U(t) = \frac{N}{2}\rho \int_0^\infty dr \, 4\pi r^2 g(r,t)v(r) \tag{9}$$

and

$$W(t) = -\frac{N}{6}\rho \int_0^\infty dr \, 4\pi r^2 g(r,t)w(r). \tag{10}$$

Here the factor of $\frac{1}{2}$ is to avoid double counting, and $\rho = N/V$ is the number density. 100% correlation means that $W(t) = \gamma U(t)$ holds for arbitrary $g(r,t)$ (a possible additive constant could be absorbed into the definition of U). In particular, we could consider $g(r,t) = \delta(r-r_0)$.[6] Substituting this into the above expressions, the integrals go away and we find $w(r_0) = -3\gamma v(r_0)$. Since r_0 was arbitrary, $v'(r) = -3\gamma v(r)/r$, which has the solution $v(r) \propto r^{-3\gamma}$. This connection between an inverse power-law potential and perfect correlations suggests that strong correlations can be attributed to an *effective inverse power-law potential*, with exponent given by three times the observed value of γ. This will be detailed in Paper II, which shows that while this explanation is basically correct, matters are somewhat more complicated than this. For instance, the fixed volume condition, under which the strong correlations are observed, imposes certain constraints on $g(r,t)$.

The celebrated Lennard-Jones potential is given[7] by

$$v_{\text{LJ}}(r) = 4\epsilon \left[\left(\frac{\sigma}{r}\right)^{12} - \left(\frac{\sigma}{r}\right)^6 \right]. \tag{11}$$

One might think that in the case of the Lennard-Jones potential the fluctuations are dominated by the repulsive r^{-12} term, but this naive guess leads to a slope of 4, rather than the 6.3 seen in Fig. 2(a). Nevertheless the observed correlation and the above mentioned association with inverse power-law potentials suggest that an effective inverse power-law description (involving short distances), with a more careful identification of the exponent, may apply. In fact, the presence of the second, attractive, term increases the steepness of the repulsive part, thus increasing the slope of the correlation, or equivalently the effective inverse power-law exponent (Fig. 3). Note the distinction between repulsive term and repulsive part of the potential: The latter is the region where $v(r)$ has a negative slope; thus, the region $r < r_m$ (r_m being the distance where the pair potential has its minimum, $2^{1/6}\sigma$ for v_{LJ}). This region involves both the repulsive and attractive terms (see
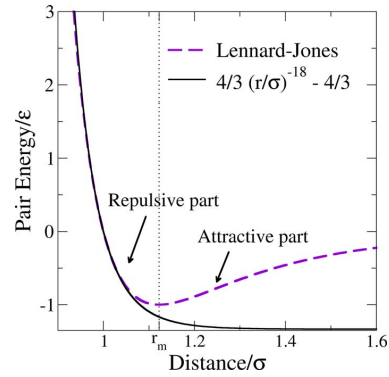
FIG. 3. (Color online) Illustration of the "effective inverse power law" chosen in this case to match the Lennard-Jones potential and its first two derivatives at the point $r = \sigma$. The vertical line marks the division into the repulsive and attractive parts of the Lennard-Jones potential.

Fig. 3, which also illustrates the approximation of the repulsive part by a power law with exponent 18). The same division was made by Weeks, Chandler, and Andersen in their noted paper of 1971,[8] in which they showed that the thermodynamic and structural properties of the Lennard-Jones fluid were dominated by the repulsive part at high temperatures for all densities, and also at low temperatures for high densities. Ben-Amotz and Stell[9] noted that the repulsive core of the Lennard-Jones potential may be approximated by an inverse power law with $n \sim 18-20$. The approximation by an inverse power law may be directly checked by computing the potential and virial with an inverse power-law potential for configurations drawn from actual simulations using the Lennard-Jones potential. The agreement (apart from additive constants) is good; see Paper II.

Consider now a system with different types of pair interactions, for example, a binary Lennard-Jones system with AA, BB, and AB interactions, or a hydrogen-bonding system modeled via both Lennard-Jones and Coulomb interactions. We can write arbitrary deviations of U and W from their mean values, denoted ΔU and ΔW, as a sum over types (indexed by t; sums over pairs of a given type are implicitly understood) as follows:

$$\Delta U = \sum_t \Delta U_t, \quad \Delta W = \sum_t \Delta W_t. \tag{12}$$

Now, supposing there is near-perfect correlation for the individual terms with corresponding slopes γ_t, we can rewrite ΔW as

$$\Delta W = \sum_t \gamma_t \Delta U_t. \tag{13}$$

If the γ_t are all more or less equal to a single value γ, then this can be factored out and we get $\Delta W \simeq \gamma \Delta U$. Thus the existence of different Lennard-Jones interactions in the same system does not destroy the correlation, since they have $\gamma_t \sim 6$. On the other hand the slope for Coulomb interaction, which as an inverse power law has perfect W, U-correlations, is $1/3$, so we cannot expect overall strong correlation in this case [Fig. 2(b)]. Indeed such reasoning also accounts for the

reduction of correlation when the total pressure and energy are considered: $\Delta E = \Delta U + \Delta K$, while (for a large atomic system) $V\Delta p = \gamma \Delta U + (2/3)\Delta K$. The fact that γ is (for the Lennard-Jones potential) quite different from $2/3$ implies that the p, E-correlation is significantly weaker than that of W, U (Fig. 1). Even in cases of unequal slopes, however, there can be circumstances under which one kind of term, and therefore one slope, dominates the fluctuations. In this case strong correlations will be observed. Examples include the high-temperature limits of hydrogen-bonded liquids (Sec. III D) and the time-averaged (total) energy and pressure in viscous liquids (Paper II).

Some of the results detailed below were published previously in letter form;[10] the aim of the present contribution is to make a comprehensive report covering more systems, while Paper II contains a detailed analysis and discusses applications. In the following section, we describe the systems simulated. In Sec. III we present the results for all the systems investigated, in particular, the degree of correlation (correlation coefficient R) and the slope. Section IV gives a summary.

II. SIMULATED SYSTEMS

A range of simulation methods, thermodynamic ensembles, and computational codes were used. One reason for this was to eliminate the possibility that strong correlations are an artifact of using a particular ensemble or code. In addition, no code can simulate the full range of systems presented. Most of the data we present are from molecular dynamics (MD) simulations, although some are from Monte Carlo[11] (MC) and event-driven[12] (ED) simulations. Most of the MD simulations (and of course all MC simulations), had fixed temperature (NVT), while some had fixed total energy (NVE). Three MD codes were used: GROMACS (GRO),[13,14] ASAP (ASAP),[15] and DIGITALMATERIAL (DM).[16] Homemade (HM) codes were used for the MC and ED simulations.

We now list the 13 systems studied, giving each a code name for future reference. The systems include monatomic systems interacting with pair potentials, binary atomic systems interacting with pair potentials, molecular systems consisting of Lennard-Jones particles joined rigidly together in a fixed configuration (here the Lennard-Jones interaction models the van der Waals forces), molecular systems that have Coulomb as well as Lennard-Jones interactions, metallic systems with a many-body potential, and a binary system interacting with a discontinuous "square-well" potential. Included with each system is a list specifying which simulation method(s), which ensemble(s), and which code(s) were used [semicolons separate the method(s) from the ensemble(s) and the ensemble(s) from the code(s)]. Details of the potentials are given in Appendix A.

CU: Pure liquid Cu simulated using the many-body potential derived from effective medium theory (EMT);[17,18] (MD; NVE; ASAP).

DB: Asymmetric "dumbbell" molecules[19] consisting of two unlike Lennard-Jones spheres connected by a rigid bond; (MD; NVT; GRO).

DZ: The potential introduced by Dzugutov[20] as a candi-date for a monatomic glass-forming system. Its distinguishing feature is a peak in $v(r)$ around 1.5σ, after which it decays exponentially to zero at a finite value of r; (MD; NVT, NVE; DM).

EXP: A system interacting with a pair potential with exponential repulsion and a van der Waals attraction; (MC; NVT; HM).

KABLJ: The Kob–Andersen binary Lennard-Jones liquid;[21] (MD; NVT, NVE; GRO, DM).

METH: The GROMOS (Ref. 22) three-site model for methanol; (MD; NVT; GRO).

MGCU: A model of the metallic alloy $Mg_{85}Cu_{15}$ using an EMT-based potential;[23] (MD; NVE; ASAP).

OTP: A three-site model of the fragile glass-former orthoterphenyl (OTP);[24] (MD; NVT; GRO).

SCLJ: The standard single-component Lennard-Jonessystem with the interaction given in Eq. (11); (MD, MC; NVT, NVE; GRO, DM).

SPC/E: The SPC/E model of water;[25] (MD; NVT; GRO).

SQW: A binary model with a pair interaction consisting of an infinitely hard core and an attractive square well;[12,26] (ED; NVE; HM).

TIP5P: A five-site model for liquid water, which reproduces the density anomaly;[27] (MD; NVT; GRO).

TOL: A seven-site united-atom model of toluene; (MD; NVT; GRO).

The number of particles (atoms or molecules) was in the range 500–2000. Particular simulation parameters (N, ρ, T, duration of simulation) are given when appropriate in Sec. III.

III. RESULTS

A. The standard single-component Lennard-Jones system

SCLJ is the system we have most completely investigated. W, U-plots are shown for a range of thermodynamic state points in Fig. 4. Here the ensemble was NVT with $N = 864$, and each simulation consisted of a 10 ns run taken after 10 ns of equilibration; for all SCLJ results so-called "argon" units are used ($\sigma = 0.34$ nm, $\epsilon = 0.997$ kJ/mol). Each elongated oval in Fig. 4 is a collection of W, U pairs for a given state point. Varying temperature at fixed density moves the oval parallel to itself, following an almost straight line as indicated by the dashed lines. Different densities correspond to different lines, with almost the same slope. In a system with a pure inverse power-law interaction, the correlation would be exact, and moreover the data for all densities would fall on the same straight line [see the discussion immediately after Eq. (5)]. Our data, on the other hand, show a distinct dependence on volume, but for a given volume, because of the strong correlation, the variation in W is almost completely determined by that of U.

Values of correlation coefficient R for the state points of Fig. 4 are listed in Table I, along with the slope γ. In Fig. 5 we show the temperature dependence of both R and γ for different densities. Lines have been drawn to indicate isochores and one isobar ($p=0$). Note that when we talk of an isobar here, we mean a set of NVT ensembles with V, T

Paper VIII   135

184507-5   Pressure-energy correlations in liquids. I.   J. Chem. Phys. **129**, 184507 (2008)
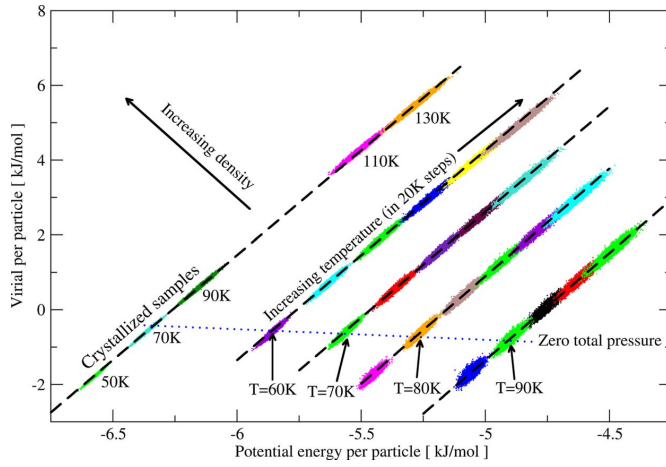
FIG. 4. (Color online) Scatter plots of the configurational parts of pressure and energy—virial vs potential energy—for several state points of the SCLJ liquid (*NVT*). Each oval represents simulations at one particular temperature and density where each data point marks instantaneous values of virial and potential energy. The dashed lines mark constant density paths with the highest density to the upper left (densities: 39.8, 37.4, 36.0, 34.6, and 32.6 mol/l). State points on the dotted line have zero average pressure. The plot includes three crystallized samples (lower left corner), discussed at the end of Sec. III A and, in more detail, in Paper II (reproduced from Ref. 10).

chosen so that the thermal average of p takes on a given value, rather than fixed-pressure ensembles. This figure makes it clear that for fixed density, R increases as T increases, while it also increases with density for fixed temperature; the slope slowly decreases in these circumstances. In fact, it eventually reaches 4, the value expected for a pure

r^{-12} interaction (e.g., at $\rho=34.6$ mol/l, $T=1000$ K, $\gamma=4.61$, see Ref. 10). This is consistent with the idea that the repulsive part, characterized by an effective inverse power law, dominates the fluctuations: Increasing either temperature or density increases the frequency of short-distance encounters while reducing the typical distances of such encounters. On the other hand, along an isobar, these two effects work against each other, since as T increases, the density decreases. The density effect "wins" in this case, which is equivalent to a statement about the temperature and volume derivative of R: Our simulations imply that

$$\left(\frac{\partial R}{\partial T}\right)_p = \left(\frac{\partial R}{\partial T}\right)_V + \left(\frac{\partial R}{\partial V}\right)_T \left(\frac{\partial V}{\partial T}\right)_p < 0, \qquad (14)$$

which is equivalent to

TABLE I. Correlation coefficients R and effective slopes γ for the SCLJ system for the state points in Fig. 4. p is the thermally averaged pressure. The last five states were chosen to approximately follow the isobar $p=0$.

ρ (mol/l)	T (K)	p (MPa)	Phase	R	γ
42.2	12	2.6	Glass	0.905	6.02
39.8	50	−55.5	Crystal	0.987	5.85
39.8	70	−0.5	Crystal	0.989	5.73
39.8	90	54.4	Crystal	0.990	5.66
39.8	110	206.2	Liquid	0.986	5.47
39.8	150	309.5	Liquid	0.988	5.34
37.4	60	−3.7	Liquid	0.965	6.08
37.4	100	102.2	Liquid	0.976	5.74
37.4	140	192.7	Liquid	0.981	5.55
37.4	160	234.3	Liquid	0.983	5.48
36.0	70	−0.7	Liquid	0.954	6.17
36.0	110	90.3	Liquid	0.969	5.82
36.0	150	169.5	Liquid	0.977	5.63
36.0	190	241.4	Liquid	0.981	5.49
36.0	210	275.2	Liquid	0.982	5.44
34.6	60	−42.5	Liquid	0.900	6.53
34.6	100	41.7	Liquid	0.953	6.08
34.6	140	114.5	Liquid	0.967	5.80
34.6	200	211.0	Liquid	0.977	5.57
32.6	70	−35.6	Liquid	0.825	6.66
32.6	90	−0.8	Liquid	0.905	6.42
32.6	110	31.8	Liquid	0.929	6.22
32.6	150	91.7	Liquid	0.954	5.95
32.6	210	172.7	Liquid	0.968	5.68
37.4	60	−3.7	Liquid	0.965	6.08
36.0	70	−0.7	Liquid	0.954	6.17
34.6	80	1.5	Liquid	0.939	6.27
32.6	90	00	Liquid	0.905	6.42
42.2	12	2.6	Glass	0.905	6.02

FIG. 5. (Color online) Upper plot, correlation coefficient R for the SCLJ system as a function of temperature for several densities (*NVT*). This figure makes clear the different effects of density and temperature on R. Lower plot, effective slope γ as a function of T. Simulations at temperatures higher than those shown here indicate that the slope slowly approaches the value 4 as T increases. This is to be expected because as collisions become harder, involving shorter distances, the effective inverse power-law exponent approaches the 12 from the repulsive term of the Lennard-Jones potential.

$$\left(\frac{\partial R}{\partial T}\right)_V < -\left(\frac{\partial R}{\partial V}\right)_T V\alpha_p = \rho\left(\frac{\partial R}{\partial \rho}\right)_T \alpha_p, \qquad (15)$$

where $\alpha_p \equiv (\partial V/\partial T)_p/V$ is the thermal expansivity at constant pressure and ρ is the particle density. This can be recast in terms of logarithmic derivatives [valid whenever $(\partial R/\partial \rho)_T > 0$] as follows:

$$\frac{\left(\dfrac{\partial R}{\partial \ln(T)}\right)_V}{\left(\dfrac{\partial R}{\partial \ln(\rho)}\right)_T} < T\alpha_p. \qquad (16)$$

Thus what we observe in the simulations, namely, that the correlation becomes stronger as temperature is reduced at fixed pressure, is *a priori* more to be expected when the thermal expansivity is large [since then the right hand side of Eq. (16) is large]. This has particular relevance in the context of supercooled liquids, which we discuss in Paper II, because these are usually studied by lowering temperature at fixed pressure. On the other hand if the expansivity becomes small, as for example, when a liquid passes through the glass transition, inequality (16) is *a priori* less likely to be satisfied. We have, in fact, observed this in a simulation of OTP: Upon cooling through the (computer) glass transition, the correlation became weaker with further lowering of temperature at constant pressure.

Remarkably, the correlation persists when the system has crystallized, as seen in the data for the highest density—the occurrence of the first-order phase transition can be inferred from the gap between the data for 90 and 110 K, but the data fall on the same line above and below the transition. One would not expect the dynamical fluctuations of a crystal, which are usually assumed to be well described by a harmonic approximation, to resemble those of the high-temperature liquid. In fact, for a one-dimensional crystal of particles interacting with a harmonic potential $v(r) = \frac{1}{2}k(r - r_m)^2$, it is easy to show (Paper II) that there is a negative correlation with slope equal to $-2/3$. To investigate whether the harmonic approximation ever becomes relevant for the correlations, we prepared a perfect fcc crystal of SCLJ particles at zero temperature and simulated it at increasing temperatures, from 0.02 to 90 K in argon units, along a constant density path. The results are shown in Fig. 6. Clearly the correlation is maintained right down to zero temperature. The harmonic approximation is therefore useless for dealing with the pressure fluctuations even as $T \to 0$, because the slope is far from $-2/3$. The reason for this is that the dominant contribution to the virial fluctuations comes from the third-order term, as shown in Paper II.

B. A case with little correlation: The Dzugutov system

Before presenting data for all the systems studied, it is useful to see what it means for the correlation not to hold. In this subsection we consider the Dzugutov system,[20] whose potential contains a peak at the second-neighbor distance (Fig. 7, see Appendix A for details) whose presence might be expected to interfere with the effectiveness of an inverse power-law description. In the next subsection we show how
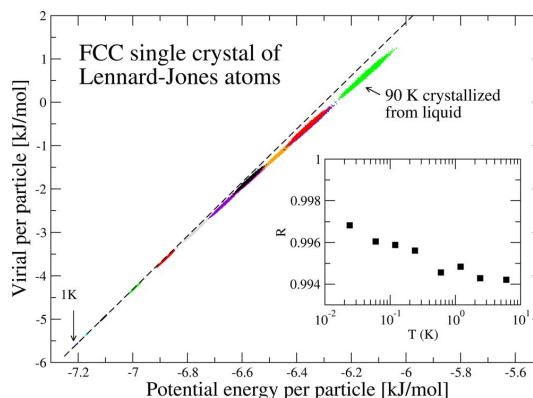
FIG. 6. (Color online) Scatter plot of the W,U-correlations for a perfect face-centered-cubic (fcc) crystal of Lennard-Jones atoms at temperatures 1, 2, 3, 5, 10, 20, 30, 40, 50, 60, 70, and 80 K, as well as for defective crystals (i.e., crystallized from the liquid) at temperatures 50, 70, and 90 K (*NVT*). The dashed line gives the best fit to the (barely visible) lowest-temperature data ($T = 1$ K). The inset shows the temperature dependence of R at very low temperatures. The crystalline case is examined in detail in Paper II, where we find that R does not converge to unity at $T = 0$, but rather to a value very close to unity. All state points refer to the highest density of Fig. 4, 39.8 mol/l.

in a specific model of water the lack of correlation can be explicitly seen to be the result of competing interactions. Figure 8 shows W,U-plots for the Dzugutov system for two nearby temperatures at the same density. The ovals are much less elongated than was the case for SCLJ, indicating a significantly weaker correlation—the correlation coefficients here are 0.585 and 0.604, respectively. In Paper II it is shown explicitly that the weak correlation is due to contributions arising from the second peak. Note that the major axes of the ovals are not aligned with the line joining the state points, given by the mean values of W and U, here identifiable as the intersection of the dashed and straight lines. On the other hand, the lines of best fit from linear regression, indicated by the dashed lines in each case, *do* coincide with the line connecting state points. This holds generally, a fact which follows from statistical mechanics (Appendix B). The interesting thing is rather that the major axes point in different directions, whereas in the SCLJ case they are also aligned

FIG. 7. (Color online) A plot of the Dzugutov pair potential, with the Lennard-Jones potential (shifted by a constant) shown for comparison.

FIG. 8. (Color online) Scatter plot of W, U-correlations for the Dzugutov system at density 0.88 and temperatures 0.65 and 0.70 (*NVE*). The dashed lines indicate the best-fit line using linear regression. These are consistent with the temperature dependence of the mean values of $\langle W \rangle$ and $\langle U \rangle$, as they should be (see Appendix B), but they clearly do not represent the direction of greatest variance. The fu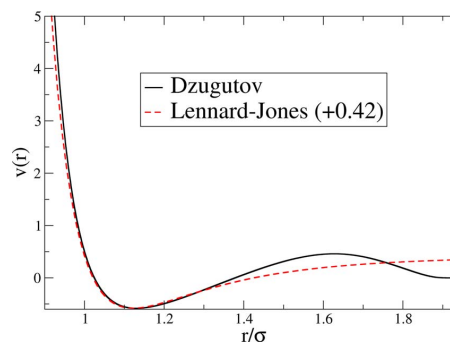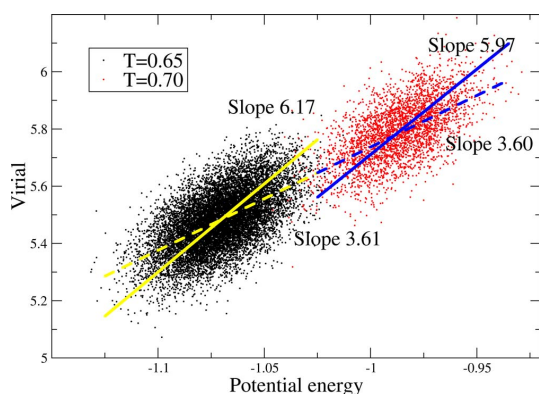ll lines have slopes equal to the ratio of standard deviations of the two quantities [Eq. (7)]. The correlation coefficient is 0.585 and 0.604 for $T=0.65$ and $T=0.70$, respectively.

with the state-point line. The linear-regression slope, being equal to $\langle \Delta U \Delta W \rangle / \langle (\Delta U)^2 \rangle$, treats W and U in an asymmetric manner by involving $\langle (\Delta U)^2 \rangle$, but not $\langle (\Delta W)^2 \rangle$. This is because a particular choice of independent and dependent variables is made. If instead we plotted U against W, we would expect the slope to be simply the inverse of the slope in the W, U-plot, but, in fact, the new slope is $\langle \Delta U \Delta W \rangle / \langle (\Delta W)^2 \rangle$. This equals the inverse of the original slope only in the case of perfect correlation, where $\langle \Delta U \Delta W \rangle^2 = \langle (\Delta W)^2 \rangle \langle (\Delta U)^2 \rangle$. For our purposes a more symmetric estimate of the slope is desired, one which agrees with the linear-regression slope in the limit of perfect correlation. We use simply the ratio of standard deviations $\sqrt{\langle (\Delta W)^2 \rangle} / \sqrt{\langle (\Delta U)^2 \rangle}$ [Eq. (7)]. This slope was used to plot the dashed line in Fig. 2(a) and the full lines in Fig. 8, where it clearly represents the orientation of the data better.[28]

C. When competition between van der Waals and Coulomb interactions kills the correlation: TIP5P water

As we shall see in the next section, the systems that show little correlation include several, which involve both van der Waals and hydrogen bonding, modeled by Lennard-Joness and Coulomb interactions, respectively. As noted already, the latter, being a pure inverse power law ($n=1$), by itself exhibits perfect correlation with slope $\gamma = 1/3$, while the Lennard-Jones part has near perfect correlation. However, the significant difference in slopes means that no strong correlation is seen for the full interaction. To check explicitly that this is the reason the correlation is destroyed we have calculated the correlation coefficients for the Lennard-Jones and Coulomb parts separately in a model of water. Water is chosen because the density of hydrogen bonds is quite high. Simulations were done with the TIP5P model of water,[27] which has the feature that the density maximum is reason-
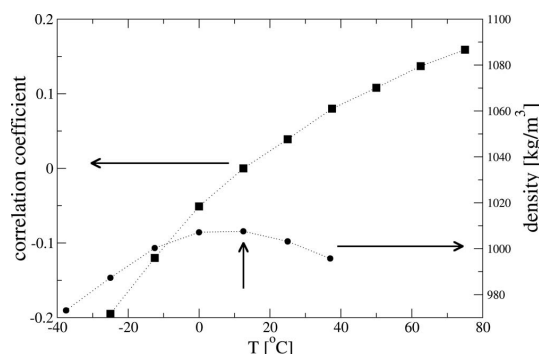
FIG. 9. Plot of R for TIP5P water in *NVT* simulations with densities chosen to give an average pressure of 1 atm. Not only is the magnitude of R low (less than 0.2) in the temperature range shown, but it changes sign around the density maximum. The vertical arrow indicates the state point used for Fig. 2(b).

ably well reproduced. This existence of the density maximum is, in fact, related to pressure and energy becoming uncorrelated, as we shall see.

Figure 9 shows the correlation coefficients and slopes for a range of temperatures; the correlation is almost nonexistent, passing through zero around where the density attains its maximum value. We have separately determined the correlation coefficient of the Lennard-Jones part of the interaction; it ranges from 0.9992 at -25 °C to 0.9977 at 75 °C, even larger than we have seen in the SCLJ system. The reason for this is that the (attractive) Coulomb interaction forces the centers of the Lennard-Jones interaction closer together than they would be otherwise; thus, the relevant fluctuations are occurring higher up the repulsive part of the Lennard-Jones pair potential. Correspondingly the slope from this interaction ranges between 4.45 and 4.54, closer to the high-T, high density limit of 4 than was the case for the SCLJ system. This is confirmed by inspection of the oxygen-oxygen radial distribution function in Ref. 27 where it can be seen that the first peak lies entirely to the left of the $v_{LJ}=0$ distance $\sigma = 0.312$ nm. Finally note that the near coincidence between the vanishing of the correlation coefficient and the density maximum, which is close to the experimental value of 4 °C, is not accidental: The correlation coefficient is proportional to the configurational part of the thermal pressure coefficient β_V (Paper II). The full β_V vanishes exactly at the density maximum (4 °C), but the absence of the kinetic term means that the correlation coefficient vanishes at a slightly higher temperature (~ 12 °C).

D. Results for all systems

In Fig. 10 we summarize the results for the various systems. Here we plot the numerator of Eq. (6) against the denominator, including factors of $1/(k_B T V)$ in both cases to make an intensive quantity with units of pressure. Since R cannot be greater than unity, no points can appear above the diagonal. Being exactly on the diagonal indicates perfect correlation ($R=1$), while being significantly below indicates poor correlation. Different types of symbols indicate differ-

FIG. 10. (Color online) W, U-correlations for all simulated liquids; $\langle \Delta W \Delta U \rangle / (k_B T V)$ plotted vs $(\langle (\Delta W)^2 \rangle \langle (\Delta U)^2 \rangle)^{1/2} / (k_B T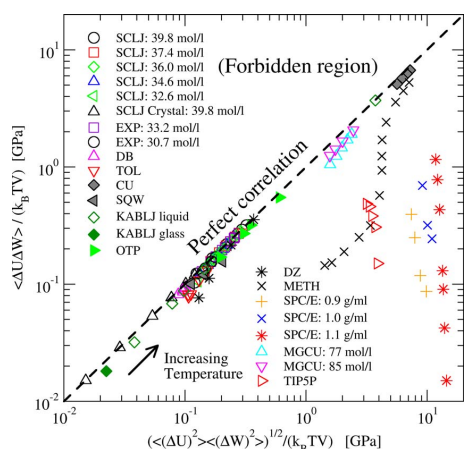 V)$. Both quantities correspond to a pressure, which is given in units of GPa; for model systems not specifically corresponding to real systems, such as SCLJ, KABLJ, and SQW, argon units were used to set the energy and length scales. If the correlation is perfect ($R=1$) the data fall on the diagonal marked by a dashed line. For the TIP5P model of water only temperatures with $R>0$ are included; volumes were chosen to give a pressure close to zero.

ent systems, as well as different densities for the same system, while symbols of the same type correspond to different temperatures.

All of the simple liquids, SCLJ, KABLJ, EXP, DB, and TOL, show strong correlations, while METH, SPC/E, and TIP5P show little correlation. Values of R and γ at selected state points for all systems are listed in Table II. What determines the degree of correlation? The Dzugutov and TIP5P cases have already been discussed. The poor correlation for METH and SPC/E is (presumably) because these models, like TIP5P, involve both Lennard-Jones and Coulomb interactions. In systems with multiple Lennard-Jones species, but without any Coulomb interaction, there is overall a strong correlation because the slope is almost independent of the parameters for a given kind of pair.

As the temperature is increased, the data for the most poorly correlated systems, which are all hydrogen-bonding organic molecules, slowly approach the perfect-correlation line. This is consistent with the idea that this correlation is observed when fluctuations of both W and U are dominated by close encounters of pairs of neighboring atoms; at higher temperature there are increasingly many such encounters, which therefore come to increasingly dominate the fluctuations. Also because the Lennard-Jones potential rises much more steeply than the Coulomb potential, the latter becomes less important as short distances dominate more. Although not obvious in the plot, we find that increasing the density at fixed temperature generally increases the degree of correlation, as found in the SCLJ case; this is also consistent with the increasing relevance of close encounters or collisions.

A system quite different from the others presented so far is the binary square-well system, SQW, with a discontinuous potential combining hard-core repulsion and a narrow attractive well (Fig. 11; see Appendix A for details). Such a po-

TABLE II. Correlation coefficients and slopes at selected state points for all investigated systems besides SCLJ. Argon units were used for DZ, EXP, KABLJ, and SQW by choosing the length parameter (of the larger particle when there were two types) to be 0.34 nm and the energy parameter to be 0.997 kJ/mol. The phase is indicated as liquid or glass. SQW data involve time averaging over periods 3.0, 3.0, 8.0, and 9.0, respectively, for the four listed state points. A minus sign has been included with the slope when $R < 0$; note that the γ values only really make sense as slopes when $|R|$ is close to unity. The ensemble was *NVT* except for CU, DZ, MGCU, and SQW, where it was *NVE*.

System	ρ (mol/l)	T (K)	Phase	R	γ
CU	125.8	1500	Liquid	0.907	4.55
CU	125.8	2340	Liquid	0.926	4.15
DB	11.0	130	Liquid	0.964	6.77
DB	9.7	300	Liquid	0.944	7.45
DZ	37.2	78	Liquid	0.585	3.61
EXP	30.7	96	Liquid	0.908	5.98
EXP	33.2	96	Liquid	0.949	5.56
KABLJ	50.7	30	Glass	0.858	6.93
KABLJ	50.7	70	Liquid	0.946	5.75
KABLJ	50.7	240	Liquid	0.995	5.10
METH	31.5	150	Liquid	0.318	22.53
METH	31.5	600	Liquid	0.541	6.88
METH	31.5	2000	Liquid	0.861	5.51
MGCU	85.0	640	Liquid	0.797	4.74
MGCU	75.6	465	Liquid	0.622	6.73
OTP	4.65	300	Liquid	0.913	8.33
OTP	4.08	500	Liquid	0.884	8.78
OTP	3.95	500	Liquid	0.910	7.70
SPC/E	50.0	200	Liquid	0.016	208.2
SPC/E	55.5	300	Liquid	0.065	48.6
SQW	60.8	48	Liquid	−0.763	−50.28
SQW	60.8	79	Liquid	−0.833	−49.11
SQW	60.8	120	Liquid	−0.938	−52.02
SQW	59.3	120	Liquid	−0.815	−30.07
TIP5P	55.92	273	Liquid	−0.051	−2.47
TIP5P	55.94	285.5	Liquid	0.000	2.51
TOL	10.5	75	Glass	0.877	7.59
TOL	10.5	300	Liquid	0.961	8.27

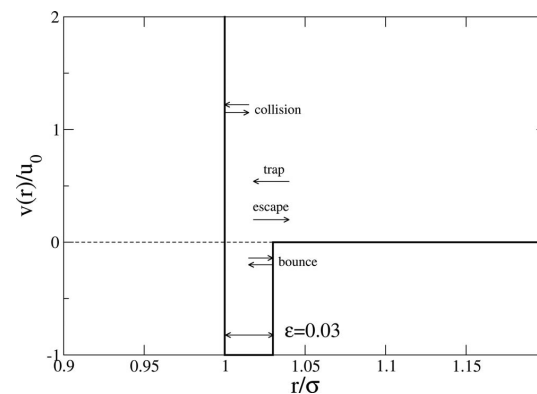
FIG. 11. Illustration of the square-well potential, indicating the four microscopic processes, which contribute to the virial.

Paper VIII

139

184507-9   Pressure-energy correlations in liquids. I.

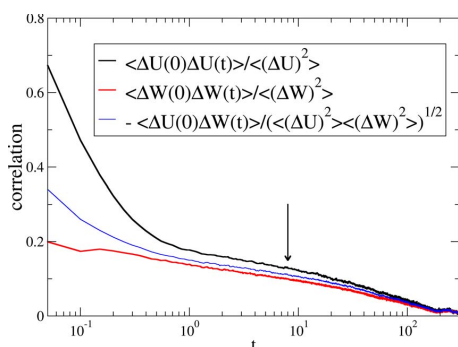J. Chem. Phys. **129**, 184507 (2008)

FIG. 12. (Color online) Energy-energy, virial-virial, and energy-virial correlation functions for SQW at packing fraction $\phi=0.595$ and temperature $T=1.0$ (normalized to unity at $t=0$). The cross correlation has been multiplied by -1. The arrow marks the time $t=8$, roughly $1/10$ of the relaxation time (determined from the long-time part of the energy-virial cross-correlation function). This time was used for averaging.

tential models attractive colloidal systems,[12] one of whose interesting features, predicted from simulations and theory, is the existence of two different glass phases, termed the "repulsive" and "attractive" glasses.[29] The discontinuous potential not only makes the simulations substantially different from a technical point of view, but there are also conceptual differences—in particular, the instantaneous virial is a sum of delta functions in time. The dynamical algorithm employed in the simulations is ED, where events involve a change in the relative velocity of a pair of particles due to hitting the hard-core inner wall of the potential or crossing the potential step. The algorithm must detect the next event, advance time by the appropriate amount, and adjust the velocities of all particles appropriately. There are four kinds of events (illustrated in Fig. 11): (1) "collisions," involving the inner repulsive core; (2) "bounces," involving bouncing off the outer (attractive) wall of the potential; (3) "trapping," involving the separation going below the range of the outer wall; and (4) "escapes," involving the separation increasing beyond the outer wall. To obtain meaningful values of the virial a certain amount of time averaging must be done—we can no longer consider truly instantaneous quantities. As shown in Appendix C the time-averaged virial may be written as the following sum over all events that take place in the averaging interval t_{av}:

$$\bar{W} = \frac{1}{3t_{av}}\sum_{\text{events } e} m_{r,e}\mathbf{r}_e \cdot \Delta\mathbf{v}_e. \qquad (17)$$

Here $\mathbf{r}_e$ and $\mathbf{v}_e$ refer to the relative position and velocity for the pair of particles participating in event e, while Δ indicates the change taking place in that event. Positive contributions to $\bar{W}$ come from collisions; the three other event types involve the outer wall, which, as is easy to see, always gives a negative contribution. The default t_{av} in the simulation was 0.05. Strong correlations emerge only at longer averaging times, however. An appropriate t_{av} may be chosen by considering the correlation functions (auto- and cross-) for virial and potential energy, plotted in Fig. 12, where the "instantaneous" values $E(t)$ and $W(t)$ correspond to averaging

over 0.05 time units. We choose $t_{av} \simeq \tau_\alpha/10$, where τ_α is the relaxation time determined from the cross-correlation function $\langle \Delta U(0)\Delta W(t)\rangle$. Data for a few state points are shown in Table II. Remarkably, this system, so different from the continuous potential systems, also exhibits strong W,U-correlations, with $R=0.94$ in the case $T=1.0$, $\phi=0.595$ (something already hinted at in Fig. 12 in the fact that the curves coincide). There is a notable difference, however, compared to continuous systems: The correlation is negative.

The reason for the negative correlation is that at high density, most of the contributions to the virial are from collisions: A particle will collide with neighbor 1, recoil, and then collide with neighbor 2 before there is a chance to make a bounce event involving neighbor 1. The number of collisions that occur in a given time interval is proportional to the number of bound pairs that is exactly anticorrelated with the energy. The effective slope γ has a large (negative) value of order -50, which does not seem to depend strongly on temperature. This example is interesting because it shows that strong pressure-energy correlations can appear in a wider range of systems that might first have been guessed. Note, however, that the ordinary hard-sphere system cannot display such correlations, since potential energy does not exist as a dynamical variable in this system, i.e., it is identically zero. The idea of correlations emerging when quantities are averaged over a suitable time interval is one we shall meet again in Paper II in the context of viscous liquids.

IV. SUMMARY

We have demonstrated a class of model liquids whose equilibrium thermal fluctuations of virial and potential energy are strongly correlated. We have presented detailed investigations of the presence or absence of such correlations in various liquids, with extra detail presented for the standard SCLJ case. One notable aspect is how widespread these correlations are, appearing not just in Lennard-Jones potentials or in potentials that closely resemble the Lennard-Jones one, but also in systems involving many-body potentials (CU and MGCU) and discontinuous potentials (SQW). We have seen how the presence of different types of terms in the potential, such as Lennard-Jones and Coulomb interactions, spoil the correlations, even though each by itself would give rise to a strongly correlating system. Most simulations were carried out in the *NVT* ensemble; R is not ensemble independent, but the $R \to 1$ limit is.

Several of the hydrocarbon liquids studied here were simulated using simplified "united-atom" models where groups such as methyl groups or even benzene rings were represented by Lennard-Jones spheres. These could also be studied using more realistic "all-atom" models, where every atom (including hydrogen atoms) is included. It would be worth investigating whether the strength of the correlations is reduced by the associated Coulomb terms in such cases.

In Paper II we provide a detailed analysis for the SCLJ case, including consideration of contributions beyond the effective inverse power-law approximation and the $T \to 0$ limit of the crystal. There we also discuss some consequences,

140   *B. Papers*

184507-10   Bailey *et al.*   J. Chem. Phys. **129**, 184507 (2008)

including a direct experimental verification of the correlations for supercritical argon and consequences of strong pressure-energy correlations in highly viscous liquids and biomembranes.

APPENDIX A: DETAILS OF INTERATOMIC POTENTIALS

Here we give more detailed information about the interatomic potentials used. These details have been published elsewhere as indicated, except for the case of EXP and TOL.

CU: Pure liquid Cu simulated using the many-body potential derived from EMT.[17,18] This is similar to the embedded atom method of Daw and Baskes,[30] where the energy of a given atom i, E_i, is some nonlinear function (the "embedding function") of the electron density due to the neighboring atoms. In the EMT, it is given as the energy of an atom in an equivalent reference system, the "effective medium," plus a correction term, $E_i = E_{C,i}(n_i) + \frac{1}{2}[\Sigma_{j \neq i} v_{ij}(r_{ij}) - \Sigma_{j \neq i}^{\mathrm{ref}} v_{ij}(r_{ij})]$. Specifically, the reference system is chosen as a fcc crystal of the given kind of atom, and "equivalent" means that the electron density is used to choose the lattice constant of the crystal. The correction term is an ordinary pair potential involving a simple exponential, but notice that the corresponding sum in the reference system is subtracted (guaranteeing that the correct reference energy is given when the configuration is in fact, the reference configuration). The parameters were $E_0 = -3.510$ eV, $s_0 = 1.413$ Å, $V_0 = 2.476$ eV, $\eta_2 = 3.122$ Å^{-1}, $\kappa = 5.178$, $\lambda = 3.602$, and $n_0 = 0.0614$ Å^{-3}.

DB: Asymmetric dumbbell molecules,[19] consisting of two unlike Lennard-Jones spheres, labelled P and M, connected by a rigid bond. The parameters were $\epsilon_p = 5.726$ kJ/mol, $\sigma_p = 0.4963$ nm, $m_p = 77.106$ u, $\epsilon_m = 0.66944$ kJ/mol, $\sigma_m = 0.3910$ nm, and $m_m = 15.035$ u; the bond length was $d = 0.29$ nm. Cross interactions, ϵ_{pm} and σ_{pm}, were set equal to the geometric and arithmetic means of the p and m parameters, respectively (Lorentz–Berthelot mixing rule[31]).

DZ: A monatomic liquid introduced by Dzugutov as a candidate for a monatomic glass-forming system.[20] The potential is a sum of two parts, $v(r) = v_1(r) + v_2(r)$, with $v_1(r) = A(r^{-m} - B)\exp(c/(r-a))$ for $r < a$ and zero otherwise, and $v_2(r) = B \exp(d/(r-b))$ for $r < b$, zero otherwise. The parameters are chosen to match the location and curvature of the Lennard-Jones potential: $m = 16$, $A = 5.82$, $c = 1.1$, $a = 1.87$, $B = 1.28$, $d = 0.27$, and $b = 1.94$.

EXP: A system interacting with a pair potential with exponential repulsion $U(r) = (\epsilon/8)[6 \exp(-14(r/\sigma - 1)) - 14(\sigma/r)^6]$. Note that the attractive term has the same form as the Lennard-Jones potential.

KABLJ: The Kob–Andersen binary Lennard-Jones liquid,[21] a mixture of two kinds of particles A and B, with A making 80% of the total number. The energy and length parameters are $\epsilon_{AA} = 1.0$, $\epsilon_{BB} = 0.5$, $\epsilon_{AB} = 1.5$, $\sigma_{AA} = 1.0$, $\sigma_{BB} = 0.88$, and $\sigma_{AB} = 0.8$. The masses are both equal to unity. We use the standard density $\rho = 1.2\sigma_{AA}^{-3}$.

METH: The GROMOS three-site model for methanol.[32] The sites represent the methyl ($M \equiv CH_3$) group ($m = 15.035$ u), the O atom ($m = 15.999$ u), and the O-bonded H atom ($m = 1.008$ u). The charges for Coulomb interactions are, respectively, $0.176e$, $-0.574e$, and $0.398e$. The M and O groups additionally interact via Lennard-Jones forces, with parameters $\epsilon_{MM} = 0.9444$ kJ/mol, $\epsilon_{OO} = 0.8496$ kJ/mol, $\epsilon_{MO} = 0.9770$ kJ/mol, $\sigma_{MM} = 0.3646$ nm, $\sigma_{OO} = 0.2955$ nm, and $\sigma_{MO} = 0.3235$ nm. Lennard-Jones interactions are smoothly cutoff between 0.9 and 1.1 nm. The $M-O$ and O–H distances are fixed at 0.136 and 0.1 nm, respectively, while the $M-O-H$ bond angle is fixed at 108.53°.

MGCU: A model of the metallic alloy $Mg_{85}Cu_{15}$, simulated by EMT with parameters as in Ref. 23. In this potential there are seven parameters for each element. However, some of the Cu parameters were allowed to vary from their original values in the process of optimizing the potential for the Mg–Cu system. The parameters for Cu are $E_0 = -3.510$ eV, $s_0 = 1.413$ Å, $V_0 = 1.994$ eV, $\eta_2 = 3.040$ Å^{-1}, $\kappa = 4.944$, $\lambda = 3.694$, and $n_0 = 0.0637$ Å^{-3}, while those for Mg were $E_0 = -1.487$ eV, $s_0 = 1.766$ Å, $V_0 = 2.230$ eV, $\eta_2 = 2.541$ Å^{-1}, $\kappa = 4.435$, $\lambda = 3.293$, and $n_0 = 0.0355$ Å^{-3}. It should be noted that there is an error in Ref. 23: The parameter s_0 for Cu is given in units of bohr instead of Å.

OTP: The Lewis–Wahnström three-site model of OTP (Ref. 24) consisting of three identical Lennard-Jones spheres located at the apices A, B, and C of an isosceles triangle. Sides AB and BC are 0.4830 nm long, while the ABC angle is 75°. The Lennard-Jones interaction parameters are $\epsilon = 4.989$ kJ/mol and $\sigma = 0.483$ nm, while the mass of each sphere, not specified in Ref. 24, was taken as one-third of the mass of an OTP molecule, $m = 76.768$ u.

SCLJ: The standard single-component Lennard-Jones system with potential given by Eq. (11).

SPC/E: The SPC/E model of water,[25] in which each molecule consists of three rigidly bonded point masses, with an OH distance of 0.1 nm and the HOH angle equal to the tetrahedral angle. Charges on O and each H are equal to $-0.8476e$ and $+0.4238e$, respectively. O atoms interact with each other via a Lennard-Jones potential with $\epsilon = 2.601$ kJ/mol and $\sigma = 0.3166$ nm.

SQW: A binary model with a pair interaction consisting of an infinitely hard core and an attractive square well:[12,26] $v_{ij}(r) = \infty$, $r < \sigma_{ij}$, $v_{ij}(r) = -u_0$, $\sigma_{ij} < r < \sigma_{ij}(1 + \epsilon)$, $v_{ij}(r) = 0$, and $r > \sigma_{ij}(1 + \epsilon)$. The radius parameters are $\sigma_{AA} = 1.2$, $\sigma_{BB} = 1$, and $\sigma_{AB} = 1.1$, while $\epsilon = 0.03$ and $u_0 = 1$. The composition was equimolar, and the masses of both particles were equal to unity.

TIP5P: In this water model[27] there are five sites associated with a single water molecule. One for the O atom, one for each H, and two to locate the centers of negative charge corresponding to the electron lone pairs on the O. The OH bond length and the HOH bond angle are fixed at the gas-phase experimental values $r_{OH} = 0.09572$ nm and $\theta_{HOH} = 104.52°$. The negative charge sites are located symmetrically along the lone-pair directions at distance r_{OL}

Paper VIII

141

184507-11   Pressure-energy correlations in liquids. I.

J. Chem. Phys. **129**, 184507 (2008)

$=0.07$ nm and with an intervening angle $\theta_{LOL}=109.47°$. A charge of $+0.241e$ is located on each hydrogen site, while charges of equal magnitude and opposite sign are placed on the lone-pair sites. O atoms on different molecules interact via the Lennard-Jones potential with $\sigma_O=0.312$ nm and $\epsilon_O=0.669$ kJ/mol.

TOL: A seven site united-atom model of toluene, consisting of six "ring" C atoms and a methyl group (H atoms are not explicitly represented). In order to handle the constraints more easily, only three mass points were used; one at the ring C attached to the methyl group ($m=40.065$ u), and one at each of the two "meta" C atoms ($m=26.038$) (note that with this mass distribution, the moment of inertia is not reproduced correctly). Parameters were derived from the information in Ref. [33]: $\epsilon_{ring}=0.4602$ kJ/mol, $\epsilon_{methyl}=0.6694$ kJ/mol, $\sigma_{ring}=0.375$ nm, and $\sigma_{methyl}=0.391$ nm. The Lorentz–Berthelot rule was used for cross interactions.[33]

APPENDIX B: CONNECTING FLUCTUATIONS TO THERMODYNAMIC DERIVATIVES

If A is a dynamical quantity that depends only on the configurational degrees of freedom, then its average in the canonical ensemble (NVT) is given by (where, for convenience, we use a discrete-state notation, with A_i referring to the value of A in the ith microstate, etc.)

$$\langle A \rangle = \frac{\Sigma_i A_i \exp(-\beta U_i)}{\Sigma_i \exp(-\beta U_i)} = \frac{\Sigma_i A_i \exp(-\beta U_i)}{Q}, \tag{B1}$$

where $\beta=1/k_B T$ and Q is the configurational partition function. Then the inverse temperature derivative of $\langle A \rangle$ can be written in terms of equilibrium fluctuations as follows:

$$\left(\frac{\partial \langle A \rangle}{\partial \beta} \right)_V = - \frac{\Sigma_i A_i \exp(-\beta U_i) U_i}{Q}$$
$$+ \frac{\Sigma_i A_i \exp(-\beta U_i) \Sigma_j \exp(-\beta U_j) U_j}{Q^2} \tag{B2}$$

$$= - (\langle AU \rangle - \langle A \rangle \langle U \rangle) \tag{B3}$$

$$= - \langle \Delta A \Delta U \rangle. \tag{B4}$$

Now taking $A=W$ and $A=U$ successively we find that

$$\left(\frac{\partial \langle W \rangle}{\partial T} \right)_V \Big/ \left(\frac{\partial \langle U \rangle}{\partial T} \right)_V = \left(\frac{\partial \langle W \rangle}{\partial \beta} \right)_V \Big/ \left(\frac{\partial \langle U \rangle}{\partial \beta} \right)_V$$
$$= \frac{\langle \Delta W \Delta U \rangle}{\langle (\Delta U)^2 \rangle}. \tag{B5}$$

This last expression is precisely the formula for the slope obtained by linear regression when plotting W against U.

Consider now volume derivatives. Because volume dependence comes in through the microstate values, A_i and U_i, and the volume derivatives of these are not necessarily re-

lated in a simple way, the corresponding expression is not as simple: The derivative of $\langle W \rangle$ with respect to volume at fixed temperature is given by

$$\left(\frac{\partial \langle W \rangle}{\partial V} \right)_T = \frac{\partial}{\partial V} (\langle p \rangle V - Nk_B T)_T \tag{B6}$$

$$= \langle p \rangle + V \left(\frac{\partial \langle p \rangle}{\partial V} \right)_T = \langle p \rangle - K_T, \tag{B7}$$

where K_T is the isothermal bulk modulus. The derivative of U can be obtained by writing pressure as the derivative of Helmholtz free energy F (K is kinetic energy) as follows:

$$\langle p \rangle = - \left(\frac{\partial F}{\partial V} \right)_T = - \left(\frac{\partial (\langle U \rangle + \langle K \rangle - TS)}{\partial V} \right)_T \tag{B8}$$

$$= - \left(\frac{\partial \langle U \rangle}{\partial V} \right)_T + T \left(\frac{\partial S}{\partial V} \right)_T. \tag{B9}$$

Then using the thermodynamic identity $(\partial S/\partial V)_T = (\partial \langle p \rangle/\partial T)_V \equiv \beta_V$, we obtain the ratio of volume derivatives of $\langle W \rangle$ and $\langle U \rangle$ as follows:

$$\left(\frac{\partial \langle W \rangle}{\partial V} \right)_T \Big/ \left(\frac{\partial \langle U \rangle}{\partial V} \right)_T = - \frac{K_T - \langle p \rangle}{T\beta_V - \langle p \rangle}, \tag{B10}$$

which becomes $-K_T/(T\beta_V)$ when the pressure is small compared to the bulk modulus. As discussed in Paper II, β_V can be expressed in terms of $\langle \Delta U \Delta W \rangle$ again, but the fluctuation expression for K_T is more complicated. Thus we cannot simply identify the lines of constant T, varying V, on a $\langle W \rangle$, $\langle U \rangle$-plot, as we could with lines of fixed V, varying T, by examining the fluctuations at fixed V, T.

APPENDIX C: VIRIAL FOR SQUARE-WELL SYSTEM

Here we derive the expression for the time-averaged virial, Eq. (17), as a convenience for the reader. The idea is to replace the step u_0 in the potential with a finite slope u_0/δ over a range δ, and take the limit $\delta \to 0$. We start by replacing a two-body interaction in three dimensions with the equivalent one-dimensional, one-body problem using the radial separation r and the reduced mass m_r. Let the potential step be at $r=r_s$ and define $x=r-r_s$ (see Fig. 13). We consider an "escape event" over a positive step, so that an initial (relative) velocity v_0 becomes a final velocity v_1 and r goes from a value less than r_0 to a value greater than $r_0+\delta$. The resulting formula also applies for the other kinds of events.
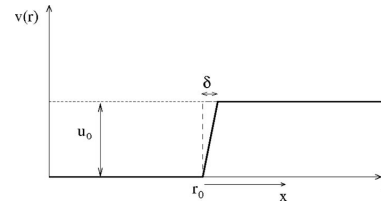

FIG. 13. Illustration of replacement of discontinuous step by a finite slope for the square-well potential for the purpose of calculating the virial. The limit $\delta \to 0$ is taken at the end.

The contribution to the time integral of the virial from this event is given by

$$\Delta = \int_0^{t_\delta} \frac{(r_0 + x)}{3} F \, dt = -\int_0^{t_\delta} \frac{(r_0 + x)u_0}{3\delta} \, dt, \tag{C1}$$

where F is the (constant) force in the region $0 < x < \delta$ and t_δ is the time taken for the "particle" (the radial separation) to cross this region. The trajectory $x(t)$ is given by the standard formula for uniform acceleration

$$x(t) = v_0 t - \frac{1}{2}\frac{u_0}{\delta m_r} t^2, \tag{C2}$$

which by setting $x(t_\delta) = \delta$ gives the following expression for t_δ:

$$t_\delta = \delta \left(\frac{m_r v_0}{u_0} - \sqrt{\left(\frac{m_r v_0}{u_0}\right)^2 - \frac{2m_r}{u_0}} \right); \tag{C3}$$

here we have taken the negative root, appropriate for a positive u_0 (we want the smallest positive t_δ). Returning to Δ, it can be split into two parts as follows:

$$\Delta = -\int_0^{t_\delta} \frac{r_0 u_0}{3\delta} \, dt - \int_0^{t_\delta} \frac{x(t)u_0}{3\delta} \, dt. \tag{C4}$$

Consider the second term: Using the expression for $x(t)$ from Eq. (C2), we see that the result of the integral will involve a term proportional to t_δ^2 and one proportional to t_δ^3. Using Eq. (C3) to replace $t_\delta \propto \delta$, and noting the δ in the denominator, the terms will have linear and quadratic dependences on δ, respectively. Thus they will vanish in the limit $\delta \to 0$. On the other hand, the first term gives

$$\Delta = -\frac{r_0 u_0}{3\delta} t_\delta = -\frac{r_0 u_0}{3}\left(\frac{m_r v_0}{u_0} - \sqrt{\left(\frac{m_r v_0}{u_0}\right)^2 - \frac{2m_r}{u_0}} \right)$$

$$= \frac{r_0 m_r}{3}(\sqrt{v_0^2 - 2u_0/m_r} - v_0). \tag{C5}$$

This expression can be simplified by writing it in terms of the change of velocity $\Delta v \equiv v_1 - v_0$. In the one-body problem conservation of momentum does not hold, and v_1 is given by energy conservation

$$\tfrac{1}{2}m_r v_0^2 = \tfrac{1}{2}m_r v_1^2 + u_0, \tag{C6}$$

from which Δv is obtained as

$$\Delta v \equiv v_1 - v_0 = \sqrt{v_0^2 - 2u_0/m_r} - v_0; \tag{C7}$$

thus, the expression for Δ becomes

$$\Delta = \frac{r_0 m_r}{3}\Delta v = \frac{m_r}{3}\mathbf{r} \cdot \Delta\mathbf{v}, \tag{C8}$$

where in the last expression a switch to three-dimensional notation was made, recognizing that for central potentials $\Delta\mathbf{v}$ will be parallel to the displacement vector between the two particles. This expression, derived for escape events, must also hold for capture events since these are time-reverses of each other, and the virial is fundamentally a configurational quantity, independent of dynamics (the above expression is time-reversal invariant because the change in the radial com-

ponent of velocity is the same either way, since although the "initial" and "final" velocities are swapped, they also have opposite sign). Bounce and collision events may be treated by dividing the event into two parts at the turning point (where the relative velocity is zero), noting that each may be treated exactly as above, then adding the results back together. If we now consider all events that take place during an averaging time t_{av}), we get the time-averaged virial as

$$\overline{W} = \frac{1}{3t_{av}}\sum_{\text{events } e} m_{r,e}\mathbf{r}_e \cdot \Delta\mathbf{v}_e. \tag{C9}$$

[1] L. D. Landau and E. M. Lifshitz, *Statistical Physics, Part I* (Pergamon, London, 1980).

[2] J. P. Hansen and I. R. McDonald, *Theory of Simple Liquids*, 2nd ed. (Academic, New York, 1986).

[3] L. E. Reichl, *A Modern Course in Statistical Physics*, 2nd ed. (Wiley, New York, 1998).

[4] M. P. Allen and D. J. Tildesley, *Computer Simulation of Liquids* (Oxford University Press, Oxford, 1987).

[5] N. P. Bailey, U. R. Pedersen, N. Gnan, T. B. Schrøder, and J. C. Dyre, J. Chem. Phys. **129**, 184508 (2008).

[6] If this seems unphysical, the argument could be given in terms of arbitrary deviations from equilibrium, $\Delta g(r,t) \equiv g(r,t) - \langle g(r)\rangle$. See, however, Paper II.

[7] J. E. Lennard-Jones, Proc. Phys. Soc. London **43**, 461 (1931).

[8] J. D. Weeks, D. Chandler, and H. C. Andersen, J. Chem. Phys. **54**, 5237 (1971).

[9] D. Ben-Amotz and G. Stell, J. Chem. Phys. **119**, 10777 (2003).

[10] U. R. Pedersen, N. P. Bailey, T. B. Schrøder, and J. C. Dyre, Phys. Rev. Lett. **100**, 015701 (2008).

[11] D. P. Landau and K. Binder, *A Guide to Monte Carlo Simulations in Statistical Physics*, 2nd ed. (Cambridge University Press, Cambridge, 2005).

[12] E. Zaccarelli, G. Foffi, K. A. Dawson, S. V. Buldyrev, F. Sciortino, and P. Tartaglia, Phys. Rev. E **66**, 041402 (2002).

[13] H. J. C. Berendsen, D. van der Spoel, and R. van Drunen, Comput. Phys. Commun. **91**, 43 (1995).

[14] E. Lindahl, B. Hess, and D. van der Spoel, J. Mol. Model. **7**, 306 (2001).

[15] Asap, Asap home page, see http://wiki.fysik.dtu.dk/asap for more information on MD codes.

[16] N. P. Bailey, T. Cretegny, J. P. Sethna, V. R. Coffman, A. J. Dolgert, C. R. Myers, J. Schiøtz, and J. J. Mortensen, e-print arXiv:cond-mat/0601236.

[17] K. W. Jacobsen, J. K. Nørskov, and M. J. Puska, Phys. Rev. B **35**, 7423 (1987).

[18] K. W. Jacobsen, P. Stoltze, and J. K. Nørskov, Surf. Sci. **366**, 394 (1996).

[19] U. R. Pedersen, T. Christensen, T. B. Schrøder, and J. C. Dyre, Phys. Rev. E **77**, 011201 (2008).

[20] M. Dzugutov, Phys. Rev. A **46**, R2984 (1992).

[21] W. Kob and H. C. Andersen, Phys. Rev. Lett. **73**, 1376 (1994).

[22] W. R. P. Scott, P. H. Hunenberger, I. G. Tironi, A. E. Mark, S. R. Billeter, J. Fennen, A. E. Torda, T. Huber, P. Kruger, and W. van Gunsteren, J. Phys. Chem. A **103**, 3596 (1999).

[23] N. P. Bailey, J. Schiøtz, and K. W. Jacobsen, Phys. Rev. B **69**, 144205 (2004).

[24] L. J. Lewis and G. Wahnström, Phys. Rev. E **50**, 3865 (1994).

[25] H. J. C. Berendsen, J. R. Grigera, and T. P. Straatsma, J. Phys. Chem. **91**, 6269 (1987).

[26] E. Zaccarelli, F. Sciortino, and P. Tartaglia, J. Phys.: Condens. Matter **16**, 4849 (2004).

[27] M. W. Mahoney and W. L. Jorgensen, J. Chem. Phys. **112**, 8910 (2000).

[28] Choosing this measure of the slope is equivalent to diagonalizing the correlation matrix (the covariance matrix where the variables have been scaled to have unit variance) to identify the independently fluctuating variable. This is often done in multivariate analysis (see, e.g., Ref. 34), rather than diagonalizing the covariance matrix, when different variables have widely differing variances.

[29] F. Sciortino, Nature Mater. **1**, 145 (2002).

[30] M. R. Daw and M. I. Baskes, Phys. Rev. B **29**, 6443 (1984).

[31] J. P. Hansen and I. R. McDonald, *Liquid and Liquid Mixtures* (Butterworths, London, 1969).

Paper VIII

184507-13   Pressure-energy correlations in liquids. I.

143

J. Chem. Phys. **129**, 184507 (2008)

[32] W. F. van Gunsteren, S. R. Billeter, A. A. Eising, P. H. Hünenberger, P. Krüger, A. E. Mark, W. R. P. Scott, and I. G. Tironi, *Biomolecular Simulation: The GROMOS96 Manual and User Guide* (Hochschul-Verlag AG an der ETH Zürich, Zürich, 1996).

[33] W. L. Jorgensen, J. D. Madura, and C. J. Swenson, J. Am. Chem. Soc. **106**, 6638 (1984).

[34] K. H. Esbensen, D. Guyot, F. Westad, and L. P. Houmøller, *Multivariate Data Analysis—In Practice*, 5th ed. (Camo, Oslo, 2002).

Pressure-energy correlations in liquids. II. Analysis and consequences

Nicholas P. Bailey,[a] Ulf R. Pedersen, Nicoletta Gnan, Thomas B. Schrøder, and
Jeppe C. Dyre
DNRF Center "Glass and Time," IMFUFA, Department of Sciences, Roskilde University,
P.O. Box 260, DK-4000 Roskilde, Denmark

We present a detailed analysis and discuss consequences of the strong correlations of the configurational parts of pressure and energy in their equilibrium fluctuations at fixed volume reported for simulations of several liquids in the previous paper [N. P. Bailey *et al.*, J. Chem. Phys. **129**, 184507 (2008)]. The analysis concentrates specifically on the single-component Lennard-Jones system. We demonstrate that the potential may be replaced, at fixed volume, by an effective power law but not simply because only short-distance encounters dominate the fluctuations. Indeed, contributions to the fluctuations are associated with the whole first peak of the radial distribution function, as we demonstrate by an eigenvector analysis of the spatially resolved covariance matrix. The reason the effective power law works so well depends crucially on going beyond single-pair effects and on the constraint of fixed volume. In particular, a better approximation to the potential includes a linear term, which contributes to the mean values of potential energy and virial, but little to their fluctuations, for density fluctuations which conserve volume. We also study in detail the zero temperature limit of the (classical) crystalline phase, where the correlation coefficient becomes very close, but not equal, to unity, in more than one dimension; in one dimension the limiting value is exactly unity. In the second half of the paper we consider four consequences of strong pressure-energy correlations: (1) analyzing experimental data for supercritical argon we find 96% correlation; (2) we discuss the particular significance acquired by the correlations for viscous van der Waals liquids approaching the glass transition: For strongly correlating viscous liquids knowledge of just one of the eight frequency-dependent thermoviscoelastic response functions basically implies knowledge of them all; (3) we reinterpret aging simulations of *ortho*-terphenyl carried out by Mossa *et al.* [Eur. Phys. J. B **30**, 351 (2002)], showing their conclusions follow from the strongly correlating property; and (4) we briefly discuss the presence of the correlations (after appropriate time averaging) in model biomembranes, showing that significant correlations may be present even in quite complex systems. © *2008 American Institute of Physics.*
[DOI: 10.1063/1.2982249]

I. INTRODUCTION

In the companion paper[1] to this work, referred to as Paper I, we detailed the existence of a strong correlation between the equilibrium fluctuations of the configurational parts of pressure and energy in several model liquids. Recall that (instantaneous) pressure p and energy E have contributions both from particle momenta and positions,[2]

$$p = Nk_BT(\mathbf{p}_1, \ldots, \mathbf{p}_N)/V + W(\mathbf{r}_1, \ldots, \mathbf{r}_N)/V, \quad (1)$$

$$E = K(\mathbf{p}_1, \ldots, \mathbf{p}_N) + U(\mathbf{r}_1, \ldots, \mathbf{r}_N), \quad (2)$$

where K and U are the kinetic and potential energies, respectively, and $T(\mathbf{p}_1, \ldots, \mathbf{p}_N)$ is the "kinetic temperature,"[2] proportional to the kinetic energy per particle. The configurational contribution to pressure is the virial W, which for a translationally invariant potential-energy function U is defined[2] by

$$W = -\frac{1}{3}\sum_i \mathbf{r}_i \cdot \nabla_{\mathbf{r}_i} U, \quad (3)$$

where $\mathbf{r}_i$ is the position of the ith particle. Note that W has dimension energy. In the case of a pair potential $U_{\text{pair}} = \Sigma_{i<j} v(r_{ij})$, the expression for the virial becomes[2]

$$W_{\text{pair}} = -\frac{1}{3}\sum_{i<j} r_{ij}v'(r_{ij}) = -\frac{1}{3}\sum_{i<j} w(r_{ij}), \quad (4)$$

where $w(r) \equiv rv'(r)$.

It is the correlation between U and W that we are interested in, quantified by the correlation coefficient

$$R = \frac{\langle \Delta W \Delta U \rangle}{\sqrt{\langle (\Delta W)^2 \rangle}\sqrt{\langle (\Delta U)^2 \rangle}}. \quad (5)$$

Paper I documented the correlation in many systems, showing that this is often quite strong, with correlation coefficient $R > 0.9$, while in some other cases it was found to be weak or almost nonexistent. The latter included in particular models with additional significant Coulombic interactions. The purpose of this paper is twofold. First we give a comprehensive

analysis of the source of the correlation in the simplest "strongly correlating" model liquid, the standard single-component Lennard-Jones (SCLJ) fluid. Paper I presented briefly an explanation in terms of an effective inverse power-law potential. Here we elaborate on that in greater detail and go beyond it. Second we discuss a few observable consequences and applications of the strong correlations. These range from their measurement in a real system to applications to systems as diverse as supercooled liquids and biomembranes.

In Sec. II we present a detailed analysis for the SCLJ case, first in terms of an effective inverse power law with exponent ~ 18. This accounts for the correlation at the level of individual pair encounters by assuming that only the repulsive part of the potential, corresponding to distances less than the minimum of the potential r_m, is relevant for fluctuations, and that this may be well approximated by an inverse power law. The value 18 is significant since this explains the "slope" γ defined as

$$\gamma \equiv \sqrt{\frac{\langle (\Delta W)^2 \rangle}{\langle (\Delta U)^2 \rangle}}, \tag{6}$$

observed to be ~ 6 for Lennard-Jones systems (Paper I). The slope is exactly $n/3$ for a pure inverse power-law potential with exponent n, a case with perfect W, U correlation (Paper I). Section II continues with a discussion of the SCLJ crystal, which is also strongly correlating. This would seem to invalidate the dominance of the repulsive part since only presumably distances around and beyond the potential minimum are important, at least at low and moderate pressure. In this case the correlation can be explained only when summation over all pairs is taken into account, thus the correlation emerges as a collective effect. There is a connection between the slope obtained in this way and that given by the effective inverse power law, in fact, they are quite similar. The third subsection in Sec. II gives a more systematic analysis of which regions dominate the fluctuations in the liquid phase using an eigenvector decomposition of the spatially resolved covariance matrix. This matrix represents the contributions to the (co-)variances of potential energy and virial from different pair separations. It is demonstrated that the region around the minimum of the potential plays a substantial role. The final subsection in Sec. II provides a synthesis of the insights from the previous subsections, resulting in an "extended effective power-law approximation," which includes a linear term. The main point is that a linear term in the pair potential will contribute to the mean values, but not to fluctuations, of W and U, if the volume is constant.

In Sec. III we discuss some consequences, starting by considering whether the instantaneous correlations can be related to a measurable quantity in the normal liquid state, and demonstrating this with data for supercritical argon, finding a correlation coefficient of 0.96. Next we focus on consequences for highly viscous liquids, where time-scale separation implies that instantaneous correlation between virial and potential energy can be related to a correlation between the time-averaged pressure and energy. The third subsection dis-

cusses consequences for aging, while the fourth briefly discusses connections with recent work by Heimburg and Jackson on biomembranes.

Finally, Sec. IV concludes with an outlook reflecting on the broader significance of strong correlation and its implications for the understanding of liquids, particularly in the context of viscous liquids (which has been our main motivation throughout this work).

II. ANALYSIS

A. The effective inverse power law

In this section we consider the SCLJ system in the hope that it is simple enough that a fairly complete understanding of the cause of strong correlations is possible. Recall that $R > 0.9$ for a wide range of states (Paper I). In order to understand the numerology better we consider a generalized Lennard-Jones potential, denoted by LJ(a, b) $(a > b)$,

$$v_{\mathrm{LJ}}^{a,b}(r) \propto (\sigma/r)^a - (\sigma/r)^b, \tag{7}$$

although the standard LJ(12,6) case will be used for most examples. Starting from the idea that short distances dominate fluctuations and that the observed correlations are suggestive of a power-law interaction, we show that at a given density, the LJ potential may be approximated by a single effective inverse power law over a range from a little less than σ (where v_{LJ} changes sign) to around r_m, the location of the potential minimum $[r_m = 2^{1/6}\sigma$ for LJ(12,6)], covering an energy range of approximately $-\epsilon$ to $+2\epsilon$, where ϵ is the well-depth. At first sight, one might expect that if this were at all the case, the effective power would be less than a, somehow a mixture of the two exponents a and b. It was noticed by Ben-Amotz and Stell,[3] however, that the repulsive core of the LJ(12,6) potential may approximated by an inverse power law with an exponent of ~ 18, in agreement with our data (Paper I). To see how we get an exponent greater than a, note that the exponent n in an inverse power law can be extracted from different ratios of derivatives,

$$v_{\mathrm{PL}}(r) = Ar^{-n} + B, \tag{8}$$

where B is a constant. This implies that

$$n = \frac{-rv'_{\mathrm{PL}}(r)}{(v_{\mathrm{PL}}(r) - B)} = \frac{-rv''_{\mathrm{PL}}(r)}{v'_{\mathrm{PL}}(r)} - 1 = \frac{-rv'''_{\mathrm{PL}}(r)}{v''_{\mathrm{PL}}(r)} - 2 = \cdots \tag{9}$$

since successive differentiation gives factors of n, then $n+1$, etc. For a potential $v(r)$, which is not an inverse power law, these expressions provide different definitions of a local effective power-law exponent [assuming $v(r) \to 0$ as $r \to \infty$],

$$n^{(0)}(r) \equiv -rv'(r)/v(r),$$

$$n^{(1)}(r) \equiv -rv''(r)/v'(r) - 1,$$

$$n^{(2)}(r) \equiv -rv'''(r)/v''(r) - 2, \tag{10}$$

$$n^{(p)}(r) \equiv -rv^{(p+1)}(r)/v^{(p)}(r) - p.$$

Paper IX

147

184508-3   Pressure-energy correlations in liquids. II

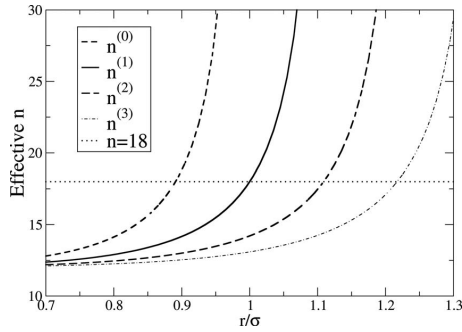J. Chem. Phys. **129**, 184508 (2008)

FIG. 1. Effective power-law exponents defined by derivative ratios of different orders [Eqs. (10)] for the standard Lennard-Jones potential LJ(12,6). All converge to 12 at small r; they diverge when the derivative in the denominator vanishes, which happens for larger r, the higher the order of this derivative. The term "effective inverse power law" in this paper refers to a power law chosen to match $n^{(1)}$ at some point $r_0 < r_m \sim 1.12\sigma$, the potential minimum where $n^{(1)}$ diverges. A convenient choice is to match at $r = \sigma$, giving 18. In Secs. II B and II C we show that $n^{(2)}(r)$ plays an important role in the understanding of fluctuations associated with pair distances close to the potential minimum ($r_m \sim 1.12\sigma$).

A plot of the first four of these is shown in Fig. 1 for LJ(12,6). All converge to $a = 12$ at short r, as they must. All increase with increasing r until the denominator vanishes, but more slowly, the higher the order p. In particular, when $n^{(p)}$ diverges it is straightforward algebra to show that $n^{(p+1)}$ has the value $a+b+p$. So $n^{(0)}$ diverges at $r = \sigma$ where the potential is zero, and is therefore unsuitable for characterizing the range which we expect to dominate the fluctuations, from energy $+\epsilon$ to energy $-\epsilon$ (it is also sensitive to the presence of an additive constant, unlike the others). Instead we use $n^{(1)}$, which at $r = \sigma$ (the zero of v and the divergence of $n^{(0)}$) takes the value $a+b$, or 18 for the LJ(12,6). Taking the factor 3 in the denominator of the virial into account, this would explain the slope ~ 6 observed in the simulations (Paper I). However first we should see how well an inverse power law with this exponent actually fits the LJ potential. We denote the point matching point r_0. With the exponent fixed, we are free to choose the multiplicative constant A and the additive one B to match the slope and value at $r = \sigma = r_0$; the resulting expression is $(4/3)((r/\sigma)^{-18} - 1)$. This is plotted in Fig. 2(a) along with v_{LJ}. We can match at different values of r by finding the expression for $n^{(1)}(r)$ for the generalized LJ potential,

$$n^{(1)}(r) = b + \frac{a-b}{1 - (b/a)(r/\sigma)^{a-b}}, \quad (11)$$

which becomes $6 + 12/(2 - (r/\sigma)^6)$ for LJ(12,6).[4]

The fact that we can choose a function (an inverse power law in this case) to match a given function and its first two derivatives is nothing special by itself; after all, a Taylor series does the same. Examples of matching power laws and Taylor series up to fourth order, at different values of r_0, are shown in Fig. 2(b), where the errors $v_{\text{LJ}}(r) - v_{\text{PL}}(r)$ or $v_{\text{LJ}}(r) - v_{\text{Taylor}}(r)$ are plotted. The magnitude of the errors are similar in the range of r shown but note that in Taylor series it was necessary to match third derivatives at r_0 to achieve
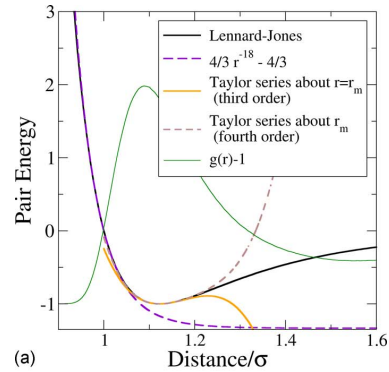
(a)
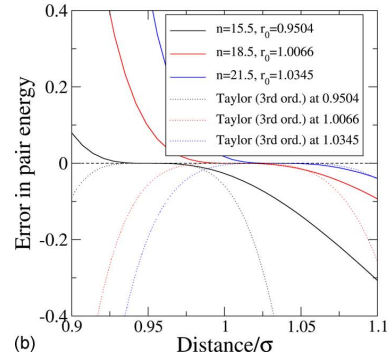
(b)

FIG. 2. (Color online) (a) The Lennard-Jones potential $v_{\text{LJ}}(r)$ fitted by an effective power-law potential $v_{\text{PL}}(r) = Ar^{-n} + B$ covering the most important part of the repulsive part of the potential. The exponent n was chosen to be 18, which optimizes agreement at $r_0 = \sigma$, where the effective power law exactly matches not just v_{LJ} but also its first two derivatives. Also shown are the Taylor series expansions of $v_{\text{LJ}}(r)$ about $r = r_m$ up to third and fourth orders. The RDF $g(r) - 1$ (at $T = 80$ K, $p = 0$) is also shown as a convenient reference for thinking about where contributions to potential energy and virial fluctuations come from. (b) Error made in approximating $v_{\text{LJ}}(r)$ with different effective power laws matched at different points r_0 and with Taylor expansions up to third order about the same point.

this, so the inverse power-law description is more compact. Moreover the power-law representation is much more useful when it comes to representing the fluctuations of total energy and virial because an inverse power law (and therefore the error) flattens out at a constant value at larger r, whereas the polynomial nature of the Taylor expansion means that away from the point of expansion, the error diverges rapidly [Fig. 2(a)].

We can test the validity of the power-law approximation for representing fluctuations in W and U as follows. For the purpose of computing the energy and virial of a configuration due to a pair interaction, all necessary information is contained in the instantaneous radial distribution function (RDF) (Ref. 2)

$$g(r,t) \equiv \frac{2}{N\rho} \sum_{i<j} \delta(r - r_{ij}(t))/(4\pi r^2), \quad (12)$$

where $\rho = N/V$ with N and V being the number of particles and the system volume, respectively. From this U and W may be computed as
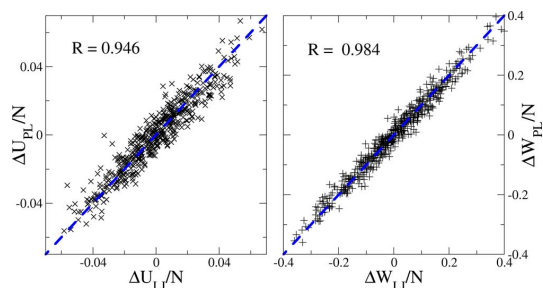
FIG. 3. (Color online) Scatter plot of true and reconstructed potential energy and virial fluctuations (dimensionless units) for the LJ liquid, where the reconstructed values U_{PL} and W_{PL} were calculated from the true configurations, assuming an inverse power-law potential with exponent of 19.2; mean values have been subtracted off. The state point is the same as in Fig. 1 of Paper I (zero average pressure, *NVT* ensemble). The correlation coefficients are displayed in the figures; the dashed lines indicate slope unity. The fact that actual and reconstructed fluctuations correlate strongly, and with slopes close to unity, support the idea that the W, U correlation is derived from an effective inverse power-law potential dominating fluctuations.

$$U_{LJ}(t) = \frac{N}{2} \rho \int_0^\infty dr 4\pi r^2 g(r,t) v_{LJ}(r), \tag{13}$$

$$W_{LJ}(t) = -\frac{N}{6} \rho \int_0^\infty dr 4\pi r^2 g(r,t) w_{LJ}(r). \tag{14}$$

Now, $U_{LJ}(t)$ is rewritten as an inverse power-law potential plus a difference term, $U_{LJ}(t) = U_{PL}(t) + U_{diff}(t)$, where

$$U_{PL}(t) = \frac{N}{2} \rho \int_0^\infty dr 4\pi r^2 g(r,t) v_{PL}(r), \tag{15}$$

$$U_{diff}(t) = \frac{N}{2} \rho \int_0^\infty dr 4\pi r^2 g(r,t)(v_{LJ}(r) - v_{PL}(r)), \tag{16}$$

and similarly $W_{LJ}(t) = W_{PL}(t) + W_{diff}(t)$. We do not include the additive constant with the power-law approximation; for practical reasons the potential function should be close to zero at a cutoff distance r_c (adding a constant to v_{PL} would only add an overall constant to U_{PL}). We refer to $U_{PL}(t)$ and $W_{PL}(t)$ as "reconstructed" potential energy and virial, respectively, to emphasize that the configurations are drawn from a simulation using the LJ potential, but these quantities are calculated using the inverse power law. In Fig. 3, we show a scatter plot of the true and reconstructed values of U and W for the same state point ($p=0$, $T=80$ K) as was shown in Figs. 1 and 2(a) of Paper I. Here the inverse power-law exponent was chosen to minimize the variances of the difference quantities $\langle (\Delta U_{diff})^2 \rangle$ and $\langle (\Delta W_{diff})^2 \rangle$. These are minimized for $n=19.3$ and 19.1, respectively, so we choose the value 19.2, which corresponds to matching the potentials at the distance of 1.015σ. Note that what are actually plotted are the deviations from the respective mean values—the means $\langle U_{LJ} \rangle$ and $\langle U_{PL} \rangle$, for example, do not coincide. However the fluctuations are clearly highly correlated, and the data lie quite close to the blue dashed lines, marking slope unity. Specifically, the correlation coefficients are 0.946 for the potential energy and 0.984 for the virial. We can also

check how much of the variance of U_{LJ} is accounted for by U_{PL}, $\langle (\Delta U_{PL})^2 \rangle / \langle (\Delta U_{LJ})^2 \rangle$, and similarly for W. This is a sensible quantity because the "PL" and "diff" parts are almost uncorrelated for the choice $n=19.2$ (cross terms account for less than 1% of the total variance in each case). We find 92% for U and 95% for W. Thus we see that the power law gives to a quite good approximation the fluctuations of W and U. The correlation follows from this with γ given by one-third of the effective inverse power-law exponent, or 6.4 for this state point. The measured slope [Eq. (6)] was 6.3, corresponding to an effective exponent of 18.9, about 2% smaller than the 19.3. A simpler way to determine the exponent would be three times the slope, although for some applications it could be advantageous to optimize the fit as described here.

B. Low-temperature limit: Anharmonic vibrations of a crystal

We turn our attention now to the fact that the correlation persists even for the crystallized samples (seen in Paper I in the lower left part of Fig. 4 and in Fig. 6). This is not trivial because the physics of solids, both crystalline and amorphous systems, is generally dominated by fluctuations about mechanically stable structures, and therefore presumably (except perhaps at very high pressure) by the form of the potential near its minimum r_m, i.e., including distances larger than the minimum. Thus the idea of the effective inverse power law would seem to be inappropriate here, in particular, since the effective exponent $n^{(1)}$ diverges at r_m—and there is apparently no reason why one should get a correlation as strong as in the liquid and with so similar a slope. In fact, there is an interval of r between r_m and the minimum of the pair virial $-w(r)/3$ where $v(r)$ increases and $-w(r)/3$ decreases, which would lead, if anything, to a negative correlation between W and U, when considering individual pair interactions. Moreover, one would expect that a harmonic approximation of the potential near the ground-state configuration would be an accurate representation of the dynamics in the low-temperature limit, but as we will see, the harmonic approximation actually implies negative W, U correlation, which is not observed. In this subsection we show why the strong positive correlation persists, and why the slope γ changes little going from liquid to crystal (at constant volume). Although the classical dynamics of a crystal is apparently of little importance, since in reality quantum effects dominate, it turns out to be very instructive to consider the low-temperature ($T\to0$) classical limit since what we find has significance also in the liquid phase (Sec. II C). The key ideas are (1) that the positive correlation emerges only after summing over all interactions—it is therefore a collective effect rather than a single-pair effect, and (2) the constraint of fixed volume—it is important to recall from Paper I that the virial-potential-energy correlation only appears under fixed-volume conditions; different volumes give approximately the same slope but different offsets (Fig. 4 in Paper I).

1. The one-dimensional crystal

For maximum clarity we start by considering the simplest possible case, a one-dimensional (1D) crystal with periodic boundary conditions and only nearest-neighbor interactions. We also suppose that the lattice spacing a_c is equal to the minimum of the potential; this assumption is not made in the subsequent treatment of the three-dimensional (3D) crystal. In a crystal the particles stay close to their equilibrium positions. It therefore makes sense to expand the pair energy (we have in mind a general pair potential with a single minimum) as a Taylor series, leaving out constant terms but keeping third order terms,

$$U = \sum_i \left(\frac{1}{2}k_2(r_{i,i+1} - r_m)^2 + \frac{1}{6}k_3(r_{i,i+1} - r_m)^3 \right)$$
$$\equiv \frac{1}{2}k_2 S_2 + \frac{1}{6}k_3 S_3, \tag{17}$$

where $r_{i,i+1}$ is the distance between particles i and $i+1$, k_p is the pth derivative of the pair potential at $r=r_m$, and we introduce the notation

$$S_p \equiv \Sigma_i (r_{i,i+1} - r_m)^p.$$

The virial is

$$W = -\frac{1}{3}\sum_i \left(k_2 r_{i,i+1}(r_{i,i+1} - r_m) + \frac{k_3 r_{i,i+1}}{2}(r_{i,i+1} + r_m)^2 \right), \tag{18}$$

which, by writing $r_{i,i+1} = r_m + (r_{i,i+1} - r_m)$, can be rewritten as

$$W = -\frac{1}{3}\left(k_2 r_m S_1 + k_2 S_2 + \frac{k_3 r_m}{2}S_2 + \frac{k_3}{2}S_3 \right). \tag{19}$$

Note that U involves S_2 and S_3 while W also has a first-order term with S_1. Evaluating the sum S_1 is very simple: $r_{i,i+1}$ can be expressed in terms of displacements from the equilibrium positions u_i as $r_{i,i+1} = r_m + u_{i+1} - u_i$, giving for S_1

$$S_1 = \sum_i (u_{i+1} - u_i). \tag{20}$$

Such a sum of consecutive relative displacements gives the change in separation of the two end particles. However the total sum must vanish because by periodic boundary conditions the "end particles" are the same particle (it does not matter which one), therefore $S_1 = 0$. In fact, periodic boundary conditions are not necessary, only that the length is fixed. Since both U and W involve at lowest order S_2, which is positive semidefinite, at sufficiently low temperature we may drop the S_3 terms. Combining Eqs. (17) and (19) we find

$$W = -\frac{1}{3}\frac{k_2 + k_3 r_m/2}{k_2/2}U = \frac{n^{(2)}(r_m)}{3}U, \tag{21}$$

where we have written the coefficient in terms of the $p=2$ effective power-law exponent defined in Eq. (10). For LJ(a, b) the coefficient evaluates to $(a+b+1)/3$, which is 6.33 for LJ(12,6), similar to the observed slope. This short calculation demonstrates the main point: summing over all interactions makes the first-order term in the virial vanish, and the

second-order term is proportional to the second-order term in the potential energy. It is also worth noting that for a purely harmonic crystal we can take $k_3 = 0$, in which case Eq. (21) implies that there is perfect negative correlation, with a slope of $-2/3$.

2. The three-dimensional crystal

We now generalize this to 3D crystals, which means allowing for transverse displacements. The calculation involves breaking overall sums into sums over 1D chains within the crystal. We also relax the condition that the lattice constant coincides with the potential minimum, which is only realistic at low pressures. We still assume only nearest-neighbor interactions are relevant (this will be justified in the next subsection). Generalization to a disordered (amorphous) solid[5] should be possible, since we observe the correlation to hold also in that case. The calculation would necessitate, however, some kind of disorder averaging, which is beyond the scope of this paper.[6]

We start by considering a simple cubic (sc) crystal of lattice constant a_c, with interactions only between nearest neighbors, so that the equilibrium bond length is a_c for all bonds. The fact that such a crystal is mechanically unstable is irrelevant for the calculation. We shall see later that the result applies also to, for instance, a face-centered-cubic (fcc) crystal. We have the same kind of expansions about $r=a_c$ as above for U and W, except a linear term is now included since we no longer assume that $a_c = r_m$. An index b is used to represent nearest-neighbor bonds, and as for the 1D case, we define

$$S_p \equiv \sum_b (r_b - a_c)^p. \tag{22}$$

We then have for U and W

$$U = \sum_{p=1}^{\infty} \frac{k_p}{p!}\sum_{\text{bonds } b} (r_b - a_c)^p = \sum_{p=1}^{\infty} \frac{k_p}{p!}S_p, \tag{23}$$

$$3W = \sum_{p=1}^{\infty} -\frac{k_p}{(p-1)!}\sum_{\text{bonds } b} r_b(r_b - a_c)^{p-1}$$
$$= -\sum_{p=1}^{\infty} \frac{k_p a_c}{(p-1)!}S_{p-1} - \sum_{p=1}^{\infty} \frac{k_p}{(p-1)!}S_p$$
$$= -k_1 a_c S_0 - \sum_{p=1}^{\infty} \left(\frac{k_p}{(p-1)!} + \frac{k_{p+1}a_c}{p!} \right)S_p, \tag{24}$$

where k_p is the pth derivative of the pair potential at $r=a_c$. It is convenient to define coefficients C_p^U and C_p^W of the dimensionless quantities S_p/a_c^p,

$$C_p^U \equiv \frac{k_p a_c^p}{p!}, \tag{25}$$

$$C_p^W \equiv -\left(\frac{k_p a_c^p}{(p-1)!} + \frac{k_{p+1}a_c^{p+1}}{p!} \right). \tag{26}$$

Dropping the constant term $-k_1 a_c S_0$ in W, since it plays no role for the fluctuations, we then have

$$U = \sum_{p=1}^{\infty} C_p^U \frac{S_p}{a_c^p}, \tag{27}$$

$$3W = \sum_{p=1}^{\infty} C_p^W \frac{S_p}{a_c^p}. \tag{28}$$

The ratio of the corresponding coefficients is given by the *p*th order effective inverse power-law exponent,

$$C_p^W / C_p^U = -\left(p + \frac{k_{p+1} a_c}{k_p}\right) = n^{(p)}(a_c). \tag{29}$$

Thus for in the limit of small a_c, where these are all similar and close to the repulsive exponent in the potential (Fig. 1), the two expansions will be proportional to each other to an infinite order. Also worth noting for later use is that the C_p's in each series increase with p. For example,

$$C_2^U / C_1^U = \frac{k_2 a_c}{2k_1} = -\frac{1}{2}(n^{(1)}(a_c) + 1), \tag{30}$$

$$C_2^W / C_1^W = \frac{k_2 a_c + k_3 a_c^2 / 2}{k_1 + k_2 a_c} = -\frac{1}{2}(n^{(1)}(a_c) + 1)\frac{n^{(2)}(a_c)}{n^{(1)}(a_c)}. \tag{31}$$

For a_c between σ and r_m, for LJ(12,6), the absolute values of these ratios lie in the intervals 9.5–∞ and 6.7–9.5, respectively.

From dimensional considerations the variance of S_p is proportional to $N\sigma_u^{2p}$, where $\sigma_u^2 \propto T$ is the variance of single-particle displacements. At low T, therefore, we expect the S_1 terms to dominate, which causes a problem since k_1 changes its sign at r_m, corresponding to the divergence of $n^{(1)}$. In 1D this was avoided by the exact vanishing of S_1. In 3D S_1 does not vanish exactly but retains terms second order in displacements, and so contributes similarly to S_2. It turns out (see below) that S_1 and S_2/a_c have similar variances and significant positive correlation, but in view of Eqs. (30) and (31) this is not even necessary for a strong W, U correlation—the coefficients of the S_1 are relatively small so that it is still the S_2 terms that dominate. That is essentially the explanation of the strong correlations in the crystal, but we now continue the analysis in more detail in order to investigate how good it becomes in the limit $T \to 0$. These general considerations will be of use again in the following subsection, where we make a similar expansion of the fluctuations in the liquid state.

We need to evaluate S_1 and S_2 in terms of the relative displacements $\mathbf{u}_b$ of the pair of particles involved in bond b.[7] We keep only terms up to second order in displacements since we are interested in the limit of low temperatures, so all S_3 terms in the expansion are dropped. In a sc crystal, all nearest-neighbor bonds are parallel to one of the coordinate (crystal) axes. Consider all bonds along the *x*-axis. These may be grouped into rows of collinear bonds. The sum along a single row is almost analogous to the 1D case except that the bond length r_b now also involves transverse displacements,

$$S_p^{\text{row}} = \sum_{b,\text{row}} (r_b - a_c)^p. \tag{32}$$

We write r_b explicitly in terms of the relative displacements and expand the resulting square root, dropping terms of higher order than the second in u,

$$\begin{aligned}
r_b - a_c &= ((a_c + u_{b,x})^2 + u_{b,y}^2 + u_{b,z}^2)^{1/2} - a_c \\
&= a_c\left(1 + \frac{2u_{b,x}}{a_c} + \frac{u_{b,x}^2}{a_c^2} + \frac{u_{b,y}^2 + u_{b,z}^2}{a_c^2}\right)^{1/2} - a_c \\
&= a_c\left(1 + \frac{1}{2}\left(\frac{2u_{b,x}}{a_c} + \frac{u_{b,x}^2 + u_{b,y}^2 + u_{b,z}^2}{a_c^2}\right)\right. \\
&\quad \left. -\frac{1}{8}\left(\frac{2u_{b,x}}{a_c}\right)^2\right) - a_c \\
&= u_{b,x} + \frac{u_{b,y}^2 + u_{b,z}^2}{2a_c}.
\end{aligned} \tag{33}$$

Now, the sum over bonds in a given row of the parallel displacements $u_{b,x}$ vanishes for the same reasons as in the 1D case. However when we sum the contributions to S_1 over the row, there are also second-order terms coming from the transverse displacements. Extending the sum to all bonds parallel to the *x*-axis, we have part of S_1, denoted as S_1^x,

$$S_1^x = \sum_{b,x} \frac{u_{b,y}^2 + u_{b,z}^2}{2a_c} = \sum_{b,x} \frac{|\mathbf{u}_{b,\perp}|^2}{2a_c}, \tag{34}$$

where $\perp$ indicates the component of the relative displacement vector perpendicular to the bond direction. Writing it this way allows us to easily include the bonds parallel to the *y*- and *z*-axes, and the total S_1 is given by
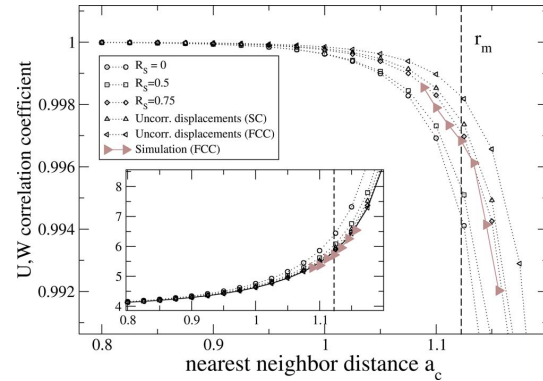
FIG. 4. (Color online) Plots of predicted W, U correlation coefficient for $T \to 0$ for a crystal of LJ(12,6) particles for different degrees of correlation between the quantities $S_1 a_c$ and S_2, and of low-temperature simulation data. The first three curves (counting from the bottom) assume that the variances of $S_1 a_c$ and S_2 are equal, and that their correlation coefficients R_S are 0, 0.5, and 0.75, respectively. The fourth curve (up triangles) results from considering an sc lattice and assuming individual particles have uncorrelated Gaussian-distributed displacements, leading to specific values for the variances and covariance of $S_1 a_c$ and S_2. The fifth (left triangles) shows the same estimate for a fcc lattice. The right triangles are data from an *NVT* simulation of a perfect fcc crystal at $T = 0.0002$ K. The conclusion from this figure is that R does not tend to unity as $T \to 0$, although it becomes extremely close. The inset shows the corresponding slopes γ [Eq. (6)].

Paper IX

184508-7   Pressure-energy correlations in liquids. II

151

J. Chem. Phys. **129**, 184508 (2008)

$$S_1 = \sum_b \frac{|\mathbf{u}_{b,\perp}|^2}{2a_c}. \tag{35}$$

Next we calculate S_2 to second order in the relative displacements $\mathbf{u}_b$. Starting with S_2^x, the part containing only bonds in the x-direction, using Eq. (33) we get

$$S_2^x = \sum_{b,x} u_{b,x}^2 = \sum_{b,x} |\mathbf{u}_{b,\|}|^2, \tag{36}$$

where $\|$ means the part of the relative displacement that is parallel to the bond. Including all bonds,

$$S_2 = \sum_b |\mathbf{u}_{b,\|}|^2. \tag{37}$$

Now we can return to our expressions for the potential-energy fluctuations [Eqs. (23) and (24)], keeping only terms in S_1 and S_2,

$$\Delta U = k_1 S_1 + \frac{k_2}{2} S_2 = \frac{k_1}{2a_c} \sum_b |\mathbf{u}_{b,\perp}|^2 + \frac{k_2}{2} \sum_b |\mathbf{u}_{b,\|}|^2. \tag{38}$$

Similarly, for the virial

$$3W = -k_2 a_c S_1 - \frac{k_3 a_c}{2} S_2 - k_1 S_1 - k_2 S_2$$

$$= -\left(\frac{k_1}{2a_c} + \frac{k_2}{2} \right) \sum_b |\mathbf{u}_{b,\perp}|^2 - \left(k_2 + \frac{k_3 a_c}{2} \right) \sum_b |\mathbf{u}_{b,\|}|^2. \tag{39}$$

3. Statistics of S_1 and S_2

It is clear that the $\|$ and $\perp$ sums are not equal, although they must be correlated to some extent. If written in terms of

single-particle displacements rather than relative displacements for bonds, a term such as $|\mathbf{u}_{b,\|}|^2$ for a bond in the x-direction becomes

$$(u_{\mathbf{R}+a_c\hat{\imath},x} - u_{\mathbf{R},x})^2 = u_{\mathbf{R}+a_c\hat{\imath},x}^2 + u_{\mathbf{R},x}^2 - 2u_{\mathbf{R}+a_c\hat{\imath},x} u_{\mathbf{R},x}, \tag{40}$$

where $\mathbf{R}$ is a lattice vector used to index particles. Summing over bonds gives

$$S_2 = 2 \sum_{\mathbf{R}} |\mathbf{u}_{\mathbf{R}}|^2 - 2 \sum (\text{para. cross terms}), \tag{41}$$

where the cross terms are products of the parallel components of displacements on neighboring particles. For S_1 we have something similar,

$$S_1 a_c = 2 \sum_{\mathbf{R}} |\mathbf{u}_{\mathbf{R}}|^2 - 2 \sum (\text{perp. cross terms}), \tag{42}$$

where here the cross terms involve transverse components. Since the term $\Sigma_{\mathbf{R}} |\mathbf{u}_{\mathbf{R}}|^2$ appears in both S_1 and S_2, these are correlated to some extent, but not 100% since different cross terms appear (note that if it were 100%, then W and U would both be proportional to $S_2 \propto S_1$ and also correlated 100%). Before considering as to what extent they are correlated, let us see how much of a difference it makes. Suppose the quantities $S_1 a_c$ and S_2 have variances σ_1^2 and σ_2^2, respectively, and are correlated with correlation coefficient R_S. Using the coefficients introduced in Eqs. (25) and (26)

$$U a_c^2 = C_1^U (S_1 a_c) + C_2^U S_2,$$
$$3W a_c^2 = C_1^W (S_1 a_c) + C_2^W S_2. \tag{43}$$

From this we obtain an expression for the W, U correlation coefficient by forming the appropriate products and taking averages,

$$R = \frac{C_1^U C_1^W \sigma_1^2 + C_2^U C_2^W \sigma_2^2 + (C_1^U C_2^W + C_1^W C_2^U)\sigma_1\sigma_2 R_S}{\sqrt{(C_1^U)^2\sigma_1^2 + (C_2^U)^2\sigma_2^2 + 2C_1^U C_2^U \sigma_1\sigma_2 R_S}\sqrt{(C_1^W)^2\sigma_1^2 + (C_2^W)^2\sigma_2^2 + 2C_1^W C_2^W \sigma_1\sigma_2 R_S}}. \tag{44}$$

This estimation of R is plotted in Fig. 4 as a function of lattice constant for $R_S = 0$, 0.5 and 0.75, for the case $\sigma_1 = \sigma_2$. Clearly the value of R_S makes little difference in the region of interest, $a_c \sim r_m$ or less, where R is above 0.99. Note that all curves drop dramatically as the lattice constant approaches the inflection point ($k_2 = 0$) of the potential (the precise value at which R becomes zero depends on the statistics of $S_1 a_c$ and S_2). In this regime, however, higher-order terms in displacements, including S_3, S_4, etc., become more important, and because of Eq. (29) their inclusion tends to restore R to a high value (we have not calculated their effect in detail). Also plotted is the estimation of R obtained by assuming that particle displacements are uncorrelated and Gaussian distributed with variance σ_u^2 for each (Cartesian) component, corresponding to an Einstein model of the vibrational dynamics. In this case tedious but straightforward al-

gebra allows the means and (co-)variances of $S_1 a_c$ and S_2 to be calculated explicitly for a given lattice. The results for sc and fcc are given in Table I. Notice that the variance of S_2 is somewhat larger than that of $S_1 a_c$, while their means are equal. This can be traced to the fact that the latter contains

TABLE I. Statistics of $S_1 a_c$ and S_2 assuming uncorrelated particle displacements with variance σ_u^2 for each Cartesian component, for sc and fcc lattices.

	sc	fcc
$\langle S_1 a_c \rangle$	$6N\sigma_u^2$	$12N\sigma_u^2$
$\langle S_2 \rangle$	$6N\sigma_u^2$	$12N\sigma_u^2$
$\mathrm{var}(S_1 a_c)$	$30N\sigma_u^4$	$108N$
$\mathrm{var}(S_2)$	$36N\sigma_u^4$	$120N$
$\mathrm{cov}(S_1 a_c, S_2)$	$24N\sigma_u^4$	$96N$
R_S	0.73	0.84

twice as many cross terms as the former, and a factor of $1/2$, so the contribution from such terms to the mean is the same in both cases, while the contribution to the variance is smaller for $S_1 a_c$. From the (co-)variances we find the correlation coefficient $R_S = 0.73$ and $R_S = 0.84$ for the sc and fcc cases, respectively. These are also plotted in Fig. 4. A more exact calculation would take into account the true normal modes of the crystal but would yield little of use: Data from the crystal simulations at very low temperature, also plotted in Fig. 4 agree within estimated numerical errors with both the sc and fcc estimates. The key point of this figure—that R is close to but less than 1—apparently would change little by taking the true crystal dynamics into account. In particular, it is important to note that if $R=1$ exactly, then this would be true no matter what kind of weighted average of configurations is taken (what kind of ensemble), so a value less than unity in the Einstein approximation is sufficient to disprove the hypothesis that $R \to 1$ as $T \to 0$.

4. The role of the coefficients $C_{1,2}^{U,W}$

Since the detailed statistics of S_1 and S_2 have little effect on the W,U correlation, it must be mainly due to the numerical values of the coefficients $C_{1,2}^{U,W}$. We can estimate the effect of these by assuming that $S_1 a_c$ and S_2 have equal variance and are uncorrelated ($R_S = 0$). Then according to Eq. (44) the W,U correlation coefficient is

$$R = \frac{C_1^U C_1^W + C_2^U C_2^W}{\sqrt{(C_1^U)^2 + (C_2^U)^2}\sqrt{(C_1^W)^2 + (C_2^W)^2}}, \tag{45}$$

which has the form of the cosine of the angle between two vectors $\mathbf{C}^U \equiv (C_1^U, C_2^U)$ and $\mathbf{C}^W \equiv (C_1^W, C_2^W)$. Thus the closeness of R to unity indicates that these vectors are nearly parallel. The tangents of the angles these vectors make with the C_1 axis in (C_1, C_2)-space are given by Eqs. (30) and (31); clearly the two angles become equal in the limit of small a_c, where $n^{(1)}$ and $n^{(2)}$ converge. On the other hand, for $a_c \sim r_m$ where $k_1 = 0$ and $n^{(1)}$ diverges, the two vectors are

$$\mathbf{C}^U = (0, k_2/2) a_c^2,$$
$$\mathbf{C}^W = -(k_2, k_2 + k_3 a_c/2) a_c^2 \tag{46}$$
$$= -k_2 a_c^2 \left(1, 1 - \tfrac{1}{2}(n^{(2)} + 2)\right)$$
$$= k_2 a_c^2 \left(-1, \frac{n^{(2)}}{2}\right).$$

Clearly $\mathbf{C}^U$ is parallel to the C_2 axis, while $\mathbf{C}^W$ deviates from it by an angle of the order of $2/n^{(2)} \sim 1/10$. The W,U correlation coefficient is then $R = \cos(1/10) \sim 1 - \tfrac{1}{2}(1/10)^2 \sim 0.995$, in agreement with the bottom curve (circles) in the main part of Fig. 4. In this case ($a_c = r_m$, $k_1 = 0$, $S_1 a_c$ and S_2 uncorrelated with equal variance), we can obtain a simple expression for the slope

$$\gamma = \sqrt{\frac{(C_1^W)^2 + (C_2^W)^2}{(C_1^U)^2 + (C_2^U)^2}}$$
$$= \frac{k_2}{3} \sqrt{\frac{1 + (n^{(2)}/2)^2}{(k_2/2)^2}}$$
$$= \frac{2}{3}\sqrt{1 + (n^{(2)}/2)^2} \sim \frac{n^{(2)}}{3} \tag{47}$$

consistent with the result from the 1D case.

Thus when we look at the "collective" correlations in the crystal, we naturally get a slope involving the effective power-law exponent $n^{(2)}$. Since the latter evaluated at the potential minimum is similar to $n^{(1)}$ at the zero of the potential, the slope is similar to that seen in the liquid phase. On the other hand, it is more typical to think about crystal dynamics starting from a harmonic approximation, adding in anharmonic terms when necessary for higher accuracy. How does it work here? If we set $k_3 = 0$ as well as $k_1 = 0$, so we consider the purely harmonic system with the nearest-neighbor distance at the minimum of the potential, then we have $\mathbf{C}^U = (0, k_2/2)$ and $\mathbf{C}^W = -(k_2/3)(1,1)$. These are not close to being parallel, so the correlation will be weaker (coming mainly from that of S_1 and S_2) but more particularly, it will be negative, thus qualitatively different from the anharmonic case. Thus the presence of the k_3 affects the results at arbitrarily low temperature, so the harmonic approximation is never good enough. This is reminiscent of thermal expansion, which does not occur for a purely harmonic crystal. In fact, the Grüneisen parameter for a 1D crystal with nearest neighbor interactions may be shown[8] to be equal to $1 + n^{(2)}(a_c)/2$.

Finally we consider the more realistic fcc crystal. First note that Eqs. (35) and (37) are unchanged as long as a_c is now interpreted as the nearest-neighbor distance rather than the cubic lattice spacing: Each position in a fcc lattice has 12 nearest neighbors, four located in each of three mutually orthogonal planes. Taking the xy and parallel planes first, the neighbors are located along the diagonal directions with respect to the cubic crystal axes. As before we can do the sum first over bonds forming a row, then over all parallel rows. For a given plane there are two orthogonal sets of rows, but the form of the sums in Eqs. (35) and (37) includes all bonds. The results of the calculation of (co-)variances of S_1 and S_2 in the Einstein model of the dynamics are changed in a way that, in fact, increases their mutual correlation and therefore the W,U correlation, as shown in Table I and Fig. 4.

To summarize this subsection, the correlation in the crystal is an anharmonic effect that persists in the limit $T \to 0$. It works because (1) the constraint of fixed volume causes the terms in U and W that are first order in particle displacements to cancel and (2) the coefficients of the "transverse" second-order terms are small compared to those of the "parallel" ones, a fact which can be traced to the resemblance of the potential to a power law at distances shorter than the potential minimum. "Small" here means of the order of $1/10$, which leads to over 99% correlation because R is essentially the cosine of this quantity. In one dimension there

Paper IX 153

184508-9   Pressure-energy correlations in liquids. II   J. Chem. Phys. **129**, 184508 (2008)

are no transverse displacements and the correlation is 100% as $T \rightarrow 0$; in more than one dimension as $T \rightarrow 0$ the correlation is very close to unity but never 100%.

To gain a more complete insight into the fluctuations, we next present an analysis that clarifies exactly the contributions to fluctuations from different distances, without approximations, now again with the liquid case in mind.

C. Fluctuation modes

In the last two subsections we considered single-pair effects (associated with $r < r_m$) and collective effects (associated with $r \sim r_m$), respectively. In this section we focus on contributions from particular pair separations without keeping track of which actual particles are involved. We identify the contributions to U and W coming from all pairs whose separation lies within a fixed small interval of separations r; fluctuations in the number of such pairs generate fluctuations in the contributions. By considering all intervals we can systematically analyze the variances and covariances of U and W in terms of pair separation, which is the purpose of this section.

The instantaneous values of U and W are given by Eq. (13) and (14), generalized to an arbitrary pair potential. By taking a time (or ensemble) average we get the corresponding expressions for $\langle U \rangle$ and $\langle W \rangle$ in terms of $g(r) \equiv \langle g(r,t) \rangle$, the usual thermally averaged RDF. Now we consider the variances $\langle (\Delta U)^2 \rangle$ and $\langle (\Delta W)^2 \rangle$, and the covariance $\langle \Delta U \Delta W \rangle$. Starting with, for example, $\Delta U(t) = 4\pi \rho N / 2 \int_0^\infty dr r^2 v(r) \Delta g(r,t)$, where $\Delta g(r,t) \equiv g(r,t) - g(r)$, averaging and taking everything except $\Delta g(r,t)$ outside the average, we have

$$\langle (\Delta U)^2 \rangle = (4\pi \rho N/2)^2 \int_0^\infty dr_1 r_1^2 \int_0^\infty dr_2 r_2^2 v(r_1) v(r_2)$$
$$\times \langle \Delta g(r_1,t) \Delta g(r_2,t) \rangle, \tag{48}$$

$$\langle (\Delta W)^2 \rangle = (4\pi \rho N/2)^2 \int_0^\infty dr_1 r_1^2 \int_0^\infty dr_2 r_2^2 w(r_1) w(r_2)$$
$$\times \langle \Delta g(r_1,t) \Delta g(r_2,t) \rangle, \tag{49}$$

$$\langle \Delta U \Delta W \rangle = (4\pi \rho N/2)^2 \int_0^\infty dr_1 r_1^2 \int_0^\infty dr_2 r_2^2 v(r_1) w(r_2)$$
$$\times \langle \Delta g(r_1,t) \Delta g(r_2,t) \rangle. \tag{50}$$

Clearly the quantity, which contains the essential statistical information about the fluctuations, is $\langle \Delta g(r_1,t) \Delta g(r_2,t) \rangle$, the covariance of the RDF with itself. Its magnitude is inversely proportional to N, so that $\langle (\Delta U)^2 \rangle$ is proportional to N, as it should be. The variances of U and W and their covariance are integrals of this function with different weightings. To make further progress, we integrate the integrands for the variances over $M \times M$ "blocks" in r_1, r_2-space. This is equivalent to considering the energy, say, as the following sum of M interval energies,

$$U(t) = \sum_{a=1}^M U_a(t), \tag{51}$$

where the interval energy $U_a(t)$ is defined as the integral between boundaries r_a and r_{a+1},

$$U_a(t) \equiv \frac{N}{2} \rho \int_{r_a}^{r_{a+1}} dr 4\pi r^2 g(r,t) v(r). \tag{52}$$

The virial can be similarly represented as a sum of contributions from the same r-intervals, $W(t) = \sum_{a=1}^M W_a(t)$. From now on we consider the primary fluctuating quantities to be $U_a(t)$ and $W_a(t)$ and seek to understand the correlation between their respective sums in terms of correlations between particular U_as and W_as. In order to achieve a reasonable degree of spatial resolution, we do not make the intervals (blocks) too big, and choose an interval width of 0.05. This gives $M = 42$ intervals: U_1 is the contribution to the energy coming from pairs with separation in the range of 0.85–0.9, marking the lower limit of nonzero RDF, while U_{42} refers to the range 2.9–2.95, marking the cutoff distance of the potential used here. We shall see explicitly that only distances up to around 1.4 contribute significantly to the fluctuations. We denote deviations from the mean as, e.g., $\Delta U_a = U_a - \langle U_a \rangle$ with the angle brackets representing the time (or ensemble) average.

We are interested in the covariance of the U_a's with themselves (including $\langle \Delta U_a \Delta U_b \rangle$, $a \neq b$), the W_a's with themselves, and the U_a's with the W_a's. These covariances are just what is obtained by integrating the integrands in Eqs. (48)–(50) over the block defined by the corresponding intervals for r_1 and r_2. These values are conveniently represented using matrices $\mathbf{\Delta}^{UU}$, $\mathbf{\Delta}^{WW}$, and $\mathbf{\Delta}^{UW}$ defined as

$$(\mathbf{\Delta}^{UU})_{ab} = \langle \Delta U_a \Delta U_b \rangle, \tag{53}$$

$$(\mathbf{\Delta}^{WW})_{ab} = \langle \Delta W_a \Delta W_b \rangle, \tag{54}$$

and

$$(\mathbf{\Delta}^{UW})_{ab} = \langle \Delta U_a \Delta W_b \rangle. \tag{55}$$

Note that the sum of all elements of $\mathbf{\Delta}^{UU}$ is the energy variance since it reproduces the double integral of Eq. (48); similarly, for the other two matrices

$$\langle (\Delta U)^2 \rangle = \sum_{a,b} (\mathbf{\Delta}^{UU})_{ab}, \tag{56}$$

$$\langle (\Delta W)^2 \rangle = \sum_{a,b} (\mathbf{\Delta}^{WW})_{ab}, \tag{57}$$

$$\langle \Delta U \Delta W \rangle = \sum_{a,b} (\mathbf{\Delta}^{UW})_{ab}. \tag{58}$$

At this point we make one further transformation. Define new matrices $\mathbf{\Delta}^{UU*}$, $\mathbf{\Delta}^{WW*}$, and $\mathbf{\Delta}^{UW*}$ by

$$\mathbf{\Delta}^{UU*} \equiv \mathbf{\Delta}^{UU} / \langle (\Delta U)^2 \rangle, \tag{59}$$

$$\mathbf{\Delta}^{WW*} \equiv \mathbf{\Delta}^{WW} / \langle (\Delta W)^2 \rangle, \tag{60}$$

and

TABLE II. First ten eigenvalues of the supercovariance matrix [Eq. (65)], their fractional contributions to the three (co-)variances [Eqs. (62)–(64)], and their effective slopes [Eq. (67)] for the SCLJ liquid with parameters as in Fig. 1 of Paper I (ρ=34.6 mol/l, T=80 K). Contributions from the dominant four eigenvectors are in boldface. The last three rows list sums of the third, fourth, and fifth columns over, respectively, the dominant four, the first ten, and all $2M$ eigenvectors. The sum of the fifth column over all eigenvectors should be compared [see Eq. (64)] to the R=0.939 listed in Table I of Paper I.

Index	Eigenvalue	U-var. contr.	W-var. contr.	Corr. coeff. contr.	Effective slope
1	1.73	0.01	0.01	0.01	5.38
2	1.55	0.04	0.06	0.05	7.63
3	**1.11**	**0.24**	**0.15**	**0.19**	**4.98**
4	**0.87**	**0.25**	**0.25**	**0.25**	**6.34**
5	**0.78**	**0.20**	**0.14**	**0.17**	**5.27**
6	**0.58**	**0.11**	**0.17**	**0.13**	**7.80**
7	0.34	0.02	0.05	0.03	10.14
8	0.23	0.01	0.03	0.01	13.67
9	0.13	0.00	0.01	0.00	116.19
10	0.10	0.01	0.00	−0.00	−3.63
$\Sigma_{3,\dots,6}$	⋯	0.797	0.709	0.742	⋯
$\Sigma_{1,\dots,10}$	⋯	0.884	0.877	0.849	⋯
$\Sigma_{1,\dots,2M}$	⋯	1.000	1.000	0.938	⋯

$$\mathbf{\Delta}^{UW*} \equiv \mathbf{\Delta}^{UW}/\sqrt{\langle(\Delta U)^2\rangle\langle(\Delta W)^2\rangle}. \tag{61}$$

This is equivalent to normalizing the U_a's by the standard deviation $\sqrt{\langle(\Delta U)^2\rangle}$ and the W_a's by $\sqrt{\langle(\Delta W)^2\rangle}$, respectively. The elements of $\mathbf{\Delta}^{UU*}$, $\mathbf{\Delta}^{WW*}$, and $\mathbf{\Delta}^{UW*}$ can be thought of as representing, in some sense, what fraction of the total (co-)variance is contributed by the corresponding block. Normalized in this way, the sum over all elements of $\mathbf{\Delta}^{UU*}$ and $\mathbf{\Delta}^{WW*}$ is exactly unity and that for $\mathbf{\Delta}^{UW*}$ equals the correlation coefficient R,

$$\sum_{a,b}(\mathbf{\Delta}^{UU*})_{ab} = 1, \tag{62}$$

$$\sum_{a,b}(\mathbf{\Delta}^{WW*})_{ab} = 1, \tag{63}$$

$$\sum_{a,b}(\mathbf{\Delta}^{UW*})_{ab} = R. \tag{64}$$

To make a direct analysis of all possible covariances, we now construct a larger $2M \times 2M$ matrix by placing $\mathbf{\Delta}^{UU*}$ and $\mathbf{\Delta}^{WW*}$ on the diagonal blocks, and $\mathbf{\Delta}^{UW*}$ and its transpose on the off-diagonal blocks,

$$\mathbf{\Delta}^{\mathrm{Sup}} \equiv \begin{bmatrix} \mathbf{\Delta}^{UU*} & \mathbf{\Delta}^{UW*} \\ (\mathbf{\Delta}^{UW*})^T & \mathbf{\Delta}^{WW*} \end{bmatrix}. \tag{65}$$

This "supercovariance" matrix contains all the information about the covariance of the contributions of energy and virial with each other. This symmetric and positive semidefinite[9] matrix can be separated into additive contributions by spectral decomposition as

$$\mathbf{\Delta}^{\mathrm{Sup}} = \sum_{\alpha} \lambda_{\alpha} v_{\alpha} v_{\alpha}^T, \tag{66}$$

where v_{α} is the normalized eigenvector whose (non-negative) eigenvalue is λ_{α}—this follows from the diagonalization of the matrix. Thus we decompose the supercovariance into a sum of parts. This method of accounting for the

variance of many variables is the basis of the technique known as principal component analysis (PCA), which is a workhorse of multivariate data analysis.[10] The eigenvectors represent statistically independent "modes of fluctuation;" the corresponding eigenvalue is the part of the variance within the $2M$-dimensional space accounted for by the mode. PCA is most effective when the eigenvectors associated with the largest few eigenvectors account for most of the variance in the set of fluctuating quantities. For example, in the extreme case where one eigenvector accounts for over 99% of the variance, we could claim that all the different apparently random fluctuations of the different contributions to energy and virial were moving in a highly coordinated way, such that a single parameter (say, the value of any one of them) would be enough to give the values of all.

In our case we are not necessarily interested in the modes with the largest eigenvalues: a large eigenvalue could describe a fluctuation mode where the individual U_a's and W_a's change a lot but their respective sums do not; this would correspond to the contributions from one interval increasing while those in others decrease, in such a way that the total is roughly constant. What we really want are those modes that contribute a lot to the variance in energy and virial and to their covariance. This is easy to do by summing all elements in the appropriate block of the matrix $\lambda_{\alpha} v_{\alpha} v_{\alpha}^T$, where v_{α}, λ_{α} are the normalized eigenvector and eigenvalue in question.[11] In Table II we list the first ten eigenvalues in decreasing order, along with their contributions to the normalized variances of energy, virial, and their covariance—the normalized covariance being equal to R_{WU}. In addition, an "effective slope" for each mode is obtained from the αth eigenvector as

$$\gamma_{\alpha} = \sqrt{\frac{\langle(\Delta W)^2\rangle}{\langle(\Delta U)^2\rangle}} \frac{\Sigma_{a=M+1}^{2M}(v_{\alpha})_a}{\Sigma_{b=1}^{M}(v_{\alpha})_b} = \gamma \frac{\Sigma_{a=M+1}^{2M}(v_{\alpha})_a}{\Sigma_{b=1}^{M}(v_{\alpha})_b}, \tag{67}$$

where the numerator gives the sum of virial contributions for that mode, and the denominator the sum of energy contribu-

Paper IX

155

184508-11   Pressure-energy correlations in liquids. II

J. Chem. Phys. **129**, 184508 (2008)

tions. The factor in front, which is numerically equal to the overall slope γ, accounts for the standard deviation that we normalized the U_a's and W_a's to define the matrices Δ^{UU*}, Δ^{WW*}, and Δ^{UW*}.

In the above equation, it looks like γ_α is determined by the overall γ, whereas we could expect more the opposite, that the overall slope is somehow an average of the individual effective mode slopes. It looks like this because of the normalization choice we made in determining the decomposition. We can relate the γ_α to the γ in a more meaningful way by writing the sums in Eqs. (62) and (63) in terms of the spectral decomposition Eq. (66),

$$1 = \frac{\sum_{a,c} \Delta^{WW}_{a,c}}{\sum_{b,d} \Delta^{UU}_{b,d}} = \frac{\sum_\alpha \sum_{a,c>M} \lambda_\alpha (v_\alpha)_a (v_\alpha)_c}{\sum_\beta \sum_{b,d \leq M} \lambda_\beta (v_\beta)_b (v_\beta)_d} \quad (68)$$

$$= \frac{\sum_\alpha \lambda_\alpha (\sum_{a>M} (v_\alpha)_a)^2}{\sum_\beta \lambda_\beta (\sum_{b \leq M} (v_\beta)_b)^2} \quad (69)$$

$$= \frac{\sum_\alpha \lambda_\alpha (\gamma_\alpha/\gamma)^2 (\sum_{a \leq M} (v_\alpha)_a)^2}{\sum_\beta \lambda_\beta (\sum_{b \leq M} (v_\beta)_b)^2}, \quad (70)$$

where in the last step Eq. (67) was used. Multiplying both sides by γ^2 we get an expression for the latter as a weighted average of the squares of the γ_α,

$$\gamma^2 = \frac{\sum_\alpha X_\alpha \gamma_\alpha^2}{\sum_\beta X_\beta}, \quad (71)$$

where the weight of a given mode slope γ_α is (apart from normalization) $X_\alpha \equiv \lambda_\alpha (\sum_{a \leq M} (v_\alpha)_a)^2$, combining the eigenvalue and the square of the summed "energy part" of the corresponding eigenvector.

Now we can notice that the third, fourth, fifth, and sixth eigenvectors, to be referred to respectively as EV3, EV4, EV5, and EV6, account for most of the three (co-)variances (totalling 0.80 out of 1.00, 0.71 out of 1.00, and 0.74 out of 0.94 for variance of U, variance W, and correlation coefficient, respectively). These four eigenvectors are represented in Fig. 5. We observe that, as expected, most of the fluctuations are associated with pair separations well within the first peak of the RDF, which extends to nearly $r = 1.6\sigma$ [see Fig. 2(a)]. In fact, not much takes place beyond $r = 1.3\sigma$. Interestingly, of the four, EV5, accounting for less that 20% of the variances, is the only one that directly fits the idea that the fluctuations take place at short distances, while the other modes extend out to $r \sim 1.3\sigma$, beyond even the inflection point of the potential (around 1.24σ).

It is instructive to repeat the fluctuation mode analysis for a nonstrongly correlating liquid, the Dzugutov liquid at $T = 0.65$. We do not show the full results here but they can be summarized as follows. There are two modes that are concentrated at distances less than and around the first minimum of the potential. These have slopes of 5.73 and 5.01 and contribute a total of about 0.35–0.4 to the variances and correlation coefficient. Since the latter is 0.585 at this temperature, these modes account for most of it. There are four more modes that contribute more than 5% to the variances, but the slopes are quite different: −9.34, 7.20, 28.43, and −0.67. These four modes all include significant contributions at dis-
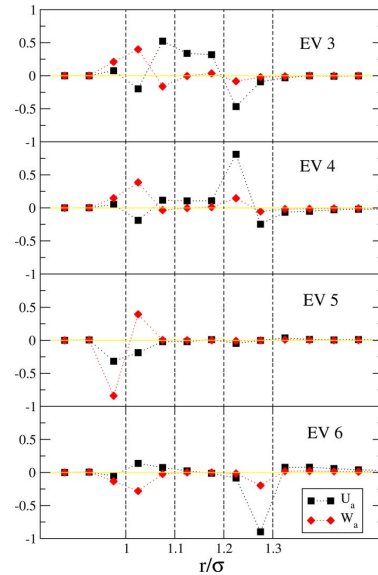

FIG. 5. (Color online) Representations of the eigenvectors 3, 4, 5, and 6 of the supercovariance matrix. Squares represent variation in U_a values for a mode; diamonds represent variation in W_a values.

tances corresponding to the peak in $v(r)$; clearly this extra peak in the potential and the associated peak in the pair-virial $w(r)$ give rise to components in the fluctuations which cannot be related in the manner of an effective inverse power law, even though fluctuations occurring around the minimum can. As a result the overall correlation is rather weak.

D. Synthesis: Why the effective power law works even at longer distances

We can apply ideas similar to those used in the crystal analysis to understand why the correlation holds even for modes active at separations larger than the minimum, why the slopes are similar to the effective power-law slopes, and why the effective power law works as well as it does. Recall the essential ingredients of the crystal analysis: the importance of summing over all pairs, the fixed-volume constraint, and the increase in the magnitude of coefficients of the Taylor expansion with order. These are equally valid here, but now we use them to constrain the allowed deviations in $g(r)$ from its equilibrium value, instead of displacements from a fixed equilibrium configuration. Define the resolved pair-density $\rho(r)$ by

$$\rho(r) \equiv (N/2) 4\pi r^2 \rho g(r). \quad (72)$$

The requirement that this integrates to the total number of pairs in the system, $\int_0^\infty \rho(r)dr = N(N-1)/2$, gives a global constraint on fluctuations of $\rho(r)$,

$$\int_0^\infty \Delta\rho(r)dr = 0. \quad (73)$$

A typical fluctuation will have peaks around the peaks of $g(r)$, but only those near the first peak will significantly af-

156   *B. Papers*

184508-12   Bailey *et al.*   J. Chem. Phys. **129**, 184508 (2008)
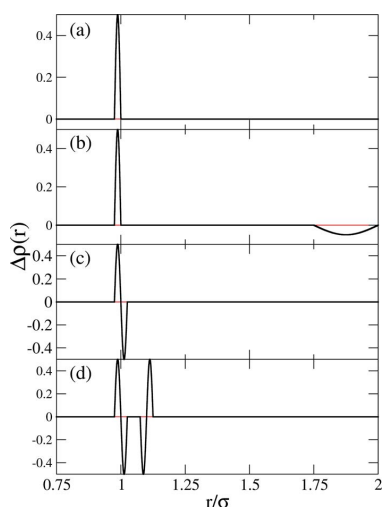

FIG. 6. (Color online) Intuitive picture of allowed and disallowed fluctuations in $\rho(r)$: (a) is not allowed because it violates the global constraint $\int \Delta\rho(r)=0$; (b) satisfies the global constraint but not locality; (c) could correspond, for instance, to a single bond becoming shorter, but this is inconsistent with fixed volume (vanishing first moment—such a change cannot happen in isolation); and (d) is allowed—it corresponds, for example, to a single particle being displaced toward one neighbor and away from another. Thus one bond shortens and one lengthens.

fect the potential energy and virial (Sec. II C). We can assume that, for a dense liquid not close to a phase transition, almost any configuration Γ may be mapped to a nearby reference configuration Γ_{ref} whose RDF is identical to the thermal average $g(r)$. "Nearby" implies that the particle displacements relating the Γ and Γ_{ref} are small compared to the interparticle spacing.[12] These displacements define the deviation $\Delta\rho(r)$ of $\rho(r)$ from its equilibrium value. Mapping to Γ_{ref} gets around the absence of a unique equilibrium configuration as in the crystal case.

Let us consider what restriction this places on $\Delta\rho(r)$; these are illustrated in Fig. 6. Because the displacements are small, $\Delta\rho(r)$ must be local: a peak in $\Delta\rho(r)$ at some r must be compensated by an opposite peak at a nearby location r_{ref} rather than one far away [thus example (b) in the figure is not allowed]—this corresponds to a bond having length r in the actual configuration and length r_{ref} in Γ_{ref} [Fig. 6(c)]. Finally fixed volume implies that a fluctuation cannot involve any substantial change in the mean nearest-neighbor bond length. This may be expressed mathematically as the near vanishing of the first moment of $\Delta\rho(r)$,

$$\int_{\text{first peak}} r\Delta\rho(r)dr \cong 0. \tag{74}$$

Thus, if a particle is displaced toward a neighbor on one side, it is displaced away from a neighbor on the opposite side, thus the resulting fluctuation is expected to look like Fig. 6(d), which is characterized by vanishing zeroth and first moments. Note that we restrict the integral to the first peak. The principle that fluctuations of $\Delta\rho(r)$ must be local allows us to write a version of Eq. (73) similarly restricted:

$$\int_{\text{first peak}} \Delta\rho(r)dr = 0. \tag{75}$$

Equations (74) and (75) cannot be literally true, since there must be contributions from fluctuations at whatever cut-off distance is used to define the boundary of the first peak. For instance, there could be a fluctuation such as Fig. 6(d) centered just to the right of this cutoff, so that only the first positive part was included in the integrals. We can ignore these contributions if we assume that the potential is truncated and shifted to zero at the boundary, as is standard in practice (although usually at larger distances). Then fluctuations right at the boundary do not contribute to the potential energy, The fact that the only contributions to the integral are at the boundary is a restatement of the locality of fluctuations.[13]

Now we make a Taylor series expansion of $v(r)$ around the maximum r_M of the first peak of $g(r)$, using $U = \int_0^\infty \rho(r)v(r)dr$,

$$\Delta U = \int_{\text{first peak}} \Delta\rho(r)\left(v(r_M) + k_1(r - r_M) \right.$$
$$\left. + \frac{1}{2}k_2(r - r_M)^2 + \cdots \right)$$
$$\equiv \sum_p \frac{k_p}{p!}M_p. \tag{76}$$

As for the crystal k_p is the pth derivative of $v(r)$ at the expansion point (r_M here), while M_p is the pth moment of $\Delta\rho(r)$,

$$M_p \equiv \int_{\text{first peak}} \Delta\rho(r)(r - r_M)^p dr. \tag{77}$$

A similar series exists for W, with coefficients given by Eq. (26),

$$3\Delta W = \sum_p \frac{C_p^W}{(r_M)^p}M_p. \tag{78}$$

The moments play a role exactly analogous to the sums S_p in the analysis of the crystal. The near vanishing of M_1 corresponds to that of S_1 in the crystal case, both following from the fixed-volume constraint; as there, it probably holds only to first order in particle displacements (except in one dimension where it is exact), but we have not tried to make a detailed estimate as we did with the crystal. Recalling that the extra contributions to the M_2 terms will be small anyway, in view of Eqs. (30) and (31), we simply set $M_1=0$, so the two series become (noting that $M_0=0$ also)

$$\Delta U = \sum_{p=2}^{\infty} C_p^U \frac{M_p}{r_M^p},$$
$$3\Delta W = \sum_{p=2}^{\infty} C_p^W \frac{M_p}{r_M^p}, \tag{79}$$

where the coefficients $C_p^{U,W}$ are those defined in Eqs. (25) and (26), but with r_M replacing a_c. The points made in
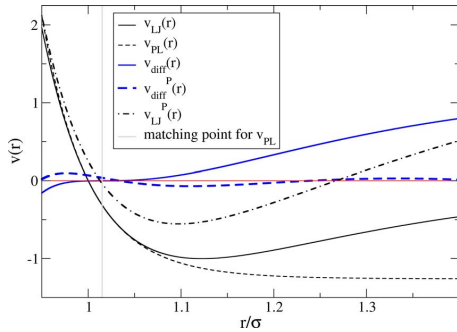
FIG. 7. (Color online) The true potential $v_{LJ}(r)$, the best effective power law $v_{PL}(r)$ (in the sense that the fluctuations in potential energy and virial reproduced most faithfully), and their difference $v_{diff}(r)$. Also shown are the projected versions $v_{LJ}^P(r)$ and $v_{diff}^P(r)$ where the constant and linear terms (determined over the interval 0.95σ to 1.4σ) have been subtracted off. It is the projected functions that should be compared in order to make a statement about the smallness of $v_{diff}(r)$ relative to $v_{LJ}(r)$ since only the projected functions contribute to fluctuations of total potential energy.

Sec. II B regarding the relation between the two series are equally valid here. At orders $p=2$ and higher, corresponding coefficients are related by the $n^{(p)}(r_M)$, which are always all above $a=12$. We expect from dimensional considerations that the variance of M_p is proportional to Nw_{FP}^{2p}, where $w_{FP} \sim 0.3r_M$ is the width of the first peak of $g(r)$. Thus moments of higher order should contribute less, and therefore M_2 should dominate, implying that the proportionality between ΔU and ΔW is essentially $n^{(2)}(r_M)$. This is in the range of 15–24 for r_M in the range of 1.05σ–1.15σ, giving slopes between 5 and 8, similar to those observed in the fluctuation modes. Unlike the low-T limit of the crystal, we cannot assume that the fluctuations are particularly localized around r_M, so it is not surprising that a range of slopes show up. Notice that we do not see arbitrarily high mode slopes corresponding to the divergence of $n^{(2)}(r)$ at the inflection point of the potential. Rather, for modes centered there, the assumption that we can neglect higher moments of the fluctuations no longer holds and there is an interpolation between $n^{(2)}(r)$ and $n^{(3)}(r)$ which is smaller (but still greater than $a=12$.

We can now understand also why the potential and virial fluctuations, as "reconstructed" using the effective power-law potential (Fig. 3), agree so well with the true fluctuations, even though the fluctuation mode analysis shows that there are significant contributions from distances around and beyond the minimum, well away from the matching point $r=1.015\sigma$. Figure 7 shows the LJ(12,6) potential, the $n=19.2$ power law (which gave the best fit in Sec. II A), and their difference, $v_{diff}(r) \equiv v_{LJ}(r) - v_{PL}(r)$. The latter is obviously very small and flat near the matching point but grows significantly in an approximately linear fashion at distances larger than $r \sim 1.05\sigma$. In view of Eqs. (16) and (72), a fluctuation of U_{diff} can be written as

$$\Delta U_{diff} = \int_0^\infty v_{diff}(r)\Delta\rho(r)dr, \tag{80}$$

which has the form of an inner product of functions. Vanishing fluctuations of U_{diff} follows if either (1) v_{diff} is identically

zero, or (2) it is nonzero, but orthogonal to the space of allowed $\Delta\rho(r)$. Given that v_{diff} is not particularly small except close to the matching point (see Fig. 7), the fact that U_{diff} fluctuations are relatively small even though they are associated with distances away from the matching point indicates that point (2) must hold approximately. Since allowed $\Delta\rho(r)$ functions are those with no constant or linear term [see Eqs. (73) and (74)], functions orthogonal to these are those with only a constant and linear term: $f(r) = Cf_0(r) + Df_1(r)$, where $f_0(r)$ is a constant function and $f_1(r)$ is a linear function with zero mean over the range of interest. It is clear in Fig. 7 that v_{diff} is not exactly of this form, but it can be well approximated by such a function. This approximation can be checked by standard methods of the linear algebra of function spaces. First we choose a range (r_1, r_2) over which functions are to be defined. For purposes this should include the range of significant contributions to W and U (Fig. 5). We choose $r_1 = 0.95\sigma$ and $r_2 = 1.4\sigma$. The normalized, mutually orthogonal basis vectors $f_0(r)$ and $f_1(r)$ are then given by

$$f_0(r) = 1/\sqrt{r_2 - r_1},$$
$$f_1(r) = \sqrt{\frac{12}{(r_2 - r_1)^3}}(r - (r_1 + r_2)/2). \tag{81}$$

The part of $v_{diff}(r)$ that is spanned by these basis functions is $v_0f_0 + v_1f_1$, where $v_i \equiv \int_{r_1}^{r_2} f_i(r)v_{diff}(r)dr$ is the inner product of $v_{diff}(r)$ and the corresponding basis vector. We define $v_{diff}^P(r)$ as the part of $v_{diff}(r)$ projected onto the space of allowed functions,

$$v_{diff}^P(r) = v_{diff}(r) - v_0f_0(r) - v_1f_1(r). \tag{82}$$

This function is also plotted in Fig. 7, where it can be seen that it is certainly small compared to $v_{diff}(r)$ itself. More importantly, it is also small compared to the projected part of $v_{LJ}(r)$, $v_{LJ}^P(r)$, defined analogously, because it is this that explains why the fluctuations of U_{diff} are small compared to those of U_{LJ} (or equivalently U_{PL}). This may be quantified by noting that the ratio of their norms is 0.09, which indicates how orthogonal $v_{diff}(r)$ is to the space of allowed $\Delta\rho(r)$. If we projected out only the constant term from $v_{diff}(r)$ and $v_{LJ}^P(r)$ (the *a priori* more obvious way to compare the size of two functions) the ratio of norms would be 0.50, and it would not be obvious why v_{PL} does as good a job as it does. Thus, again, constant-volume constraint, implying Eq. (74), is important.

The above discussion applies equally well to the virial. We can now write a more accurate approximate expression for $v_{LJ}(r)$, which we call the extended effective inverse power-law approximation,

$$v_{LJ}(r) \simeq Ar^{-n} + B + Cr, \tag{83}$$

where A, B, and C are constants. The associated pair virial $(w(r) \equiv rv'(r))$ is then

$$w_{LJ}(r) \simeq -nAr^{-n} + Cr, \tag{84}$$

which has the same form. In both cases the term Cr contributes to the mean value but not the fluctuations because $\int r\rho(r)dr$ is nonzero, while $\int r\Delta\rho(r)dr \cong 0$ for those $\Delta\rho(r)$

which are allowed at fixed volume. Note also that the contribution to the mean values from Cr will depend on volume because $g(r)$ and, hence, $\rho(r)$ do. Thus we can see that although there are significant contributions to fluctuations away from the matching point where the power law fits the true potential well, these are essentially equal for both the power law and the true potential because the difference between the two potentials in this region is almost orthogonal to the allowed fluctuations in $\rho(r)$. This also explains why the fluctuation only holds at fixed volume (which would not be explained by the assumption that short-distance encounters dominate the fluctuations).

The extended power-law approximation, determined empirically by the projection procedure, provides an alternative way to understand why the effective exponent $n^{(1)}$ evaluated at $r \sim \sigma$ agrees well with $n^{(2)}$ evaluated around the minimum r_m. For the extended effective power-law approximate [Eq. (83)], we get

$$n^{(1)}(r) = \frac{-n(n+1)Ar^{-(n+1)}}{-nAr^{-(n+1)}+C} - 1,$$

$$n^{(2)}(r) = \frac{n(n+1)(n+2)Ar^{-(n+2)}}{n(n+1)Ar^{-(n+2)}} - 2 = n. \tag{85}$$

Note that $n^{(2)}(r)$ is constant and equal to the exponent n of the power law, while $n^{(1)}(r)$ only approaches n when r is small enough that C in the denominator can be neglected [for the true potential $n^{(2)}(r)$ increases with r and eventually diverges (see Fig. 1)]. This emphasizes the greater usefulness of $n^{(2)}$ in identifying the effective power-law exponent. Recall also that our analysis earlier in this section indicates that $n^{(2)}(r)$, involving that the second and third derivatives of $v(r)$ near its minimum, is more fundamentally the cause of the W, U correlations, explaining something like 80% of the correlation in the liquid phase and over 99% in the crystal phase. The fact that Eq. (83) is a good approximation for the Lennard-Jones potential pushes the correlation to over 90% also in the liquid phase.

To summarize the last two subsections, we have shown here that the source of the fluctuations is indeed pair separations within the first peak, although only a relatively small fraction of the variances come from the short-r region where the approximation of the pair potential by a power law is truly valid. We have also seen how the Taylor-series analysis (which involves the crucial step of taking a sum over all pairs) may be extended to cover the whole first peak area, with all terms giving roughly the same effective slope, given essentially by the second-order effective exponent: $\gamma \sim n^{(2)}(r_m)/3$. The fact that this matches the first-order effective exponent at the shorter distance $r \sim \sigma$ is equivalent to the extended effective power-law approximation [Eq. (83)], which given a constant volume is what justifies the replacement of the potential by a power law (empirically demonstrated in Fig. 3).

III. SOME CONSEQUENCES OF STRONG PRESSURE-ENERGY CORRELATIONS

This section gives examples of consequences of strong pressure-energy correlations. The purpose is to show that these are important, whenever present. Clearly, more work needs to be done to identify and understand all consequences of strong pressure-energy correlations.

A. Measurable consequences of instantaneous W, U correlations

The observation of strong W, U correlations is of limited interest if it can only ever be observed in simulations. How can we make a comparison with experiment? In general, fluctuations of dynamical variables are related to thermodynamic response functions,[14–16] for example, those of U are related to the configurational part of the specific heat, C_V^{conf}. The latter is obtained by subtracting off the appropriate kinetic term, which for a monatomic system such as argon is $3Nk_B/2$. The virial fluctuations, however, although related to the bulk modulus, are not directly accessible because of another term that appears in the equation, the so-called hypervirial, which is not a thermodynamic quantity.[2] Fortunately this difficulty can be handled.

Everything in this section refers to the *NVT* ensemble. First we define the various response functions and configurational counterparts, the isothermal bulk modulus K_T, C_V, and the "pressure coefficient," β_V,

$$K_T \equiv -V\left(\frac{\partial \langle p \rangle}{\partial V}\right)_T, \quad K_T^{\text{conf}} \equiv K_T - \frac{Nk_BT}{V},$$

$$C_V \equiv \left(\frac{\partial E}{\partial T}\right)_V, \quad C_V^{\text{conf}} \equiv C_V - \frac{3}{2}Nk_B,$$

$$\beta_V \equiv \left(\frac{\partial \langle p \rangle}{\partial T}\right)_V, \quad \beta_V^{\text{conf}} \equiv \beta_V - \frac{Nk_B}{V}, \tag{86}$$

$$p^{\text{conf}} \equiv p - \frac{Nk_BT}{V} = \frac{W}{V}.$$

We also define $c_V \equiv C_V/V$. The following fluctuation formulas are standard (see, for example, Ref. 2)

$$\frac{\langle (\Delta W)^2 \rangle}{k_BTV} = \frac{Nk_BT}{V} + \frac{\langle W \rangle}{V} - K_T + \frac{\langle X \rangle}{V}, \tag{87}$$

$$\frac{\langle (\Delta U)^2 \rangle}{k_BT^2} = C_V - \frac{3}{2}Nk_B = C_V^{\text{conf}}, \tag{88}$$

$$\frac{\langle \Delta U \Delta W \rangle}{k_BT^2} = V\beta_V - Nk_B = V\beta_V^{\text{conf}}. \tag{89}$$

Here X is the so-called "hypervirial," which gives the change in virial upon an instantaneous volumetric scaling of positions. It is not a thermodynamic quantity and cannot be determined experimentally, although it is easy to compute in simulations. For a pair potential $v(r)$, X is a pair-sum,

Paper IX

159

184508-15   Pressure-energy correlations in liquids. II

J. Chem. Phys. **129**, 184508 (2008)

$$X = \sum_{\text{pairs}} x(r)/9, \tag{90}$$

where $x(r) = rw'(r)$. If we use the extended effective power-law approximation (including the linear term) discussed in the last section, then from Eq. (84) we get $x(r) \simeq n^2 A r^{-n} + Cr$. Summing over all pairs, and recalling that when the volume is fixed the Cr term gives a constant, we have a relation between the total virial and total hypervirial,

$$X = (n/3)W + \text{const.} \tag{91}$$

This constant survives, of course, when we take the thermal average $\langle X \rangle$, as do the corresponding constants in $\langle U \rangle, \langle W \rangle$. To get rid of these constants, one possibility would be to take derivatives with respect to T, but this can be problematic when analyzing experimental data. Instead we simply compare quantities at any temperature to those at some reference temperature T_{ref}; this effectively subtracts off the unknown constants. Taking first the square of the correlation coefficient, we have

$$R^2 = \frac{(\langle \Delta U \Delta W \rangle)^2}{\langle (\Delta U)^2 \rangle \langle (\Delta W)^2 \rangle}, \tag{92}$$

which implies

$$R^2 \frac{\langle (\Delta W)^2 \rangle}{k_B T V} = \frac{1}{k_B T V} \frac{(\langle \Delta U \Delta W \rangle)^2}{\langle (\Delta U)^2 \rangle}. \tag{93}$$

Inserting the fluctuation formulas [Eqs. (87) and (89)] gives

$$R^2 \left(\langle p \rangle - K_T + \frac{\langle X \rangle}{V} \right) = \frac{1}{k_B T V} \frac{(k_B T^2 V \beta_V^{\text{conf}})^2}{k_B T^2 C_V^{\text{conf}}} \tag{94}$$

$$= T \frac{(\beta_V^{\text{conf}})^2}{c_V^{\text{conf}}}. \tag{95}$$

Defining quantities $\tilde{A} \equiv \langle p \rangle - K_T + \langle X \rangle / V$ and $B \equiv T(\beta_V^{\text{conf}})^2/c_V^{\text{conf}}$ (the reason for the tilde on A will become clear), we have $R^2 \tilde{A} = B$. This is an exact relation. To deal with the hypervirial we first take differences with the quantities at T_{ref}, assuming that the variation in R is much smaller than the $\tilde{A}$ and B variations:

$$R^2(\tilde{A} - \tilde{A}_{\text{ref}}) = B - B_{\text{ref}}, \tag{96}$$

where $\tilde{A}_{\text{ref}} = \tilde{A}(T_{\text{ref}})$, etc. $\tilde{A} - \tilde{A}_{\text{ref}}$ written out explicitly is

$$\tilde{A} - \tilde{A}_{\text{ref}} = (\langle p \rangle - K_T) - (\langle p \rangle_{\text{ref}} - K_{T\text{ref}}) + \frac{\langle X \rangle - \langle X \rangle_{\text{ref}}}{V}. \tag{97}$$

Next we use the power-law approximation to replace $\langle X \rangle - \langle X_{\text{ref}} \rangle$ with $(n/3)(\langle W \rangle - \langle W_{\text{ref}} \rangle)$. This is the crucial point: whereas it is often not a good approximation that $\langle X \rangle = (n/3)\langle W \rangle$ due to the unknown additive constants discussed above, subtracting two state points considers *changes* in $\langle X \rangle$ and $\langle W \rangle$ with temperature. Recall from Sec. III B of Paper I that the changes in mean values $\Delta \langle W \rangle$ and $\Delta \langle X \rangle$ between (nearby) temperatures are related as the linear regression of the fluctuations of those quantities at one (nearby or intermediate) temperature. The linear relation between subtracted mean values holds if the instantaneous W and X are strongly
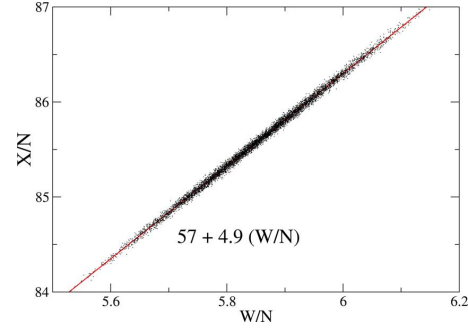

FIG. 8. (Color online) Scatter plot of instantaneous virial and hypervirial (in dimensionless units) for a SCLJ system at $\rho = 1.0$, $T = 0.80$ (*NVE*). The correlation coefficient between these quantities is 0.998. The hypervirial is the main contribution to the configurational part of the bulk modulus; it gives (after dividing by volume) the change in virial for a given relative change in volume. The sizable constant term in the linear fit shows that Eq. (91) is a poor approximation. The slope is 4.9, about 10% smaller than $\gamma \sim 5.4$ for this state point. The difference reflects the limit of the validity of the power-law description—in fact, a more detailed analysis shows that the relation between W and X is dominated by $n^{(3)}(r)$, which is smaller than $n^{(2)}(r)$ (Fig. 1).

correlated in the region of interest. The latter is confirmed by our simulations; indeed the correlation of instantaneous values of X and W is even stronger than for W and U, with approximately the same slope (Fig. 8). Thus Eq. (97) becomes

$$\tilde{A} - \tilde{A}_{\text{ref}} \simeq (\langle p \rangle - K_T) - (\langle p \rangle_{\text{ref}} - K_{T\text{ref}}) + \frac{n}{3} \frac{\langle W \rangle - \langle W \rangle_{\text{ref}}}{V} \tag{98}$$

$$= A - A_{\text{ref}}, \tag{99}$$

where $A \equiv \langle p \rangle - K_T + (n/3)(\langle W \rangle / V)$ (no tilde) contains quantities that are all directly accessible to experiment except for the effective power-law exponent n. This can be obtained by noting that if there were perfect correlation, one could interchange ΔW and $(n/3)\Delta U$; thus,

$$\frac{\beta_V^{\text{conf}}}{C_V^{\text{conf}}/V} = \frac{\beta_V^{\text{conf}}}{c_V^{\text{conf}}} = \frac{\langle \Delta U \Delta W \rangle}{\langle (\Delta U)^2 \rangle} = \frac{n}{3}, \tag{100}$$

which gives for A

$$A = \langle p \rangle - K_T + \frac{\langle p \rangle^{\text{conf}} \beta_V^{\text{conf}}}{c_V^{\text{conf}}}. \tag{101}$$

Thus to compare with experiment one should plot $B - B_{\text{ref}}$ against $A - A_{\text{ref}}$; the prediction, in the case of near perfect correlation, $R^2 \simeq 1$, is a straight line with slope close to unity. Figure 9 shows data for argon for T between 200 and 660 K. Argon was chosen because as a monatomic system there are no rotational or vibrational modes contributing to the heat capacity and it is therefore straightforward to subtract off the kinetic part. Also we restrict to a relatively high temperature to avoid quantum effects. The correlation coefficient R given as the square root of the slope of a linear fit is 0.96. Note that the assumed constancy of R is confirmed (going to lower temperatures there are increasingly large de-
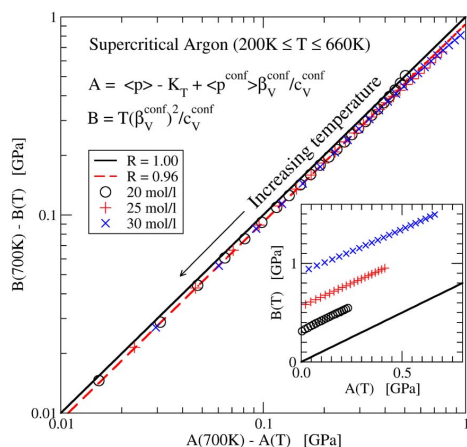
FIG. 9. (Color online) Data from the NIST database (Ref. 45) for supercritical argon at three different densities covering the temperature range of 200 K–660 K showing a strong virial-potential-energy correlation ($R=0.96$) (reproduced from Ref. 4). Here $K_T \equiv -V(\partial \langle p \rangle / \partial V)_T$, $p^{\mathrm{conf}} \equiv p - Nk_B T/V = W/V$ $\beta_V^{\mathrm{conf}} \equiv (\partial \langle p \rangle / \partial T)_V - Nk_B/V$, and $c_V^{\mathrm{conf}} \equiv C_V/V - (3/2)Nk_B/V$. The diagonal line corresponds to perfect correlation. The inset shows "unsubtracted" values for A and B; the fact that the data do not fall on the solid line indicates that a power-law description does not hold for the full thermodynamics.

viations). The importance of subtracting from a reference state point is highlighted by the inset, which shows that $A(T)=B(T)$ does not hold: There is a correlation in the fluctuations which is not present in the full equation of state.[4]

B. Time averaging: Pressure-energy correlations in highly viscous liquids

We have observed and discussed in Paper I that when volume is held constant, the correlations tend to become more perfect with increasing T, while along an isobar (considering still fixed-volume simulations, choosing the volume to give a prescribed average pressure) they become more perfect with decreasing T. This fact makes the presence of correlations highly relevant for the physics of highly viscous liquids approaching the glass transition. Basic questions such as the origins of nonexponential relaxations and non-Arrhenius temperature dependence are still vigorously debated in this field of research.[17–20] Instantaneous correlations of the kind discussed in this work would seem to be relevant only to the high frequency properties of a highly viscous liquid; their relevance to the long time scales on which structural relaxation occurs follows from the separation of time scales as explained below.

A question that is not actively debated in this research field (but see, e.g., Refs. 21–23) is whether a single parameter is enough to describe a highly viscous liquid. The consensus for more than 30 years is that with few exceptions these liquids require more than just one parameter, a conclusion scarcely surprising given their complexity. The meaning of "having a single parameter" can be understood as follows. Following a sudden change in volume, both pressure and energy relax to their equilibrium values over a time scale of

minutes or even hours, sufficiently close to the glass transition. If a single parameter governs the internal relaxation of the liquid, then both pressure and energy relax with the same time scale, and, in fact, the normalized relaxation functions are identical.[21,23] This behavior can be expressed in the frequency domain, as a certain quantity, the dynamic Prigogine–Defay ratio, being equal to unity.[23] A key feature of highly viscous liquids is the separation of time scales between the slow structural ("alpha") relaxation (up to order seconds) and the very short times (of order picoseconds) characterizing the vibrational motion of the molecules. This separation allows a more direct experimental consequence of W, U correlations than that described in the previous subsection: Suppose a highly viscous liquid has perfectly correlated W, U fluctuations. When W and U are time averaged over, say, one-tenth of the alpha relaxation time τ_α,[24] they still correlate 100%. Since the kinetic contribution to pressure is fast, its time average over $\tau_\alpha/10$ is just its thermal average, and thus the time-averaged pressure equals the time average of W/V plus a constant. Similarly, the time-averaged energy equals the time-averaged potential energy plus a constant. Thus the fluctuations of the time-averaged W and U equal the slowly fluctuating parts of pressure and energy, so these slow parts will also correlate 100% in their fluctuations. In this way we get from the nonobservable quantities W and U to the observable ones E and p (we similarly averaged to observe the correlation in the SQW system in Paper I). The upper part of Fig. 10 shows normalized fluctuations of energy and pressure for the commonly studied Kob–Andersen binary Lennard-Jones system[25] (referred to as KABLJ in Paper I), time averaged over one-tenth of τ_α. In the lower part we show the dynamic Prigogine–Defay ratio,[12] which in the NVT ensemble is defined as follows:

$$\Lambda_{TV}(\omega) \equiv -\frac{c_V''(\omega)(1/\kappa_T(\omega))''}{T[\beta_V''(\omega)]^2}. \tag{102}$$

Here $\kappa_T = 1/K_T$ is the isothermal compressibility and $''$ denotes the imaginary part of the complex frequency-dependent response function. A way to interpret this quantity can be found by considering the fluctuation-dissipation theorem expressions for the response functions. For example the frequency-dependent constant-volume specific heat $c_V(\omega)$ is given[26] by

$$c_V(\omega) = \frac{\langle (\Delta E)^2 \rangle}{k_B T^2} - \frac{i\omega}{k_B T^2} \int_0^\infty \langle \Delta E(0) \Delta E(t) \rangle \exp(-i\omega t) dt, \tag{103}$$

where E is the total energy. Taking the imaginary part we have

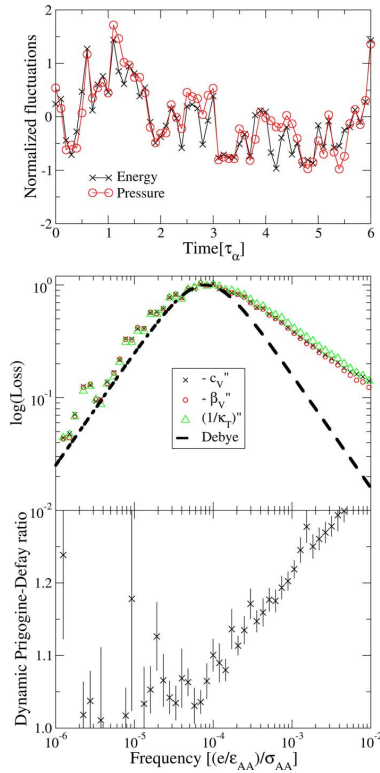$$c_V''(\omega) = -\frac{\omega}{k_B T^2}(\mathcal{L}\{\langle \Delta E(0) \Delta E(t) \rangle\})', \tag{104}$$

Paper IX

184508-17   Pressure-energy correlations in liquids. II

161

J. Chem. Phys. **129**, 184508 (2008)

FIG. 10. (Color online) Upper panel, time-averaged (over $\tau_\alpha/10$, where τ_α is the structural relaxation time) normalized fluctuations of E and p in NVT simulations of the Kob–Andersen (Ref. 20) binary Lennard-Jones (KABLJ) system, plotted against time in units of $\tau_\alpha \sim 10^3 \sigma_{AA} \sqrt{m/\epsilon_{AA}}$. The density was $1.2\sigma_{AA}^{-3}$, and the temperature was $0.474\epsilon_{AA}$. Middle panel, imaginary parts of the three response functions $-c_v(\omega)$, $-\beta_V(\omega)$; and $1/\kappa_T(\omega)$, scaled to the maximum value. Lower panel, dynamic Prigogine–Defay ratio for the same simulation. The approach toward unity at frequencies smaller than the loss-peak frequency $(\sim 1/\tau_\alpha)$ is exactly equivalent to the correlation between time-averaged quantities shown in the upper panel (reproduced from Ref. 19).

where we use $\mathcal{L}$ to represent Laplace transformation. Similarly,

$$(1/\kappa_T)''(\omega) = \frac{\omega V}{k_B T}(\mathcal{L}\{\langle \Delta p(0)\Delta p(t)\rangle\})' \qquad (105)$$

and

$$\beta_V''(\omega) = -\frac{\omega}{k_B T^2}(\mathcal{L}\{\langle \Delta E(0)\Delta p(t)\rangle\})'. \qquad (106)$$

Forming the Prigogine–Defay ratio then gives, after cancelling factors of k_B, T, V, and ω,

$$\Lambda_{TV}(\omega) = \frac{(\mathcal{L}\{\langle \Delta E(0)\Delta E(t)\rangle\})'(\mathcal{L}\{\langle \Delta p(0)\Delta p(t)\rangle\})'}{(\mathcal{L}\{\langle \Delta E(0)\Delta p(t)\rangle\})'^2}. \qquad (107)$$

We can see that the right-hand side has a similar structure to a correlation coefficient, if we take the inverse square root. So in a loose sense the dynamic Prigogine–Defay ratio can

be thought of as the inverse square of a correlation coefficient, referred to a particular time scale. This gives an intuitive reason for why it is in general greater or equal to unity, with equality only achieved in the case of perfect correlation.[23] The lower panel of Fig. 10 shows this quantity for a range of frequencies for the KABLJ system. It clearly approaches one at low frequencies and stays within 20% of one in the main relaxation region. In the sense above, this corresponds to $R > 0.9$, or strongly correlation.

The line of reasoning presented here opens for a new way of utilizing computer simulations to understand ultraviscous liquids. Present-day computers are barely able to simulate 1 μs of real-time dynamics, making it difficult to predict the behavior of liquids approaching the laboratory glass transition. We find that pressure-energy correlations are almost independent of viscosity, however, which makes it possible to make predictions regarding the relaxation properties even in the second or hour range of characteristic times. Thus if a glass-forming liquid at high temperatures (low viscosity) has very strong pressure-energy correlations $(R \sim 1)$, its eight thermoviscoelastic response functions at ultraviscous conditions may basically be expressed in terms of just one, irrespective of temperature (or viscosity).

C. Aging and energy landscapes

We now discuss the significance of the present results for the interesting results reported in 2002 by Mossa *et al.*[27] who studied the inherent states (ISs) visited by the Lewis-Wahnström model[28] of the glass-forming liquid *ortho*-terphenyl (OTP) during aging, i.e., the approach to equilibrium. An IS is a local minimum of the so-called potential-energy landscape (PEL) to which a given configuration is mapped by steepest-descent minimization.[29,30] The PEL formalism involves modeling the distributions and averages of properties of the IS in the hope of achieving a compact description of the thermodynamics of glass-forming liquids.[31,32] The thesis of Mossa *et al.*[27] and of the previous work[33] is that an equation of state can be derived using this formalism which is valid even for nonequilibrium situations. This involves including an extra parameter, namely, the average IS (potential) energy, $\langle e_{IS}\rangle$, so that the equation of state takes the form

$$p(T,V,\langle e_{IS}\rangle) = p_{IS}(\langle e_{IS}\rangle,V) + p_{vib}(T,V,\langle e_{IS}\rangle), \qquad (108)$$

where p_{IS} is the ensemble averaged IS pressure—for a given configuration it is the pressure of the corresponding IS—and $p_{vib} \equiv p - p_{IS}$. The usefulness of splitting in this way lies in the fact that p_{IS} does not explicitly depend on T.

At equilibrium $\langle e_{IS}\rangle$ is determined by V and T. The conclusion of Ref. 22 is that knowledge of $\langle e_{IS}\rangle$ in nonequilibrium situations is enough to predict the corresponding pressure (given also T and V). This was based on the extensive simulations of various aging schedules. Thus the authors concluded that the ISs visited by the system while out of equilibrium must be in some sense the "same" ones sampled during equilibrium conditions. Same is effectively defined by their results that averages of various IS properties (V, e_{IS}, p_{IS}, as well as a measure of the IS curvature) are all related to

each other the same way under nonequilibrium conditions as under equilibrium conditions. It was similarly found that the volume could be determined from $\langle e_{IS} \rangle$ following a pressure jump in a pressure-controlled simulation. On the other hand, subsequent work by the same group found that this was not at all possible for glassy water during compression/decompression cycles.[34]

Now, our results (Paper I) for the same OTP model show that it is a strongly correlating liquid. Thus we expect a general correlation between individual, not just average, values of p_{IS}, the inherent state pressure (which lacks a kinetic term and therefore equals the inherent state virial divided by volume) and e_{IS}, for a given volume. Therefore, for any given collection of ISs with the same volume—not just equilibrium ensembles—the mean values of U and W will fall on the same straight line as the instantaneous values. Note that this would not hold if the correlation was nonlinear. Correspondingly, for a given p_{IS}, there is a general correlation between individual values of e_{IS} and V. In fact, any two of these quantities determine the third with high accuracy, and this is true at the level of individual configurations, including ISs.

To see how this works for cases involving fixed volume, we write the total (instantaneous) pressure as a sum of an IS part, which involves the virial at the corresponding IS, plus a term involving the difference in the true virial from the IS virial, plus the kinetic term:

$$p = \frac{W_{IS}}{V} + \frac{W - W_{IS}}{V} + \frac{N k_B T}{V}. \tag{109}$$

The first term is linearly related to the IS energy for a strongly correlating liquid. Moreover, the difference term is similarly expressed in terms of the corresponding energy difference, $W - W_{IS} = \gamma(U - e_{IS})$. Taking averages over the (possibly nonequilibrium, although we assume equilibrium within a given potential-energy basin) ensemble, we expect that $\langle U - e_{IS} \rangle$ depends only on T and V (a slight e_{IS} dependence can appear in γ since this is slightly state-point dependent). Thus it follows that p can be reconstructed from a knowledge of (average) e_{IS}, V, and T, without any assumptions about the nature of the ISs visited. In particular, no conclusion can be drawn regarding the latter. The failure of the pressure reconstruction in the case of water[23] is not surprising since water models are generally not strongly correlating (which as we saw in Paper I is linked to the existence of the density maximum).

D. Biomembranes

A completely different area of relevance for the type of correlations reported here relates to the recent work of Heimburg and Jackson,[35] who proposed a controversial new theory of nerve signal propagation. Based on experiment and theory they suggest that a nerve signal is not primarily electrical but a soliton sound wave.[36] Among other things this theory explains how anaesthesia works (and why one can dope people with the inert gas xenon): anaesthesia works simply by a freezing-point depression that changes the membrane phase transition temperature and affects its ability to carry the soliton sound wave. A crucial ingredient of the

TABLE III. Data from NpT simulations of fully hydrated phospholipid membranes of 1,2-dimyristoyl-sn-glycero-3-phosphocholine (DMPC), 1,2-dimyristoyl-sn-glycero-3-phospho-L-serine with sodium as counter ion (DMPS-Na), hydrated DMPS (DMPSH), and DPPC (Refs. 40 and 44). The columns list temperature, correlation coefficient between volume and energy, average lateral area per lipid, simulation time in equilibrium, and total simulation time.

	T (K)	R_{EV}	A_{lip} (Å^2)	t (ns)	t_{tot} (ns)
DMPC	310	0.885	53.1	60	114
DMPC	330	0.806	59.0	50	87
DMPS-Na	340	0.835	45.0	22	80
DPPC	325	0.866	67.3	13	180

theory is the postulate of proportionality between volume and enthalpy of microstates, i.e., that their thermal equilibrium fluctuations should correlate perfectly. This should apply even through the first-order membrane *melting* transition. The theory was justified in part from previous experiments by Heimburg showing proportionality between compressibility and specific heat through the phase transition.[37] The postulated correlation—including the claim that is survives a first-order phase transition—fits precisely the pattern found in our liquid simulations.

By re-examining existing simulation data[38,39] as well as carrying out extensive new simulations,[40] we have investigated whether the correlations are also found in several model membrane systems, five of which are listed in Table III. The simulations involved a layer of phospholipid membrane surrounded by water, in the L_α phase (that is, at temperatures above the transition to the gel-state), at constant p and T. When p, rather than V, is constant, the relevant quantities that may correlate are energy and volume. As with viscous liquids (Sec. III B) and the square well system (Paper I), time averaging is necessary for a correlation to emerge, where now

$$\Delta \overline{E(t)} \simeq \gamma^{vol} \Delta \overline{V(t)}. \tag{110}$$

When an averaging time of 1 ns is chosen, a significant correlation emerges, with correlations between 0.8 and 0.9 (Table III; note these R_{EV} values fall slightly short of our criterion of 0.9 for "strong correlations"). The time series of time-averaged normalized E and V for one case are shown in Fig. 11. The necessity of time averaging stems from the presence of water, which we know does not exhibit strong correlations. Since the membrane dynamics are much slower than those of the water, they can be isolated by time averaging.

IV. CONCLUSIONS AND OUTLOOK

In Paper I and this work we have demonstrated several cases of strongly correlating liquids and some cases where the correlation is weak or absent (at least under normal conditions of pressure and temperature). An important next step is to continue to document the existence or nonexistence of correlations, particularly in different kinds of model systems, such as nonpair potential systems and systems with interactions computed using quantum mechanics (e.g., by density functional theory). It is noteworthy in this respect that after
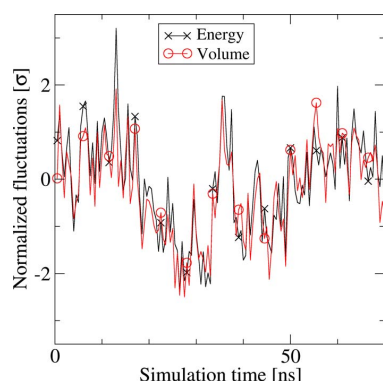
FIG. 11. (Color online) Normalized fluctuations of energy ($\times$) and volume ($\bigcirc$) for a 1,2-dipalmitoyl-sn-glycero-3-phosphocholine (DPPC) membrane at 325 K (Ref. 44). Each data point represents a 0.5 ns average. Energy and volume are correlated with a correlation coefficient of $R=0.87$ (NpT).

suitable time averaging the correlations may appear in systems where they are otherwise unexpected. One example was the square-well (SQW) case, where the correlation was between the time-averaged virial and potential energy. In the case of viscous liquids time averaging allowed a correlation to appear between the more accessible energy and pressure, while for the biomembranes it made it possible to remove the nonstrongly correlating contributions from the water. In all cases time averaging is relevant because of a separation of time scales: the SQW system because the time scale over which the average number of neighbors changes is long compared to the time between collisions; viscous liquids because the vibrational dynamics (which includes the kinetic contributions) is fast compared to the slow configurational dynamics; biomembranes because the membrane dynamics is slow compared to those of the water. Note that in this case it was necessary to consider an NpT ensemble and study the correlations between energy and volume because only a part of the system is strongly correlating, and this part cannot be constrained to a particular volume. It is worth noting that even with fixed volume, the correlation coefficient depends on whether the ensemble is NVT or NVE, although the strongly correlating limit of $R \to 1$ is independent of ensemble.

A point which has been mentioned, but which is worth emphasizing again, is that the replacement of the potential by an appropriate inverse power law can only reproduce the fluctuations, and not the mean values of (potential) energy and virial, nor their first derivatives with respect to T and V. These determine the equation of state, in particular features such as the van der Waals loop that are absent in a pure power-law system, even if changes in the exponent are allowed. The generalization to the extended effective inverse power-law approximation, however, allows in principle such features to be described.

Finally, consider again viscous liquids, which are typically deeply supercooled. The most common way of classifying them involves the fragility parameter introduced by Angell,[41] related to the departure from Arrhenius behavior of the temperature dependence of the viscosity. Strong liquids, having the most Arrhenius behavior, have traditionally been considered the easiest ones to understand because Arrhenius temperature dependence is well-understood. However it may well be that strongly correlating liquids are in fact the simplest.[42] The connection with the long-discussed question of whether a single-order parameter describes highly viscous liquids has been discussed briefly in Sec. III B and is discussed further in Ref. 21. As an example, a direct application of the strongly correlating property concerns diffusion in supercooled liquids. Recent work of Coslovich and Roland[43] has shown that the diffusion constant in viscous binary Lennard-Jones mixtures may be fitted by an expression $D = F(\rho^\gamma/T)$, where γ reflects the effective inverse power of the repulsive core. "Density scaling" has also been observed experimentally.[46–49] It is natural, given the results of Coslovich and Roland, to hypothesize that the scaling exponent is connected to pressure-energy correlations, and in Ref. 4 it was conjectured that density scaling applies if and only if the liquid is strongly correlating. We have recently studied the relationship between the two quantitatively[50] and have found that (1) density scaling does indeed hold to the extent that the liquids are strongly correlating, and (2) the scaling exponent is given accurately by the slope γ of the correlations (hence our use of the same symbol). This finding supports the conjecture that strongly correlating liquids may be simpler than liquids in general.

In summary, the property of strong correlation between the equilibrium fluctuations of virial and potential energy allows a new way to classify liquids. It is too soon to tell how fruitful this will turn out in the long term, but judging from the applications briefly presented here, it seems at least plausible that it will be quite useful.

[1] N. P. Bailey, U. R. Pedersen, N. Gnan, T. B. Schrøder, and J. C. Dyre, J. Chem. Phys. **129**, 184507 (2008).
[2] M. P. Allen and D. J. Tildesley, *Computer Simulation of Liquids* (Oxford University Press, Oxford, 1987).
[3] D. Ben-Amotz and G. Stell, J. Chem. Phys. **119**, 10777 (2003).
[4] U. R. Pedersen, N. P. Bailey, T. B. Schrøder, and J. C. Dyre, Phys. Rev. Lett. **100**, 015701 (2008).
[5] K. Binder and W. Kob, *Glassy Materials and Disordered Solids: An Introduction to Their Statistical Mechanics* (World Scientific, Singapore, 2005).
[6] The analysis of fluctuations in the liquid in Sec. II C can be applied to the case of a disordered solid, explaining the high correlation also there, but it is not accurate enough to get as good an estimate for the low-temperature limit as we do our analysis of the crystal.
[7] "Displacement" refers to the displacement of a given particle from its equilibrium position, while the "relative displacement" is the difference in this quantity for the given pair of particles.
[8] N. W. Ashcroft and N. D. Mermin, *Solid State Physics* (Saunders College, Rochester, 1976).
[9] This follows since if v is an arbitrary vector and $A_{ab}=\langle \Delta x_a \Delta x_b \rangle$ is the covariance matrix of a set $\{x_a\}$ of random variables, then $v^T A v$ is the variance of the random variable $w = \Sigma_a v_a x_a$, and thus non-negative.
[10] K. H. Esbensen, D. Guyot, F. Westad, and L. P. Houmøller, *Multivariate*

Data Analysis—In practice, 5th ed. (Camo, Oslo, 2002).

[11] The sums over the diagonal blocks are non-negative since λ_α is, and the sum over the first (last) components of $v_\alpha v_\alpha^T$ is the dot product of the first (last) half of v_α with itself, which is also non-negative.

[12] The configuration Γ_{ref} is analogous to the inherent state configuration often used to describe viscous liquid dynamics (Refs. 29 and 30), which is obtained by minimizing the potential energy starting from configuration Γ.

[13] We have checked the statements that the zeroth and first moments of $\rho(r)$ over the first peak are constant apart from contributions at the cutoff by computing orthogonalized versions of them (using Legendre polynomials defined on the interval from 0.8 σ to 1.4 σ) and showing that they are strongly correlated (correlation coefficient 0.9) with a slope corresponding to the cutoff itself.

[14] L. D. Landau and E. M. Lifshitz, *Statistical Physics, Part I* (Pergamon Press, London, 1980).

[15] J. P. Hansen and I. R. McDonald, *Theory of Simple Liquids*, 2nd ed. (Academic, New York, 1986).

[16] L. E. Reichl, *A Modern Course in Statistical Physics*, 2nd ed. (Wiley, New York, 1998).

[17] W. Kauzmann, Chem. Rev. (Washington, D.C.) **43**, 219 (1948).

[18] S. Brawer, *Relaxation in Viscous Liquids and Glasses* (American Ceramic Society, Columbus, 1985).

[19] C. A. Angell, K. L. Ngai, G. B. McKenna, P. F. McMillan, and S. W. Martin, J. Appl. Phys. **88**, 3113 (2000).

[20] J. C. Dyre, Rev. Mod. Phys. **78**, 953 (2006).

[21] N. P. Bailey, T. Christensen, B. Jakobsen, K. Niss, N. B. Olsen, U. R. Pedersen, T. B. Schrøder, and J. C. Dyre, J. Phys.: Condens. Matter **20**, 244113 (2008).

[22] J. W. P. Schmelzer and I. Gutzow, J. Chem. Phys. **125**, 184511 (2006).

[23] N. L. Ellegaard, T. Christensen, P. V. Christiansen, N. B. Olsen, U. R. Pedersen, T. B. Schrøder, and J. C. Dyre, J. Chem. Phys. **126**, 074502 (2007).

[24] U. R. Pedersen, T. Christensen, T. B. Schrøder, and J. C. Dyre, Phys. Rev. E **77**, 011201 (2008).

[25] W. Kob and H. C. Andersen, Phys. Rev. Lett. **73**, 1376 (1994).

[26] J. K. Nielsen and J. C. Dyre, Phys. Rev. B **54**, 15754 (1996).

[27] S. Mossa, E. La Nave, F. Sciortino, and P. Tartaglia, Eur. Phys. J. B **30**, 351 (2002).

[28] L. J. Lewis and G. Wahnström, Phys. Rev. E **50**, 3865 (1994).

[29] M. Goldstein, J. Chem. Phys. **51**, 3728 (1969).

[30] F. H. Stillinger, Science **267**, 1935 (1995).

[31] F. Sciortino, J. Stat. Mech.: Theory Exp. **2005**, 35.

[32] A. Heuer, J. Phys.: Condens. Matter **20**, 373101 (2008).

[33] E. La Nave, S. Mossa, and F. Sciortino, Phys. Rev. Lett. **88**, 225701 (2002).

[34] N. Giovambattista, H. E. Stanley, and F. Sciortino, Phys. Rev. Lett. **91**, 115504 (2003).

[35] T. Heimburg and A. D. Jackson, Proc. Natl. Acad. Sci. U.S.A. **102**, 9790 (2005).

[36] T. Heimburg and A. D. Jackson, Biophys. J. **92**, 3159 (2007).

[37] H. Ebel, P. Grabitz, and T. Heimburg, J. Phys. Chem. B **105**, 7353 (2001).

[38] U. R. Pedersen, C. Leidy, P. Westh, and G. H. Peters, Biochim. Biophys. Acta **1758**, 573 (2006).

[39] U. R. Pedersen, G. H. Peters, and P. Westh, Biophys. Chem. **125**, 104 (2007).

[40] U. R. Pedersen, G. H. Peters, T. B. Schrøder, and J. C. Dyre, AIP Conf. Proc. **982**, 407 (2008).

[41] C. A. Angell, in *Relaxations in Complex Systems*, edited by K. L. Ngai and G. B. Wright (U.S. GPO, Washington, D.C., 1985), p. 3.

[42] A. Le Grand, C. Dreyfus, C. Bousquet, and R. M. Pick, Phys. Rev. E **75**, 061203 (2007).

[43] D. Coslovich and C. M. Roland, J. Phys. Chem. B **112**, 1329 (2008).

[44] U. R. Pedersen, G. H. Peters, T. B. Schrøder, and J. C. Dyre (unpublished).

[45] E. W. Lemmon, M. O. McLinden, and D. G. Friend, in *NIST Chemistry WebBook, NIST Standard Reference Database Number 69*, edited by P. J. Linstrom and W. G. Mallard (NIST, Gaithersburg, 2005), URL http://webbook.nist.gov.

[46] G. Tarjus, D. Kivelson, S. Mossa, and C. Alba-Simionesco, J. Chem. Phys. **120**, 6135 (2004).

[47] C. Dreyfus, A. L. Grand, J. Gapinski, W. Steffen, and A. Patkowski, Eur. Phys. J. B **42**, 309 (2004).

[48] R. Casalini and C. M. Roland, Phys. Rev. E **69**, 062501 (2004).

[49] C. Roland, S. Hensel-Bielowka, M. Paluch, and R. Casalini, Rep. Prog. Phys. **68**, 1405 (2005).

[50] T. B. Schrøder, U. R. Pedersen, and J. C. Dyre, e-print arXiv:0803.2199.

Computer simulations of phospholipid-membrane thermodynamic fluctuations

Ulf R. Pedersen* (urp@ruc.dk), Günther H. Peters[†],
Thomas B. Schrøder* and Jeppe C. Dyre*

*DNRF Centre "Glass and Time," IMFUFA, Department of Sciences,
Roskilde University, Postbox 260, DK-4000 Roskilde, Denmark.
[†]Center for Membrane Biophysics (MEMPHYS), Department of Chemistry,
Technical University of Denmark, DK-2800 Kgs. Lyngby, Denmark

November 20, 2008

Abstract

This paper reports all-atom computer simulations of five phospholipid membranes, DMPC, DPPC, DMPG, DMPS, and DMPSH, with a focus on the thermal equilibrium fluctuations of volume, energy, area, thickness, and order parameter. For the slow fluctuations at constant temperature and pressure (defined by averaging over 0.5 nanosecond) volume and energy exhibit strong correlation. These quantities on the other hand do not correlate significantly with area, thickness, or order parameter. The correlations are mainly reported for the fluid phase, but we also give results for the ordered (gel) phase of two membranes, showing a similar picture. The strong correlations reported here confirm an assumption of a recent theory for nerve signal propagation proposed by Heimburg and Jackson (2005). The cause of the observed strong correlations is identified by splitting volume and energy into contributions from tails, heads, and water, showing that the slow volume-energy fluctuations derive from the tail region's van der Waals interactions and are thus analogous the similar strong correlations recently observed in computer simulations of the Lennard-Jones and other simple van der Waals type liquids.

In 2005 Heimburg and Jackson showed that biomembranes may carry solitonic sound waves with a maximum amplitude and a minimum velocity of the solitons that is close to the propagation velocity in myelinated nerves [1]. Their paper concluded: "It would be surprising if nature did not exploit these features." Subsequent works by the same authors argue directly that nerve signals are not primarily electrical, but solitonic sound waves carried by the nerve cell membrane [2]. The conventional wisdom is that nerve signals propagate via electrical current as formulated in the Hodgkin-Huxley theory [3]. The

Heimburg-Jackson theory, which is obviously controversial, explains anaesthesia as a straightforward effect of melting-point depression of the order-disorder transition that biomembranes (for otherwise biologically unknown reasons) have at temperatures close to physiological temperatures [4].

The Heimburg-Jackson nerve-signal theory motivated this study. An element of the theory is the assumption that volume and enthalpy correlate strongly in their thermal equilibrium fluctuations, at least as regards the slow parts of these fluctuations. This assumption was justified by observations that membrane specific heat and compressibility are proportional in their temperature dependence, even across the phase transition [5, 6]. Such a postulated strong correlation between thermodynamic variables of microstates is quite unusual in the statistical mechanical literature. Below we present first results from extensive computer simulations of different phospholipid membranes performed in order to investigate whether strong volume-energy correlations are observed and – if they are – what causes them.

Recently we studied equilibrium thermodynamic fluctuations of much simpler systems, namely various model liquids like the standard Lennard-Jones (LJ) liquid and similar systems [7, 8, 9, 10]. In many such simple liquids one finds a strong correlation between equilibrium fluctuations of the virial W and the potential energy U, when fluctuations are studied at constant particle number N, constant volume V, and constant temperature T (the so-called NVT ensemble [11]). Recall [12] that the virial $W = W(t)$ gives the non-ideal contribution to the instantaneous pressure $p = p(t)$ via the defining equation: $p(t)V = (2/3)Nk_BT(t) + W(t)$ where $T(t)$ is the instantaneous temperature defined via the instantaneous kinetic energy. The virial determines the part of the pressure that comes from interactions, i.e., in addition to the ideal gas contribution; the virial is a function of the particle positions [12]. For the LJ liquid, as well as for a united-atom toluene model, a dumbbell model, the Kob-Andersen binary LJ liquid [13], and other liquids, W and U correlate better than 90% in their equilibrium fluctuations. This reflects an effective inverse power-law potential dominating fluctuations, as detailed in Refs. [9, 10]. Liquids with poor $W - U$ correlation include water and methanol [8]. In these cases the correlations are ruined by the hydrogen bonds that are conventionally modelled via Coulomb forces – the existence of competing interactions prevents strong $W - U$ correlation in hydrogen-bonded liquids.

For liquids with time-scale separation like highly viscous liquids, strong $W - U$ correlations are particularly significant. Thus it has been shown [7, 14] that viscous liquids with strong $W - U$ correlations are close to being "single-order-parameter liquids" in the classical Prigogine-Defay sense [15]. This implies that complex frequency-dependent thermoviscoelastic response functions like the isobaric/isochoric dynamic specific heat, dynamic thermal expansion coefficient, dynamic compressibility, etc, are all given by a single function [14]. In particular, these cannot "decouple" [16] from one another – they must all exhibit relaxations in the same frequency range. It has also been shown that strongly correlating viscous liquids obey density scaling, i.e., that if the relaxation time τ is measured at different temperatures and density ρ, τ is a unique function

of ρ^x/T [17]. Moreover, the exponent x may be determined from studies of $W - U$ correlations at a single state point [18]. Finally, it was recently found that strongly correlating viscous liquids have much simpler ageing properties than do viscous liquids in general (unpublished).

Fluctuations are ensemble dependent, of course, and one may ask what happens if fluctuations are instead studied in the ensemble of constant temperature and pressure (NpT ensemble). In this case virial fluctuations are not interesting, but in the NpT ensemble there are equally strong correlations for simple liquids between the fluctuations of volume and potential energy [7]. This is the ensemble used below for studying biomembrane thermodynamic fluctuations.

Based on the findings for simple model liquids and the Heimburg-Jackson theory we found it would be interesting to simulate phospholipid membranes in order to investigate whether the Heimburg-Jackson assumption of strong $V - U$ correlations is confirmed even for such complex systems. A phospholipid has both van der Waals interactions between its acyl chains and hydrogen bonds in the head region. Similarities to simple liquids are not at all obvious, and the microscopic origin of the enthalpy/volume correlations tentatively derived from experiments [5, 6] is not trivial.

Because of the large amount of water in the system one does not expect strong instantaneous correlations of phospholipid membrane thermodynamic fluctuations. The Heimburg-Jackson theory, however, in reality only relates to strong correlations of the biomembrane's slow degrees of freedom (on millisecond time scales), and so do the experiments they quote indicating strong correlations [5, 6]. This is analogous to the situation for highly viscous liquids where time-scale separation between the fast, vibrational degrees of freedom and the much slower configurational is also essential.

Phospholipids are the major constituent of biological membranes. Close to physiological temperature membranes undergoes a transition from a disordered phase (L_α phase) to an ordered phase (L_β) [4, 19]. Below we evaluate the strength of $V - U$ correlations for both the disordered and ordered phases with main focus on the high-temperature disordered phase. The correlation strength was calculated on a range of time scales. We show that $V - U$ correlate strongly, but only on long time scales. We furthermore investigated how well membrane area as well as membrane order-parameter fluctuations correlate with V and U fluctuations; such correlations are generally poor. Finally, the cause of the correlations is identified by splitting volume as well as energy into contributions from tails, heads, and water: The slow, strongly correlating $V - U$ fluctuations are shown to derive from the tails that are dominated by van der Waals interactions, thus establishing a conceptual link to the strong correlations of the slow pressure-energy fluctuations – the virial/potential energy correlations – of simple van der Waals liquids [8].

Simulations details

Details of the seven membrane simulations performed are listed in Tabel 1. The following abbreviations are used: DMPC-f: a fully hydrated di-myristoyl-phosphatidyl-choline membrane in the fluid phase. DMPC-g: a fully hydrated di-myristoyl-phosphatidyl-cholin membrane in the ordered phase. DPPC-f: a fully hydrated di-palmitoyl-phosphatidyl-choline membrane in the fluid phase. DPPC-g: a fully hydrated di-palmitoyl-phosphatidyl-choline membrane the ordered phase. DPPG: a fully hydrated di-palmitoyl-phosphatidyl-glycerol membrane in the fluid phase with calcium counter ions. DPPS: a fully hydrated di-myristoyl-phosphatidyl-serine membrane in the fluid phase with calcium counter ions. DMPSH: a fully hydrated and protonated di-myristoyl-phosphatidyl-serine membrane in the fluid phase.

In all simulations a time step of 1.0 fs was used. Temperature and pressure were controlled by the Langevin thermostat (damping coefficient: 5 ps^{-1}) and Nose-Hoover Langevin barostat (anisotropic regulation; piston oscillation time: 100 fs; damping time: 50 fs) [11]. Electrostatic interactions were evaluated using the Particle-Mesh-Ewald method [20, 21] with a grid spacing ~ 1Å and were updated every 4 fs. Van der Waals interactions were cut-off at 12 Å in combination with a switching function starting at 10 Å. Periodic boundary conditions were applied in all three dimensions. Simulations were carried out using NAMD [22].

The simulations of DMPC-f, DPPC-f, DPPG, DPPS, DMPS and DMPSH started from configurations taken from Refs. [23, 24, 25]. Initial configurations of DMPC-g and DPPC-g were built from a membrane simulated by Venable and co-workers [26]. The acyl chains remain in an ordered structure (as shown on Fig. 1), and they are referred to as "ordered".

Thermal equilibrium was ensured by monitoring the membrane area; only trajectories with no drift (compared to the thermal fluctuations) were used in the data analysis. The length of the equilibrium trajectories is listed in Table 1 in the column under t_{prod}. The importance of equilibrium should be emphasized, since an apparent strong correlation would appear if volume and energy relax from some (arbitrary) out-of-equilibrium state.

Results

The following collective quantities were evaluated every 0.5 ps: Potential energy U, simulation box volume $V = XYZ$ (where X, Y and Z are the box dimensions), projected membrane area $A = XY$, box thickness Z, and average chain order parameter $\langle S_{CD} \rangle_{ch}$. The latter parameter, which characterizes the overall acyl-chain order [27], is defined as $\langle S_{CD} \rangle_{ch} = |\langle \frac{3}{2}\cos^2(\theta_{CD}) - \frac{1}{2}\rangle_{ch}|$ where θ_{CD} is the angle between the membrane normal and ($\vec{z}$) the C-H bond of a given methylene group, and $\langle \ldots \rangle_{ch}$ denotes an average over all methylene groups in all chains.

First, we consider the fluid DMPC-f membrane. The instantaneous fluctu-

Table 1: Overview of simulations details and results

(A) System abv. (phase)	t_{sim} [ns]	t_{prod} [ns]	N_{lip}	T [K]	N_{wat}/N_{lip}
DMPC-f (fluid)	151	121	128	330	33
DMPC-g (ordered)	65	36	64	286	33
DPPC-f (fluid)	180	124	72	325	29
DPPC-g (ordered)	78	48	64	304	33
DMPG (fluid)	149	49	128	330	33
DMPS (fluid)	139	49	128	340	36
DMPSH (fluid)	136	35	128	340	37

(B) System abv. (phase)	$R_{\bar{U}\bar{V}}$	γ	$R_{\bar{U}\bar{U}_t}$	$R_{\bar{U}\bar{A}}$	$R_{\bar{V}\bar{A}}$	$R_{\bar{A}\bar{S}_{CD}}$	$R_{\bar{U}\bar{S}_{CD}}$	$R_{\bar{V}\bar{S}_{CD}}$
DMPC-f (fluid)	0.77	6.7	0.82	0.50	0.57	-0.75	-0.49	-0.54
DMPC-g (ordered)	0.47	4.3	0.31	0.02	0.05	-0.64	0.12	0.14
DPPC-f (fluid)	0.87	7.1	0.89	-0.29	-0.36	0.00	-0.61	-0.71
DPPC-g (ordered)	0.75	4.6	0.71	-0.16	0.12	-0.67	0.09	-0.07
DMPG (fluid)	0.82	5.9	0.80	0.41	0.40	-0.76	0.01	0.08
DMPS (fluid)	0.59	5.3	0.64	0.30	0.28	-0.71	0.04	0.20
DMPSH (fluid)	0.78	9.2	0.84	0.43	0.51	-0.50	0.05	0.14

(A) t_{sim}: Total simulation time in nanoseconds. t_{prod}: Length of production run in nanoseconds (only membranes in quasi-equilibrium, i.e., with no detectable drift in the area per molecule, were included in the data analysis); N_{lip}: Number of lipid molecules; T: Temperature in Kelvin; N_{wat}/N_{lip}: Number of water molecules per lipid molecule. (B) $R_{\bar{U}\bar{V}}$: Energy-Volume correlation coefficient (see Eq. 1); γ: Energy-volume scaling factor in Å^3 mol/kcal (see Eq. 13); $R_{\bar{U}\bar{U}_t}$: Energy-"Energy of acyl groups" correlation coefficient. $R_{\bar{U}\bar{A}}$: Energy-Area correlation coefficient; $R_{\bar{V}\bar{A}}$: Volume-Area correlation coefficient. $R_{\bar{A}\bar{S}_{CD}}$: Area-"chain order-parameter" correlation coefficient; $R_{\bar{U}\bar{S}_{CD}}$: Energy-"chain order-parameter" correlation coefficient; $R_{\bar{V}\bar{S}_{CD}}$: Volume-"chain order-parameter" correlation coefficient.
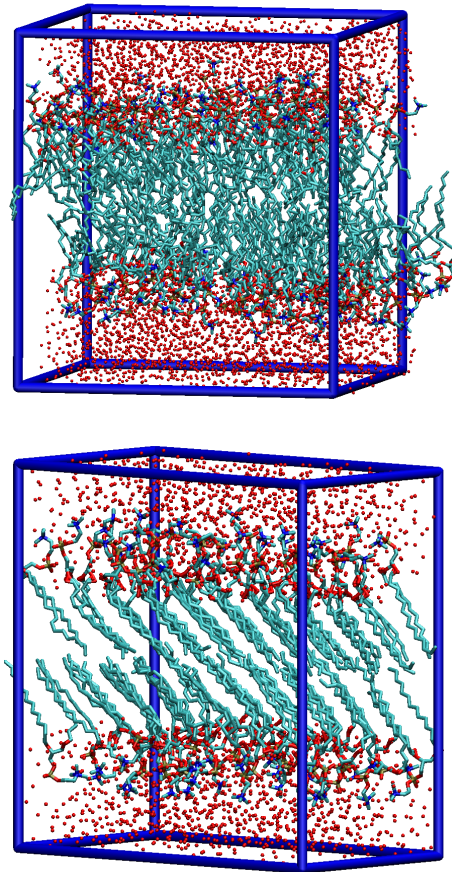
Figure 1: Snapshots of DMPC membrane in the fluid phase (DMPC-f; top) and in the ordered phase (DMPC-g; bottom). The red atoms are the oxygen atoms of water molecules; hydrogen atoms were removed for visual clarity (but included in the simulations). The green strings are the acyl chains. The frame indicates the periodic boundary box.

ations of volume and energy do not show any significant correlation (data not shown). This is not surprising, since a significant part of the simulation box is water and water is known not to have such correlation [8]. However, if fluctuations are averaged over time windows of 0.5 nanosecound, volume and energy are strongly correlated as shown in Fig. 2A for DMPC-f. This is quantified by the correlation coefficient,

$$R_{\bar{U}\bar{V}} = \frac{\langle \Delta\bar{U}\Delta\bar{V} \rangle}{\sqrt{\langle(\Delta\bar{U})^2\rangle\langle(\Delta\bar{V})^2\rangle}} = 0.77, \tag{1}$$

where the bar here and henceforth indicates a 0.5 ns average. $R = 0$ corresponds to no correlation, $|R| \cong 1$ corresponds to strong correlation. For comparison the correlation coefficient without averaging (R_{UV}) is 0.35.

One possible explanation for the observed strong correlation could be that the order of the acyl chains is the single controlling parameter of the fluctuations. If chains, as a result of a thermal fluctuation, become more ordered, one expects: decrease of energy, volume, and area, but increase of thickness and $\langle S_{CD} \rangle_{ch}$. We find $R_{\bar{U}\bar{A}} = 0.50$ and $R_{\bar{V}\bar{A}} = 0.57$. The correlation has the right sign but is significantly lower. The same is the case for Z and $\langle S_{CD} \rangle_{ch}$. Fig. 2B shows the full correlation matrix. Clearly a single parameter description is not sufficient. We need two parameters to describe the thermodynamic fluctuations: one parameter controlling V and U and one "geometrical" parameter controlling A, Z, and $\langle S_{CD} \rangle_{ch}$.

Table 1 shows that the DMPC-f, DPPC-g, DPPC-g, DMPG, DMPS, and DMPSH have strong volume-energy correlation ($R \geq 0.75$). The volumes DMPC-g and DMPS show less correlation with energy – a point returned to below.

The term "slow fluctuations" has so far been arbitrary, defined via the 0.5 ns averaging time window. A more general approach is to investigate the time-dependent correlation coefficient

$$\Gamma_{UV}(t) = \frac{\langle \Delta U(0)\Delta V(t) \rangle}{\sqrt{\langle \Delta U(0)\Delta U(t)\rangle\langle \Delta V(0)\Delta V(t)\rangle}} \, . \tag{2}$$

Similarly, one defines the time-dependent energy-area correlation coefficient $\Gamma_{UA}(t)$.

Fig. 3 shows $\Gamma_{UV}(t)$ and $\Gamma_{UA}(t)$ for all seven investigated system. In contrast to $\Gamma_{UA}(t)$ we observe strong correlation on slow time scales for $\Gamma_{UV}(t)$ where this function approaches unity. In the next section the slow parts of the volume and energy fluctuations are investigated via the autocorrelation functions $\langle \Delta V(0)\Delta V(t) \rangle$ and $\langle \Delta U(0)\Delta U(t) \rangle$.

Locating the slow volume and energy fluctuations

A membrane is a highly anisotropic system, and it is reasonable to divide it into regions. In the following three regions are defined: t, h, and w, where t (tail) refers to the hydrophobic acyl-chain atoms (i.e., atoms of methylene- and
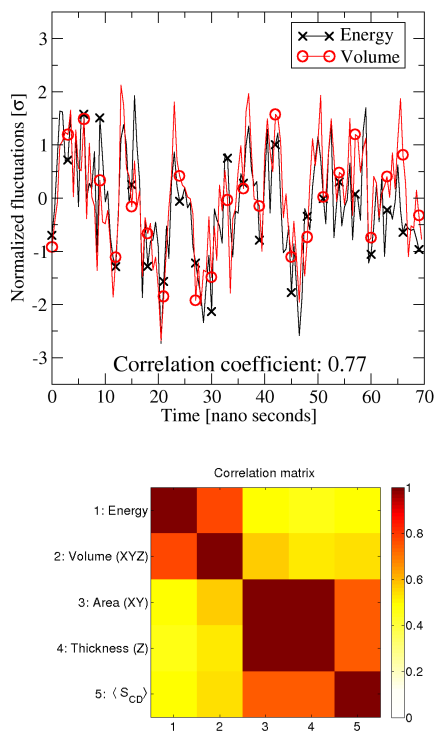
Figure 2: Correlations in the slow thermal equilibrium fluctuations of volume and energy (top) and correlation matrix for the DMPC-f membrane (bottom). The normalized fluctuations of volume and potential energy shown are averaged over time intervals of 0.5 nanosecond. Data are shifted and scaled such that the average value is zero and the standard deviation is unity. A significant correlations is observed quantified by the correlation coefficient, $R_{UV} = 0.77$ (this strong correlations can be associated to the acyl chains as seen by the similarities between this figure and the below Fig 5). The bottom panel represents the absolute values of the elements of the correlation matrix of energy, volume, membrane area, thickness and the average chain order-parameter where dark red illustrates strong correlation. Membrane area, thickness, and average chain order-parameter are strongly correlated, but these quantities only correlate weakly with energy and volume. Similar results are found for the other fluid membranes (except for DMPC-g and DMPS where the energy-volume correlation is only 0.47 and 0.59, respectively), see Table 1.

8

methyl groups in the acyl-chain), h (head) refers to the hydrophilic atoms (the remaining of the lipid atoms), and w refers to the water atoms.

To identify the origin of the slow volume fluctuations, we construct Voronoi polyhedra [28] of heavy atoms (i.e., ignoring hydrogen) and sum the Voronoi volumes for the regions t, h and w. In this way the total volume of the simulation box is divided into three terms,

$$V = V_t + V_h + V_w \,. \tag{3}$$

The auto-correlation function of the volume in Eq. 2 can now be split into a sum of three auto- and three cross-correlation functions,

$$
\begin{aligned}
\langle \Delta V(0) \Delta V(t) \rangle &= \langle \Delta V_t(0) \Delta V_t(t) \rangle \\
&+ \langle \Delta V_h(0) \Delta V_h(t) \rangle \\
&+ \langle \Delta V_w(0) \Delta V_w(t) \rangle \\
&+ 2\langle \Delta V_t(0) \Delta V_h(t) \rangle \\
&+ 2\langle \Delta V_t(0) \Delta V_w(t) \rangle \\
&+ 2\langle \Delta V_h(0) \Delta V_w(t) \rangle .
\end{aligned}
\tag{4}
$$

Fig. 4A shows these six functions for the DMPC-f membrane. The only nonvanishing function at long times (responsible for the slow fluctuations) is the auto-correlation function of the hydrophobic (tail) part of the membrane, $\langle \Delta V_t(0) \Delta V_t(0) \rangle$. This is quantified by $R_{V V_t} = 0.94$ being close to unity.

In the simulation, the potential energy of the system consists of a sum of Lennard-Jones terms, Coulomb pair energy terms, and intramolecular binding-energies:

$$U = U^{\mathrm{intra}} + \frac{1}{2} \sum_i \sum_{j \neq i} U_{ij}^{\mathrm{coul}} + \frac{1}{2} \sum_i \sum_{j \neq i} U_{ij}^{\mathrm{LJ}}\,. \tag{5}$$

Again we split the total potential energy into contributions from regions of tails, heads and water,

$$U = U_t + U_h + U_w \tag{6}$$

where

$$U_x = U_x^{\mathrm{intra}} + \frac{1}{2} \sum_{i\,=\,x} \sum_{j\,=\,\mathrm{all}} U_{ij}^{\mathrm{coul}} + \frac{1}{2} \sum_{i\,=\,x} \sum_{j\,=\,\mathrm{all}} U_{ij}^{\mathrm{LJ}}\,, \tag{7}$$

with x either tail, head, or water,

$$U_{ij}^{\mathrm{LJ}} = 4\varepsilon_{ij}((\sigma_{ij}/r_{ij})^{12} - (\sigma_{ij}/r_{ij})^6)\,, \tag{8}$$

and

$$U_{ij}^{\mathrm{coul}} = q_i q_j / (4\pi\epsilon_0 r_{ij})\,. \tag{9}$$

As for the volume, the auto-correlation function of the energy fluctuations in Eq. 2 is also split into a sum of three auto- and three cross correlation functions,

$$
\begin{aligned}
\langle \Delta U(0)\Delta U(t)\rangle &= \langle \Delta U_t(0)\Delta U_t(t)\rangle \\
&+ \langle \Delta U_h(0)\Delta U_h(t)\rangle \\
&+ \langle \Delta U_w(0)\Delta U_w(t)\rangle \\
&+ 2\langle \Delta U_t(0)\Delta U_h(t)\rangle \\
&+ 2\langle \Delta U_t(0)\Delta U_w(t)\rangle \\
&+ 2\langle \Delta U_h(0)\Delta U_w(t)\rangle .
\end{aligned}
\tag{10}
$$

Fig. 4B shows the six auto- and cross correlation functions of U_t, U_h and U_w. Again, the slow fluctuations are dominated by the tail region. It should be noted, though, that the head-head and water-water auto-correlation remaining functions are not close to vanishing, as was the case for the volume fluctuations. This is quantified by $R_{\bar{U}\bar{U}_t} = 0.82$ (Tabel 1) not being as close to unity as $R_{\bar{V}\bar{V}_t} = 0.94$.

Fig. 4C shows the auto- and cross-correlation functions corresponding to a further splitting of the tail energy into "intramolecular interactions", "Coulombic interactions" and "van der Waals interactions" given in Eq. 7. The van der Waals energies dominate the energy fluctuations of the tail region.

The above analysis shows that the slow energy-volume correlation originate from van der Walls interactions in the tail region; thus:

$$
\Delta \bar{V}_t \propto \Delta \bar{U}_t^{LJ} ,
\tag{11}
$$

where

$$
U_t^{LJ} = \frac{1}{2} \sum_{i=\text{tails}} \sum_{j=\text{all}} U_{ij}^{\text{LJ}}
\tag{12}
$$

This is in good agreement with the findings for simple strongly correlations liquids [9, 10]. It should be remembered, however, that we discarded some non-vanishing energy correlation functions. If we correlate the slow fluctuations (by doing a 0.5 ns average) of the Voronoi volume of the acyl chains and the van der Waals energy of tails, we find a correlation coefficient of $R_{\bar{V}_t \bar{U}_t^{LJ}} = 0.87$ (Fig. 5). The same number for the fluctuations for whole simulation box was $R_{\bar{V}\bar{U}} = 0.77$. The loss of correlation is associated with the energy terms neglected. Consistent with this, Table 1 shows a general correlation between $R_{\bar{V}\bar{U}}$ and $R_{\bar{U}\bar{U}_t}$.

It is convenient to define a volume-energy scaling factor via

$$
\gamma = \sqrt{\frac{\langle (\Delta V)^2\rangle}{\langle (\Delta U)^2\rangle}} .
\tag{13}
$$

For DMPC the experimentally found volume-energy scaling factor, $\gamma = (7.788 \pm 0.110) \times 10^{-4}$ mL/J $= (5.418 \pm 0.077)$ Å·mol/kcal [6], is in good agreement with the scaling factors given in Table 1.
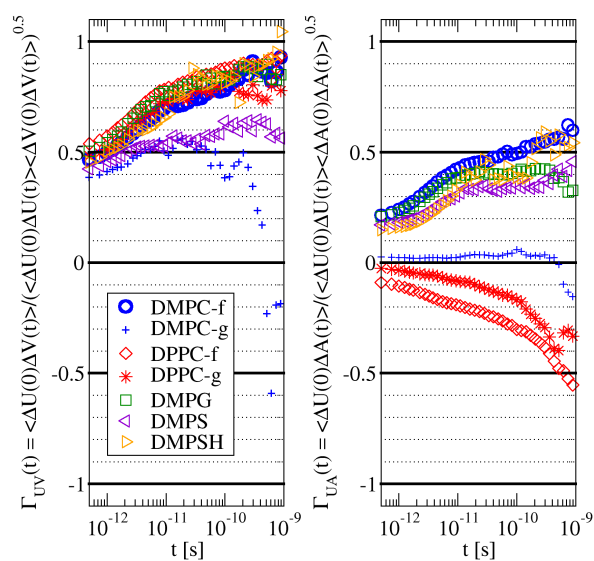
10

Figure 3: Time-dependent correlation coefficient $\Gamma(t)$ of volume-energy (left) and area-energy (right) of membranes in the fluid phase (the definition of $\Gamma(t)$ is given on the y-axis). The fast fluctuations of volume and energy, e.g. $t < 10^{-11}$ second, correlate only weakly, whereas the slow fluctuations, e.g. $t \simeq 10^{-9}$ second, are strongly correlated. The area and energy fluctuations are only weakly correlated.
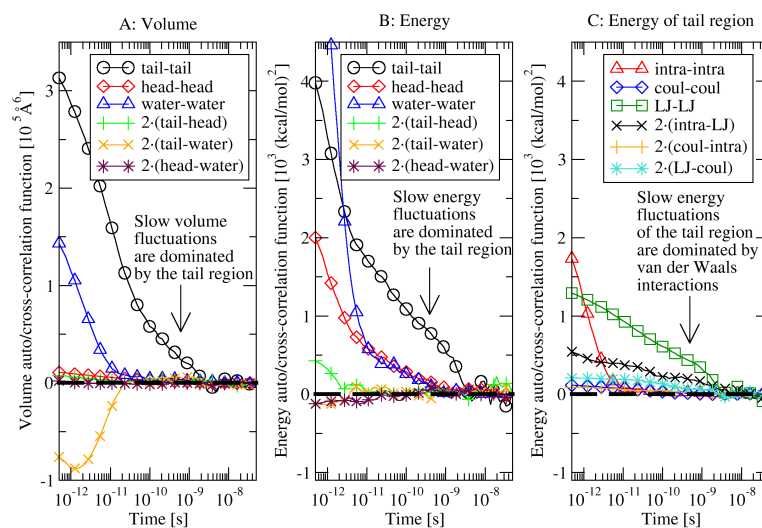
11

Figure 4: Six auto- and cross-correlations for the DMPC-f membrane. Panel A: Volume correlations of the three regions (Eq. 4): tails (methylene and methyl groups), heads, and water. From these correlations it can be concluded that the slow volume fluctuations are dominated by the acyl chains. Panel B: Energies of the three regions (Eq. 10). Again, slow fluctuations are dominated by the tail region. Panel C: Energy correlations split into intramolecular, Lennard-Jones (LJ) and Coulombic energies (Eq. 6).
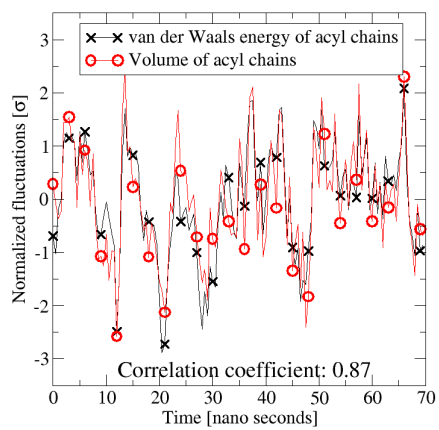
Figure 5: Normalized fluctuations of Voronoi volume and van der Waals energy of the acyl chains of the DMPC-f membrane. Data are shifted and scaled so the average value is zero and the standard deviation is unity. The correlation is strong with a correlation coefficient of 0.87. Note the similarity to Fig. 2A.

Conclusions

This paper reports a study of biomembranes' thermodynamic equilibrium fluctuations. On the long time scale we identify strong volume-energy correlations of a kind that were previously only observed for simple model liquids [7, 8]. These correlations are mainly documented in the fluid phase, but we also show that they exist in the membrane's gel phase.

It may seem surprising that a complex system like a biomembrane exhibits such strong thermodynamic correlations. The identification of the origin of the correlations as deriving from the van der Waals interactions of the hydrophobic part of the membrane, however, points to a common origin of strong thermodynamic correlations in simple van der Waals liquids and biomembranes. This is consistent with the finding that there are strong energy-volume correlations in both fluid and gel phases: The correlations do not depend on the degree of chain order, as for simple liquids where the strong correlations survive crystallization [9, 10].

Regarding the Heimburg-Jackson nerve signal theory, our findings largely confirm the assumption of this theory that volume and energy (enthalpy) correlate for microstates. We find a strong correlation only on the nanosecond and longer time scales, which are however the relevant times for nerve signals. One caveat is that, although we do find strong energy-volume correlations in both the fluid and gel phases, the proportionality constant γ is not the same in both phases (Table 1). This shows that the nature of the correlations changes when passing the phase transition, in contrast to our findings for crystallization of the standard Lennard-Jones liquid [9, 10]. More work is needed to clarify the cause of this difference between biomembranes and simple liquids.

Acknowledgments

References

[1] Heimburg T, Jackson AD (2005) On soliton propagation in biomembranes and nerves. *PNAS* 102:9790-9795.

[2] Heimburg T, Jackson AD (2007) The thermodynamics of general anesthesia. *Biophys. J.* 92:3159-3165.

[3] Hodgkin, AL, Huxley, AF (1952) A quantitative description of membrane current and its applications to conducting and excitation in nerve. *J. Physiol. (London)* 117:500-544.

[4] Nielsen LK, Bjørnholm T, Mouritsen OG (2007) Thermodynamic and real-space structural evidence of a 2D critical point in phospholipid monolayers. *Langmuir* 23:11684-11692.

[5] Heimburg, T (1998) Mechanical aspects of membrane thermodynamics. Estimation of the mechanical properties of lipid membranes close to the chain melting transition from calorimetry. *Biochim. Biophys. Acta* 1415:147-162.

[6] Ebel H, Grabitz P, Heimburg, T (2001) Enthalpy and volume changes in lipid membranes. I. The proportionality of heat and volume changes in the lipid melting transition and its implication for the elastic constants. *J. Phys. Chem. B* 105:7353-7360.

[7] Pedersen UR, Christensen T, Schrøder TB, Dyre JC (2008) Feasibility of a single-parameter description of equilibrium viscous liquid dynamics. *Phys. Rev. E* 77:011201.

[8] Pedersen UR, Bailey NP, Schrøder TB, Dyre JC (2008) Strong pressure-energy correlations in van der waals liquids. *Phys Rev. Lett.* 100:015701.

[9] Bailey NP, Pedersen UR, Gnan N, Schrøder TB, Dyre JC (2008) Pressure-energy correlations in liquids. I. Results from computer simulations. *J. Chem. Phys.*, in press.

[10] Bailey NP, Pedersen UR, Gnan N, Schrøder TB, Dyre JC (2008) Pressure-energy correlations in liquids. II. Analysis and consequences. *J. Chem. Phys.*, in press.

[11] Feller SE, Zhang YH, Pastor RW and Brooks BR (1995) Constant pressure molecular dynamics simulations: the Langevin piston method. *J. Chem. Phys* 103:4613-4621

[12] Allen MP, Tildesley DJ (1989) *Computer simulation of liquids* (Oxford University Press).

[13] Kob W, Andersen HC (1994) Scaling behavior in the beta-relaxation regime of a supercooled Lennard-Jones mixture. *Phys. Rev. Lett.* 73:1376-1379.

[14] Ellegaard NL, *et al.* (2007) Single-order-parameter description of glass-forming liquids: A one-frequency test. *J. Chem. Phys.* 126:074502.

[15] Davies RO, Jones GO (1952) The irreversible approach to equilibrium in glasses. *Proc. Roy. Soc. A (London)* 217:26-42.

[16] Angell CA (1991) Relaxation in liquids, polymers and plastic crystals - strong fragile patterns and problems. *J. Non-Cryst. Solids* 131:13-31.

[17] Roland CM, Hensel-Bielowka S, Paluch M, Casalini R (2005) Supercooled dynamics of glass-forming liquids and polymers under hydrostatic pressure. *Rep. Prog. Phys.* 68:1405-1478.

[18] Schrøder TB, Pedersen UR, Dyre JC (2008) Density scaling as a property of strongly correlating viscous liquids. *arXiv.org* arXiv:0803.2199.

[19] Zhang R, *et. al.*, (1995) Critical Fluctuations of Membranes. *Phys. Rev.* 74:2832-2835.

[20] Darden T, York D, Pedersen L (1993) Particle mesh ewald: an $N \cdot \log(N)$ methods for Ewald sums in large systems. *J. Chem. Phys.* 98:10089-10092.

[21] Essmann U, *et al.* (1995) A smooth particle mesh Ewald method. *J. Chem. Phys.* 103:8577-8593.

[22] Kale L, *et al.* (1999) NAMD2: Greater Scalability for Parallel Molecular Dynamics. *J. Comput. Phys.* 151:283-312.

[23] Pedersen UR, Leidy C, Westh P, Peters GH (2006) The effect of calcium on the properties of charged phospholipid bilayers. *Biochim. Biophys. Acta, Biomembr.* 1758:573-582.

[24] Pedersen UR, Peters GH, Westh P (2007) Molecular packing in 1-hexanol-DMPC bilayers studied by molecular dynamics simulation. *Biophysical Chemistry* 125, 104-111.

[25] Sonne J, Jensen MØ, Hansen FY, Hemmingsen L, Peters GH (2007) Reparameterization of all-atom dipalmitoylphosphatidylcholine lipid parameters enables simulations of fluid bilayers at zero tension. *Biophys. J.* 92:4157-4167.

[26] Venable RM, Brooks B., Pastor RW (2000) Molecular dynamics simulations of gel (L-beta I) phase lipid bilayers in constant pressure and constant surface area ensembles. *J. Chem. Phys.* 112, 4822-4832.

[27] Tieleman DP, Berendsen HJC (1996) Molecular dynamics simulations of a fully hydrated dipalmitoyl phosphatidylcholine bilayer with different macroscopic boundary conditions and parameters. *J. Chem. Phys.* 105:4871-4880.

[28] Voronoi G (1908) New parametric applications concerning the theory of quadratic forms - Second announcement. *J. Reine Angew. Math.* 134:198-287.

Stability of supercooled binary liquid mixtures

Søren Toxvaerd, Ulf R. Pedersen, Thomas B. Schrøder, and Jeppe C. Dyre

DNRF centre "Glass and Time," IMFUFA, Department of Sciences,
Roskilde University, Postbox 260, DK-4000 Roskilde, Denmark

(Dated: January 6, 2009)

The supercooled Kob-Andersen binary Lennard-Jones (KABLJ) mixture crystallizes partially in lengthy Molecular Dynamics simulations by forming pure FCC crystals of the majority component. The general thermodynamic and kinetic stability of supercooled binary mixtures is discussed, emphasizing the importance of negative mixing enthalpy whenever present. Based on this a modification of the KABLJ mixture is proposed that is less prone to crystallization and faster to simulate; this is obtained by removing the like-particle attractions by switching to Weeks-Chandler-Andersen type potentials while maintaining the unlike-particle attraction.

I. INTRODUCTION

As computers get faster, simulations of the highly viscous liquid phase preceding glass formation become increasingly realistic. In this context it is nice to have a standard model system, something like the Ising model for critical phenomena. For several years binary binary Lennard-Jones (BLJ) mixtures have served this purpose – in particular the Wahnström and Kob-Andersen systems [1, 2], because they are easy to simulate and were never found to crystallize. The Kob-Andersen BLJ consists of two types of Lennard-Jones particles, 80% large (A) particles and 20% small (B) particles. The BLJ potentials are modifications of the potentials devised by Weber and Stillinger [3], who constructed the pair potentials for the binary mixture based of physical-chemical data for the $Ni_{80}P_{20}$ alloy. The Kob-Andersen potentials describe a strongly non-ideal mixture due to an AB attraction that is three times stronger than the BB attraction. This ensures a large negative mixing enthalpy (and energy), which suppresses crystallization into pure A crystals as detailed below.

Recently, both the Wahnström (Wa) and the Kob-Andersen (KA) systems were shown to crystallize in lengthy computer runs [4]. This motivated the present paper that has three purposes. First, we briefly review the general theory of thermodynamic and kinetic stability of supercooled binary mixtures (Sec. II). Secondly, we detail the crystallization of the Kob-Andersen systems (Sec. III), while the crystallization of the Wahnström liquid will be described elsewhere [5]. Finally, we suggest a modification of the KA binary system that is more stable and faster to simulate; in fact, we have not been able to crystallize the new system even in month long simulations. The idea is to keep the KA system's large negative mixing enthalpy, but remove the AA and BB attractions by adopting Weeks-Chandler-Andersen (WCA) type potentials between like particles (Sec. IV). Section V gives a brief discussion.

II. GENERAL TREATMENT

Consider a binary mixture of N_A solvent (A) particles and N_B solute (B) particles, with total number of particles $N = N_A + N_B$. The thermodynamic stability of this system against crystallization is expressed by the melting temperature of a pure A crystal, $T_{\text{fus,A}}$, as a function of the concentration of A particles. The latter quantity is conveniently expressed in terms of the fraction $x_{\text{B}} = N_B/N$ of B particles ($x_{\text{A}} + x_{\text{B}} = 1$). We consider the usual case of externally controlled temperature T and pressure p. At the melting temperature of the pure A crystalline phase in the AB mixture, the chemical potential of the A particles in the crystal equals the chemical potential of the A particles of the liquid mixture. The chemical potential is the Gibbs free energy per particle. The change in Gibbs free energy per A particle at melting, $\Delta G_{\text{trans,A}}$ can be divided into two therms, $\Delta G_{\text{fus,A}}$ and $\Delta G_{\text{mix,A}}$, where $\Delta G_{\text{fus,A}}$ is the change in Gibbs free energy per A particle upon melting an A crystal into pure A liquid, and $\Delta G_{\text{mix,A}}$ is the change in Gibbs free energy per A particle going from pure to mixed liquid. The melting temperature $T_{\text{fus,A}}$ is determined by

$$\Delta G_{\text{trans,A}} = \Delta G_{\text{fus,A}}(T_{\text{fus,A}}) + \Delta G_{\text{mix,A}}(T_{\text{fus,A}}) = 0.$$
(1)

The case of pure A ($x_{\text{B}} = 0$) will be denoted by an asterisk, thus $T^*_{\text{fus,A}}$ is the melting point of the pure A crystal into pure A liquid. In this case $\Delta G_{\text{trans,A}} = \Delta G^*_{\text{fus,A}}$ and since $G = H - TS$, one has

$$\Delta H^*_{\text{fus,A}} - T^*_{\text{fus,A}} \Delta S^*_{\text{fus,A}} = 0$$
(2)

where here and henceforth all thermodynamic quantities are per A atom. When deriving the standard expression for the freezing point depression one makes the approximation that crystal and liquid have the same specific

heats, i.e that $\Delta H_{\text{fus,A}}$ and $\Delta S_{\text{fus,A}}$ are temperature independent, or from Eq. (2)

$$\Delta H_{\text{fus,A}} - T^*_{\text{fus,A}}\Delta S_{\text{fus,A}} = 0 \qquad (3)$$

In the general case where $x_{\text{B}} \neq 0$ one has from (1)

$$\Delta H_{\text{fus,A}} - T_{\text{fus,A}}\Delta S_{\text{fus,A}} = -\Delta G_{\text{mix,A}} \qquad (4)$$

and by using Eq. (3) to eliminate $\Delta S_{\text{fus,A}}$ in Eq. (4) one obtains

$$\frac{\Delta T_{\text{fus,A}}}{T^*_{\text{fus,A}}} = -\frac{\Delta G_{\text{mix,A}}}{\Delta H_{\text{fus,A}}} \qquad (5)$$

for the melting point depression $\Delta T_{\text{fus,A}} = T^*_{\text{fus,A}} - T_{\text{fus,A}}$. In the standard textbook treatment one assumes that $\Delta H_{\text{mix,A}} = 0$ and that the mixing entropy is ideal, i.e., that the mixing entropy divided by $N = N_A + N_B$ is given by $\Delta S_{\text{mix}} = -k_B[x_{\text{A}}\ln(x_{\text{A}}) + x_{\text{B}}\ln(x_{\text{B}})]$. This expression separates into a contribution from the A particles and one from the B particles. Per A particle we thus have $\Delta S_{\text{mix,A}} = -k_B\ln(x_{\text{A}}) = -k_B\ln(1 - x_{\text{B}})$. In the limit $x_{\text{B}} \to 0$ Eq. (5) under these assumptions reduces to the well-known expression

$$\frac{\Delta T_{\text{fus,A}}}{T^*_{\text{fus,A}}} \cong \frac{k_B T_{\text{fus,A}}}{\Delta H^*_{\text{fus,A}}} x_{\text{B}} \qquad (6)$$

More generally, $\Delta H_{\text{mix,A}} = 0$ does not apply – in fact for the Kob-Andersen liquid the mixing enthalpy is large (and negative) and this term cannot be ignored. For small concentrations of the solute, x_{B}, the mixing entropy is still given by $\Delta S_{\text{ideal mix,A}}$. For this more general case Eq. (5) becomes

$$\frac{\Delta T_{\text{fus,A}}}{T^*_{\text{fus,A}}} = -\frac{\Delta H_{\text{mix,A}} + k_B T_{\text{fus,A}}\ln(x_{\text{A}})}{\Delta H_{\text{fus,A}}} \qquad (7)$$

A negative mixing enthalpy (i.e. exotherm) clearly implies a further melting point depression beyond that of the traditional treatments. If there is a large negative mixing enthalpy, this effect is important.

The stability of a supercooled liquid mixture depends not only on its absolute (thermodynamic) stability against crystallization, but is also affected by kinetic effects. Thus the less supercooled the liquid is, the larger is the critical nucleus and the more stable is the liquid. This means that it takes longer time before a critical nucleus is generated by a thermal fluctuation, i.e., the supercooled liquid is more stable. At a given temperature the supercooled liquid is more stable the more negative $\Delta G_{\text{mix,A}}$ becomes. To see this divide the creation of a crystal nucleus of pure A particles in the mixture

$$N_{\text{A}}(\text{mix}) \to N_{\text{A}}(\text{crystal}, x_{\text{A}} = 1) \qquad (8)$$

into two steps:

$$\begin{aligned} N_{\text{A}}(\text{mix}) &\to N_{\text{A}}(\text{liquid}, x_{\text{A}} = 1) \\ N_{\text{A}}(\text{liquid}, x_{\text{A}} = 1) &\to N_{\text{A}}(\text{crystal}, x_{\text{A}} = 1). \end{aligned} \qquad (9)$$

The first reaction is a density fluctuation from the mixture to a pure liquid domain of A particles, the second is crystallization. The crystallization is (qualitatively) described by classical nucleation theory (CNT). In its simplest formulation the number of particles, N^*, in the critical nucleus is given [6] by

$$N^* = \frac{32\pi\gamma_\infty^3}{3\rho_s^2\Delta\mu_{\text{A}}^3}, \qquad (10)$$

where γ_∞ is the solid-liquid surface tension, ρ_s is the crystal number density and $\Delta\mu_{\text{A}}$ is the change in Gibbs free energy per A particle by going from the crystal to pure A liquid. When the creation of a pure A crystal takes place in a mixture, the lowering of Gibbs free energy by the crystallization process is reduced by $\delta\mu = -\Delta G_{\text{mix,A}} = -\Delta H_{\text{mix,A}} + T_{\text{fus,A}}\Delta S_{\text{mix,A}} \approx -\Delta_{\text{A,mix}}u_{pot} - k_B T_{\text{fus,A}}\ln(x_{\text{A}})$. Since the size of the critical nucleus N^* varies as $N^* \propto (\Delta\mu_{\text{A}})^{-3}$, when $\Delta\mu_{\text{A}}$ is replaced by $\Delta\mu_{\text{A}} - \delta\mu_{\text{A}}$ to lowest order the change in critical nucleus size δN^* is given by $\delta N^*/N^* = 3\delta\mu_{\text{A}}/\Delta\mu_{\text{A}}$, thus

$$\frac{\delta N^*}{N^*} = -3\frac{\Delta_{\text{A,mix}}u_{pot}(x_{\text{A}}) + k_B T_{\text{fus,A}}\ln(x_{\text{A}})}{\Delta\mu_{\text{A}}}. \qquad (11)$$

Both the negative mixing energy and the mixing entropy terms tend to increase the size of the critical nucleus. Note, however, that if the crystallization is instead to, e.g., an AB-crystal from an B-rich mixture with positive AB binding energy, the size of the critical nucleus is reduced. This prediction agrees with our simulations of crystallization in supercooled mixtures of varying composition.

The above stability considerations indicate that if a binary mixture crystallizes into, e.g., an AB-type crystal, a negative mixing energy will enhance the tendency of crystallization by decreasing the size of the critical nucleus. Confirming this, we find that increasing the fraction of B particles to $x_{\text{B}}=0.5$ for KA-type BLJ mixtures results in systems that more quickly crystallize into an AB (CsCl structure) crystal. This is consistent with the results of Fernandez and Harrowell [7], who found that the $T = 0$ equilibrium phase of the KABLJ mixture consists of co-existing pure A (FCC) and AB (CsCl structure) crystals. The mixing energy term also plays an important role for the KA mixture and here we observe (see later) that the nucleation time depends on details in the truncation of the pair potentials in agreement with Eq. (11).

III. THE WAHNSTRÖM AND THE KOB-ANDERSEN BINARY LENNARD-JONES MIXTURES

The simplest case of a realistic mixture is that given by the semi-empirical Lorentz-Berthelot (LB) rules [8] relating the energy parameters σ and ϵ in the pair potentials between the different species of the AB mixture:

$$\sigma_{AB} = (\sigma_{AA} + \sigma_{BB})/2 \qquad (12)$$
$$\epsilon_{AB} = \sqrt{\epsilon_{AA}\epsilon_{BB}} \qquad (13)$$

These rules apply for atoms with weak dispersion attractions [9], and they work well for simple mixtures of for instance noble-gas atoms [8], i.e., for interactions between spherically symmetric atoms with unperturbed valence-electron orbitals.

There are two standard models for highly viscous supercooled binary mixtures, the model introduced by Wahnström (WA) [1] and the model by Kob and Andersen (KA) [2]. Both models involve Lennard-Jones potentials (LJ).

$$u_{LJ}(r_{ij}) = 4\epsilon_{ij}\left[\left(\frac{\sigma_{ij}}{r_{ij}}\right)^{12} - \left(\frac{\sigma_{ij}}{r_{ij}}\right)^{6}\right] \qquad (14)$$

between particle i and j. The WA model obeys the LB-rules by having

$$\sigma_{AB} = (\sigma_{AA} + \sigma_{BB})/2 \qquad (15)$$

with $\sigma_{BB} = 1/1.2\sigma_{AA}$ and $\epsilon_{AB} = \epsilon_{AA} = \epsilon_{BB} = 1$. The KA model strongly disobeys the LB-rules: The LJ-potential parameters for the KA mixture are $\sigma_{AB} = 0.8\sigma_{AA}$, $\sigma_{BB} = 0.88\sigma_{AA}$, $\epsilon_{AB} = 1.5\epsilon_{AA}$, and $\epsilon_{BB} = 0.5\epsilon_{AA}$. This results in a tendency for the small solute B particles to "glue" to the A particles. This mixture has a significant non-ideal mixing energy and it is considerably more stable against crystallization than the WA mixture.

We have calculated [10] the melting point temperature at constant pressure ($p\sigma_{AA}^3/\epsilon_{AA}$=10) for small solute concentrations, x_B, and using Eq. (7) for these two models. The result is shown in Figure 1. The melting point depression by mixing is traditionally given at constant pressure. Most MD simulations are, however performed for isochores where $T_{fus,A}(x_B)$ depends on the partial volumes of the species in the mixture.

As can be seen from the figure the negative mixing energy lowers the melting point temperature significantly. The WA model is indeed more prone to crystallization than the KA model and recently Pedersen and co-workers reported crystallization of the WA model after lengthy computer runs [5]. The crystal is the MgZn$_2$ phase consisting of particles in the ratio 1:2, different from the 1:1 ratio defining the Wahnström BLJ. Thus concentration fluctuations precede (or at least correlate with) crystal formation. These findings inspired us to investigate whether the more widely studied KA model also crystallizes in lengthy computer runs.

We performed molecular dynamics simulations of 1000 (and 10000) particles of the standard Kob-Andersen binary Lennard-Jones liquid in the NVE and NVT ensembles. The system was simulated at the density 1.2 in dimensionless units at varying temperatures. The standard time-reversible leap-frog (NVT) algorithm [11] was used with a time step of 0.005 (in Argon units: $\approx 10^{-14}$ s). The software used has been described elsewhere [12]; it utilizes a double sorting of neighbor particles that makes it possible to simulate 1 μs within 2-3 days of computing on a standard computer.

For temperatures above 0.45 no crystallization was detected. In the temperature interval $[0.39, 0.45]$ a suspicious drop in pressure taking place typically after $\approx 10^8$ time steps indicates that something is happening. It turns out that the system phase separates such that the A particles form fairly large regions with no B particles present. Linked to this phase separation is a crystallization of the A particles. Ten simulations were performed in the $[0.39, 0.45]$ temperature interval; after $4.\times10^8$ time steps ($\approx 4\mu$s) eight of these ten simulations phase separated with crystallization of the A particles. Figure 2 shows a representative example of our results, giving the positions of the particles after crystallization at T=0.40 (NVT-MD). There is a large region of pure A particles showing clear crystalline order.

The general theory of stability by supercooling a mixture shows that if a binary mixture can crystallize into e.g. a AB-type crystal, the mixing energy can enhance the tendency of crystallization, in CNT by decreasing the size of the critical nucleus. We find that increasing the fraction of B-particles to x_B=0.5 results in that the KA-mixture quickly crystallizes into an AB (CsCl structure) crystal in accordance with the CNT prediction. The result is as mentioned consistent with the results of Fernandez and Harrowell [7], who found that the $T = 0$ equilibrium phase of the KA consists of a coexisting A (fcc) and AB (CsCl structure) crystals.

The stability of the supercooled mixture depends on details in the cut-off of the potentials. Originally Kob and Andersen used a cut-off at $2.5\sigma_{\alpha,\beta}$ (α, β = A,B). If one instead uses the same cut-off for all three pair potentials, i.e. $2.5\sigma_{AA}$, this corresponds to a shift from 2.5 σ_{AB} to 3.125 σ_{AB}. By this extension of the range of the AB attraction the mixing energy becomes more negative than in the original KA mixture by an amount of 0.04 ϵ_{AA}. This may seem insignificant, but according to Eq. (11) the corresponding change in the critical nucleus size is of order 10%. Consistent with this we find that the KABLJ mixture with this cutoff must typically be simulated three times longer before it crystallizes than when using the original KA parameters.

IV. A MODIFIED BINARY MODEL SYSTEM LESS PRONE TO CRYSTALLIZATION

With the general theory for melting point depression and nucleation in mind it is possible to modify the existing models in such a way that they are less prone to crystallization. We want to maintain the success of the existing models, which are set up to simulate real supercooled mixtures, in the case of KA-model a binary mixture of $Ni_{80}P_{20}$ alloy. For this reason the sizes of the molecules in the KA-mixture, given by the σ_{ii} values, are maintained. We also want to have the same structure of the KA-mixture, given by their correlation functions. A modified KA-mixture with only repulsive forces between A-A and B-B particles, but where the attraction between A- and B-particles is maintained. With Lennard-Jones (LJ) potentials between particle i and j the modified potentials are

$$u_{ij}(r_{ij}) = \begin{cases} u_{LJ}(r_{ij}) - u_{LJ}(r_{ij}(icut)), & r_{ij} < r_{ij}(cut) \\ 0, & r \geq r_{ij}(cut), \end{cases} \tag{16}$$

with

$$r_{i,i}(cut) = 2^{1/6}\sigma_{ii} \tag{17}$$

$$r_{AB}(cut) = 2.5\sigma_{AB} \tag{18}$$

and meets these requirements. *A priory* it is to be expected [13] that the structure of the mixture only deviates marginally from the originally KA-model because the repulsive parts of the potential interactions are not changed from the original KA-model. The modified binary model is indeed much more stable and we have so far not been able to crystallize it (for a particle fraction $x_B = 0.2$). The system was cooled and at a new and lower temperature the system was equilibrated until the diffusion constant remained constant, and the system was then simulated 10^{10} time steps (corresponding to ≈ 0.1 ms) for nine temperatures in the interval $T \in [0.25, 0.40]$. There are two reasons for this resistance against crystallization by supercooling. First the melting point temperature, $T^*_{fus,A}$, of the pure solvent particles is lowered significantly (see Figure 1). Secondly, the relative importance of the mixing energy, $\Delta_{A,mix}u_{pot}(x_B)$ is bigger due to a stronger violation of the LB-rules for the energy and thereby a lower melting point temperature and an increase of the size of the critical fcc-nucleus.

The question arises, however, whether the modified system is a supercooled system or a highly viscous (equilibrium) liquid. As mentioned most MD simulations are performed at constant density, and the result shown in Figure 1 for $p = 10$ cannot be used to obtain the melting point temperature in the modified system at ρ=1.2 and x_B =0.2, and to determine whether the system is in a supercooled state. The KA-mixture crystallizes into a pure A-particle fcc-structure for small particle fraction, x_B, and into a CsCl (A,B) crystal for $x_B \approx 0.5$.

In between there might be other stable crystal arrangements [14]. The relative strength of the binding energy between A- and B particles is increased when the attraction between A,A- and B,B particles are removed, but with unchanged attraction between A- and B particles. This change stabilizes the CsCl-like crystal relative to the liquid, and the melting point temperature at x_B =0.5 is increased, whereas the melting point temperature of the fcc crystal for small x_B is decreased (as shown in Figure 1). The qualitative change in melting point temperature by the modification, and at constant pressure is shown in Figure 3. There is, however, a simple computer experiment to investigate whether the modified system at ρ=1.2 and x_B =0.2 is in a supercooled state at the low temperature: First we crystallized the modified system at a particle fraction x_B=0.5. Then the system with ρ=1.2 and x_B =0.2 was grafted with a CsCl crystal of 200 A and 200 B-particles, taken from the x_B=0.5 system and surrounded by 600 A-particles at a density $\rho = 1.2$, and the melting point temperature of this crystal was directly determined by heating/cooling. The melting point temperature of the CsCl grafted system at x_B =0.2 and ρ=1.2 is $T_m \approx 0.32$, and the modified system is indeed a supercooled highly viscous liquid at the low temperatures investigated. For a temperature of T =0.30 and below the system with the A,B crystal of 400 particles remained; but the remaining A-particle crystallized into a fcc-structure. The configuration is shown in Figure 4. The computer experiment demonstrates that the supercooled system is below what corresponds to the eutectic point temperature in a constant pressure system, but the actual phase diagram might be even more complicated than given here [14].

An further advantage of the modified system is that it is much faster to simulate by using a two-step sorting of nearest neighbor [12]. In addition to that one can use a bigger value of the time increment in the MD simulation due to the lower temperature, so not only does the mixture not crystallizes; but it can also be cooled further down under equilibrium condition (see Figures 8-10) and followed for much longer times ($0.1ms$).

The structure of the modified mixture is, as expected, almost the same as in the KA-mixture. Figure 5, 6 and 7 show the radial distribution functions, $g_{\alpha,\beta}(r)$ for the modified mixture and for the KA-mixture. The similarity is well known. (The so-called WCA- system [13] with only repulsive LJ forces has been used in perturbation theories for dense liquid.) As can be seen from the figures only the distribution, $g_{B,B}(r)$ of the B-particles is affected. This change in $g_{B,B}(r)$ is due to the relative increased "binding-energy" between the solvent A-particles and the solute of B-particles which, however, is not so visible in $g_{A,B}(r)$ due to the many A-B configurations (notice the different y-scales of the two figures).

The KA- and the modified mixture were cooled down from T=1.5. The KA- mixture crystallizes as mentioned in the temperature interval T $\in [0.39, 0.45]$; but it is possible to quench the KA-system down to T=0.375 and

still determine the self diffusion constant, D. The modified mixture was cooled down to T=0.25. At each (low) temperature the system was followed $10^{10} \approx$ one $0.1 ms$ time step. The diffusion constant, at T=0.25, for the A-particles is $D(A) \approx 1.0 \times 10^{-08}$. The B particles behave in a similar way, but as the temperature is decreased the ratio $D(B)/D(A)$ changes from 1.7 for T=1.5 to 9.7 for T=0.25. The values of the self-diffusion constants $D(T)$ were obtained from the slopes of the mean square displacements as a function of the time. At the low temperatures the ballistic- and diffusive time-regimes are very well separated, a log-log plot of the mean-square displacement as a function of time and for different temperatures (Figure 8) shows this separation.

The diffusion constants for A- and B-particles are shown in Figure 9 together with low temperature data for the KA-mixture (A-particles) [15]. It is possible to scale the diffusion constants for the two mixtures as is demonstrated in Figure 10, where log(D) for the KA-mixture (+) connected with dots, is plotted as a function of 1/(T*0.81). A similar "fragility invariance" for a system with different repulsive power potentials (r^{-n}) has been observed of [16].

V. DISCUSSION

The highly viscous fluid state below the equilibrium melting point temperature is found in many systems ranging from simple organic one-component systems and alloys to complex biochemical substances and ionic liquids. Along with the increasing interest in this state of matter it is important to have models that are less prone to crystallisation. The general thermodynamics theory for (equilibrium) melting and classical nucleation theory gives an indication of how to create models which suppress crystallisation by cooling. We have given one simple example by modifying the Kob-Andersen model which is the most used MD model for binary highly viscous fluids, but it is straightforward to extend the model to include other interactions and a more refined energy functions without loosing its stability against crystallization. A general recipe of energy functions for stable highly viscous liquids is, however, difficult to set up since many mixtures exhibits "reacting systems" with crystals with mixed compositions where an increased binding-or mixing energy can enhance crystallization of e.g. A,B crystals. Both the Kob-Andersen and the Wahnström models are examples of this phenomenon.

The modified model enhances the relative attraction between unlike species by removing the attraction between the A,A- and B,B-interactions. Supercooled liquid (WCA-) mixtures with solely repulsive LJ-potentials have been reported before [17], [18], but we observe that both systems [17], [18] phase separated and crystallized by cooling. By maintaining the attraction between unlike species the highly viscous state is stabilized. The modified mixture disobeys the LB-energy rule even more than the KA-mixture. The LB-energy rule is a geometric mean of interaction energy between two particles with energy scaling parameters, ϵ_{AA} and ϵ_{BB}. The two models have the same energy scaling parameters, $\epsilon_{\alpha\beta}$; but a much stronger violation of the energy rule in the interaction interval $r_{\alpha\beta} \in [2^{1/6}\sigma_{i,i}, \infty]$ where the WCA-potentials are zero. The result of this "cut and shift" is that the B-particles are almost "covalently" bounded to the A-particles and the violation of the LB-rule for the mixing energy gives a recipe for creating fragile and stable supercooled liquid mixtures.

---

[1] G. Wahnström, Phys. Rev. A **44**, 3752 (1995).

[2] W. Kob and H. C. Andersen, Phys. Rev. E **51**, 4626 (1993); *ibid.* **52**, 4134 (1995).

[3] T. A. Weber and F. H. Stillinger, Phys. Rev. B **31**, 1954 (1985).

[4] U. R. Pedersen, N. P. Bailey, J. C. Dyre, and T. B. Schrøder, arXiv:0706.0813 (2007); S. Toxvaerd, T. B. Schrøder, and J. C. Dyre, arXiv:0712.0377 (2007).

[5] U. R. Pedersen, P. Harrowell, T. B. Schrøder, and J. C. Dyre, in preparation (2008).

[6] See, e.g., A. Laaksonen, R. McGraw and H. Vehkamäki, J. Chem. Phys. **111**, 2019 (1999) and references therein.

[7] J. R. Fernandez and P. Harrowell, Phys. Rev. E **67**, 011403 (2003).

[8] J. S. Rowlinson, *Liquid and Liquid Mixtures* (Butterworths, London, 1969).

[9] J. O. Hirschfelder, C. F. Curtiss, and R. B. Bird, *Molecular Theory of Gases and Liquids* (Wiley, New York, 1954) Chap. 13.3.

[10] The $T_{\text{fus,A}}$ can be obtained from Eq. (7) for small x_B: The melting temperature for a pure LJ-system at $p = 10$ is, $T^*_{\text{fus}}=1.4017(3)$ and the corresponding densities are $\rho(s)^* = 1.0630(8)$ and $\rho(l)^* = 0.98665(3)$ of solid(s) fcc LJ-particles and liquid(l): E. A. Mastny and J. J. de Pablo, J. Chem. Phys. **127**, 104504 (2007), from where also the melting enthalpy, $\Delta_{\text{fus}}H^*$ can obtained using the (exact) Clapeyron equation; it is $\Delta_{\text{fus}}H^* = 1.675$. The mixing potential energy per solvent A-particle, $\Delta_{\text{mix}}u_{\text{pot}}(T^*_{\text{fus,A}}, x_B)$ at $p = 10$ are obtained from MD simulations. The mixing potential energy is self-consistently with the approximation in Eq. (3) assumed to be temperature independent for small x_B.

[11] S. Toxvaerd, Mol. Phys. **72**, 159 (1991).

[12] J. J. Morales, L. F. Rull, and S. Toxvaerd, Comp. Phys. Comm. **56**, 129 (1989).

186

[13] J. Weeks, D. Chandler, and H. C. Andersen, J. Chem. Phys. **54**, 5237 (1971).

[14] F. Calvo, T. V. Bogdan, V. K. de Souza and D. J. Wales, J. Chem. Phys. **127**, 044508 (2007).

[15] S. S. Ashwin and S. Sastry, J. Phys.: Condens. Matter **15**, 1253 (2003).

[16] C. De Michele, F. Sciortino and A. Coniglio, J. Phys.: Condens. Matter **16**, L489 (2004).

[17] S. R. Williams and D. J. Evans, Phys. Rev. Lett. **96**, 015701 (2006).

[18] L. O. Hedges, L. Maibaum, D. Chandler, and J. P. Garrahan, J. Chem. Phys. **127**, 211101 (2007).

Figure Captions

Figure 1.

Melting point temperature $T_{\text{fus,A}}$ of the solvent of A-particles at the external pressure $p{=}10$ as a function of the particle fraction x_{B} of solute particles, and in the concentration interval $x_{\text{B}} \in [0, 0.2]$ where the system crystallizes into a crystal of pure (fcc) A-particles. With full line is $T_{\text{fus,A}}(x_{\text{B}})$ for an ideal mixture and the Wahnström-model [1] (no visible difference), with small dashes is for the Kob-Andersen mixture [2], and with long dashes is the present modified mixture (see Sec. IV).

Figure 2.

(a) Particle positions projected onto a plane for the standard Kob-Andersen binary Lennard-Jones liquid (the large (A) particles are green, the small (B) particles are black). The system is shown after 1.5 μs of simulation (Argon units) at T=0.40 and density 1.2 (dimensionless units). After this simulation time the A particles phase separated and formed a large crystal, as is clear in the second figure showing the same configuration with all A particles removed.

Figure 3.

Schematic illustration of the change in melting point temperature, $T_m(x_{\text{B}})$ as a function of the particle fraction, x_{B} by removing the attraction between the A,A- and B,B pair interactions.

Figure 4.

Particle positions of the frozen system after it first was grafted with a small CsCl (A,B) crystal and at $T = 0.30$. The A-particles are green and the B-particles are red. (a) The hole system of 1000 particles at the density $\rho = 1.2$ and $x_{\text{B}} = 0.20$. (b) A central part of the frozen system where the two coexisting crystal forms, fcc (A) and CsCl (AB) clearly can be seen. (The frozen system contains several defects).

Figure 5.

Radial distribution functions $g_{\text{AA}}(r)$ for the A-A distribution particles at the density $\rho{=}1.2$ and the temperature T=0.50 for a mixtures with particle fraction $x_{\text{B}}{=}0.2$ of B-particles. Full line is for a KA-mixture and the dashed curve is for the modified mixture.

Figure 6.

Radial distribution functions $g_{\text{AB}}(r)$ for the A-B distribution at the density $\rho{=}1.2$ and the temperature T=0.50 for a mixtures with particle fraction $x_{\text{B}}{=}0.2$ of B-particles. Full line is for a KA-mixture and the dashed curve is for the modified mixture.

Figure 7.

Radial distribution functions $g_{\text{BB}}(r)$ for the B-B distribution at the density $\rho{=}1.2$ and the temperature T=0.50 for a mixtures with particle fraction $x_{\text{B}}{=}0.2$ of B-particles. Full line is for a KA-mixture and the dashed

Paper XI 187

curve is for the modified mixture.

Figure 8.
$log - log$ plot of the mean square displacement for A-particles as a function of time (in unit $\sigma\sqrt{m/\epsilon} \approx 2. \times 10^{-12}s$)and for different temperatures (from the left): T=1.00, 0.40, 0.35, 0.325, 0.30, 0.275 and 0.25. respectively.

Figure 9.
An Arrhenius plot, logD(1/T), of the self diffusion constant D. With + is D(A) for the KA mixture, and the points given by $\times$ and connected with lines is D(A) for the modified binary mixture (see III B). The diffusion constants, D(B) for the smaller B-particles in the modified binary mixture are shown with $\star$.

Figure 10.
With full line is the logD(1/T) for the modified mixture (the data points from Fig.9 are just connected by straight lines) and with dashes are the corresponding scaled KA-

data log(D)$(\frac{1}{0.81T})$, where the temperatures are scaled by an empirical factor 0.81.
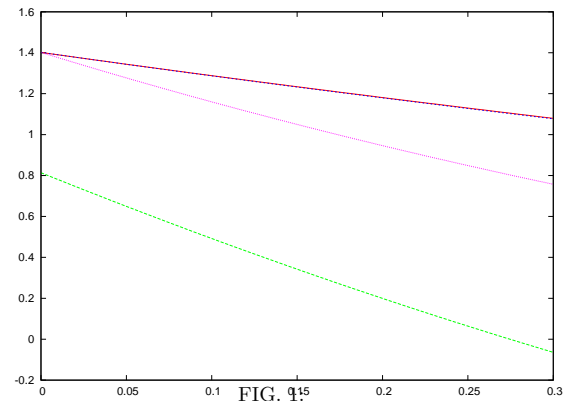
FIG. 1.
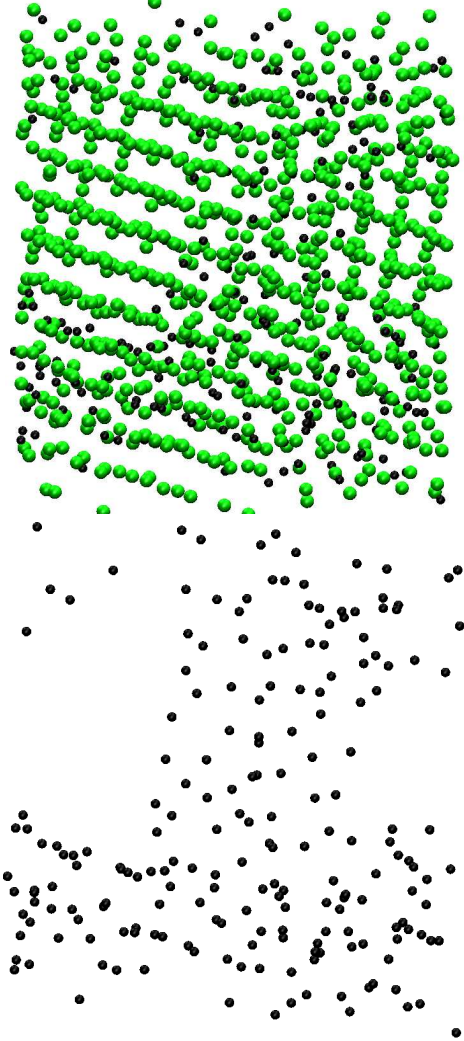
FIG. 2:
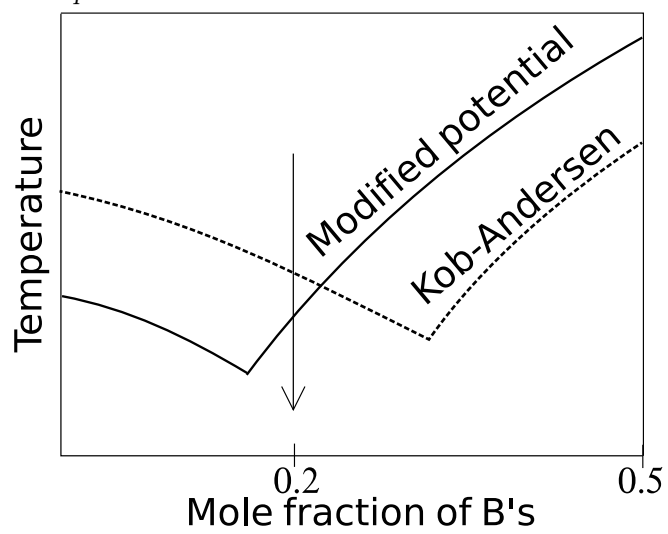
FIG. 3:
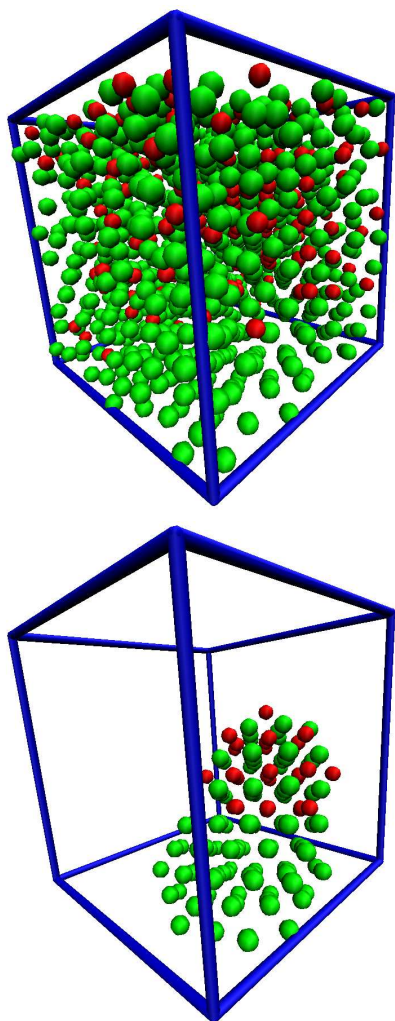
FIG. 4:
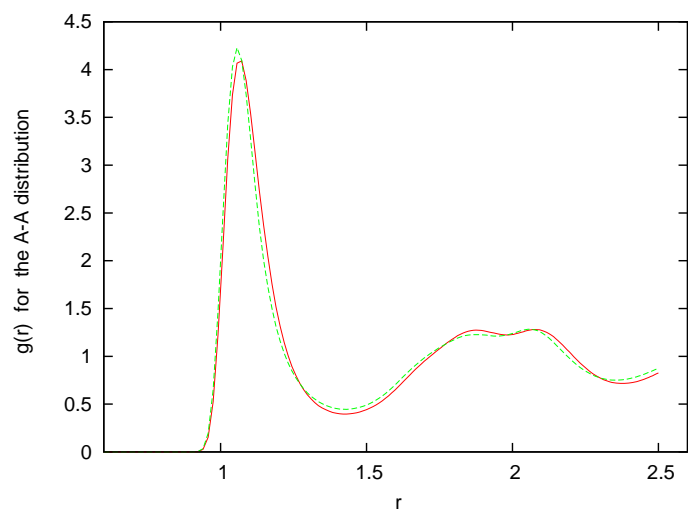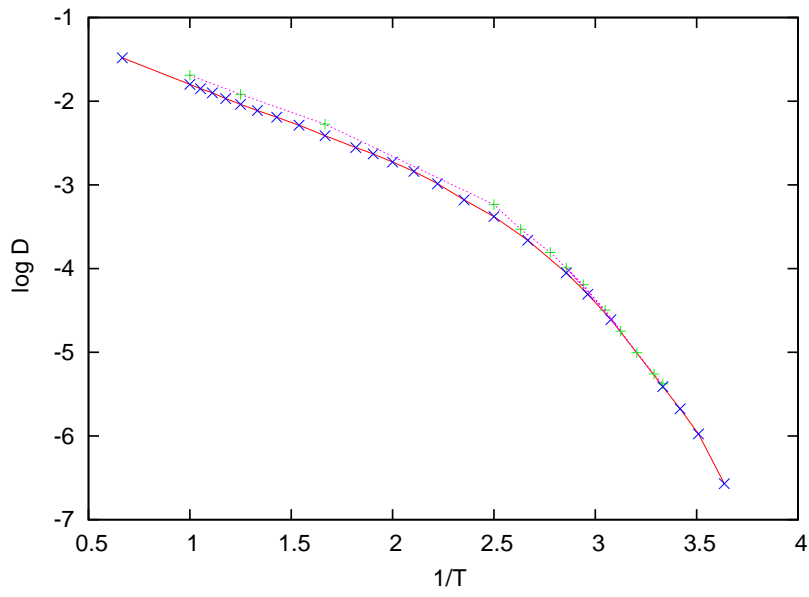
FIG. 5:
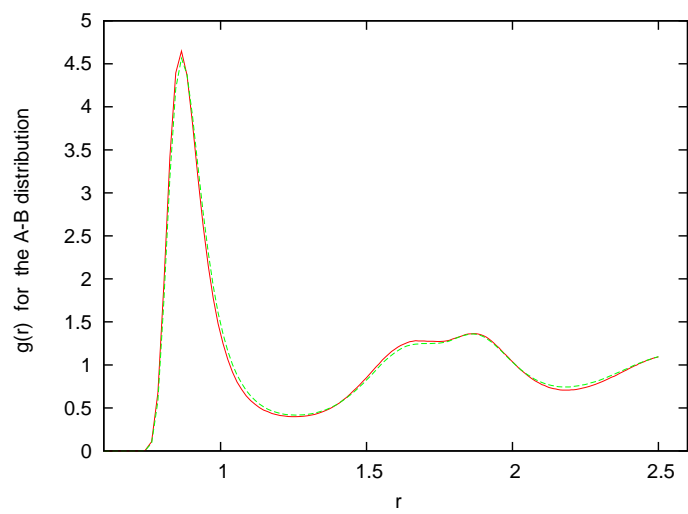
FIG. 6:
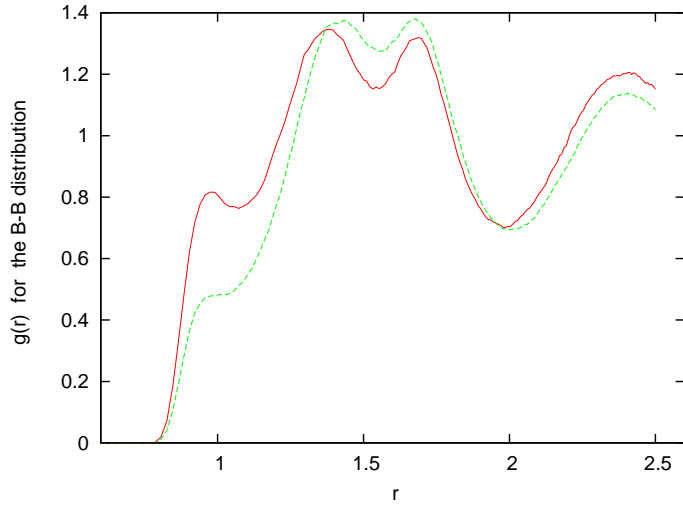
FIG. 7:
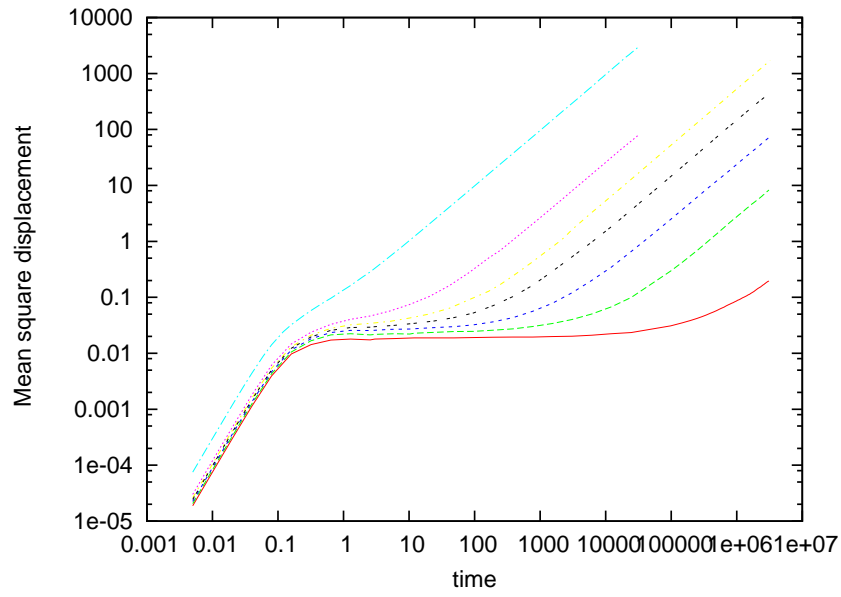
FIG. 8:
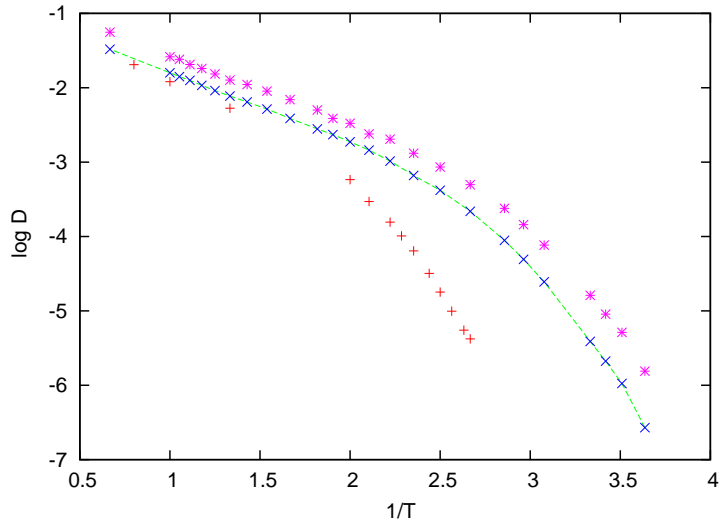
FIG. 9:

FIG. 10:

Termiske fluktuationer – er der noget nyt under Solen?

Af Ulf Rørbæk Pedersen, Thomas B. Schrøder og Jeppe C. Dyre, Danmarks Grundforskningsfonds center for seje væskers dynamik, "Glas og Tid", Roskilde Universitet

I computersimuleringer af en række simple væsker har det for nyligt vist sig, at tryk og energi korrelerer meget stærkt i deres fluktuationer i termisk ligevægt. Artiklen fortæller kort om denne opdagelse og dens konsekvenser.

Termiske fluktuationer og statistik

Tænk på molekylerne i et glas vand – eller på atomerne i en klump kobber. Et sådant system er utroligt kompliceret hvis man forestiller sig at skulle holde rede på alle molekylernes positioner og bevægelser. Men heldigvis er langt de fleste frihedsgrader uinteressante. Interessante størrelser er fx den samlede energi, volumenet, trykket, temperaturen – eller det samlede elektriske dipolmoment. For et glas vand i termisk ligevægt er disse størrelser ganske veldefinerede og konstante i tiden. Men betragter man systemet "med mikroskopet," vil man se at størrelserne faktisk fluktuerer en smule. Dette fænomen afhænger af randbetingelserne, fx gælder for et isoleret system at energien er bevaret og derfor ikke kan fluktuere. Men den typiske situation er at makroskopiske størrelser, som tiden går, fluktuerer en lille smule omkring deres middelværdier.

Situationen er ikke anderledes end uden for fysikken, faktisk er statistik jo netop opfundet til at kunne skelne tilfældige fluktuationer fra ikke-tilfældige. En nyttig erkendelse fra statistikken er den såkaldte $1/\sqrt{N}$ regel, en regel man kan komme forbavsende langt med. Hvis man fx slår plat og krone 10.000 gange vil der i gennemsnit komme 5.000 gange plat og 5.000 gange krone. Men selvfølgelig vil disse tal ikke passe helt præcist, og $1/\sqrt{N}$ reglen siger at den typiske relative afvigelse i dette eksempel er omkring 1/100 af de 10.000, altså af størrelsesorden 100 til hver side. Det betyder at hvis man fx observerer krone 6.000 gange, er det tale om en meget interessant mønt! Men hvis man observerer krone 5.060 gange er der ingen grund til mistænksomhed. Når man ofte læser at en Gallup-undersøgelse har en usikkerhed på 3% kommer det fra, at man typisk interviewer omkring 1.000 mennesker.

Einsteins formel for varmekapaciteten

$1/\sqrt{N}$ reglen betyder at jo større N er, jo mindre er fluktuationerne relativt. Jo større et glas vand, jo mindre fluktuerer middelenergien. Man skulle derfor mene at termiske fluktuationer ingen særlig betydning har for makroskopiske systemer. For godt 100 år siden viste Einstein imidlertid at det er forkert. Han udregnede, at varmekapaciteten ved konstant volumen for et system i termisk ligevægt med omgivelserne er proportional med systemets energifluktuationer. Kalder vi energien for E og betegnes afvigelser fra ligevægt med ΔE, defineres energifluktuationernes størrelse ved $\sqrt{<(\Delta E)^2>}$, hvor de spidse parenteser signalerer middelværdi over tid. Einstein viste ved en simpel udregning, at denne størrelses kvadrat er proportional med varmekapaciteten C_V:

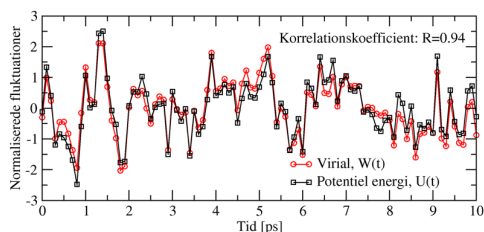$$C_V = \frac{<(\Delta E)^2>}{k_B T^2}, \qquad (1)$$

hvor k_B er Boltzmanns konstant og T er temperaturen. Varmekapaciteten er selvfølgelig proportional med antallet af molekyler, så ifølge Einsteins formel er energifluktuationernes størrelse proportional med $\sqrt{N}$. Da energien går som N, betyder det at den *relative* energifluktuation varierer som $1/\sqrt{N}$. I Einsteins formel for varmekapaciteten genfinder vi altså statistikkens $1/\sqrt{N}$ regel!

I løbet af 1920'erne og 1930'erne blev det gradvist klart at termiske fluktuationer også bestemmer andre såkaldte lineær-respons størrelser. For eksempel er kompressibiliteten (sammentrykkeligheden) proportional med volumenfluktuationerne og dielektricitetskonstanten er proportional med fluktuationerne af det elektriske dipolmoment uden et ydre felt. Endnu mere generelt gælder det såkaldte *fluktuations-dissipations (FD) teorem*, der udtaler sig om det tidsafhængige respons af et system der forstyrres lidt fra ligevægt, fx ved at det påføres et ydre elektrisk eller magnetisk felt. FD-teoremet afspejler den dybe erkendelse at fluktuationer og lineært respons er to sider af samme sag; teoremet gør det muligt at beregne det tids/frekvens-afhængige respons på et ydre felt alene ud fra fluktuationerne i termisk ligevægt (mere præcist: ud fra ligevægts tidsautokorrelationsfunktioner). Dette resultat, som er grundlæggende i den moderne statistiske mekanik, blev endeligt etableret i løbet af 1950'erne og kendes for den elektriske ledningsevnes vedkommende som "Kubo-formlen". Også på dette område var Einstein altså en pioner.

Korrelation af virial og potentiel energi i væsker

På grund af FD-teoremet ved vi i dag at termiske fluktuationer ikke er ligegyldig støj, men tværtimod indeholder væsentlig information. De fleste fysikere ville nok mene der ikke er mere at sige om denne sag. Ved grundforskningscenteret "Glas og Tid" på RUC studerer vi sejtflydende væskers egenskaber både eksperimentelt og teoretisk, blandt andet med henblik på at forstå glasovergangen – den proces hvor væsken

gradvist størkner til et fast, ikke krystallinsk stof [1-5]. Vi udfører i den forbindelse omfattende computersimuleringer. Her opdagede vi for nyligt noget mærkeligt... Det viste sig at at tryk- og energi-fluktuationerne næsten helt følges ad i tiden for rigtig mange væsker [6]. Se fx på figur 1 som viser resultater fra en computersimulering af den såkaldte Lennard-Jones væske (der i øvrigt ikke er sejtflydende!). Lennard-Jones (LJ) væsken har gennem mange år fungeret som standard modelsystem for studiet af væsker – den danner bl.a. grundlag for diverse numeriske protein-modeller – og den er givetvis et af de mest simulerede systemer i computerens tidlige historie. LJ-væsken består af en række partikler som vekselvirker via par-kræfter med en stærk, kortrækkende frastødning og en svagere, mere langtrækkende tiltrækning. Den kortrækkende frastødning modellerer molekyl-molekyl frastødningen, som i sidste ende stammer fra Pauli-princippet for elektronerne. LJ-systemet er imidlertid rent klassisk og studeres ved "molecular dynamics" metoden som simpelthen løser Newtons anden lov numerisk.


Figur 1. Normerede fluktuationer som funktioner af tiden af virial, W, og potentiel energi, U, i computersimuleringer af Lennard-Jones væsken (middelværdien er fratrukket og der er divideret med spredningen). T=80 K og p=0. Vi anvender såkaldte "Argon units", dvs. de parametre for Lennard-Jones potentialet der bedst reproducerer termodynamiske data for Argon. De viste data er et lille udsnit af en 10 nanosekunder lang simulering. W og U er tydeligvis stærkt korrelerede. Dette er kvantificeret med korrelationskoefficienten: $R \equiv <\Delta W \Delta U>/\sqrt{<(\Delta W)^2><(\Delta U)^2>}$. R=1 svarer til perfekt korrelation, medens R=0 svarer til ingen korrelation overhovedet. Figuren er en dansk version af en figur fra ref. [6].

Figur 1 viser faktisk ikke trykket p og energien E – mere præcist er det det såkaldte *virial W* og den *potentielle energi U* der vises. Som bekendt er energien summen af den kinetiske og den potentielle energi; sidstnævnte er den del af energien som afhænger af molekylernes positioner. På samme måde har trykket et "trivielt" bidrag fra molekylernes bevægelse (deres impulser) og et bidrag som afspejler det intermolekylære potential. Førstnævnte er der altid – også når molekylerne ikke vekselvirker; det fører til idealgasligningen (med sædvanlige betegnelser), $pV = Nk_BT$. Virialet W giver så per definition resten af trykket:

$$pV = Nk_BT + W. \quad (2)$$

Bemærk at virialet har dimension energi. Når man plotter virial og potentiel energi som funktioner af tiden for LJ-væsken i termisk ligevægt (figur 1) finder man altså at størrelserne følges pænt ad i deres normaliserede

fluktuationer. I det viste eksempel, der er typisk, er W og U 94% korrelerede.
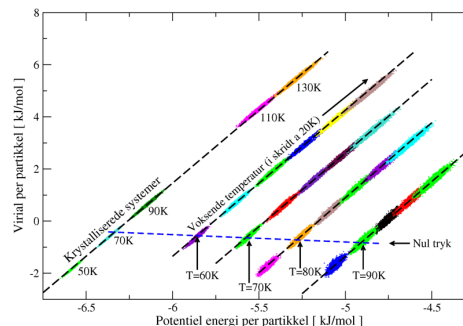
Figur 2. Illustration af de stærke $W - U$ korrelationer i computersimuleringer af Lennard-Jones væsken for forskellige termodynamiske tilstande. Hver farvet ellipse består af punkter der giver sammenhørende værdier af virial og potentiel energi til givne tidspunkter i tidsudviklingen. De ellipser der ligger på samme skrå sorte stiplede linie er simuleret ved samme densitet. Densiteterne er fra højre mod venstre: 32,6; 34,6; 36,0; 37,4 og 39,8 mol/l. De ellipser der krydses af den næsten vandrette blå stiplede linie har nul tryk. Det at de farvede ellipser er langstrakte viser, at der er stærke korrelationer mellem virial og potentiel energi. Den orange ellipse mærket "T=80 K" er resultatet af den simulering der er illustreret i figur 1, med $R = 0,94$. For alle de termodynamiske tilstande der er vist her gælder $R > 0,9$, undtaget væske-tilstandene med negativt tryk (under den blå stiplede linie) hvor R er lidt mindre end 0,9. Figuren er en dansk version af en figur fra ref. [6].

Figur 2 viser samhørende værdier af W og U for en række termodynamiske tilstande af LJ-væsken. For hver tilstand (farvet klynge) vises øjeblikkelige værdier; hver tilstand danner på denne måde en langstrakt ellipse af punkter. Det at den er langstrakt udtrykker netop de stærke korrelationer. De stiplede linier markerer forskellige densiteter.

Ingen har tilsyneladende bemærket disse korrelationer før – eller i hvert fald publiceret det. Vi havde en del problemer med selv at få resultatet publiceret, nogle reviewere mente det var forkert :-(, nogle at det var trivielt :-(, men heldigvis var der også nogle som mente det er interessant :-) . Et overraskende forskningsresultat rejser altid følgende spørgsmål: Hvad er forklaringen? Hvor almen er fænomenet? Og: Er det overhovedet vigtigt, dvs har det afgørende konsekvenser – og i givet fald hvilke? Hvad angår det første, vil vi ikke her bruge så megen plads på forklaringen (se reference [7]); det viser sig at for en række væsker kan potentialet til en god approximation beskrives som en invers potenslov af afstanden mellem to molekyler. Dette betyder at disse væsker har stærke $W - U$ korrelationer – de er "strongly correlating". Dermed afgrænses en klasse af væsker som omfatter van der Waals væsker og formentlig de fleste metaller, mens væsker med stærke hydrogenbindinger og væsker med kovalente bindinger ikke er "strongly correlating". Men som vist i detaljer i ref. [7] er forklaringen lidt mere kompliceret end som så; fx er korrelationerne i Lennard-Jones krystallen faktisk endnu stærkere end i

væsken. Korrelationerne overlever altså krystallisering (se nederste venstre hjørne i figur 2), hvilket er meget usædvanligt for en første-ordens faseovergang.

Argon er stærkt korreleret

Der er en hel del der tyder på at "strongly correlating" væsker i flere sammenhænge er simplere end væsker i almindelighed. Vi er for tiden i "Glas og Tid"-gruppen i fuld gang med at kortlægge fænomenet teoretisk. Men hvilke eksperimentelle konsekvenser har stærke $W - U$ korrelationer? Noget af det første vi kiggede på var argon, den klassiske modelvæske. Ved at analysere allerede eksisterende eksperimentelle data har vi vist at der er 96% korrelation mellem virial og potentiel energi i deres termiske fluktuationer for superkritisk argon. Dette er det første direkte bevis for at "strongly correlating liquids" eksisterer i virkeligheden og ikke kun i computeren. Figur 3 viser termodynamiske data for argon i et plot hvor diagonalen svarer til 100% korrelation.
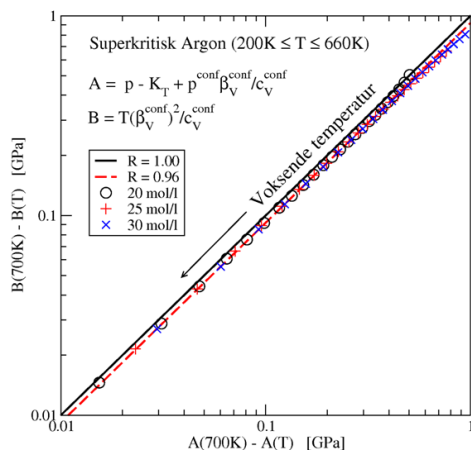
Figur 3. Stærke $W - U$ korrelationer i eksperimentelle data for superkritisk Argon. Data for tre forskellige densiteter og en række temperaturer er plottet på en sådan måde (se reference 6) at de skulle falde på den sorte diagonal hvis virial og potential energi var perfekt korreleret ($R = 1$). Dette er ikke tilfældet, men vi finder $R = 0,96$ (den røde stiplede linie) – altså ganske stærke korrelationer. Figuren er en dansk version af en figur fra ref. [6].

Mellem væske og fast stof

En måske vigtigere konsekvens vedrører sejtflydende væsker, der er vores primære interesse i "Glas og Tid". En sådan væske er kendetegnet ved at have meget lang relaxationstid [1-5] – den tid det tager væsken at komme i ligevægt efter en ydre forstyrrelse. Mens relaxationstiden for vand er 1 picosekund, kan den nemt være millisekunder, sekunder, timer, osv, for ekstremt seje væsker. Dette medfører, kan man vise, at en række termodynamiske størrelser som fx varmekapacitet, termiske udvidelseskoefficient eller kompressibilitet, alle er komplekse og frekvens-afhængige (ligesom fx en elektrisk impedans). Hvis væskens relaxationstid er τ, vil disse "termoviskoelastiske responsfunktioner" have signifikant frekvensafhængighed for frekvenser

omkring $1/\tau$. Dette kan kvalitativt forstås på følgende måde. Når vi måler ved frekvenser der er væsentligt højere end $1/\tau$, kan væskens struktur ikke nå at reagere på den påvirkning den udsættes for, simpelthen fordi dens relaxationstid er for lang. Det betyder at man vil se en opførsel der er karakteristisk for et fast stof. Måler vi derimod ved en frekvens der er væsentligt lavere end $1/\tau$, har væsken god tid til at reagere på den påvirkning vi udsætter den for, og den udviser karakteristisk væske-opførsel. Det vil sige at størrelser som varmekapacitet, kompressibilitet og udvidelseskoefficient er høje ved lave frekvenser (væske-opførsel) og lave ved høje frekvenser (faststof-opførsel). Ved frekvenser omkring $1/\tau$ slår relaxationsprocesserne igennem og medfører at responsfunktionerne bliver komplekse.

Dette er helt generelt for alle de grundlæggende otte termodynamiske responsfunktioner som findes (se fx ref. [8]). Men for "strongly correlating liquids" kan man vise [8], at i grænsen hvor der er 100% korrelation mellem virial og potentiel energi, vil alle ovennævnte responsfunktioner have samme frekvensafhængighed. Faktisk gælder også omvendt, at hvis responsfunktionerne har samme frekvensafhængighed, så vil væsken være "strongly correlating". Dette resultat illustrerer den ny væskeklasses relevans for seje væskers fysik. Men det er endnu ikke eftervist eksperimentelt. Grunden er, at der i dag ikke findes metoder til pålidelig måling af termoviskoelastiske responsfunktioner. Vi arbejder på at udvikle sådanne i "Glas og Tid"-gruppen. Det vil føre for vidt at forklare hvorfor det er så svært at måle responsfunktionerne; den interesserede læser kan få noget af forklaringen i ref. [9] der påviser at gængse metoder til måling af den frekvensafhængige isobare varmekapacitet ikke er pålidelige.

Nervesignaler

Et sidste eksempel på betydningen af korrelationer involverer en biofysisk anvendelse. For nyligt har Thomas Heimburg og Andrew Jackson fra Niels Bohr Institutet fremsat en helt ny teori for hvordan et nervesignal propagerer [10]. Idéen er at nervesignaler ikke primært er elektriske signaler, men u-lineære (soliton-)lydbølger som forplanter sig i nervecellemembranen. Teorien, som naturligvis er kontroversiel, forklarer bedøvelse som en effekt af at membran-smeltetemperaturen sænkes, hvilket delvis forhindrer lydbølgens forplantning [11].

Et vigtigt input i Heimburg-Jackson teorien er at membran-varmekapacitet og -kompressibilitet er proportionale i deres variation med temperaturen. Det kan vises at dette er opfyldt til en god approximation hvis membranens mikroskopiske energifluktuationer korrelerer stærkt med dens volumenfluktuationer (ved konstant tryk), altså en korrelation af samme type som den ovenfor diskuterede. Vi har undersøgt om det er tilfældet ved, i samarbejde med Günther Peters fra MEM-PHYS DTU, at foretage nogle omfattende computer-simuleringer. Resultaterne ses i figur 4. Rent faktisk finder vi stærke korrelationer, hvilket bestemt ikke er

trivielt i lyset af hvor kompliceret en biomembran er. Simuleringerne støtter altså Heimburg-Jackson teorien.
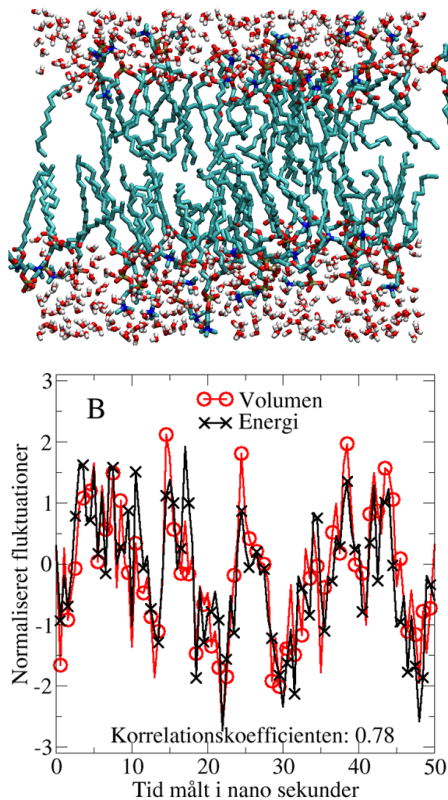
Figur 4. Øverst ses et udsnit af en computersimulereret membran bestående af phospholipider. Et phospholipid molekyle består af en hydrofil del (elsker vand) samt en hydrofob del (hader vand). I vand vil lipiderne spontant ordne sig så hydrofobe dele er skærmet fra vand mens hydrofile grupper er i kontakt med vand, som det er ses på figuren. Hovedbestandelen af disse biomembraner er phospholipider, og de benyttes derfor ofte som model-system for disse. Nederst vises hvordan volumen og energi midlet over 1/2 nanosekund fluktuerer som funktion af tid i en simulering af en membran. Med det blotte øje ses at volumen og energi "følges ad", dvs. de er stærkt korreleret. Det kan nævnes at øjeblikkelige volumener og energier kun er svagt korreleret. Det skyldes bl.a. at vandmolekyler bidrager til korttids-fluktuationer og at vand ikke er en "strongly correlating"-væske (se tekst). Det er altså kun for de langsomme membranfluktuationer man finder stærk korrelation.

Der forestår nu et større arbejde med at kortlægge egenskaberne af "strongly correlating liquids". Vores arbejdshypotese er som nævnt at disse væsker er særligt simple. Det er påvist at tryk-temperatur-afhængigheden af relaxationstiden i det væsentlige kan beregnes ud fra ligevægtsfluktuationerne [12], og seje væskers "aging" egenskaber er også ret simple (upubliceret).

Den lidt tilfældige opdagelse af stærke $W - U$ korrelationer, kan således måske med tiden føre til en bedre forståelse af seje væskers fysik.

Litteratur

[1] M.D. Ediger, C.A. Angell og S.R. Nagel (1996), *J. Phys. Chem.* **100**, s. 13200-13212.

[2] C.A. Angell, K.L. Ngai, G.B. McKenna, P.F. McMillan og S.W. Martin (2000), *J. Appl. Phys.* **88**, s. 3113-3157.

[3] P.G. Debenedetti og F.H. Stillinger (2001), *Nature* **410**, s. 259-267.

[4] J.C. Dyre (2006), *Rev. Mod. Phys.* **78**, s. 953-972.

[5] J. Dyre og T. Schrøder (2006), *Kvant* **17** (1), s. 12-15.

[6] U.R. Pedersen, N.P. Bailey, T.B. Schrøder, and J.C. Dyre (2008), *Phys. Rev. Lett.* **100**, 015701.

[7] N.P. Bailey, U.R. Pedersen, N. Gnan, T.B. Schrøder og J.C. Dyre (2008), "Pressure-energy correlations in Liquids." I og II, *J. Chem. Phys.* **129**, 184507 (I) og *J. Chem. Phys.* **129**, 184508 (II)

[8] N.L. Ellegaard, T. Christensen, P.V. Christiansen, N.B. Olsen, U.R. Pedersen, T.B. Schrøder og J.C. Dyre (2007), *J. Chem. Phys.* **126**, 044502.

[9] T. Christensen, N.B. Olsen og J.C. Dyre (2007), *Phys. Rev. E* **75**, 041502.

[10] T. Heimburg og A.D. Jackson (2005), *Proc. Natl. Acad. Sci.* **102**, 9790-9795.

[11] T. Heimburg og A.D. Jackson (2007), *Biophys. J.* **92**, 3159-3165.

[12] T.B. Schrøder, U.R. Pedersen, J.C. Dyre (2008), arXiv:0803.2199.

Ulf Rørbæk Pedersen er ph.d-studerende ved "Glas og tid". Han benytter molekyldynamik-simuleringer til at undersøge egenskaber af de stærkt korrelerede væsker, "strongly correlating liquids", som artiklen omhandler, såvel som metastabilitet af underafkølede væsker og phospholipidmembraner.

Thomas B. Schrøder, som er lektor i fysik, forsker i computersimuleringer af seje væskers dynamik og søger at opstille simple modeller, der afspejler disse egenskaber. Han har tidligere arbejdet med simulering af modeller for AC elektrisk ledning i uordnede stoffer, samt protein- og polymerdynamik.

Jeppe Dyre, der er professor i fysik, arbejder på at opstille fænomenologiske modeller for seje væskers dynamiske egenskaber. Modellerne opstilles i dialog med RUC glasgruppens eksperimentalfysikere. Målet er en model som gælder for alle seje væsker, uanset kemisk sammensætning.

Hidden scale invariance in molecular van der Waals liquids: A simulation study

Thomas B. Schrøder, Ulf R. Pedersen, Nicholas Bailey, Søren Toxværd, and Jeppe C. Dyre

DNRF Centre "Glass and Time," IMFUFA, Department of Sciences,
Roskilde University, Postbox 260, DK-4000 Roskilde, Denmark
(Dated: December 29, 2008)

We demonstrate that there is a "hidden" approximate scale invariance in van der Waals liquids. For an asymmetric dumbbell model, we provide direct evidence that the potential energy fluctuations are accurately described by inverse power law (IPL) potentials. We show that the radial distribution functions are accurately reproduced by the IPL's, and that the radial distribution functions obey the IPL predicted scaling properties. IPL scaling of the long time dynamics is also found to apply to this liquid – as well as to the Lewis-Wahnström model of ortho-terphenyl – with the scaling exponent predicted by the equilibrium fluctuations.

A phenomenon is scale invariant if it has no characteristic length or time. Scale invariance emerged as a paradigm in the early 1970's following the tremendous successes of the theory of critical phenomena. Liquids described by scale-invariant potentials are a theorist's dream by having a number of simple properties [1]. If potentials vary with distance as r^{-n}, the configurational free energy F as a function of density $\rho \equiv N/V$ and temperature T may be written $F = Nk_BTf(\rho^\gamma/T)$ where $\gamma = n/3$. Dynamical properties of inverse power law (IPL) liquids are also simple, because their relaxation time τ may be written as

$$\tau = g(\rho^\gamma/T) \qquad (1)$$

with the exponent γ that characterizes the thermodynamics. Unfortunately the predicted equation of state does not fit data for real fluids, and IPL liquids do not have stable low pressure states. Both problems derive from the absence of molecular attractions; these define the spatial scale of one intermolecular distance at low pressure. Thus real liquids have apparently little in common with scale-invariant liquids. In this paper we demonstrate that there is nevertheless a "hidden" approximate scale invariance in a large class of liquids, the van der Waals liquids. Consequently several properties of IPL liquids apply to van der Waals liquids, leading to experimentally testable predictions.

It was recently shown [2, 3, 4] that a number of model liquids exhibit strong correlations between the equilibrium fluctuations of the potential energy U and the virial W (defining the contribution to pressure coming from the intermolecular interactions via $pV = Nk_BT + W$). The class of "strongly correlating liquids" includes [4] the standard Lennard-Jones liquid, a liquid with exponential short-range repulsion, the Kob-Andersen binary Lennard-Jones liquid, a seven-site united-atom model of toluene, the three-site Lewis-Wahnström toy model of ortho-terphenyl (OTP), as well as a model consisting of asymmetric "dumbbell" type molecules.

For inverse power-law potentials $\propto r^{-n}$ there is 100% correlation between virial and potential energy fluctuations as function of time: $\Delta W(t) = \gamma \Delta U(t)$ where

$\gamma = n/3$ [1]. By reference to the single-component Lennard-Jones system it was argued in Ref. [4] that strongly correlating liquids are well approximated by inverse power-law potentials as regards their thermal equilibrium fluctuations. The present paper presents concrete proofs that this is the case – even for *molecular* model liquids with van der Waals type interactions (i.e., excluding hydrogen- and covalent bonds). The main conclusions below are:

- *At a given density and temperature the energy surface of a strongly correlating molecular liquid may to a good approximation be replaced by that of inverse power law potentials.*

- *State points having similar γ's are connected by a number of IPL scaling properties to a good approximation.*

For an asymmetric dumbbell model we provide direct evidence below that the potential energy fluctuations are accurately described by inverse power law potentials (varying as r^{-18}). We show that the radial distributions functions are all accurately reproduced by the r^{-18} IPL's, and that the radial distribution functions obey the IPL predicted scaling properties. Proceeding to the dynamics we show that that the so-called "density scaling" (Eq. (1)) applies to this liquid – as well as to the Lewis-Wahnström OTP model – with scaling exponent γ predicted by the equilibrium fluctuations.

We performed NVT molecular dynamics simulations [5, 6, 7, 8] of two molecular liquids: i) 512 asymmetric dumbbell molecules consisting of pairs of Lennard-Jones (LJ) spheres connected by rigid bonds; the dumbbells were parameterized to mimic toluene [9]. ii) the Lewis-Wahnström OTP model [12]. Both models are strongly correlating for the range of state points investigated here. For the dumbbell model we find for the correlation coefficient $0.95 < R < 0.97$; for the OTP model $0.91 < R < 0.92$. Fig. 1a illustrates the strong WU-correlation for the asymmetric dumbbell model. Since $R \approx 1$ it follows that $\Delta W(t) \approx \gamma \Delta U(t)$ in their instantaneous fluctuations [3], and consequently we refer to γ
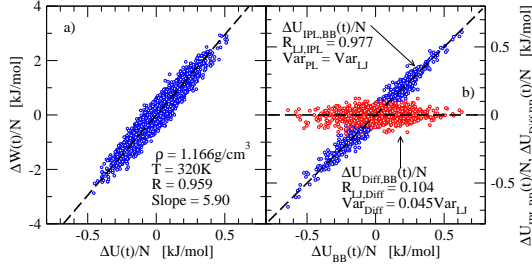
FIG. 1: **a)** $\Delta W(t)/N$ vs. $\Delta U(t)/N$ for the asymmetric dumbbell model. The strong correlations are quantified by the correlation coefficient, $R \equiv \langle \Delta W \Delta U \rangle / \sqrt{\langle (\Delta W)^2 \rangle \langle (\Delta U)^2 \rangle} = 0.959$. The dashed line has the slope $\gamma \equiv \sqrt{\langle (\Delta W)^2 \rangle / \langle (\Delta U)^2 \rangle} = 5.90$. **b)** For configurations taken from the simulation reported in Fig. 1a we evaluated $U_{\rm IPL,BB}(t) \equiv \sum_{i>j} \phi_{\rm IPL,BB}(r_{ij}(t))$ with $\phi_{\rm IPL,BB}(r) \equiv C_{\rm BB} \epsilon_{\rm BB} (\sigma_{\rm BB}/r)^{18}$. The constant $C_{\rm BB} = 1.489$ ($C_{\rm AA} = 1.075$, $C_{\rm AB} = 1.237$) was chosen to make the variance of $U_{\rm IPL,BB}(t)$ equal to the variance of $U_{\rm BB}(t) \equiv \sum_{i>j} \phi_{\rm LJ,BB}(r_{ij}(t))$. $U_{\rm IPL,BB}(t)$ strongly correlates with $U_{\rm BB}(t)$ with a correlation coefficient of 0.977. In comparison $U_{\rm Diff,BB}(t) \equiv U_{\rm BB}(t) - U_{\rm IPL,BB}(t)$ has small variance, 0.045 times the variance of $U_{\rm BB}(t)$ and is only weakly correlated with the latter. Redoing the analysis with $n = 3 \times 5.90$ (the IPL exponent suggested by the fluctuations, see Fig. 1a) gives almost identical results.

as the 'slope'.

Fig. 1b details the origin of the strong correlations, focusing on the strongest interaction in the dumbbell model, the 'BB' interaction ('B' indicating the large "phenyl" spheres). The fluctuations in $U_{\rm BB}(t)$ are well described by an IPL pair potential $\phi_{\rm IPL,BB}(r) \propto r^{-18}$. The same conclusion applies for the AA and AB interactions (data not shown). The reason that $\phi_{\rm Diff,\alpha\beta}(r) \equiv \phi_{\rm LJ,\alpha\beta}(r) - \phi_{\rm IPL,\alpha\beta}(r)$ contributes little to the fluctuations at constant volume is that this term is approximately linear in the region of the first peak of the pair correlation function [4]: When one pair-distance is increased, other pair-distance(s) are decreased by (approximately) the same amount, keeping the change in $U_{\rm Diff,\alpha\beta}(t) \equiv \sum_{i>j} \phi_{\rm Diff,\alpha\beta}(r_{ij}(t))$ small. Switching the ensemble from NVT to NpT (p=1.32GPa) reduces the WU-correlation from 0.959 to 0.866, illustrating the importance of the constant volume constraint.

The fluctuations tell us that the relevant part of the potential energy surface is well approximated by a corresponding 'IPL' system, i.e., the system where the LJ pair potentials are replaced by the IPL potentials discussed in Fig. 1b. To test how far this correspondence holds, we simulated the IPL system at the same density and temperature. Fig. 2a compares the pair distribution functions; the agreement is striking. This is the first proof
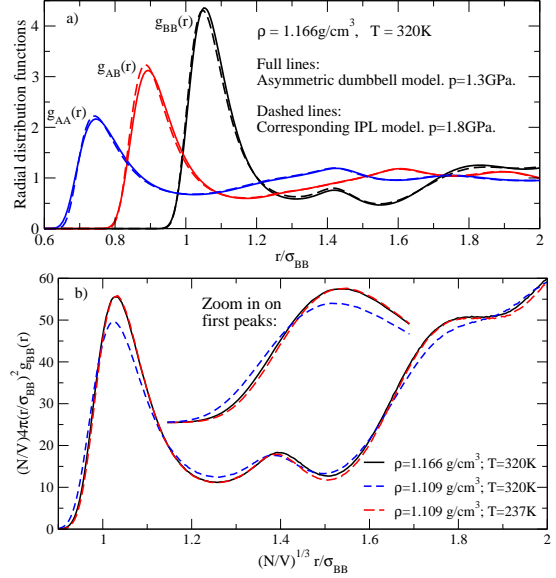
FIG. 2: **a)** Radial distribution function for the asymmetric dumbbell model (full lines), and the corresponding IPL model (dashed lines, see text). **b)** Scaled $g_{BB}(r)$ for three state points; the two state points with the same $\Gamma = \rho^\gamma/T$ (black full line and red long dashed line; $\gamma = 6$) have almost identical (scaled) structure. There is a small but significant difference in the left part of the first peak, reflecting the existence of the fixed bond. Similar scaling is found also for the AA and AB interactions (data not shown).

that the structure of a molecular liquid is well reproduced by an IPL liquid. In contrast, the average pressures of the two models are different, because the IPL system does not include the contributions from $\phi_{\rm Diff,\alpha\beta}(r)$.

Consider now changing density and temperature, conserving the parameter $\Gamma = \rho^\gamma/T$. For an $n = 3\gamma$ IPL liquid this means that we are studying the same system but with scaled length and time units [1]. Fig. 2b shows that the real (LJ) system inherits this scaling behavior to a good approximation. Note that there is only a small effect of the fixed bond connecting the LJ spheres. The average pressure and potential energy do *not* follow the IPL scaling; $\phi_{\rm Diff,\alpha\beta}(r)$ contributes differently to these at different state points, thus the IPL describes the structure and dynamics (see below), not the equation of state.

We now turn to the long time dynamics. To the degree that the IPL approximation holds over a range of state-points, the long time dynamics is a function of $\Gamma = \rho^\gamma/T$ where γ is one third of the IPL exponent n, i.e., the "density" scaling of Eq. (1) is predicted to apply. This type of scaling has in recent years become a well established empirical fact for a large number of viscous liquids
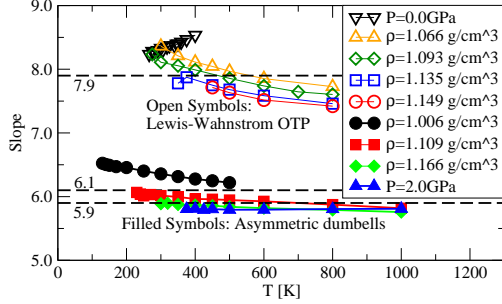
FIG. 3: The 'slopes', $\gamma \equiv \sqrt{\langle (\Delta W)^2 \rangle / \langle (\Delta U)^2 \rangle}$ plotted as a function of temperature for two molecular models. Both models are strongly correlating. For the Lewis-Wahnström OTP model the zero pressure isobar covers densities in the interval 1.008 g/cm^3 to 1.089 g/cm^3. For the asymmetric dumbbell model the 2.0GPa isobar covers densities in the interval 1.120 g/cm^3 to 1.217 g/cm^3. For the three dumbbell isochores the pressures at the lowest temperatures are -0.02GPa, 0.67GPa, and 1.28GPa respectively.

[13, 14]. Other forms of scaling have been suggested, but it has been argued that the scaling reflects an underlying IPL [14, 15, 16, 17], and thus that Eq. (1) is the correct scaling.

A potential complication for the IPL explanation of density scaling, is that the IPL exponent suggested by the fluctuations ($n = 3\gamma$) depends on state point [4]. This is illustrated for the two models in Fig. 3. Note that while the suggested exponent is slightly dependent on state point for each model, the fluctuations clearly point towards different exponents for the two models. For the OTP model we test density scaling with the slope averaged over all state points: $\gamma = 7.9$. For the dumbbell model we consider two values of the scaling exponent: the slope averaged over all state points; $\gamma = 6.1$, and the slope averaged over the three data sets with the smallest slopes; $\gamma = 5.9$, i.e., the "best" compromise if we ignore the $\rho = 1.006$ g/cm^3 isochore. Following Coslovich and Roland [16] we apply density scaling to the reduced diffusion coefficient, $D^* \equiv (N/V)^{1/3}(k_BT/m)^{-1/2}D$ where m is the mass of the molecules and D is the diffusion coefficient estimated from the long-time behavior of the mean-square displacement.

Fig. 4 applies density scaling to the Lewis-Wahnström OTP model. Density scaling works neither with $\gamma = 9.0$ or $\gamma = 7.0$, whereas it does work well with $\gamma = 7.9$ - the exponent we chose from the fluctuations (Fig. 3).

In Fig. 5 density scaling is applied to the asymmetric dumbbell model. Density scaling works neither with $\gamma = 7.0$ or $\gamma = 5.0$. Comparing the scaling with $\gamma = 6.1$ to the data without scaling ($\gamma = 0$, open symbols), we find good data collapse; by far most of the density dependence is captured by the density scaling with $\gamma = 6.1$. With
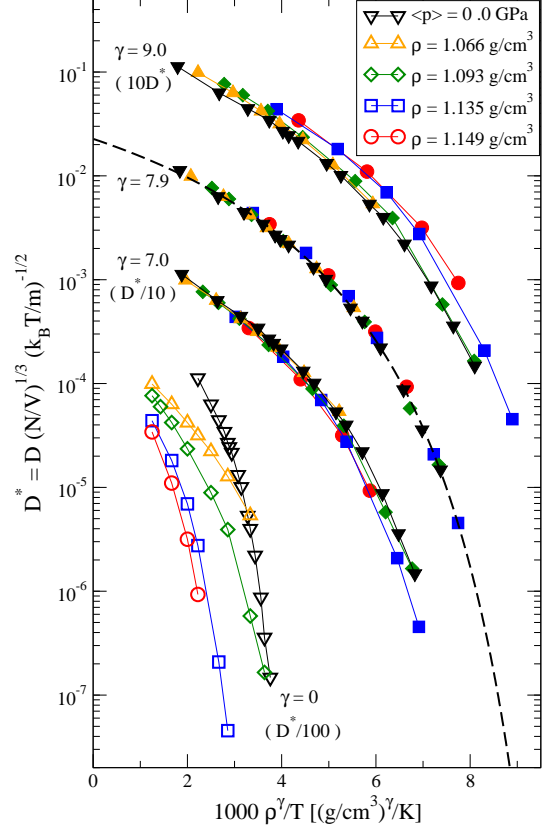

FIG. 4: The reduced diffusion coefficient for Lewis-Wahnström OTP [12]. Open symbols: D^* plotted without scaling ($\gamma = 0$, D^* divided by 100). Filled symbols: D^* scaled according to Eq. (1) with three different scaling exponents: $\gamma = 9.0$ (Upper set of curves, D^* multiplied by 10), $\gamma = 7.9$ (Second set of curves), $\gamma = 7.0$ (Third set of curves, D^* divided by 10).

$\gamma = 5.9$ the data collapse is even better for three of the data sets, whereas one data set deviates from the master curve comprised of these three sets. This is the isochore $\rho = 1.006$ g/cm^3, i.e., the one that was ignored when choosing $\gamma = 5.9$ (Fig. 3).

The above results demonstrate that density scaling is a consequence of the underlying IPL scale invariance. The scaling is only perfect for true IPL liquids - for "real" liquids a larger region of state points makes the scaling less perfect (compare Fig. 5, $\gamma = 6.1$ and 5.9) for two reasons: the apparent IPL exponents ($n = 3\gamma$) change more, and the effect of intra-molecular interactions that do not obey the IPL scaling (here the fixed bonds) is larger. Note that even small density changes are experimentally relevant;
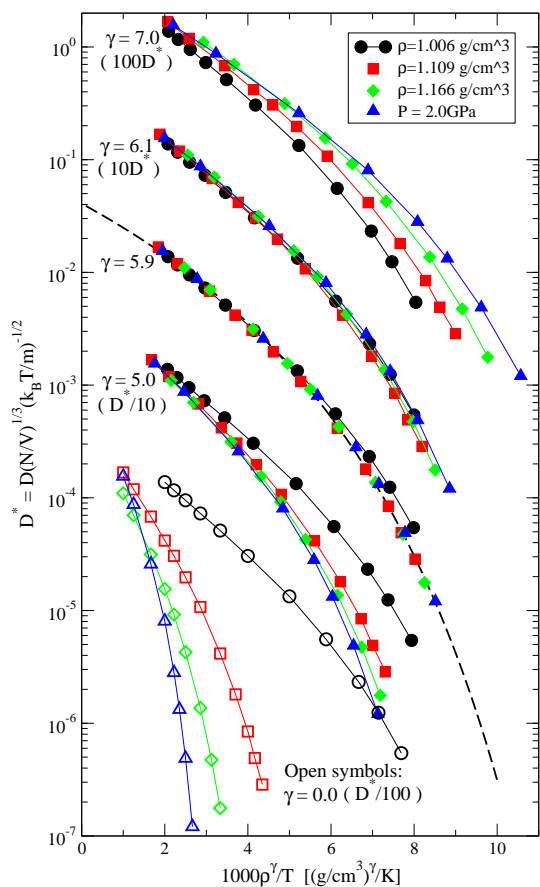
FIG. 5: The reduced diffusion coefficient for the asymmetric dumbbell model. Open symbols: D^* plotted without scaling ($\gamma = 0$, D^* divided by 100). Filled symbols: D^* scaled according to Eq. (1) with four different scaling exponents: $\gamma = 7.0$ (Upper set of curves, D^* multiplied by 100), $\gamma = 6.1$ (Second set of curves, D^* multiplied by 10), $\gamma = 5.9$ (Third set of curves), and $\gamma = 5.0$ (Fourth set of curves, D^* divided by 10).

changing density of, e.g., phenylphthalein-dimethylether by 2% can change the relaxation time by more than two decades [18].

We have provided direct evidence for an underlying IPL scale invariance in model molecular van der Waals liquids, leading to two experimentally testable predictions for these liquids: i) The density scaling exponent γ can be identified from the equilibrium fluctuations via the fluctuation-dissipation theorem determining the frequency-dependent linear thermoviscoelastic response functions [2, 19]; ii) Different state points with same ρ^γ/T – same values of D^* and τ_α – should have same scaled

structure factors.

[1] W. G. Hoover, M. Ross, K. W. Johnson, D. Henderson, J. A. Barker, and B. C. Brown, J. Chem. Phys. **52**, 4931 (1970); W. G. Hoover, S. G. Gray, and K. W. Johnson, J. Chem. Phys. **55**, 1128 (1971); Y. Hiwatari, H. Matsuda, T. Ogawa, N. Ogita, and A. Ueda, Prog. Theor. Phys. **52**, 1105 (1974); D. Ben-Amotz and G. J. Stell, J. Chem. Phys. **119**, 10777 (2003); C. De Michele, F. Sciortino, and A. Coniglio, J. Phys.: Condens. Matter **16**, L489 (2004).
[2] U. R. Pedersen, T. Christensen, T. B. Schrøder, and J. C. Dyre, Phys. Rev. E **77**, 011201 (2008).
[3] U. R. Pedersen, N. P. Bailey, T. B. Schrøder, and J. C. Dyre, Phys. Rev. Lett. **100**, 015701 (2008).
[4] N. P. Bailey, U. R. Pedersen, N. Gnan, T. B. Schrøder, and J. C. Dyre, J. Chem. Phys. **129**, 184507 (2008); J. Chem. Phys. **129**, 184508 (2008).
[5] NVT simulations were carried out using Gromacs software [6] using the Nosé-Hoover thermostat [7]. Molecules were kept rigid using the LINCS [8] algorithm.
[6] H. J. C. Berendsen, D. van der Spoel, and R. van Drunen, Comp. Phys. Comm. **91**, 43 (1995); E. Lindahl, B. Hess, and D. van der Spoel, J. Mol. Mod. **7**, 306 (2001).
[7] S. A. Nosé, Mol. Phys. **52**, 255 (1984); W. G. Hoover, Phys. Rev. A **31**, 1695 (1985).
[8] B. Hess, H. Bekker, H. J. C. Berendsen, and J. G. E. M. Fraaije, J. Comp. Chem. **18**, 1463 (1997).
[9] The large LJ sphere, mimicking the phenyl group, is similar to the one in the Lewis-Wahnström OTP model [10] with the parameters $m_p = 77.106$ u, $\sigma_p = 0.4963$ nm and $\epsilon_p = 5.726$ kJ/mol. The small sphere, mimicking the methyl group, was taken from UA-OPLS [11] with $m_m = 15.035$ u, $\sigma_m = 0.3910$ nm and $\epsilon_m = 0.66944$ kJ/mol. Bond length: $d = 0.29$ nm. The interaction between unlike particles is determined by the Lorentz-Berthelot mixing rules.
[10] G. Wahnström and L. J. Lewis, Physica A **201**, 150 (1993); L. J. Lewis and G. Wahnström, Phys. Rev. E **50**, 3865 (1994).
[11] W. L. Jorgensen, J. D. Madura, and C. J. Swenson, J. Am. Chem. Soc. **106**, 6638 (1984).
[12] $N = 324$ molecules consisting of three LJ particles (with $\sigma = 0.483$ nm, $\varepsilon = 600$ K$k_B \simeq 4.989$ kJ/mol and $m = 76.768$ u) placed in the corners of a rigid isosceles triangle with two sides of length $\sigma = 0.483$ nm and one angle of $75°$ [10]. LJ potentials were cut at $r_c = 2.5\sigma$ using a shift function [6] with $r_1 = 2.3\sigma$.
[13] A. Tölle, Rep. Prog. Phys. **64**, 1473 (2001); C. Dreyfus, A. Aouadi, J. Gapinski, M. Matos-Lopes, W. Steffen, A. Patkowski, and R. M. Pick, Phys. Rev. E **68**, 011204 (2003); C. Alba-Simionesco, A. Cailliaux, A. Alegria, and G. Tarjus, Europhys. Lett. **68**, 58 (2004); C. M. Roland, S. Hensel-Bielowka, M. Paluch, and R. Casalini, Rep. Prog. Phys. **68**, 1405 (2005).
[14] R. Casalini and C. M. Roland, Phys. Rev. E **69**, 062501 (2004).
[15] C. M. Roland and R. Casalini, J. Phys.: Condens. Matter

19, 205118 (2007).

[16] D. Coslovich and C. M. Roland, J. Phys. Chem. B **112**, 1329 (2008); arXiv:0810.5692 (2008).

[17] T. B. Schrøder, U. R. Pedersen, and J. C. Dyre, arXiv:0803.2199 (2008).

[18] M. Paluch, R. Casalini, and C. M. Roland, Phys. Rev. B **66**, 092202 (2002).

[19] N. L. Ellegaard, T. Christensen, P. V, Christiansen, N. B. Olsen, U. R. Pedersen, T. B. Schrøder, and J. C. Dyre, J. Chem. Phys. **126**, 074502 (2007).

5